AD-A187 337 DEVELOPMENT OF ADVANCEDCONSTITUTIVE MODELS FOR PLAIN AND REINFORCED CONCRETE(U) S-CUBED LA JOLLA CA G A HEGEMIER ET AL MAR 87 SSS-R-87-8454 1/3

UNCLASSIFIED AFOSR-TR-87-1391 F49620-84-C-0029 F/G 13/3 NL

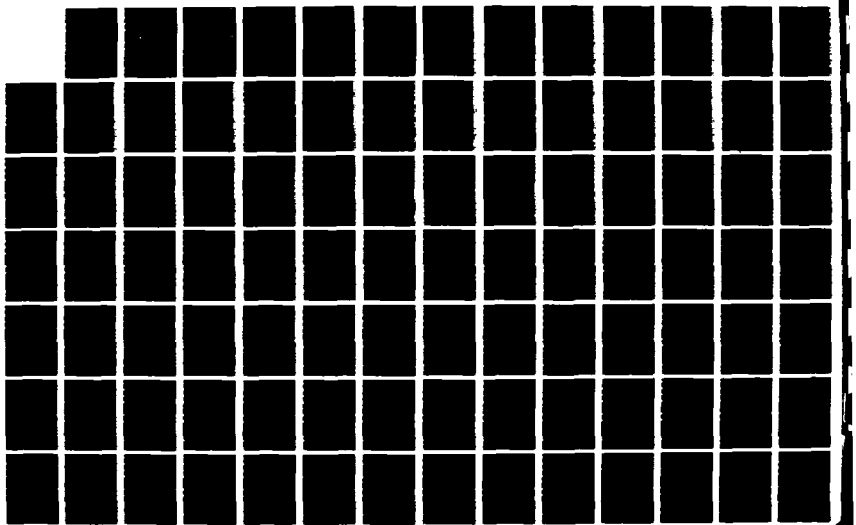

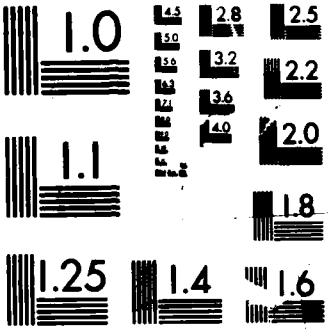

Unclassified
SECURITY CLASSIFICATION OF THIS PAGE

AD-A187 357

REPORT DOCUMENTATION PAGE

Form Approved OMB No. 0704-0188

1a. REPORT SECURITY CLASSIFICATION: Unclassified	1b. RESTRICTIVE MARKINGS
2a. SECURITY CLASSIFICATION AUTHORITY	3. DISTRIBUTION/AVAILABILITY OF REPORT: Approved for public release; distribution is unlimited.
2b. DECLASSIFICATION/DOWNGRADING SCHEDULE	
4. PERFORMING ORGANIZATION REPORT NUMBER(S): SSS-R-87-8454	5. MONITORING ORGANIZATION REPORT NUMBER(S): AFOSR-TR- 87-1391
6a. NAME OF PERFORMING ORGANIZATION: S-CUBED; 6b. OFFICE SYMBOL (If applicable):	7a. NAME OF MONITORING ORGANIZATION: AFOSR/NA
6c. ADDRESS (City, State, and ZIP Code): P O Box 1620, La Jolla, CA 92038	7b. ADDRESS (City, State, and ZIP Code): Building 410, Bolling AFB DC 20332-6448
8a. NAME OF FUNDING/SPONSORING ORGANIZATION: AFOSR/NA; 8b. OFFICE SYMBOL (If applicable): NA	9. PROCUREMENT INSTRUMENT IDENTIFICATION NUMBER: F49620 84-C-0029
8c. ADDRESS (City, State, and ZIP Code): Building 410, Bolling AFB DC 20332-6448	10. SOURCE OF FUNDING NUMBERS: PROGRAM ELEMENT NO. 61102F; PROJECT NO. 2302; TASK NO. C2; WORK UNIT ACCESSION NO.

11. TITLE (Include Security Classification): (U) Development of Advanced Constitutive Models for Plain and Reinforced ~~Concr~~ Concrete

12. PERSONAL AUTHOR(S): G A Hegemier, H E Read, K C valanis, H Murakami

13a. TYPE OF REPORT	13b. TIME COVERED	14. DATE OF REPORT (Year, Month, Day)	15. PAGE COUNT
Annual	FROM 1Mar86 TO 28 Feb87	1987 ~~August 31~~ March	268

16. SUPPLEMENTARY NOTATION

17. COSATI CODES		
FIELD	GROUP	SUB-GROUP

18. SUBJECT TERMS (Continue on reverse if necessary and identify by block number): Concrete Failure Models; Continuous Damage Model; Dowel Action; ~~Evaluation Equation;~~ Endochronic Theory; ~~Mixture Theory;~~ Reinforced Concrete.

19. ABSTRACT (Continue on reverse if necessary and identify by block number)

This report summarizes research conducted by S-Cubed to develop advance constitutive models of plain and reinforced concrete for ultimate use in the cost-effective design and hardness assessmnet of concrete protective structur The specific goals of the research are: (1) development of a mixtu theory which can accurately account for steel-concrete interaction and (2) formulati of an advanced constitutive theory for plain concrete which can accurately portray its nonlinear, inelastic behavior including damage and microcracking for arbitrary loading histories. The importance of the steel-concrete interaction and the nonlinear inelastic behavior of the palin concrete, including cracking, is emphasized. Keywords:

20. DISTRIBUTION/AVAILABILITY OF ABSTRACT	21. ABSTRACT SECURITY CLASSIFICATION
☒ UNCLASSIFIED/UNLIMITED ☒ SAME AS RPT ☐ DTIC USERS	Unclassified
22a. NAME OF RESPONSIBLE INDIVIDUAL: Spencer T Wu	22b. TELEPHONE (Include Area Code): (202) 767-4935; 22c. OFFICE SYMBOL: AFOSR/NA

DD Form 1473, JUN 86 — Previous editions are obsolete. — SECURITY CLASSIFICATION OF THIS PAGE

87 8

Unclassified

S-CUBED
A Division of Maxwell Laboratories, Inc.

AFOSR-TR- 87-1391
SSS-R-87-8454

DEVELOPMENT OF ADVANCED CONSTITUTIVE MODELS FOR PLAIN AND REINFORCED CONCRETE

G. A. Hegemier
H. E. Read
K. C. Valanis
H. Murakami

ANNUAL REPORT

Submitted to:

Air Force Office of Scientific Research
Bolling AFB
Washington, DC 20332

March, 1987

P. O. Box 1620, La Jolla, California 92038-1620
(619) 453-0060

S-CUBED
A Division of Maxwell Laboratories, Inc.

SSS-R-87-8454

DEVELOPMENT OF ADVANCED CONSTITUTIVE MODELS FOR PLAIN AND REINFORCED CONCRETE

G. A. Hegemier
H. E. Read
K. C. Valanis
H. Murakami

ANNUAL REPORT

Submitted to:

Air Force Office of Scientific Research
Bolling AFB
Washington, DC 20332

March, 1987

P. O. Box 1620, La Jolla, California 92038-1620
(619) 453-0060

ABSTRACT

This report summarizes research conducted by S-CUBED to develop advanced constitutive models of plain and reinforced concrete for ultimate use in the cost-effective design and hardness assessment of concrete protective structures. The specific goals of the research are two-fold; namely, (1) development of a mixture theory which can accurately account for steel-concrete interaction and (2) formulation of an advanced constitutive theory for plain concrete which can accurately portray its nonlinear, inelastic behavior, including developing damage and macrocracking, for arbitrary loading histories. The importance of the steel-concrete interaction and the nonlinear inelastic behavior of the plain concrete, including cracking, is emphasized. The progress made toward achieving these goals is described.

FOREWORD

This final report summarizes the research performed by S-CUBED under AFOSR Contract F49620-84-C-0029 during the period from March 1, 1984 to February 28, 1987. Partial support for portions of the research was provided by the Defense Nuclear Agency under Contract DNA001-84-C-0127. The Co-Principal Investigators for the project were Dr. G. A. Hegemier and Dr. H. E. Read. The AFOSR Contract Technical Monitors were, initially, Lt. Col. L. D. Hokanson and, later on, Dr. Spencer T. Wu.

Drs. Hegemier and Murakami, consultants to S-CUBED, are also, respectively, Professor and Associate Professor of Applied Mechanics at the University of California, San Diego. Dr. Valanis, an S-CUBED Consultant, is on leave from his position as Professor of Mechanics at the University of Cincinnati, Cincinnati, Ohio.

The authors express their appreciation to Dr. D. H. Brownell and Mr. R. G. Herrmann, who provided excellent computational support throughout the course of the research.

TABLE OF CONTENTS

TABLE OF CONTENTS (Continued)

TABLE OF CONTENTS (Continued)

TABLE OF CONTENTS (Concluded)

LIST OF ILLUSTRATIONS

LIST OF ILLUSTRATIONS (Continued)

LIST OF ILLUSTRATIONS (Continued)

LIST OF ILLUSTRATIONS (Continued)

LIST OF ILLUSTRATIONS (Continued)

LIST OF ILLUSTRATIONS (Concluded)

Section 1

INTRODUCTION

1.1 BACKGROUND.

The Air Force has, for some time now, had a major interest in reinforced concrete protective structures, which ranges from missile silos -- to buried facilities for personnel and equipment -- to above ground shelters for tactical aircraft. For example, during the past several years, the Air Force has been deeply involved in an extensive effort to develop and assess the feasibility and relative effectiveness of various candidate modes for basing the MX strategic weapons system. In most of these basing modes, the key elements are large reinforced concrete structures (protective structures) which are designed to protect a missile from the shock loads prescribed by the design attack scenarios. The enormous costs involved in constructing the large number of such structures required by the system dictates that their design be not only safe but cost-effective as well.

The current methods for designing protective structures are largely empirical, with heavy reliance upon engineering experience gained from the design of structures for prior defense systems, and insight obtained from the results of pertinent field tests conducted on small-scale structures. Full-scale testing of such structures under simulated explosive environments is extremely rare due to the enormous costs involved. Analytical simulations with finite element codes are often performed, but because of the crudeness of the material models for the plain and reinforced concrete used, little confidence is placed in the results so obtained, especially when nonlinear effects dominate the behavior. At best, relatively simple elasto-plastic models of plain concrete, normally developed from quasi-static, low pressure laboratory data, are combined with simple overlay approaches to account for the steel reinforcement. The resulting models of reinforced concrete are unable to properly account for the interaction that occurs between plain concrete and rebar during deformation. Inasmuch as such models are generally developed on the basis of quasi-static, low pressure data, they are not capable of describing the response of concrete to the high pressure, impulsive loading environments of interest. It is therefore not surprising that, at present, the collapse (failure) load of a missile silo cannot be analytically predicted to within a factor of 2. Clearly, there is a crucial need to understand how complex reinforced concrete structures fail under complex loads applied at high loading rates.

The inability of the current constitutive models to adequately describe the nonlinear behavior of plain and reinforced concrete is the main reason for the lack of confidence in numerical simulations of structural response. Without a valid numerical simulation capability, there is little hope of arriving at a cost-effective design. The inaccuracies associated with the current constitutive models of reinforced concrete stem from two main sources, namely, (1) inadequate models of plain concrete behavior, especially for high pressures and high rates of loading and (2) overly simplified methods used in mixing plain concrete and steel rebar to obtain a model of reinforced concrete. In both cases, the nature of the problem requires research at a fundamental level, since the basic technology is missing. Although extensive research has been conducted over the past fifty years on reinforced concrete, the emphasis has not been on the high pressure, dynamic response regime. Therefore, if methods are to be developed which can lead to cost-effective, reliable designs for concrete defense structures, improved modeling of the response of plain and reinforced concrete to high pressure loading environments is needed, as well as corresponding experiments to validate the modeling. This requires a significant advancement in current technology.

1.2 IMPORTANCE OF STEEL-CONCRETE INTERACTIONS.

Over the response regime of interest to the defense community, the behavior of reinforced concrete is dominated by complex nonlinear interactions between steel and concrete. In particular, it is well known that such interactions can have a major effect on global structural characteristics such as stiffness, strength, damping and ductility. In addition, steel-concrete interactions can have a primary influence on damage accumulation and failure modes.

To illustrate the above statement, consider the example of reinforced concrete in direct tension. Practical steel percentages (in the direction of loading) range from 3 percent ("dense" layout) to 0.5 percent ("sparse" layout). If one examines the unload-reload tangent modulus associated with the global stress and strain in the direction of loading, then one finds that the initial (uncracked concrete) modulus drops by approximately 65 percent for 3 percent steel, as damage in the form of progressive cracking and steel-concrete bond degradation, accumulates with increasing global deformation (extension). For 0.5 percent steel, this number becomes approximately 95 percent! For the global deformation domain of practical relevance, the initial modulus is too high for computational purposes and the asymptotic (steel only)

modulus is too low. The required modulus lies in the transitional region between the two extremes. However, behavior in this transitional domain can be predicted only if steel-concrete interactions are considered. For the example cited, the problem of predicting the appropriate stiffness is a classical problem known as "tension stiffening".

Thus, it is evident that a model of reinforced concrete must, in some sense, reflect steel-concrete interactions. In the past, practitioners have attempted to account for some of these interactions in an effort to fit test data by "adjusting" the constitutive relations of either the steel or the concrete (usually the latter). However, such an empirical approach requires a myriad of costly experiments -- costly since the specimen size must be "large" when compared to the typical steel spacing (material "microstructural" dimension), if a continuum description of reinforced concrete is to be used. In the final analysis, the empirical method does not furnish the simulation accuracy and capability that are needed for the proper treatment of current defense problems concerning the design and analysis of reinforced concrete protective structures.

1.3 OBJECTIVES.

The primary objective of the research described here is to construct an advanced, nonlinear, multiaxial constitutive model of reinforced concrete that will provide simulation accuracy in the nonlinear response regime that is superior to existing models. A secondary objective is to develop a rational method, based on physics, for accurately accounting for the effect of steel-concrete interactions on the overall response of reinforced concrete. A final objective is to develop an accurate constitutive model of plain concrete which is capable of describing its behavior over a wide range, from the onset of microcracking to the development of complete failure through macrocracking. These objectives are consistent with the technological/operational needs exemplified under subsection 1.1 above.

1.4 GENERAL METHODOLOGY.

An innovative methodology has been selected to achieve the primary objective of the research program. This methodology consists of synthesizing the global properties of reinforced concrete from knowledge of the plain concrete and steel properties, the concrete-steel interface properties, and the geometry of the steel reinforcement. Such

a non-phenomenological procedure offers the potential of maximum model simulation accuracy/capability via inclusion of the important physical phenomena, and minimizes the number and type of expensive tests necessary to define the model parameters.

A non-phenomenological reinforced concrete theory requires, as input, constitutive models for each of the basic constituents, namely, steel rebar and plain concrete. The accuracy of the resulting reinforced concrete theory depends heavily on the accuracy with which one can model these two constituents. The constitutive properties of steel are well known and can be adequately represented by reasonably simple elasto-plastic models. Plain concrete, on the other hand, is perhaps the most complex structural material in current use and, despite numerous efforts in recent years to mathematically model its properties, there is today still no model which can adequately describe its nonlinear constitutive properties over a wide range of behavior, including damage accumulation and post-cracking response. In addition, a non-phenomenological reinforced concrete theory requires constitutive descriptions of the steel-concrete interfaces, and a procedure for analytically *mixing* or *homogenizing* steel, concrete, and steel-concrete interfaces to furnish a global model of the composite.

As a result, the major challenges that one faces in attempting to develop an accurate constitutive theory for reinforced concrete are twofold, namely (1) development of an analytic mixing procedure (mixture theory) which accurately accounts for the interaction between the rebar and plain concrete, and (2) formulation of a constitutive theory for plain concrete which adequately describes its nonlinear, inelastic properties, including damage and cracking, for arbitrary, multi-axial load paths. Accordingly, these two major areas of research have been pursued in parallel, concurrent efforts under the present program.

1.5 PRESENT REPORT.

This final report describes the progress made during the contract period toward achieving the goals described above. The report has been prepared with the intention of providing the reader with a general overview of the research accomplishments, without becoming cumbersome with extensive detail. Those interested in pursuing the various topics in greater depth are referred to the publications that have resulted from this study (see Section 2) and to the appendices of this report where a number of topics that have not appeared in publication are discussed in detail.

Section 2

PUBLICATIONS AND INTERACTIONS

2.1 PUBLICATIONS.

The following is a cumulative list of the publications prepared by the contract staff members on the research conducted under the present AFOSR contract:

1. Read, H. E., and G. A. Hegemier, "Strain Softening of Rock, Soil and Concrete," *Mechanics of Materials*, Vol. 3, (1984), 271.

2. Hegemier, G. A., and H. E. Read, "Strain Softening", (Discussion), Theoretical Foundations for Large-Scale Computations for Nonlinear Material Behavior, edited by S. Nemat-Nasser, R. J. Asaro and G. A. Hegemier, Martinus Nijhoff, Publ. (1984).

3. Hegemier, G. A., H. Murakami, and L. J. Hageman, "On Tension Stiffening in Reinforced Concrete," *Mechanics of Materials*, 4 (2), (1984).

4. Hegemier, G. A., and H. Murakami, "A Nonlinear Theory for Reinforced Concrete," *Proc. Second Symp. on the Interaction of Non-Nuclear Munitions with Structures*, Panama City, FLA (1985).

5. Hegemier, G. A., and H. E. Read, "On Deformation and Failure of Brittle Solids: Some Outstanding Issues," *Mechanics of Materials*, Vol. 4 (3), (1985), 215.

6. Read, H. E., Discussion of "Hysteretic Endochronic Theory for Sand" by Z. P. Bazant, R. J. Krizek and C.-L. Shieh, *J. Engr. Mechanics, ASCE*, Vol. 111(1) (1985), 103.

7. Read, H. E., "Strain Rate Effects in Concrete: A Review of Experimental Methods," S-CUBED, Topical Report SSS-R-85-6081 (1985).

8. Valanis, K. C., and H. E. Read, "An Endochronic Plasticity Theory for Concrete," *Proc. Second Symp. on the Interaction of Non-Nuclear Munitions with Structures*, Panama City Beach, FLA., April 1985.

9. Hegemier, G. A., H. E. Read, K. C. Valanis and H. Murakami, "Development of Advanced Constitutive Models for Plain and Reinforced Concrete," S-CUBED, La Jolla, California, First Annual Report, SSS-R-85-7150 April, 1985.

10. Hageman, L. J., H. Murakami and G. A. Hegemier, "On Simulating Steel-Concrete Interaction in Reinforced Concrete, Part II: Validation Studies," *Mechanics of Materials*, Vol. 5, (1986), 187.

11. Hegemier, G. A., and H. Murakami, "On Simulating the Nonlinear Planar Hysteretic Response of Reinforced Concrete and Concrete Masonry," Third ASCE EMD Specialty Conference on Dynamics of Structures, UCLA, Los Angeles, March 31 - April 2, 1986.

12. Murakami, H., and G. A. Hegemier, "On Simulating Steel-Concrete Interaction in Reinforced Concrete. Part I: Theoretical Development," *Mechanics of Materials*, Vol. 5, (1986), 171.

13. Murakami, H., and G. A. Hegemier, "A Nonlinear Dowel Action Model," submitted to *Int. J. Solids Structs.*, (1986).

14. Hegemier, G. A., H. E. Read, K. C. Valanis and H. Murakami, "Development of Constitutive Models for Plain and Reinforced Concrete," S-CUBED, La Jolla, California, Second Annual Report, SSS-R-86-7914, April, 1985.

15. Murakami, H., and H. E. Read, "Endochronic Plasticity: Some Basic Properties of Plastic FLow and Failure," *Intl. J. Solids and Structures*, Vol. 23, (1987), 133.

16. Valanis, K. C., and H. E. Read, "An Endochronic Plasticity Theory for Concrete," *Mechanics of Materials*, Vol. 5(3), (1986), 277.

17. Hegemier, G. A., H. E. Read, K. C. Valanis and H. Murakami, "On the Synthesis of Response and Damage in Reinforced Concrete," *Proceedings of the AFOSR Workshop on the Performance of Concrete and Cement Materials*, Wright-Patterson AFB, Ohio, October 9-10, 1986.

18. Valanis, K. C., "Endochronic Theory of Soils and Concrete," Proc. 2nd Intl. Confr. and Short Course on Constitutive Laws for Engineering Matls: Theory and Application," The University of Arizona, Tucson, Arizona, January 5-10, 1987.

2.2 INTERACTIONS.

The following is a cumulative list of the interactions (coupling activities) by the contract staff members which have occurred during the course of this contract on research done under the contract:

1. Murakami, H., "Some Basic Inelastic Response Features of the New Endochronic Theory," Oral presentation at the 21st Annual Meeting of the Soc. Engrg. Sci., VPI, Blacksburg, VA, October 15, 1984.

2. Hegemier, G. A., "On Deformation and Flow of Brittle Solids," General Lecture presented at the Workshop on Inelastic Deformation and Failure Modes, Northwestern University, Evanston, Illinois, November 18-21, 1984.

3. Valanis, K. C., "An Endochronic Plasticity Theory for Concrete," Oral presentation at the Workshop on Inelastic Deformation and Failure Modes," Northwestern University, Evanston, Illinois, November 18-21, 1984.

4. Read, H. E., "Inelastic Response Characteristics of the New Endochronic Theory with Singular Kernel," Oral presentation at the Workshop on Inelastic Deformation and Failure Modes, Northwestern University, Evanston, Illinois, November 18-21, 1984.

5. Read, H. E., "On Modeling the Dynamic Behavior of Plain Concrete," Oral presentation at DNA Concrete Material Properties Meeting, Terra Tek, Salt Lake City, Utah, March 7, 1984.

6. Hegemier, G. A., "Development of an Advanced Constitutive Model for Reinforced Concrete," Oral presentation at DNA Concrete Material Properties Meeting, Terra Tek, Salt Lake City, Utah, March 7, 1984.

7. Read, H. E., "An Endochronic Plasticity Theory for Concrete," Oral presentation at the 2nd Symp. on the Interaction of Non-Nuclear Munitions with Structures, Panama City, FLA, April 1985.

8. Hegemier, G. A., "A Nonlinear Theory for Reinforced Concrete," Oral presentation at the 2nd. Symp. on the Interaction of Non-Nuclear Munitions with Structures, Panama City, FLA, April 1985.

9. Read, H. E., and G. A. Hegemier, "Some Outstanding Issues Pertaining to the Modeling of Plain and Reinforced Concretes," Oral presentation at the DNA Concrete Material Properties Meeting, Terra Tek, Salt Lake City, Utah, April 3, 1985.

10. Hegemier, G. A., "A Nonlinear Model of Reinforced Concrete," Oral presentation at the U.S.-Japan Cooperative Conference on Earthquake Engineering, Tokyo, Japan, Aug. 1985.

11. Read, H. E., and G. A. Hegemier, "Development of Advanced Constitutive Theories for Plain and Reinforced Concrete," Oral presentation at the Air Force Weapons Laboratory, Civil Engineering Research Seminar, Albuquerque, New Mexico, Sept. 1985.

12. Hegemier, G. A., and H. Murakami, "On Simulating the Nonlinear Planar Hysteretic Response of Reinforced Concrete and Concrete Masonry," 3rd ASCE EMD Specialty Conference on Dynamics of Structures, UCLA, Los Angeles, March 31 -April 2, 1986.

13. Read, H. E., and G. A. Hegemier, "Advanced Methods for Modeling Plain and Reinforced Concretes," Oral presentation at the DNA Concrete Material Properties Meeting, Stanford Research Institute, Menlo Park, California, April 22, 1986.

14. Valanis, K. C., and H. E. Read, "Endochronic Plasticity: Application to Plain Concrete," Oral presentation at the 10th U.S. National Congress of Applied Mechanics, University of Texas, Austin, Texas, June 1986.

15. Murakami, H., "Basic Flow Properties of Endochronic Plasticity," Oral presentation at the 10th U.S. National Congress of Applied Mechanics, University of Texas, Austin, Texas, June 1986.

16. Hegemier, G. A., "On the Synthesis of Response and Damage in Reinforced Concrete," Oral presentation at the AFOSR Workshop on the Performance of Concrete and Cement Materials, Wright-Patterson AFB, Ohio, October 9-10, 1986.

17. Valanis, K. C., "Endochronic Theory of Soils and Concrete." Oral presentation at 2nd Intl. Confr. and Short Course on Constitutive Laws for Engineering Materials: Theory and Application," University of Arizona, Tucson, Arizona, January 5-10, 1987.

Section 3

REINFORCED CONCRETE

This section presents the results of research conducted on the theoretical description of reinforced concrete. The discussion covers objectives, general methodology, mathematical forms, and validation problems which are intended to demonstrate the capability and accuracy of the modeling procedure.

3.1 BASIC OBJECTIVES.

The nonlinear global response of reinforced concrete protective structures to intense dynamic loads in dominated by two fundamental phenomena: (1) the behavior of the plain concrete under high strain rates and complex multiaxial stress states; and (2) interactions between the reinforcing steel and the concrete. This section is concerned with steel-concrete interaction.

It is generally recognized that steel-concrete interaction (SCI) can have a dramatic influence on the nonlinear response of a reinforced concrete (R/C) structure. In particular, important response characteristics such as global stiffness, ductility, damage type and evolution, and failure modes/conditions are strong functions of SCI.

In view of the importance of SCI and the current lack of adequate SCI descriptions in operational R/C computer codes, the present research program was undertaken to address this need. One of the basic objectives of this project was to construct an advanced model of R/C that properly reflects SCI.

3.2 ACCOMPLISHMENTS.

A fundamentally new mathematical framework for describing the nonlinear response of reinforced concrete has been constructed and validated against a suite of experimental data. This framework is nonphenomenological on the macroscale in the sense that the global properties of reinforced concrete are synthesized from the properties and geometries of the components (steel and concrete) and component interfaces. Such a model, while far more difficult to construct than a phenomenological model, offers the possibility of increased simulation capability and accuracy with a minimum number of experiments necessary to evaluate material parameters.

The foregoing modeling effort has proceeded in a sequence of stages that represents increasing levels of generality. While this sequence is not yet complete, the

success of the validations performed to-date point to a significant breakthrough in the theoretical description of SCI.

3.3 METHODOLOGY.

As was noted previously, the nonphenomenological approach implies that a model is to be constructed by synthesizing the global properties of R/C from the properties and geometries of the basic components of the "composite", i.e., steel, concrete, interfaces, and cracks. Mathematically, this problem falls into the general category of "homogenization." The term, as used here, implies construction of a "macro" model via "micromechanical" considerations together with appropriate smoothing or averaging operations.

As use of the prefixes "micro" and "macro" above imply, homogenization typically enters the picture when one wishes to determine the response of a continuum for which two widely different length scales can be identified. The large or "macroscale" is determined by the specimen geometry and/or the loading condition. The small or "microscale" is determined by material heterogeneity. In the case of reinforced concrete, the typical steel spacing constitutes the appropriate microscale.

The homogenization problem is parameterized by the small ratio of the above two length scales, ϵ. The fundamental problem is to determine the "proper" macroscopic response equations as $\epsilon \to 0$. Once obtained, it is natural to introduce asymptotic notions into the analysis to determine a physically meaningful sequence of equations ordered in powers of ϵ. The higher order equations are intended to provide additional simulation capability on the macroscale.

Using homogenization concepts, nonlinear R/C model frameworks have been constructed for both "dense" and "sparse" unidirectional steel layouts. Typical such layouts are depicted in Figures 3.1(a,b). The construction technique is based on the use of multivariable (two-space) asymptotic expansions, a variational principle, and certain smoothing operations. The resulting models have been cast in the form of a binary mixture which resembles an overlay of two continua: steel and concrete. The continua interact via body forces which are functionals of the relative global displacements of the continua. Mathematical descriptions of the model and the construction procedure can be found in Murakami and Hegemier (1986), Hegemier, Murakami, and Hageman (1985), Hegemier and Murakami (1985). Comprehensive

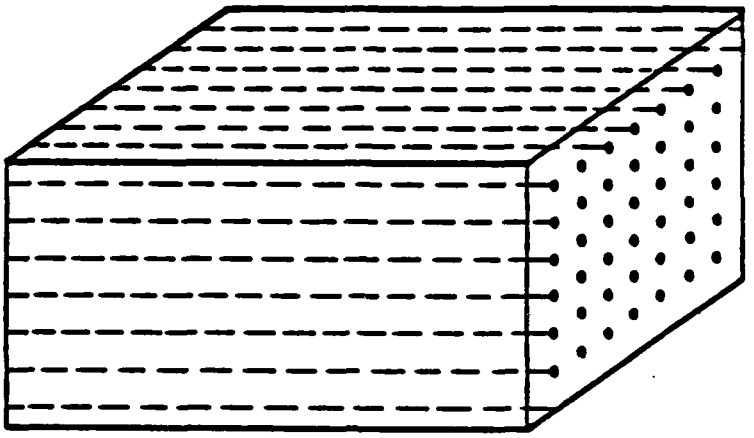

(a) Rectilinear

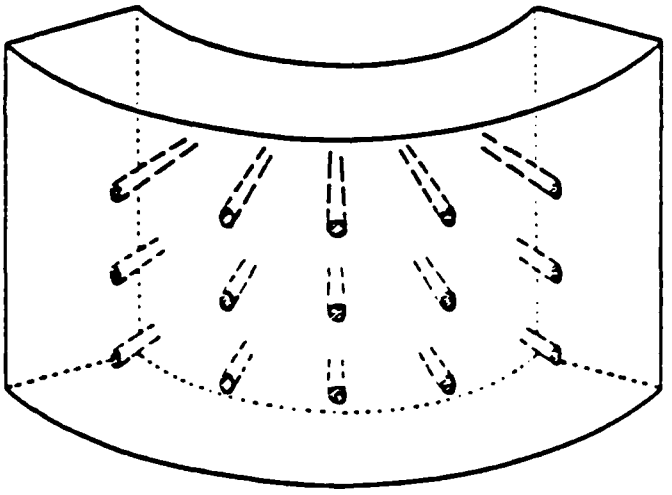

(b) Curvilinear

Figure 3.1. Unidirectional dense steel arrays.

treatment of the model construction problem is furnished collectively by Appendices C - I.

3.4 REMARKS ON MIXTURE FRAMEWORK.

It was noted previously that the new R/C model has been cast in the form of a "mixture." Some clarification concerning mixture descriptions are presented below.

Both phenomenological and nonphenomenological continuum models of R/C have features that resemble a binary mixture. This mixture assumes the form of a two-phase medium with various types of constraints.

Currently operational computer programs for the analysis of R/C structures are typically based on phenomenological models which require, as a constraint, the deformation gradient or strain tensor of the steel and concrete to be the same at spatial points where they are overlayed or "smeared." In what follows, such a description will be denoted as an "elementary" mixture.

At the other end of the spectrum are mixtures which allow relative deformation of the components, i.e., they exhibit distinct strain fields. Further, these models incorporate steel-concrete interface physics. Such descriptions will be denoted "advanced" mixtures.

For the purpose of demonstrating the difference between advanced and elementary mixture descriptions, consider the case of a unidirectionally reinforced specimen subject to global uniaxial tension, Figure 3.2. Within the context of a quasi-one-dimensional discussion, an advanced mixture would have the form:

(a) Equilibrium equations,

$$n^{(1)}\sigma^{(1)}_{11,1} + P_1 = 0 \quad , \quad n^{(2)}\sigma^{(2)}_{11,1} - P_1 = 0 \quad . \tag{3-1}$$

(b) Component constitutive relations,

$$\dot{\sigma}^{(1)}_{11} = E^{(1)}\dot{U}^{(1)}_{1,1} + C^{(1)}\dot{U}^{(2)}_{1,1} \quad , \quad \dot{\sigma}^{(2)}_{11} = E^{(2)}\dot{U}^{(2)}_{1,1} + C^{(2)}\dot{U}^{(1)}_{1,1} \tag{3-2}$$

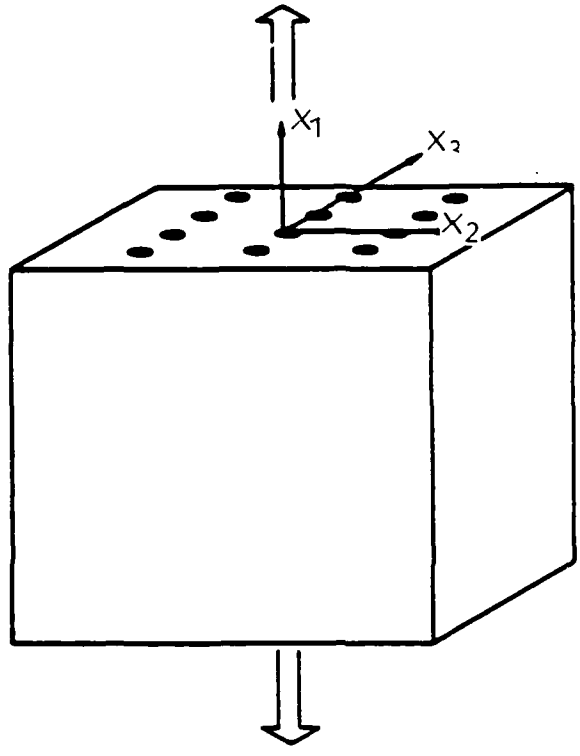

Figure 3.2. Global uniaxial loading.

(c) Interface constitutive relation

$$P_1 = F([[U_1]]) \ , \quad [U_1] \equiv U_1^{(2)} - U_1^{(1)} . \tag{3-3}$$

Here σ_{11}, U_1 denote averaged (over a typical "cell" containing an element of steel and a representative concrete cover) axial stress, displacement; E, C, are tangent moduli, $n^{(1)}$ and $n^{(2)}$ are volume fractions; superscripts 1 and 2 refer to steel and concrete, respectively; and P_1 represents an interaction term which is related to an effective steel-concrete interface shear stress $\tau^* \equiv \sigma^*_{rx}$ according to:

$$P_1 = 2\tau^*/r^{(1)} \tag{3-4}$$

where $r^{(1)}$ is the steel radius and the superscript "*" denotes "interface." The notation F in (3-3) implies a functional. Equations (3-1) - (3-3) resemble an overlay of two materials (steel and concrete) which interact via a "body force" P_1. These equations involve four field variables: $\sigma_{11}^{(\alpha)}$ and $U_1^{(\alpha)}$, $\alpha = 1,2$.

A conventional description , or elementary mixture, can be obtained from the foregoing relations by imposing the constraint: $U_1^{(1)} = U_2^{(2)} \equiv U_1$. Thus, the displacements and hence the strains in each material are identical. The governing equations then reduce to:

(a) Equilibrium

$$\sigma_{11,1} = 0 \ , \ \sigma \equiv n^{(1)}\sigma_{11}^{(1)} + n^{(2)}\sigma_{11}^{(2)} \tag{3-5}$$

(b) Constitutive

$$\dot{\sigma}_{11} = [n^{(1)}\bar{E}^{(1)} + n^{(2)}\bar{E}^{(2)}]\dot{U}_{1,1} \ , \ \bar{E} \equiv E + C \ . \tag{3-6}$$

The field now involves only two variables: σ_{11} and U_1. The component stresses can be recovered from:

$$\dot{\sigma}_{11}^{(1)} = \bar{E}^{(1)}\dot{U}_{1,1} \ , \ \dot{\sigma}_{11}^{(2)} = \bar{E}^{(2)}\dot{U}_{1,1} \ . \tag{3-7}$$

Elementary and advanced mixtures generally exhibit drastically different simulation features and capabilities. For example, if the concrete is modeled as elastic-brittle fracture, and the steel as elastic, then the elementary model in extension predicts a constant tangent modulus, E_t, Figure 3-3(a), or at best, a piecewise constant tangent modulus (drop occurs when tensile failure strain of concrete is reached), Figure 3-3(b). Here $E_t \equiv \sigma/e$ where $e \equiv U_{1,1}$.

In contrast, the advanced mixture model is capable of exhibiting realistic behavior as depicted in Figure 3-3(c). Corresponding differences in the global stress-strain response are shown schematically in Figure 3-4 for elastic-perfectly plastic rebar. Note that, in contrast to the elementary model, the advanced mixture simulates both stiffness degradation and hysteresis. The interaction term P_1 and its functional dependence on $[U_1]$ is responsible for both phenomena. [In Figure 3-4(c), e is now defined as $\Delta\ell/\ell_o$ where ℓ_o = initial steel specimen length and $E_t \equiv (n^{(1)}\sigma_{11}^{(1)} + n^{(2)}\sigma_{11}^{(2)})/e$.]

In addition to the obvious differences in global response features between elementary and advanced mixtures, there is a difference of a fundamental nature which concerns the prediction of failure. As was noted previously, the elementary mixture assumes the same strains in the steel and concrete at a spatial point. The advanced mixture, on the other hand, allows distinct strain fields. In the former case, failure is predicted when the global extensional strain e reaches the rebar failure strain, $e_f^{(1)}$. In the latter case (i.e., with use of the advanced mixture) the global and local strains can differ significantly, Figure 3-5. Here one finds that failure depends not only on the value of the global strain, but also on the rebar geometry, the steel-concrete bond characteristics, and the rebar hardening properties. An example of this situation is given by Figure 3-6. [In Figure 3-6, D_s = rebar diameter, ℓ = crack spacing, $e_f^{(s)} \equiv e_f^{(1)}$ = rebar failure strain, $\sigma_f^{(s)}$ = ultimate rebar stress, $\sigma_y^{(s)}$ = initial rebar yield stress.] Generally, the elementary mixture will predict extensional failure strains considerably in excess of actual values; hence ductility predictions will be nonconservative. On the other hand, an advanced mixture can simulate failure conditions with reasonable accuracy.

3.5 THEORETICAL STUDIES.

The primary theoretical development involves a number of key steps; these include: (1) a judicious scaling of the problem variables; (2) introduction of multiple

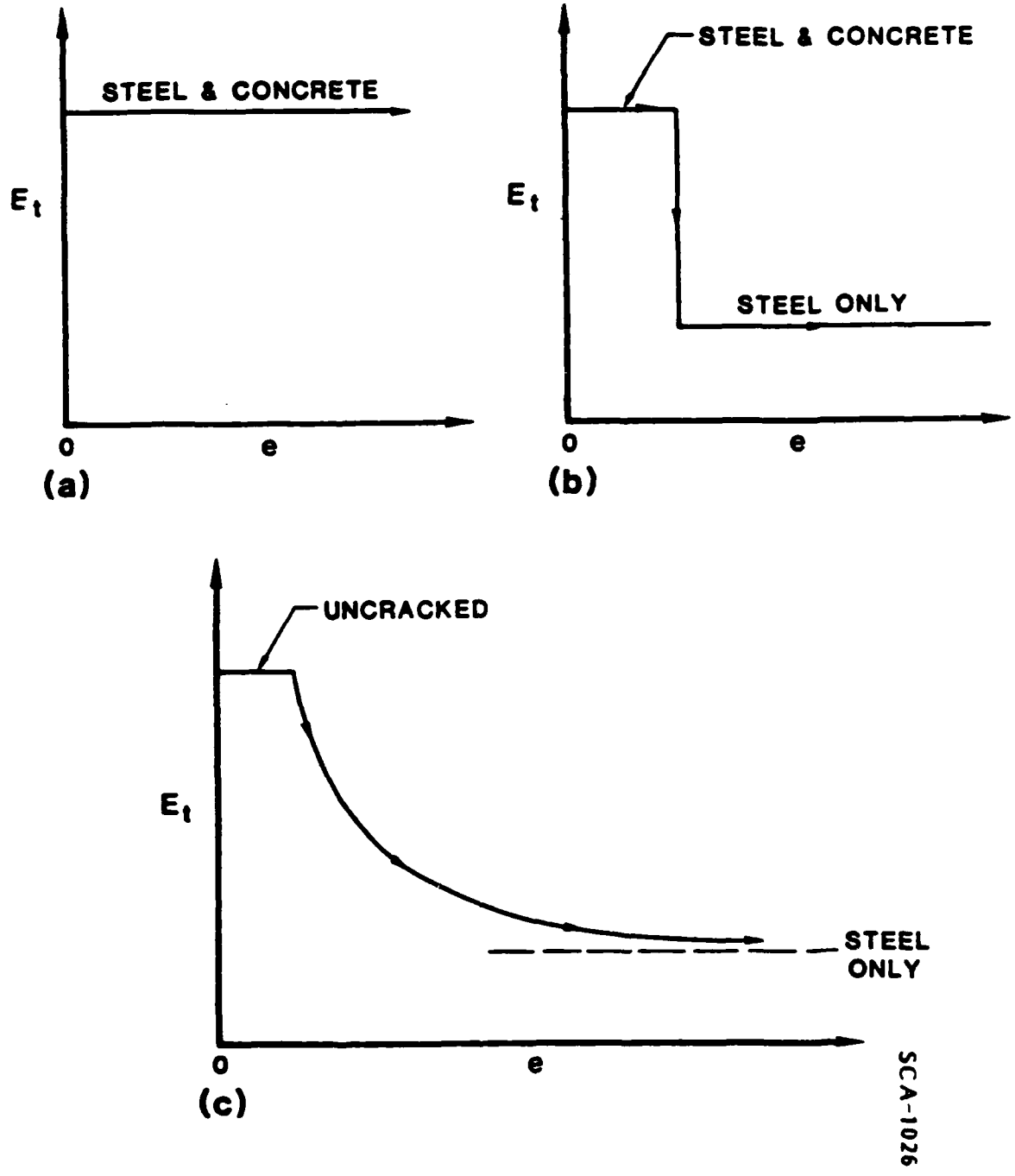

Figure 3.3. Comparison of elementary and advanced mixture models.

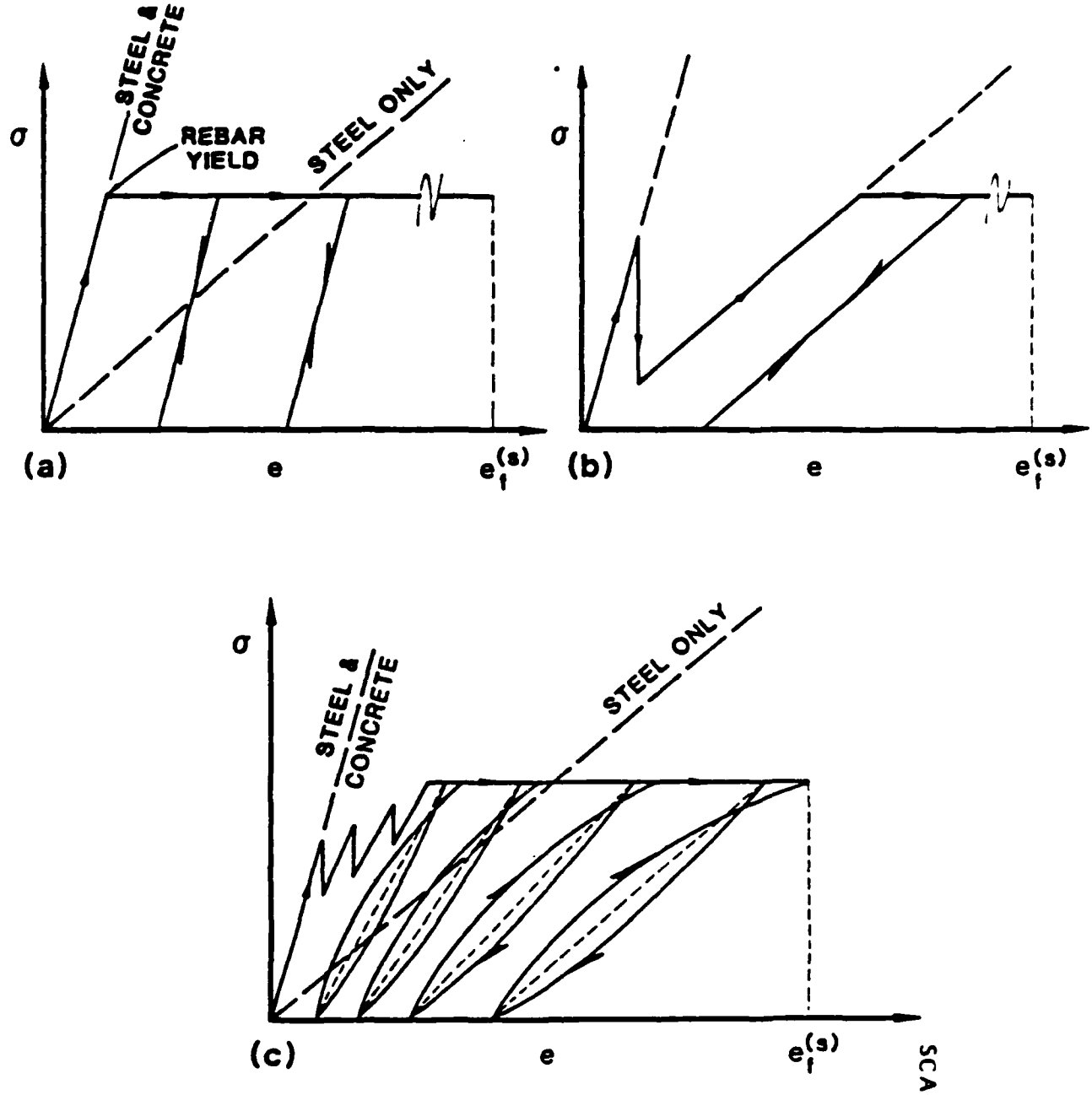

Figure 3.4. Global stress-strain responses.

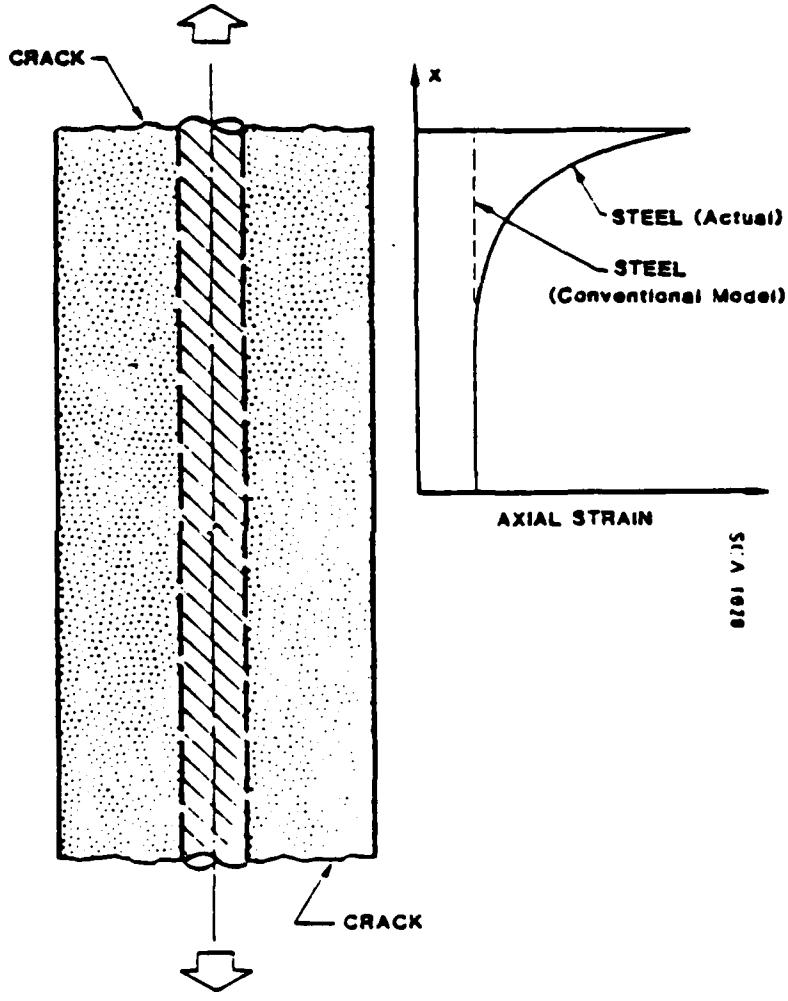

Figure 3.5. Comparison of predicted steel strains.

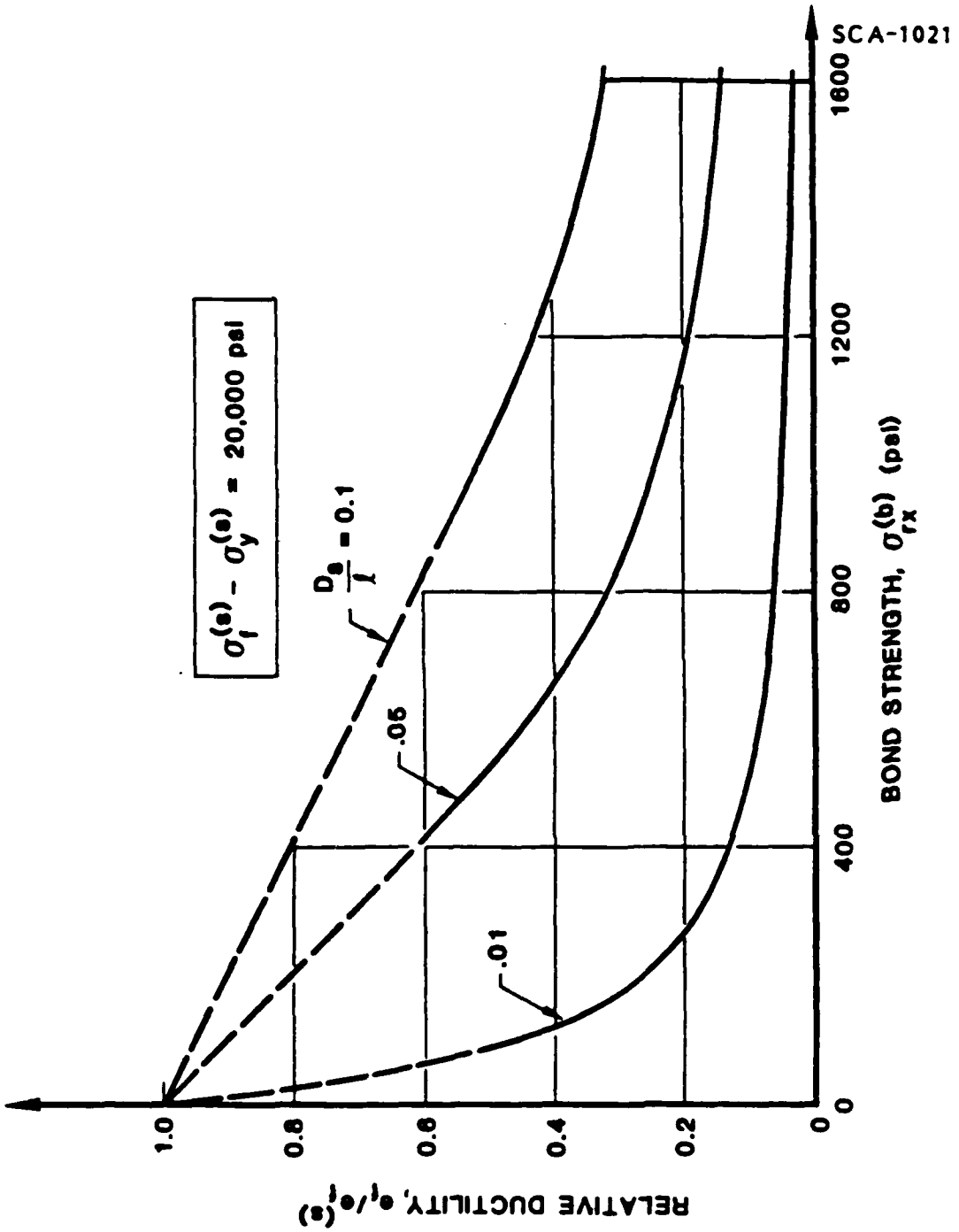

Figure 3.6. Ductility of a R/C element.

scales (coordinates) which include one set of "macrocoordinates" and another set of "microcoordinates," and representation of all field variables by a two-space asymptotic method; (3) introduction of a local periodicity condition; (4) derivation and application of a variational principle; and (5) conduct of an asymptotic analysis to ascertain appropriate test (trial) functions for the variational principle. Complete details concerning the theoretical construction process are furnished in Appendices C - I.

To-date, several mixture formulations have been derived and explored. The various models differ in their form and completeness. The form differences are a consequence of the particular variational principle used and the associated trial functions employed, as well as the description (i.e., Eulerian, Lagrangian, up-dated Lagrangian, etc.). A brief description of these efforts follows.

3.5.1 Description of Main Theoretical Efforts.

(1) Direct Variational Method -- A very general set of mixture equations has been generated using a "direct" variational principle in which only displacements are varied. This work is described in detail in Appendix C. The resulting model includes large deformations and nonlinear material and interface behavior. The latter are assumed in an incrementally linear form which includes a large class of elastoplastic and elastoplastic-brittle fracture relations. The theoretical construction process has been performed for both dense and sparse steel layouts. These layouts are assumed to be unidirectional. They may, however, be curvilinear.

(2) Mixed Variational Method -- The use of a direct variational scheme in which only the displacement field is varied is theoretically convenient from the point of a model construction process, but has several inherent drawbacks. For example, the displacement and stress microfields do not exhibit the same order of accuracy. Also,. the governing relations for the interaction terms do not evolve naturally from the development. In addition, the partial differential equations that result from a direct method tend to be too "stiff" in some applications. In an effort to improve this situation, the use of a "mixed" variational principle was explored with considerable success. This work is described in detail in Appendices D - G. In Appendix D, the basic mixed variational principle is established. In Appendix E, a mixture model is established for a dense, unidirectional steel layout for 3-D deformations. In Appendix F, a mixture model is developed for R/C plates with unidirectional steel layouts. This work is further specialized to a R/C rod in Appendix H; the latter model is necessary

to properly interpolate certain laboratory test data. The foregoing models include nonlinear material and interface behavior; however the treatments are restricted to small global or macro deformations.

(3) Oblique Steel Layouts -- The models developed under (1) and (2) above are applicable to general global (macro) coordinate systems. However, considerable care must be exercised in this connection since (a) there are two coordinate systems associated with the analysis: macro and micro, and (b) the microcoordinates must be aligned with the steel layout; hence the microcoordinate system is a material system. Specific equations applicable to general global coordinate systems are developed in Appendix G.

(4) Large Microrotations -- Some problems require the inclusion of large rotations of the steel on the microcoordinate level even though the global deformations may be small. An example of such a problem concerns the transfer of global shear stress across a crack when rebar penetrates the crack surface. For the purpose of exploring problems of this type, a special nonlinear theory was developed for which small deformations are imposed on the macroscale, but moderate rotations of steel elements are allowed. This work is described in detail in Appendix I.

3.5.2 Theoretical Approach.

An extremely brief sketch of the theoretical approach is provided next. The reader is referred to Appendix C for complete details.

Consider a uniaxial steel layout with a (initial) local periodic array occupying a volume $\bar{V}_o$ with boundary $\partial\bar{V}_o$ in the initial configuration as illustrated in Figure 3-7. In the current configuration the corresponding volume and surface will be denoted as $\bar{V}$ and $\partial\bar{V}$, respectively. Let the conservation and constitutive relations for each material (steel and concrete) be denoted collectively by

$$\underset{\sim}{\mathcal{Z}}^{\alpha}\left[\bar{\underset{\sim}{f}}^{(\alpha)}\left(\bar{\underset{\sim}{x}},\bar{t}\right)\right] = 0 \quad (\alpha = 1,2) \ , \tag{3-8}$$

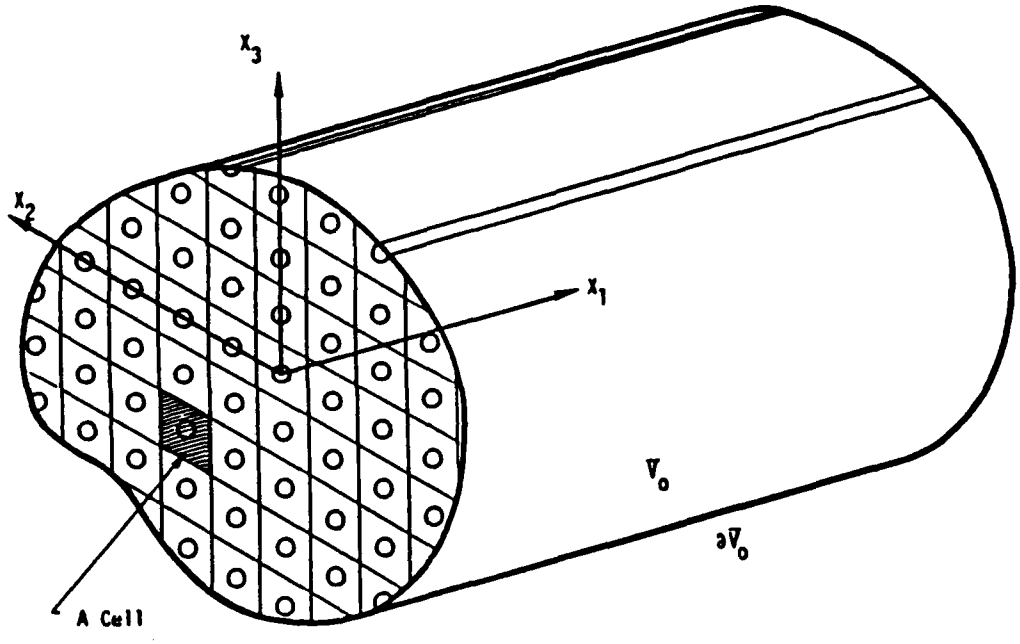

Figure 3.7. Densely reinforced concrete; initial configuration.

where $\alpha = 1,2$ refer to steel, concrete respectively (no sum on α); $\bar{\underset{\sim}{x}}$, $\bar{t}$ denote the position vector, time respectively; $\underset{\sim}{f}^{(\alpha)}$ is the collection of all field variables; and $\underset{\sim}{\mathscr{L}}$ is a nonlinear operator. The form (3-8) represents a system of equations.

It is essential to, at the outset, nondimensionalize (scale) the basic equations (3-8). For this purpose, two fundamental scales are introduced: $\bar{\Lambda}$ and $\bar{\Delta}$. Here $\bar{\Lambda}$ is a typical macrosignal wavelength, and $\bar{\Delta}$ represents the typical steel spacing. With the aid of these quantities, the field equations are scaled, and new independent variables are introduced according to $\underset{\sim}{x} = \bar{\underset{\sim}{x}}/\bar{\Lambda}$, $t = \bar{t}/\bar{t}_{(m)}$ where $\bar{t}_{(m)}$ is a typical macrosignal travel time. In terms of the nondimensional variables, the field equations assume the form

$$\underset{\sim}{\mathscr{L}}^{(\alpha)}\left[\underset{\sim}{f}^{(\alpha)}(\underset{\sim}{x},t;\epsilon)\right] = 0 \quad . \tag{3-9}$$

The quantity $\epsilon \equiv \bar{\Delta}/\bar{\Lambda}$ in (3-9) is the ratio of micro-to-macro dimensions of the problem.

Next, the concepts of microcoordinates and two-space asymptotic representations of all field variables is introduced. This proceeds as follows: It is expected that stress and deformation will vary significantly with respect to two basic length scales: (1) a "global" or "macro" length typical of the body size or loading condition and (2) a "micro" length typical of a "cell" planar dimension as depicted in Figure 3.8. These macro- and micro-dimensions will be associated with the variables $\bar{\Lambda}$, $\bar{\Delta}$ respectively. Further, it is expected that these scales will differ by at least one order of magnitude in most cases. Thus, $\epsilon << 1$. This suggests the use of multivariable asymptotic techniques, Hegemier, *et al.* (1979). This approach commences by introducing new independent variables according to

$$\begin{aligned} &\underset{\sim}{x}^{*} = \phi^{-1}(\epsilon)\underset{\sim}{x} \quad , \quad \phi(\epsilon) \to 0 \text{ as } \epsilon \to 0 \ , \\ &\tilde{\underset{\sim}{x}} = \psi(\epsilon)\underset{\sim}{x} \quad , \quad \psi(\epsilon) \to 1 \text{ as } \epsilon \to 0. \end{aligned} \tag{3-10}$$

For the present problem, it will suffice to set

$$\phi(\epsilon) = \epsilon \ , \ \psi(\epsilon) = 1 \ . \tag{3-11}$$

Thus, all field variables are now assumed to be functions of the "microcoordinates" $\underset{\sim}{x}^*$ as well as the "macrocoordinates" $\underset{\sim}{\tilde{x}} \equiv \underset{\sim}{x}$, i.e.,

$$\underset{\sim}{f}(\underset{\sim}{x},t) = \underset{\sim}{F}(\underset{\sim}{x},t;\underset{\sim}{x}^*;\epsilon) \quad . \tag{3-12}$$

Spatial derivatives of a function $\underset{\sim}{f}(\underset{\sim}{x},t)$ then take the form

$$\underset{\sim}{\nabla} \underset{\sim}{f} = \underset{\sim}{\nabla} \underset{\sim}{F} + \epsilon^{-1} \underset{\sim}{\nabla}^* \underset{\sim}{F} \tag{3-13}$$

where $\underset{\sim}{\nabla}$, $\underset{\sim}{\nabla}^*$ denote gradient operators with respect to $\underset{\sim}{x}$ and $\underset{\sim}{x}^*$ coordinates, respectively.

Under (3-13), the field equations (3-9) take the form

$$\underset{\sim}{\mathcal{L}}^{(\alpha)} \left[\underset{\sim}{F}^{(\alpha)} (\underset{\sim}{x},t;\underset{\sim}{x}^*;\epsilon) \right] = 0 \tag{3-14}$$

Next, local periodicity of all field variables is assumed with respect to the microcoordinates $\underset{\sim}{x}^*$. This condition, which is an extrapolation from linear analysis yet is expected to provide good correlation with exact results, allows one to consider a typical cell, Figure 3.8 for the purpose of determining the variation of $\underset{\sim}{F}^{(\alpha)}$ with respect to $\underset{\sim}{x}^*$. This cell contains a representative area of steel, $A^{(1)}$, and concrete, $A^{(2)}$.

The field equations (3-14) are now satisfied in an average sense. Weak solutions of (3-14) are obtained via a weighted residual procedure which takes the form:

$$\int_V \sum_{\alpha=1}^{2} \int_{A^{(\alpha)}} \underset{\sim}{\mathcal{L}}^{(\alpha)} \left[\underset{\sim}{F}^{(\alpha)} (\underset{\sim}{x},t;\underset{\sim}{x}^*;\epsilon) \right] \cdot \underset{\sim}{W}^{(\alpha)} (\underset{\sim}{x};\underset{\sim}{x}^*;\epsilon) \, dA^* \, dV = 0 \tag{3-15}$$

where $\underset{\sim}{W}^{(\alpha)}$ denote weighting functions, and $\cdot$ denotes an appropriate inner product.

The *residual procedure* (3-15) is converted to a variational principle by selecting a subset of the weighting functions as variations of velocity (Direct Method) or a combination of variations in velocity and stresses (Mixed Method). The Euler equations of the variational process are the desired mixture relations. The $\underset{\sim}{x}^*$ dependence of the weighting functions is suggested by a separate asymptotic analysis.

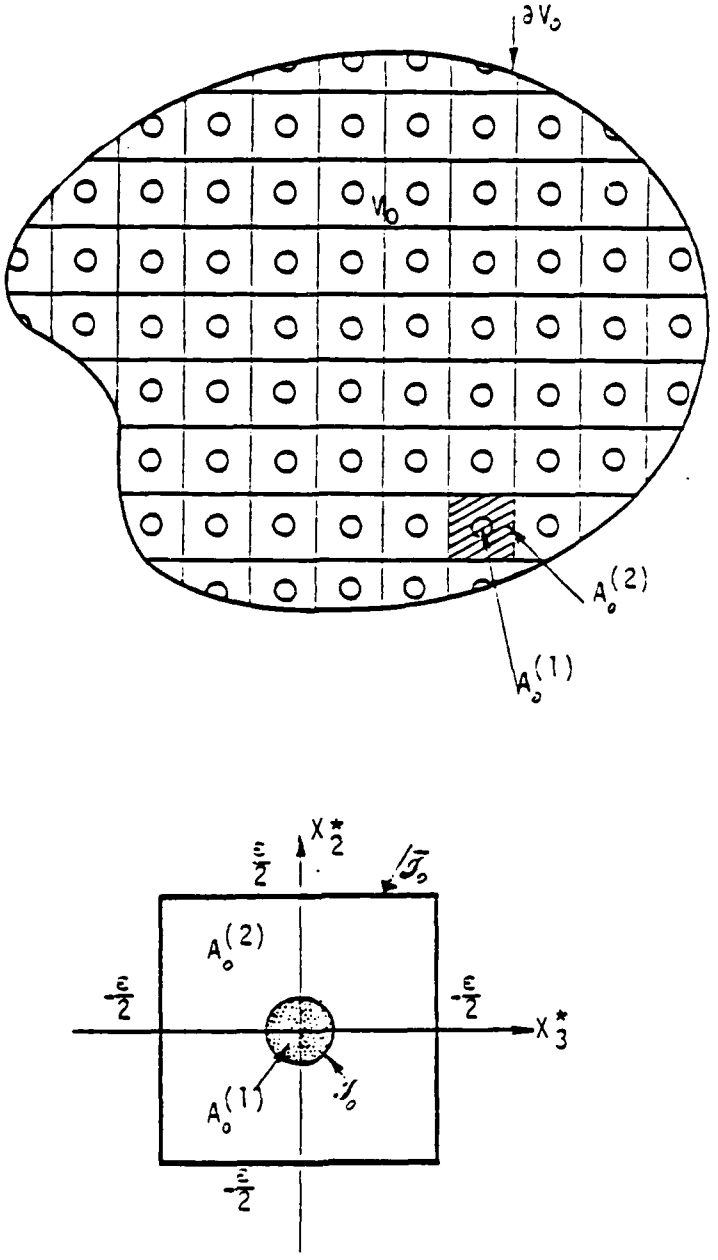

Figure 3.8. **Cell geometry for densely reinforced concrete (shown in initial configuration).**

3.5.3 Typical Mixture Form.

In the case of the Direct Method, the velocity field of each constituent is given by

$$\underset{\sim}{v}^{(\alpha)}\left(\underset{\sim}{x},t;\underset{\sim}{x}^{*};\epsilon\right) = \dot{\underset{\sim}{U}}^{(\alpha)}\left(\underset{\sim}{x},t\right) + \epsilon\underset{\sim}{S}^{K(\alpha)}(x,t)g^{K(\alpha)}\left(\underset{\sim}{x}^{*}\right) + 0(\epsilon^2) \tag{3-16}$$

The dependence on $\underset{\sim}{x}^{*}$ reflects variations of the velocity field over the cell, i.e., the microstructure. The functions $g^{K(\alpha)}$ (sum over K from 1 to n) are given. The variables $\underset{\sim}{U}$ and $\underset{\sim}{S}$ are displacement-type dependent variables.

When (3-16) is used as trial functions, the basic mixture relations take the form

$$\underset{\sim}{\nabla} \cdot \underset{\sim}{N}^{(\alpha)} + (-1)^{\alpha+1}\,\underset{\sim}{P} = 0 \quad \text{in } V, \quad (\alpha = 1,2) \tag{3-17}$$

$$\underset{\sim}{N}^{(\alpha)} = \underset{\sim}{\mathcal{F}}\left[\underset{\sim}{\nabla}\dot{\underset{\sim}{U}}^{(\alpha)}\ ,\ \underset{\sim}{\nabla}\underset{\sim}{S}^{K(\alpha)}\ ,\ \underset{\sim}{S}^{K(\alpha)}\right], \quad (\alpha = 1,2) \tag{3-18}$$

$$\underset{\sim}{P} = \underset{\sim}{\mathcal{H}}\left[\left[\dot{\underset{\sim}{U}}^{(1)} - \dot{\underset{\sim}{U}}^{(2)}\right]\ ,\ \underset{\sim}{\nabla}\underset{\sim}{S}^{K(\alpha)}\right]. \quad (\alpha = 1,2) \tag{3-19}$$

In the above, $\underset{\sim}{N}^{(\alpha)}$ is a stress average over $A^{(\alpha)}$, $\underset{\sim}{P}$ is an interaction term, and $\underset{\sim}{\mathcal{F}}$, $\underset{\sim}{\mathcal{H}}$ are functionals. Equations (3-17) - (3-19), which represent a static problem, have the form of an overlay of two continua which interact via $\underset{\sim}{P}$. Equation (3-17) is the equilibrium condition, equation (3-18) is the constitutive relation, and equation (3-19) is the constitutive relation for the interaction term.

The mixture relations (3-17) - (3-19) account for the behavior of concrete, steel, and steel-concrete interaction. The latter coupling occurs via the quantity $\underset{\sim}{P}$. Thus, for example, bond slip and degradation is reflected by (3-19). The operators $\underset{\sim}{\mathcal{F}}$ and $\underset{\sim}{\mathcal{H}}$ are defined once the steel, concrete, and steel-concrete interface behavior is analytically described.

It is noted that cracks in the concrete, according to the present modeling scheme, are treated explicitly. This furnishes maximum simulation capability. Another level of smoothing (smoothing of steel and intact concrete results in the mixture

relations (3-17) - (3-19)) is possible wherein the crack field is smoothed. The problem with such an operation, however, is that damage progresses from a sparse crack field to a dense field and the entire range of behavior may be important. Further, many failures are localized, not distributed.

3.6 VALIDATION STUDIES.

The purpose of this section is to explore the simulation accuracy and capability of the developed mixture theory framework, and to illucidate certain important features of the model. To aid in this task, several basic problem types have been selected for detailed studies. These include

- Steel-concrete slip and pullout
- Behavior under direct tension
- Behavior under biaxial stress states
- Behavior in shear (the dowel problem)
- Behavior in direct compression.

3.6.1 Simulation of Steel-Concrete Slip and Pullout.

This problem type plays a central role in the evaluation of certain interaction terms in the mixture formulation. Its relevance is as follows: The concept of steel-concrete "bond" and "slip" is manifested theoretically via Equation (3-19) or Equation (14) of Appendix C. What is required in these equations, and in the mixture model, is a local traction versus slip relation, e.g., interface shear stress versus local interface displacement difference between the rebar and concrete. However, such a relation cannot be obtained directly via experimental techniques. Although some measures of local slip can be obtained using, e.g., slip-wire techniques, the local shear stress cannot be measured. One must, in fact, back the local interface behavior out of a boundary value problem. And solution of a boundary value problem requires a theoretical model. Thus, a model must first be postulated, then a boundary value problem formulated which adequately represents the bond-slip test, and finally the desired result backed out of a suite of simulations of the test.

To illustrate the above statements, consider the test schematic of Figure 3.9 which shows a typical pullout test. Suppose that the mixture theory developed herein is adopted as the governing model of the experiment. Then, for small deformations and elastic component response, the theory developed in Appendix G reduces to

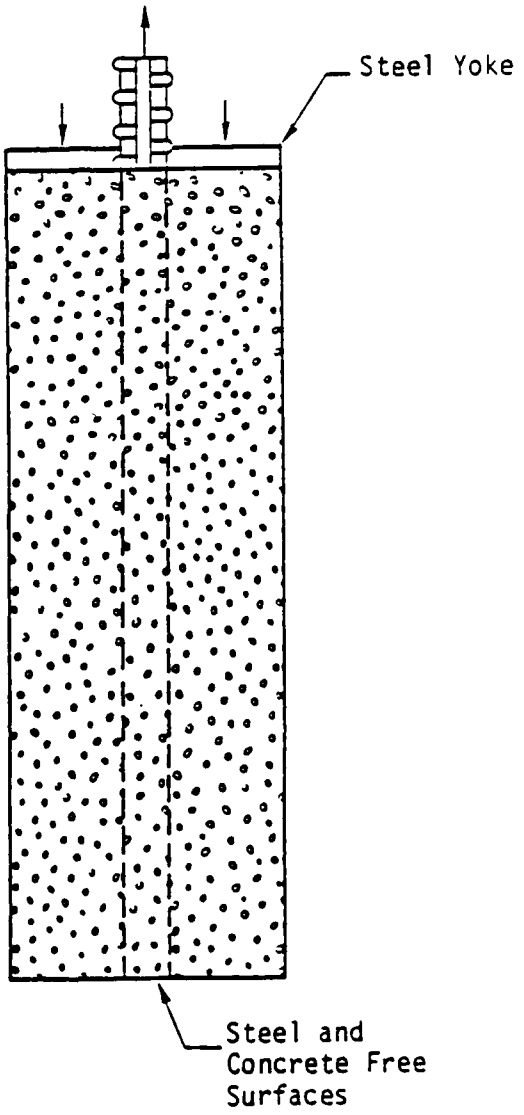

Pull-Out Test

Figure 3.9. Typical pullout test specimen.

$$N_{11,1}^{(1p)} + P_1 = 0 \quad , \quad N_{11,1}^{(2p)} - P_1 = 0 \quad , \tag{3-20}$$

$$\dot{N}_{11}^{(\alpha p)} = n^{(\alpha)} \dot{N}_{11}^{(\alpha a)} = n^{(\alpha)} E^{(\alpha)} \dot{U}_{1,1} \quad (\alpha = 1,2) \quad , \tag{3-21}$$

$$\dot{P}_1 = K_{ep} [\dot{U}_1] \quad , \quad [\dot{U}_1] \equiv [\dot{U}_1^{(1)} - \dot{U}_1^{(2)}] \quad . \tag{3-22}$$

In the above, $\alpha = 1,2$ refer to steel, concrete, respectively; $U_1^{(\alpha)}$, $N_{11}^{(\alpha a)}$ denote axial displacement and axial stress (average), respectively; K_{ep} is a tangent modulus; $n^{(\alpha)}$ denotes the volume (area) fraction of material α; and $()_{,1} \equiv \partial()/\partial x_1$, $\dot{()} \equiv \partial()/\partial t$ where t represents time.

The relations (3-20) are the equilibrium equations for each material; the latter interact via the interaction body force P_1 which reflects interface shear transfer between the steel and concrete. If σ_{rx}^* denotes the interface shear stress, then

$$P_1 = 2\sqrt{n^{(1)}}\, \sigma_{rx}^* / \epsilon \quad . \tag{3-23}$$

Equations (3-21) are the constitutive equations for each material. For elastic component response, the constants $E^{(\alpha)}$ are given by Young's modulus.

Prior to interfacial slip, the mixture theory developed herein (e.g., see Appendix H) predicts that

$$(K_{ep})^{-1}_{\substack{no \\ slip}} = \frac{\epsilon^2}{8} \left\{ \frac{1}{\mu^{(1)}} - \frac{[2 + n^{(2)} + (2\ell n\, n^{(1)}/n^{(2)})]}{n^{(2)} \mu^{(2)}} \right\} \equiv K^{-1} \quad . \tag{3-24}$$

Thus, prior to slip, the behavior of the interaction term P_1 is linear in $[U_1]$. Recall that $U_1^{(\alpha)}$ represents the <u>average</u> axial displacement of material α; Thus, even for the case of no local slip at the steel-concrete interface, the quantity $[U_1]$ does not vanish, i.e., $U_1^{(1)} \neq U_1^{(2)}$. The relation between the local slip and $[U_1]$ can be deduced from microstructural relations.

When steel-concrete slip occurs, Equation (3-24) must be generalized. For monotonic global deformation, a simple elastic-perfectly plastic model, Figure 3.10(b) will often suffice. When the elastic deformations of the concrete and steel are subtracted, this corresponds to a local rigid-plastic description of the interface bond

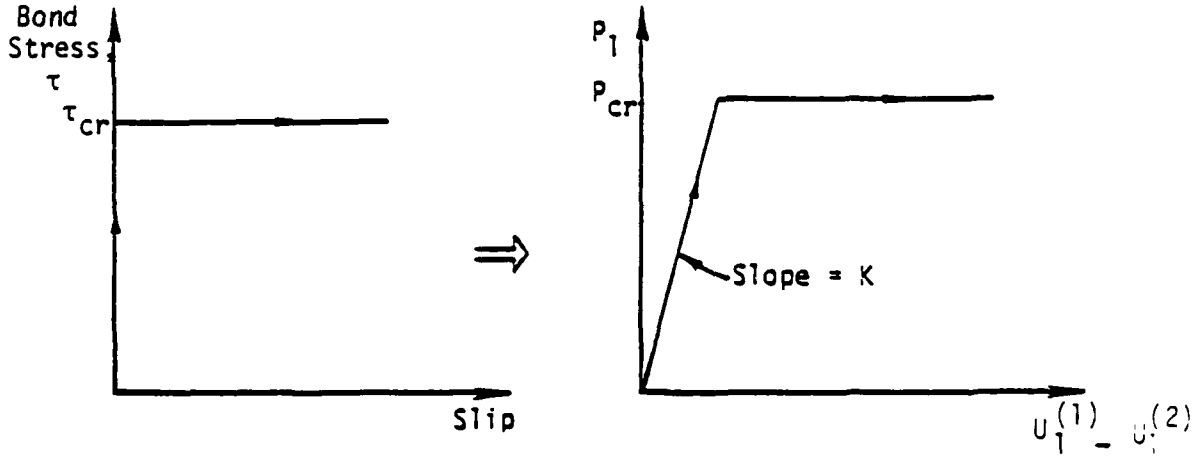

(a) Bond

(b) Interaction term, P_1

Figure 3.10. Interaction term P_1 for monotonic extension.

stress as depicted in Figure 3.10(a). Additional accuracy can be obtained by more complex interface descriptions such as depicted in Figure 3.11.

Let us turn now to experimental versus theoretical comparisons. Using the above mixture model, simulations of a number of pullout tests from different laboratories were performed. For this purpose, a boundary value problem was defined wherein the actual specimen geometry and properties were accounted for. Simulations were conducted by numerical solution of (3-20) - (3-22). Typical results are illustrated in Figure 3.12. The elementary elastic-perfectly plastic interaction term (rigid-perfectly plastic interface shear stress versus local slip) is observed to furnish adequate accuracy whereas the more complex multilinear bond-slip relation provides excellent agreement. Another comparison between simulation and experiment is given in Figure 3.13. Here again, excellent accuracy is observed.

Based upon a collection of simulation results, the piece-wise linear description of local bond stress versus local slip furnished in Figure 3.11 was found to provide an adequate description of interface behavior for a variety of concrete strengths and concrete covers. Using this description, simulation accuracy was found to vary from the excellent results of Figure 3.13 to the adequate results of Figure 3.14.

For hysteretic deformation, the above description of the interaction term must be generalized considerably. Several bond-slip models that have been explored for this purpose are depicted in Figure 3.15.

3.6.2 Simulation of R/C Under Uniaxial Tension.

One important form of damage in R/C occurs because the maximum global (composite) stress is positive, i.e., tension. Such stress states can result in progressive crack accumulation and associated steel-concrete interface slip. One manifestation of such damage is stiffness degradation. This phenomenon plays a dominant role in the bending and nonlinear stretching of R/C beams, plates, and shells.

To understand how well the mixture formulation simulates the nonlinear response of R/C when the maximum principal stress is positive, the classical tension-stiffening problem was selected for simulation. Details of the resulting studies can be found in

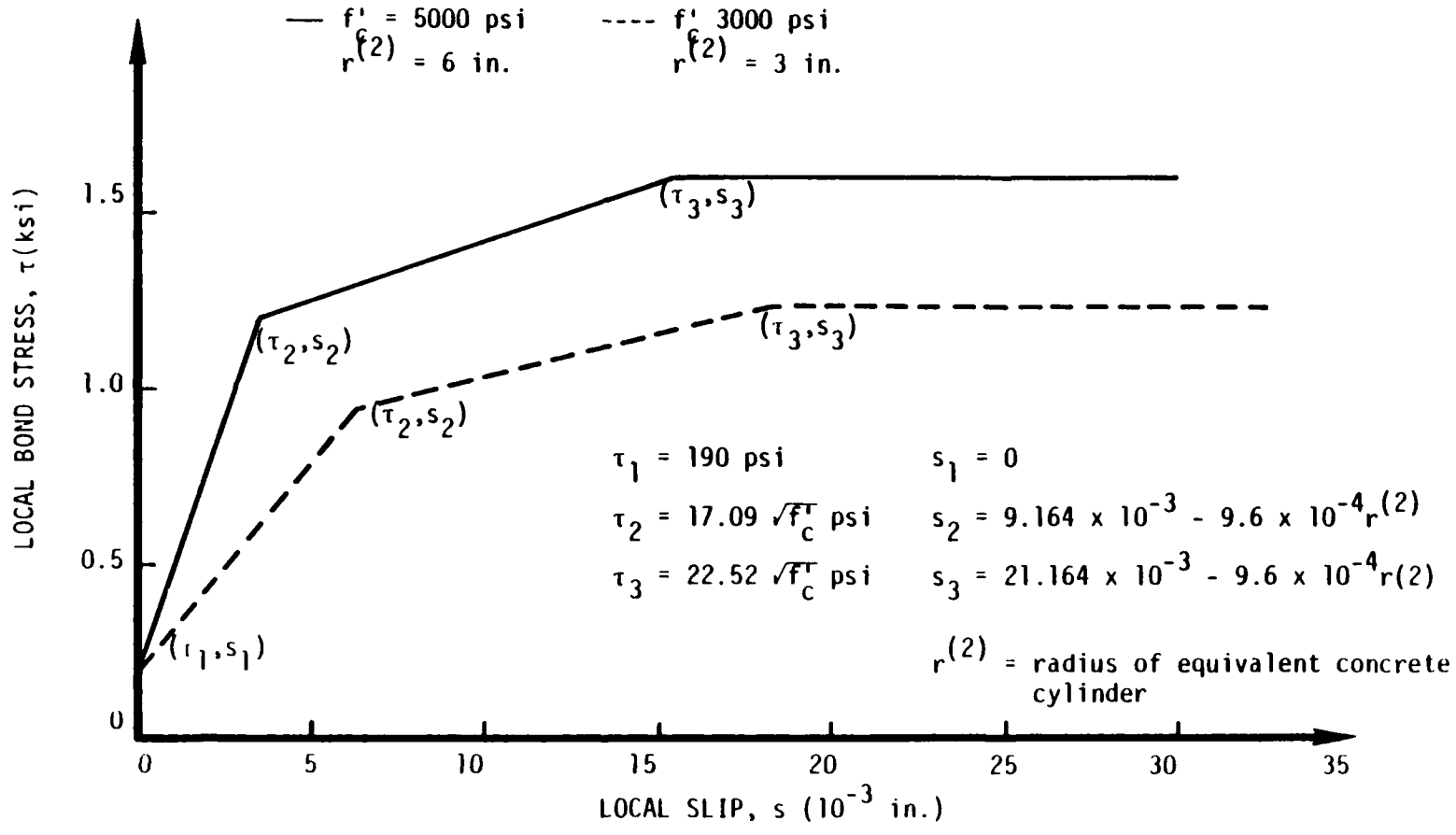

Figure 3.11. **Local bond slip relation for specimens axially reinforced with deformed bars as a function of concrete strength and cover.**

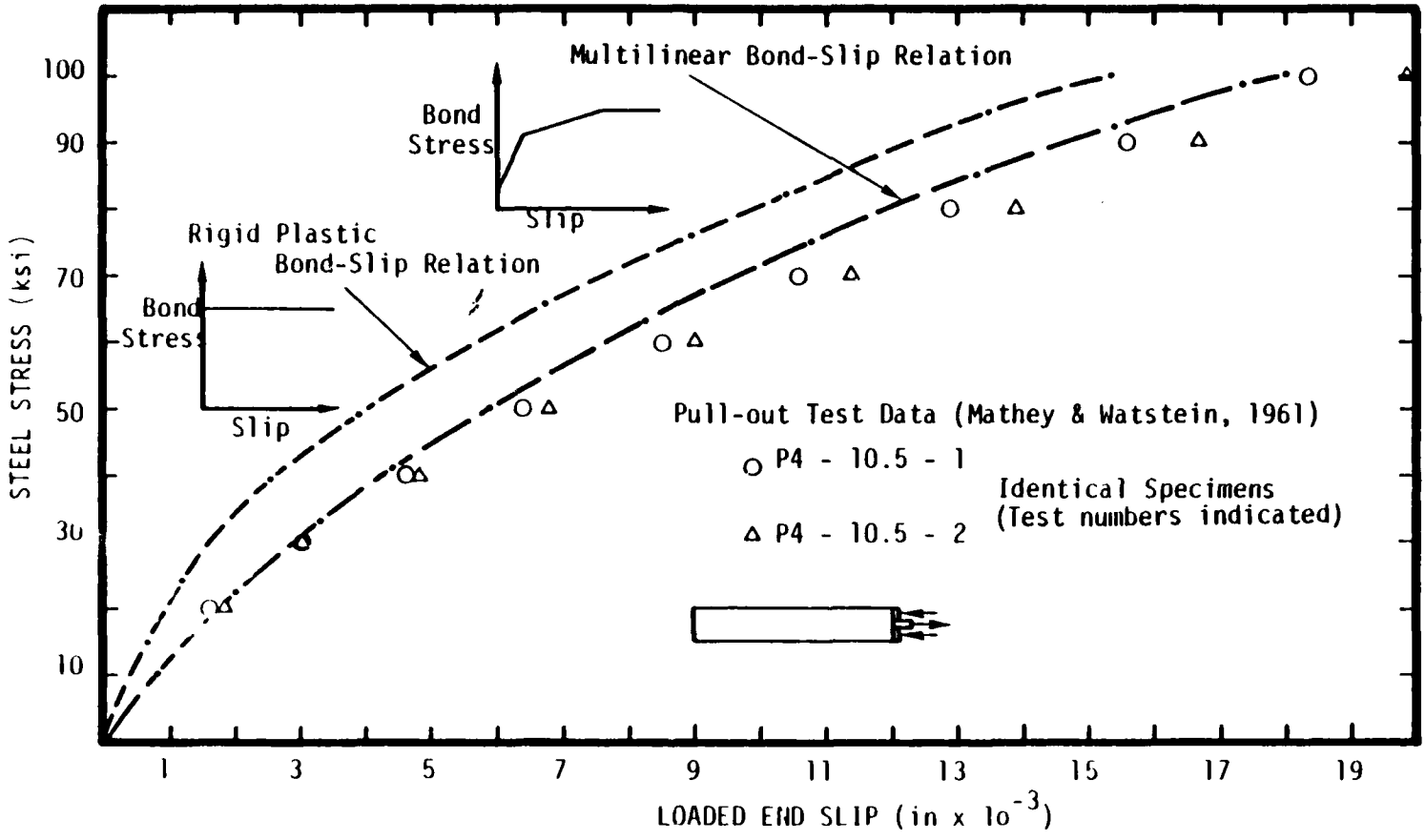

Figure 3.12. Simulation versus experiment for pullout tests.

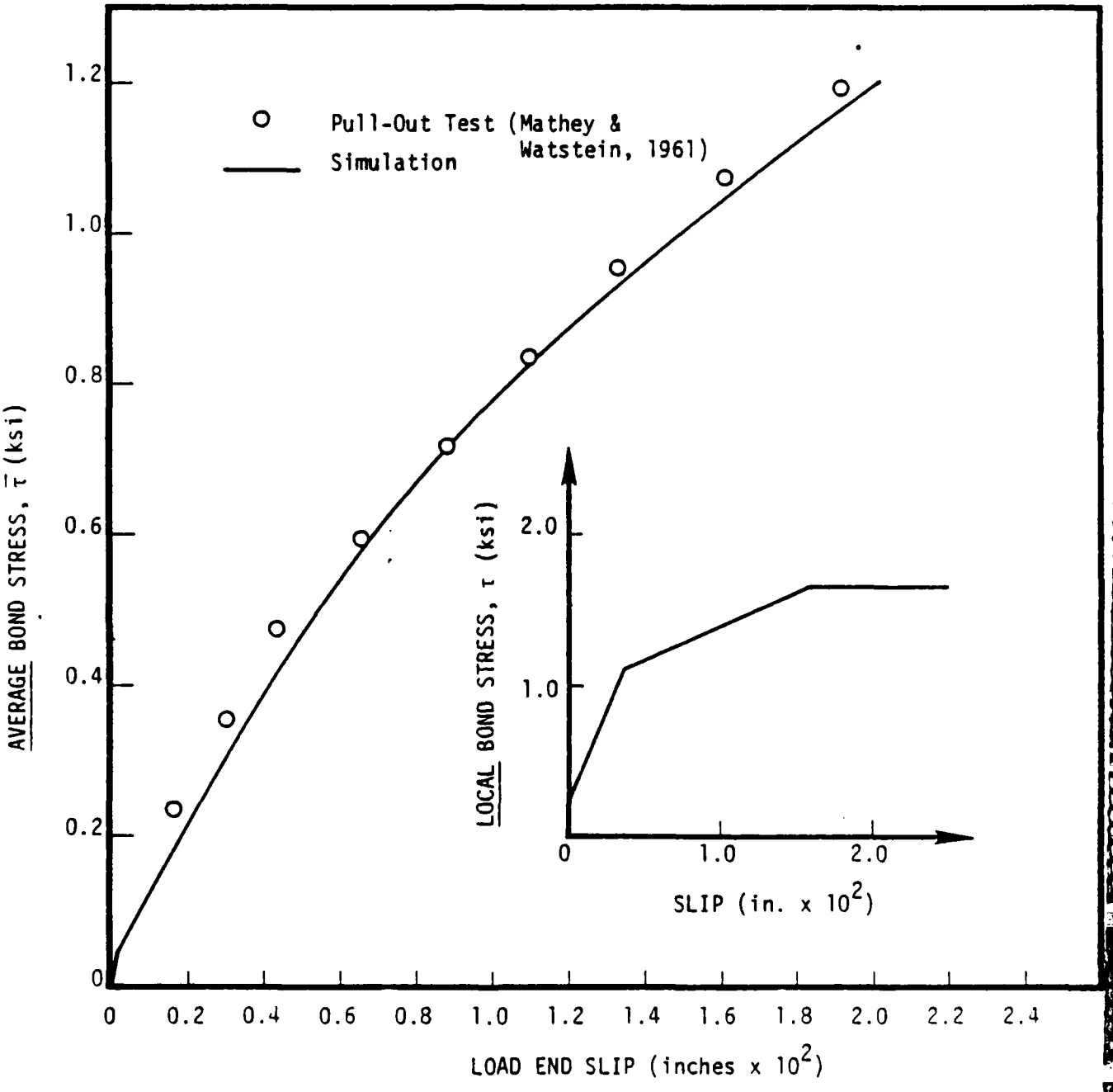

Figure 3.13. **Simulation of pullout test (average bond stress, $\bar{\tau}$, is the pullout force divided by the steel surface area).**

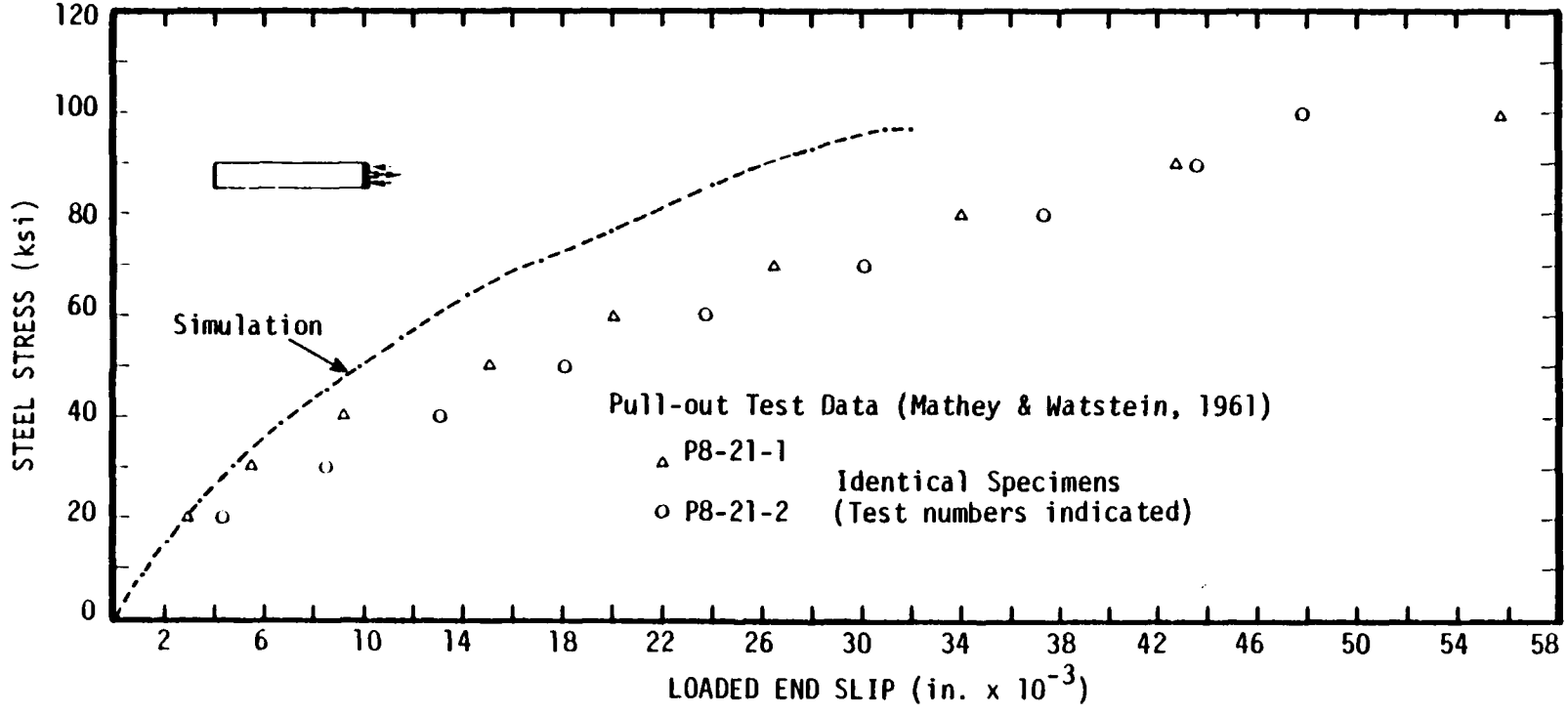

Figure 3.14. Simulation versus experiment for pullout tests.

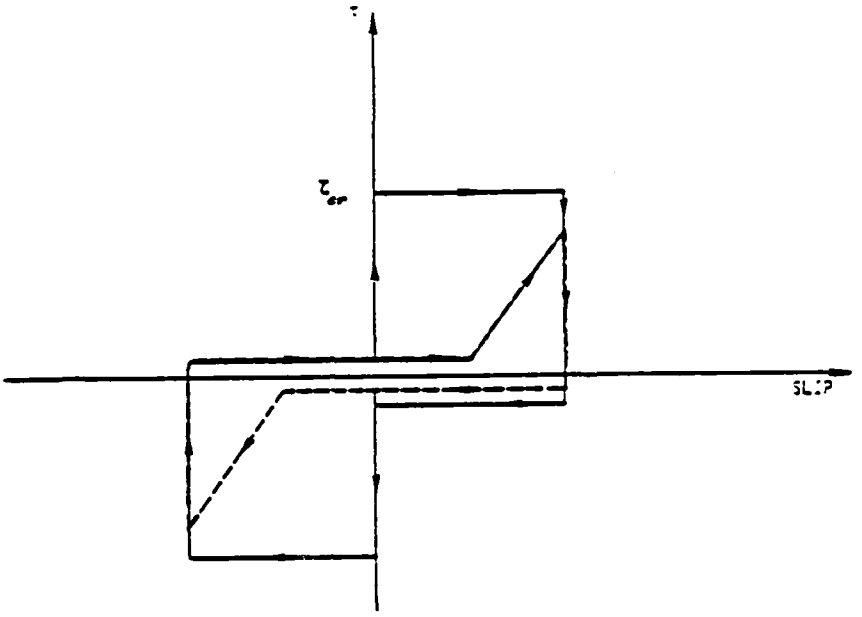

Figure 3.15a. Proposed local bond-slip relation for reversed load cycles with fixed slip limits. The first cycle is represented by solid lines, all subsequent cycles by dashed lines.

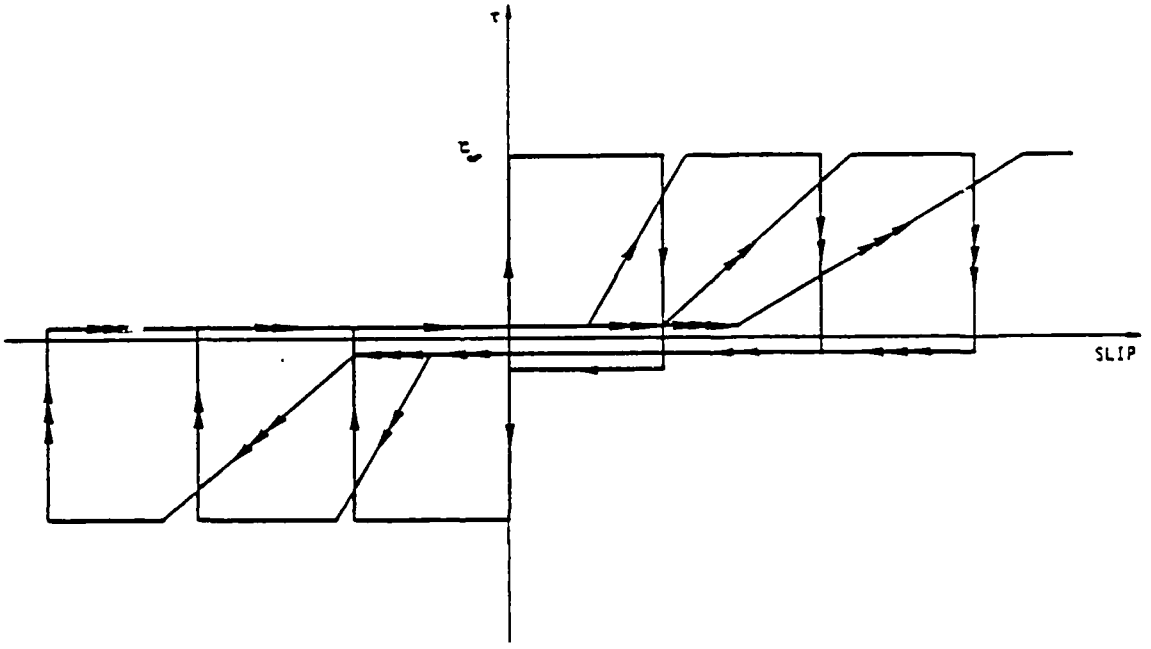

Figure 3.15b. Proposed local bond-slip relation for reversed load cycles with increasing slip limits.

Hegemier, *et al.*, (1985), Murakami and Hegemier (1986), and Hageman, *et al.*, (1986). In what follows the basic features of the problem and the results are sketched.

Consider the problem of simulating the global response of a unidirectionally reinforced concrete specimen subject to a state of global uniaxial stress applied in the steel direction (principal stresses that are oblique to the steel will be considered later) as depicted in Figure 3.2. If, as in the previous section, small deformations are assumed, then the theory developed in Appendix E reduces to

$$N_{11,1}^{(1p)} + P_1 = 0 \ , \quad N_{11,1}^{(2p)} - P_1 = 0 \ , \tag{3-25}$$

$$\dot{N}_{11}^{(\alpha p)} = n^{(\alpha)}\dot{N}_{11}^{(\alpha a)} = n^{(\alpha)}E_{ep}^{(\alpha)}\dot{U}_{1,1}, \tag{3-26}$$

$$\dot{P}_1 = K_{ep}\left[\dot{U}_1\right] \ , \quad \left[\dot{U}_1\right] \equiv \left[\dot{U}_1^{(1)} - \dot{U}_1^{(2)}\right] \tag{3-27}$$

Equations (3-25) - (3-27) are similar in form to (3-20) - (3-22). They differ, however, in the definition of the tangent moduli. Prior to bond slip, and for the elastic response regime, the tangent moduli in (3-26) and (3-27) are given by

$$E_{ep}^{(\alpha)} = (\lambda + 2\mu)^{(\alpha)} - \lambda^{(\alpha)2}/(\lambda + \mu)^{(\alpha)} \ , \tag{3-28}$$

$$K_{ep}^{-1} = \frac{\epsilon^2}{8}\left\{\frac{1}{\mu^{(1)}} - \frac{\left[2 + n^{(2)} + \left(2\ell n\, n^{(1)}/n^{(2)}\right)\right]}{n^{(2)}\mu^{(2)}}\right\} \equiv K^{-1} \tag{3-29}$$

where $\lambda^{(\alpha)}$, $\mu^{(\alpha)}$ are the Lamé constants of material α.

When steel-concrete slip occurs, Equation (3-29) must be generalized. For monotonic global deformation, a simple elastic-perfectly plastic model is sufficient. For hysteretic deformation detailed studies of steel-concrete pull-out specimens have guided the construction of an elementary bond-slip model which is depicted in terms of the interaction term P_1 in Figure 3.16. For a range of concretes, the following selection of parameters is appropriate:

$$P_{cr} = 2\sqrt{n^{(1)}}\,(\sigma_{rx})_{cr}/\epsilon \ , \ P_F = -\,P_G = 0.8\,P_{cr} \ , \qquad (3\text{-}30)$$

$$P_{IJ} = 0.2\,P_{cr} \ , \ P_{DE} = -\,P_{GH} = 0.1\,P_{cr} \ .$$

The model depicted in Figure 3.16 is easily placed in analytical incremental form. The description involves two parameters, K as defined by (3-29) and $(\sigma_{rx})_{cr}$ which represents a critical steel-concrete interface shear stress.

Outside of the elastic response regime, the components will be modeled as follows: (1) concrete: elastic-brittle fracture; (2) steel:elastic-plastic with strain hardening. This behavior is depicted in terms of tangent moduli in Figure 3.17.

(1) Monotonic Extension.

The response of the R/C type noted above involves three primary nonlinear phenomena: (1) steel-concrete bond slip, (2) plastic deformation of the rebar, and (3) progressive cracking of the concrete. Items (1) and (2) are simulated by the basic mixture relations once the appropriate tangent moduli are specified. However, item (3) requires comment. In the current mixture formulation, cracks are treated explicitly, i.e., they are not smoothed. This furnishes maximum simulation capability and allows treatment of both sparse and dense crack fields. However, this approach requires one to follow the entire crack evolution sequence. For the present uniaxial stress problem, only primary (through) cracks are considered. The development of such cracks are based on a simple stress criteria. The stress measure used in this case is the average axial concrete tensile stress, $N_{11}^{(2a)}$. Between two cracks, the variation of this stress is as depicted in Figure 3.18. Thus, new cracks always form halfway between old cracks (neglecting statistical variations in tensile strength). For simulation purposes, the boundary value problem depicted in Figure 3.19 was assumed. This Figure also shows the resulting crack sequence.

Consider now monotonic extension. Figure 3.20 shows simulation versus experimental (Mirza and Houde (1979)) data for two sizes of tension specimens. The specimen geometry is depicted in Figure 3.21. Agreement is considered to be satisfactory when one considers the data scatter that is typical of such tests. It is emphasized that the bond slip law defined by Figure 3.11 was used in the simulations. It is noted that no effort was made to "tune" the model to the data.

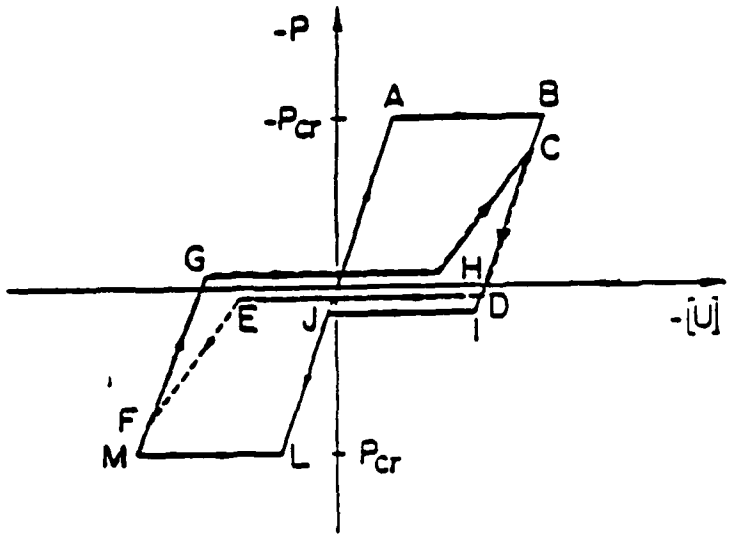

Figure 3.16 Bond-slip model.

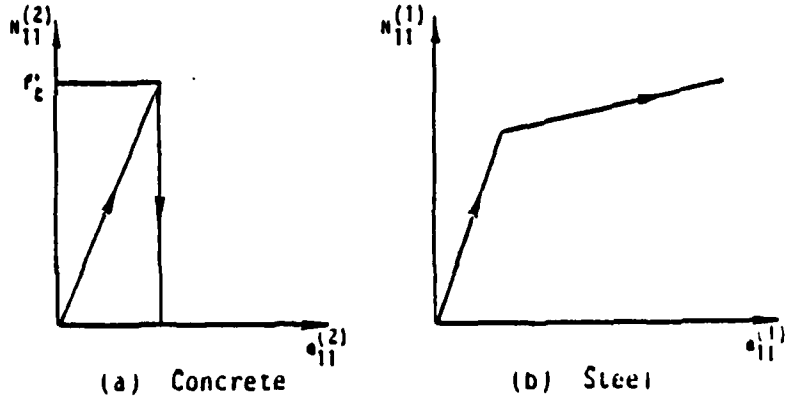

Figure 3.17. Behavior of constituents for monotonic extension.

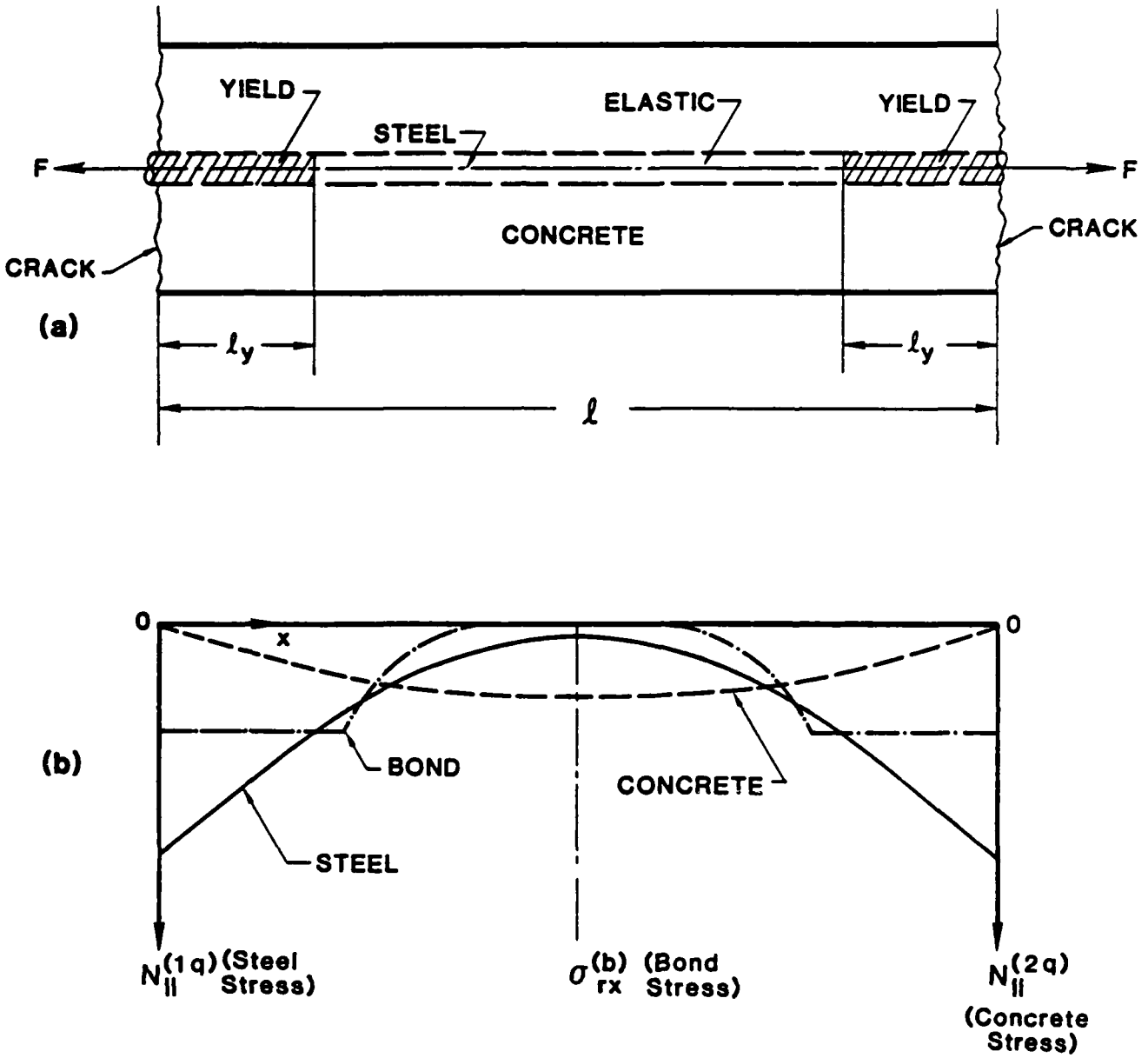

Figure 3.18. Stresses on steel and concrete and at interface.

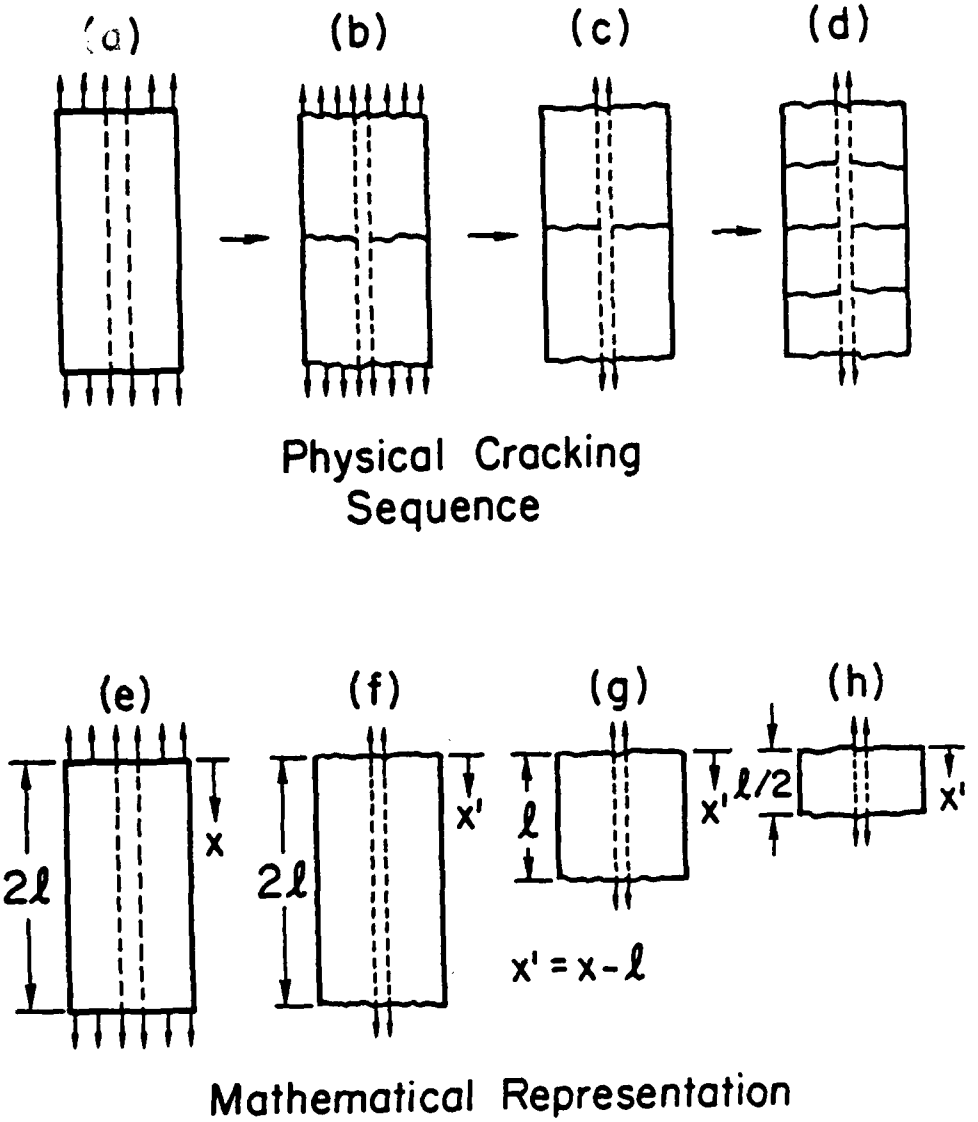

Figure 3.19. Cracking sequence assumed.

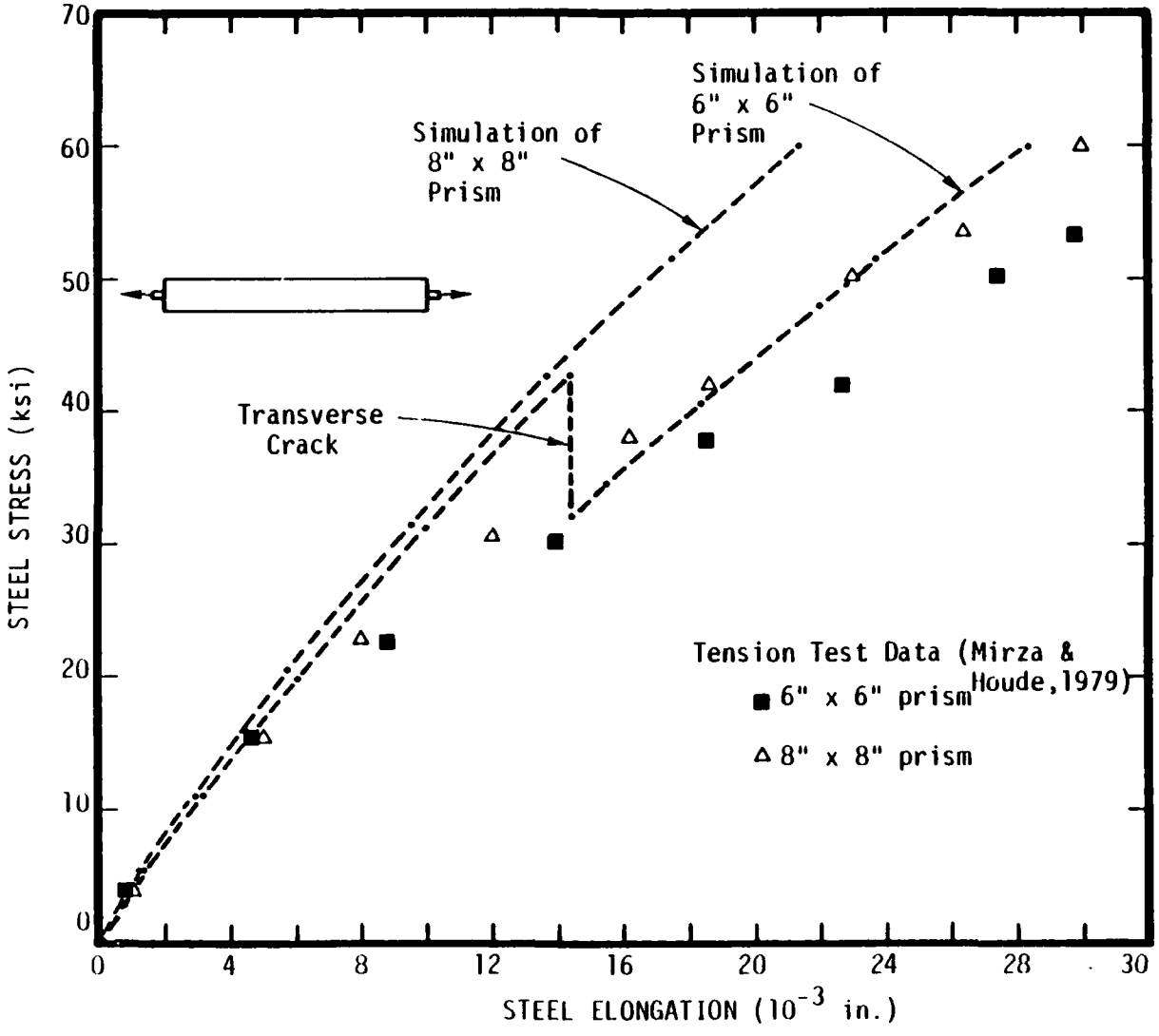

Figure 3.20. Simulation versus experiment for tension tests.

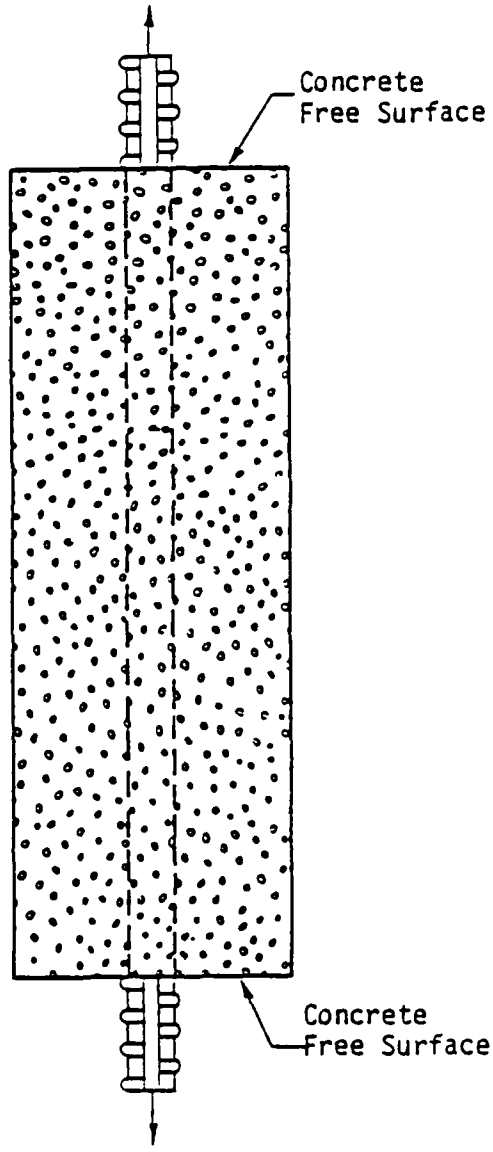

Figure 3.21. Tension test.

Another comparison that was made involves monotonic extension of scaled R/C specimens with a dense unidirectional steel layout, Figure 3.22. Experimental (Somoyaji (1979)) versus theoretical comparisons for load controlled tests are shown in Figures 3.23 -- 3.25. Figure 3.23 illustrates the behavior of one particular specimen whereas Figures 3.24 - 3.25 depict comparisons for a suite of tests. Because of the load-control, the tests in this series were not "clean." In particular, expected sharp drops in global stress due to progressive fracture of the concrete are "smeared" due to the specimen loading procedure. In addition, the method of testing led to significant data scatter. Nevertheless, the experimental-theoretical comparisons shown demonstrate that the mixture formulation is capable of good simulations for a wide range of steel layouts in all major response ranges, Figure 3.26. The latter consists of: Elastic response with no cracking, debonding, or slip (Stage I), progressive cracking with debonding and slip (Stage II), and slip only (Stage III). In addition to global stress-strain response, reasonable agreement has been observed between predicted and observed crack patterns.

(2) Hysteretic Extension.

In addition to monotonic extension, comparisons were also made between simulations and experimental data for hysteretic extension. The case considered involved cyclic loading (tension-compression) of full-scale plate-type (64 in. x 64 in. x 8 in.) specimens reinforced with No. 5 rebar. In contrast to the scaled R/C specimen tests, the experiments in this series were carefully conducted under displacement control (Hegemier, Nunn and Arya (1978)). Figures 3.27 and 3.28 indicate typical experimental versus theoretical comparisons of global (composite) stress-strain response. Figure 3.29 compares simulated and measured specimen stiffness degradation as measured by average unload-reload slopes. The agreement of test results and theoretical predictions is observed to be excellent. It is noted that both bond slip and progressive cracking of the concrete were active in these tests and simulations.

In addition to the above global stress-strain envelop and stiffness comparisons, detailed comparisons were made between theory and experiment for each unload-reload cycle. A sample of these comparisons is furnished in Figure 3.30. It is evident that the mixture model formulation is capable of simulating complex details concerning the hysteretic response with remarkable accuracy.

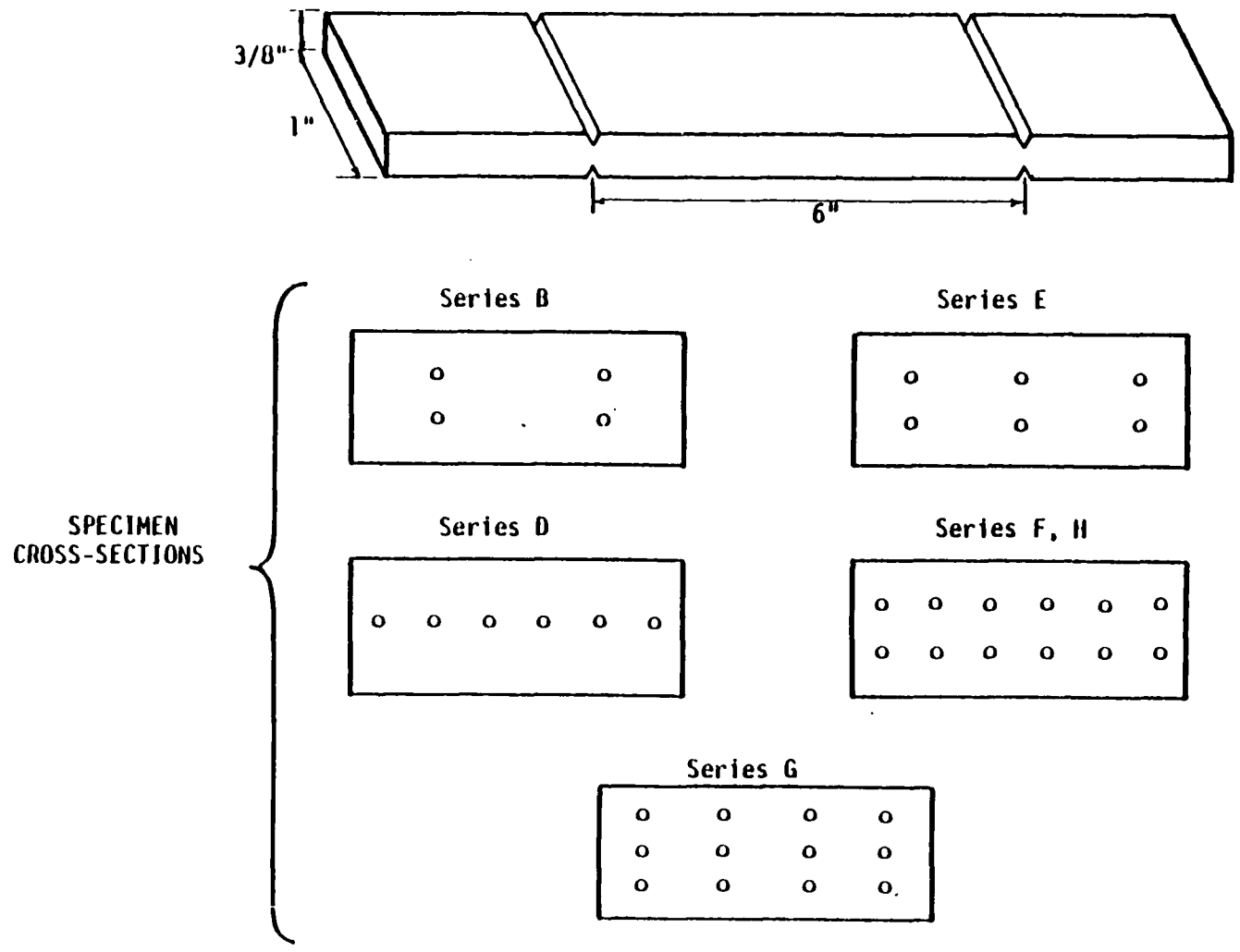

Figure 3.22. Specimen geometry.

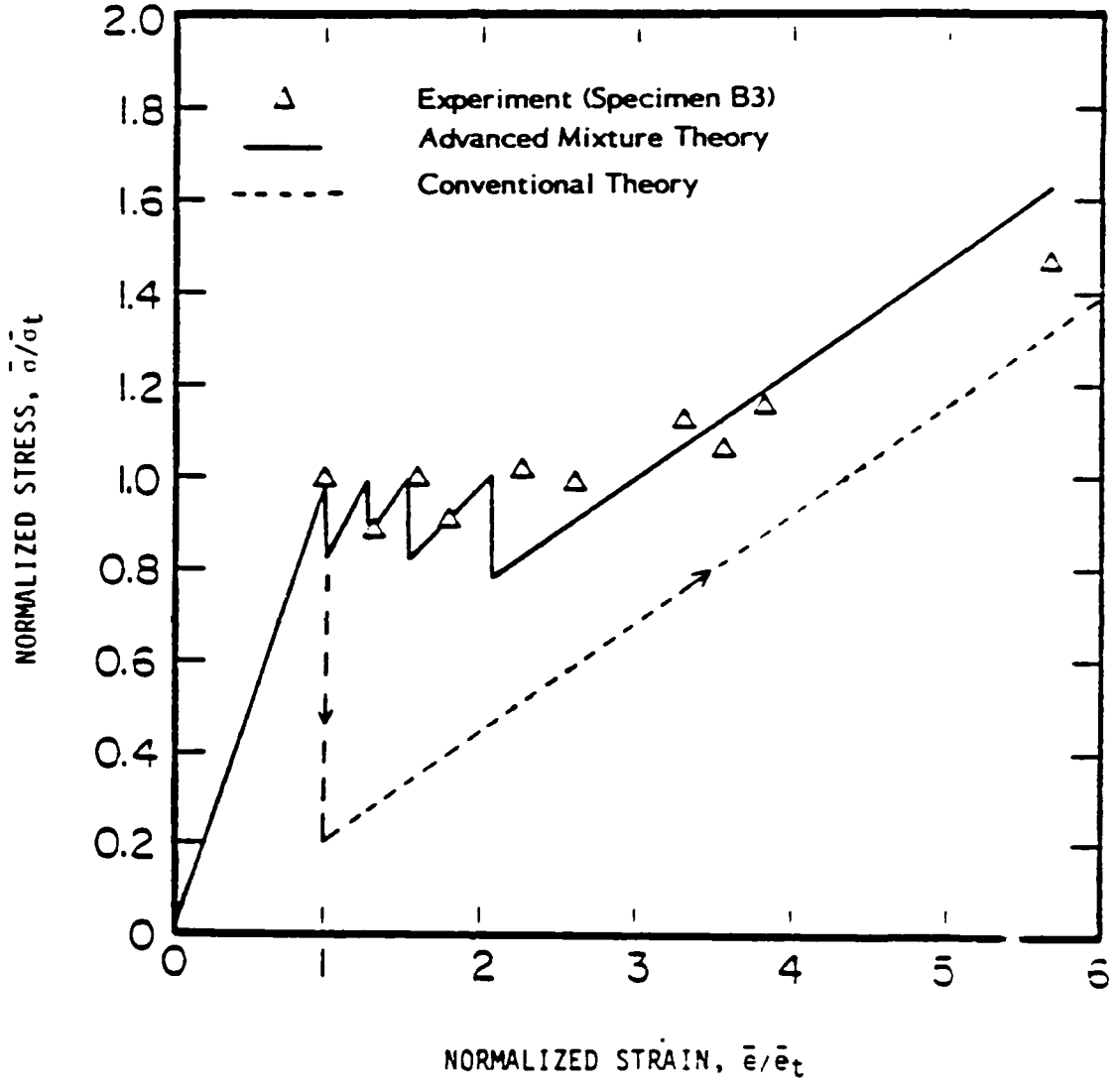

Figure 3.23. **Comparison of conventional and advanced mixture models in extension.**

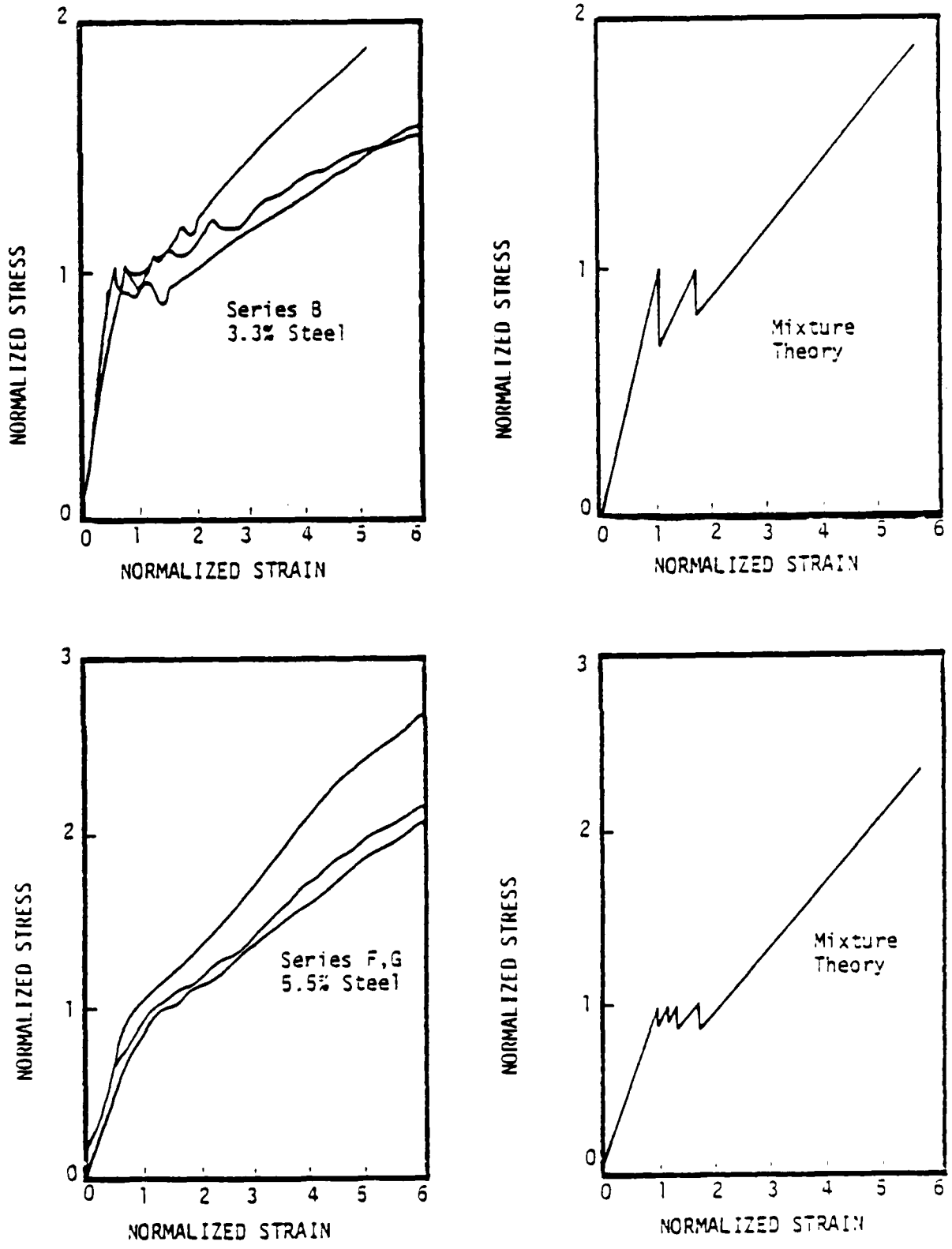

Figure 3.24. Comparisons of experiment and theory.

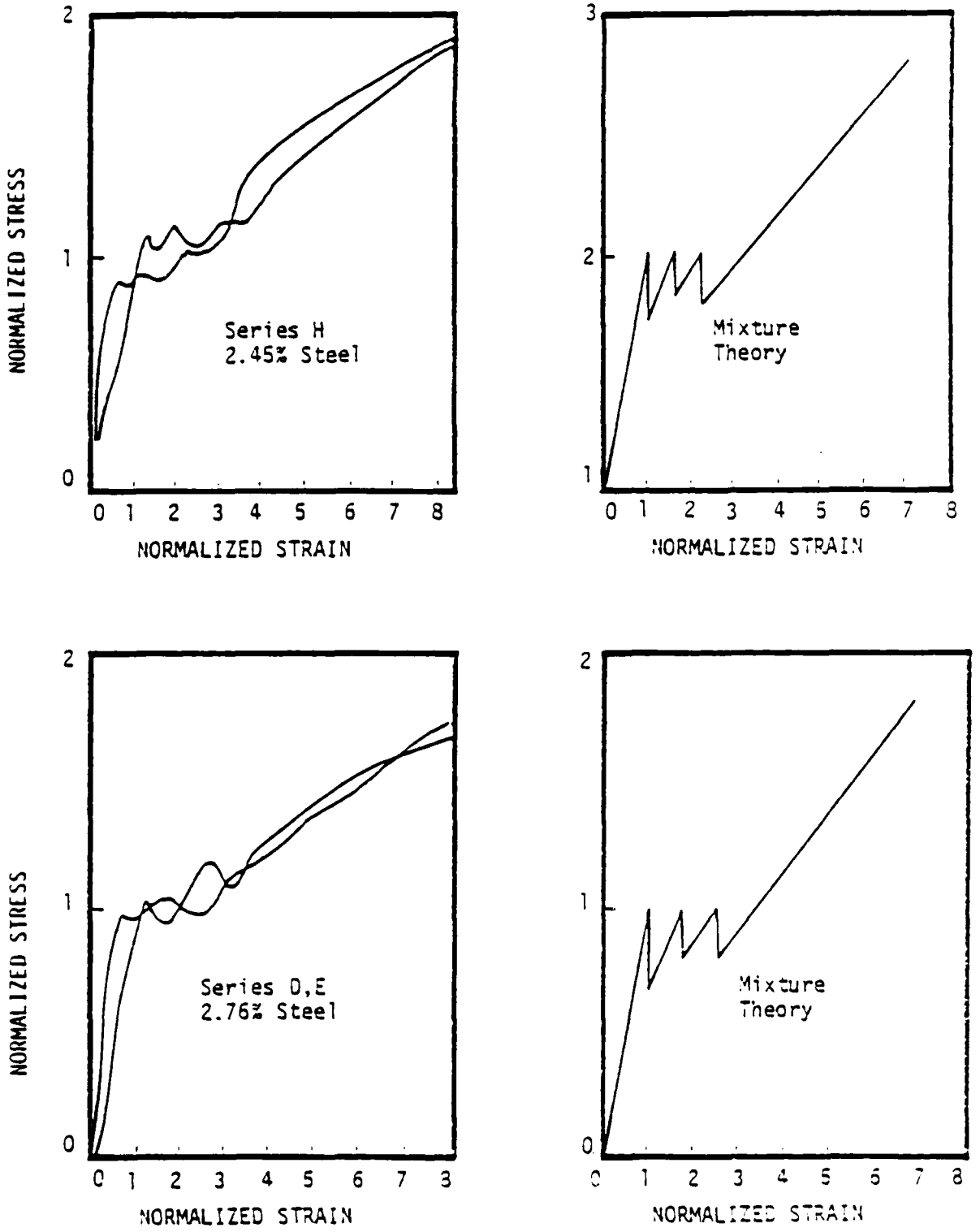

Figure 3.25. Comparisons of experiment and theory.

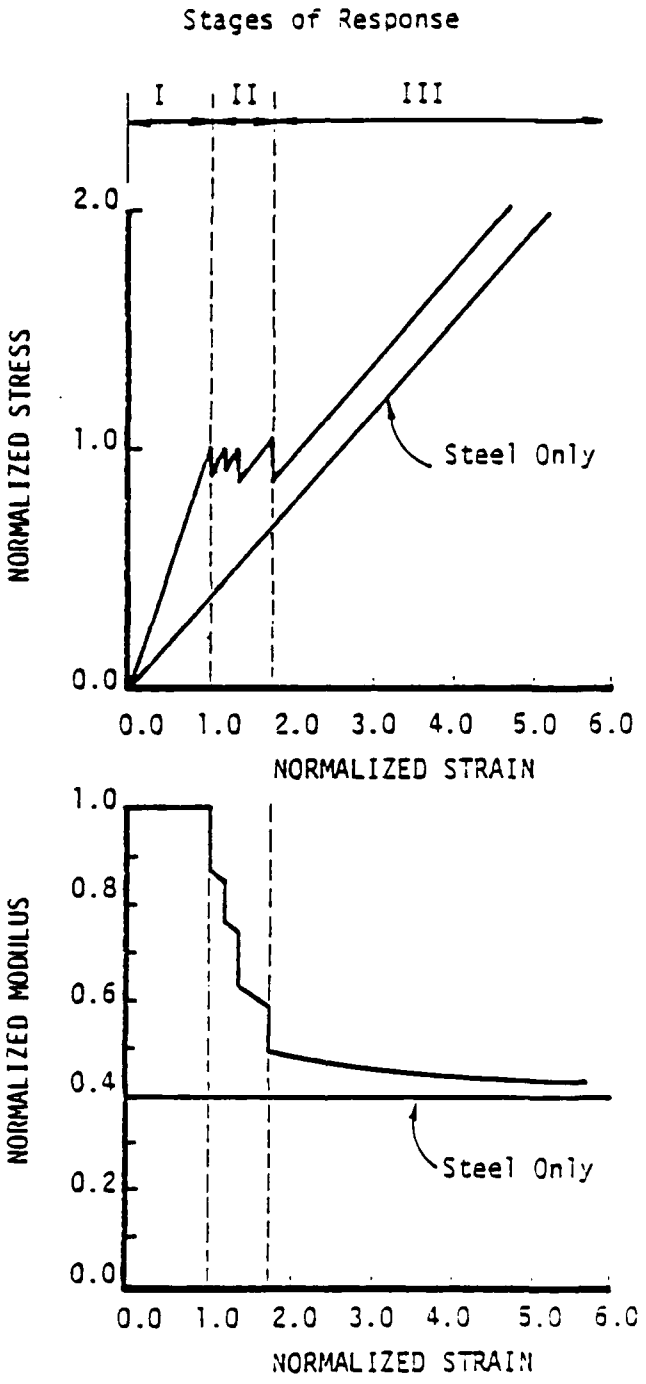

Figure 3.26. Stages of response predicted theoretically.

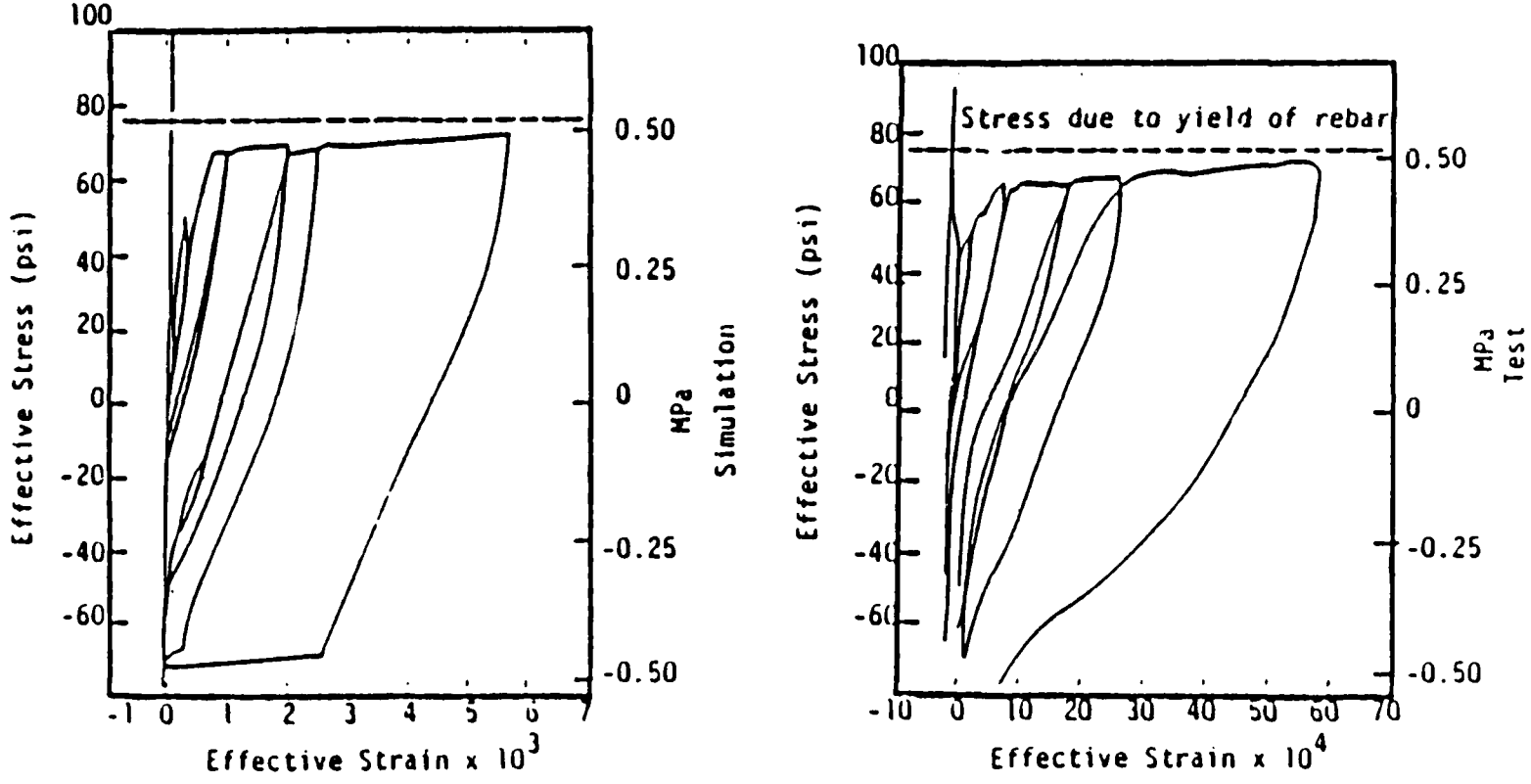

Figure 3.27. Comparison of test and simulation.

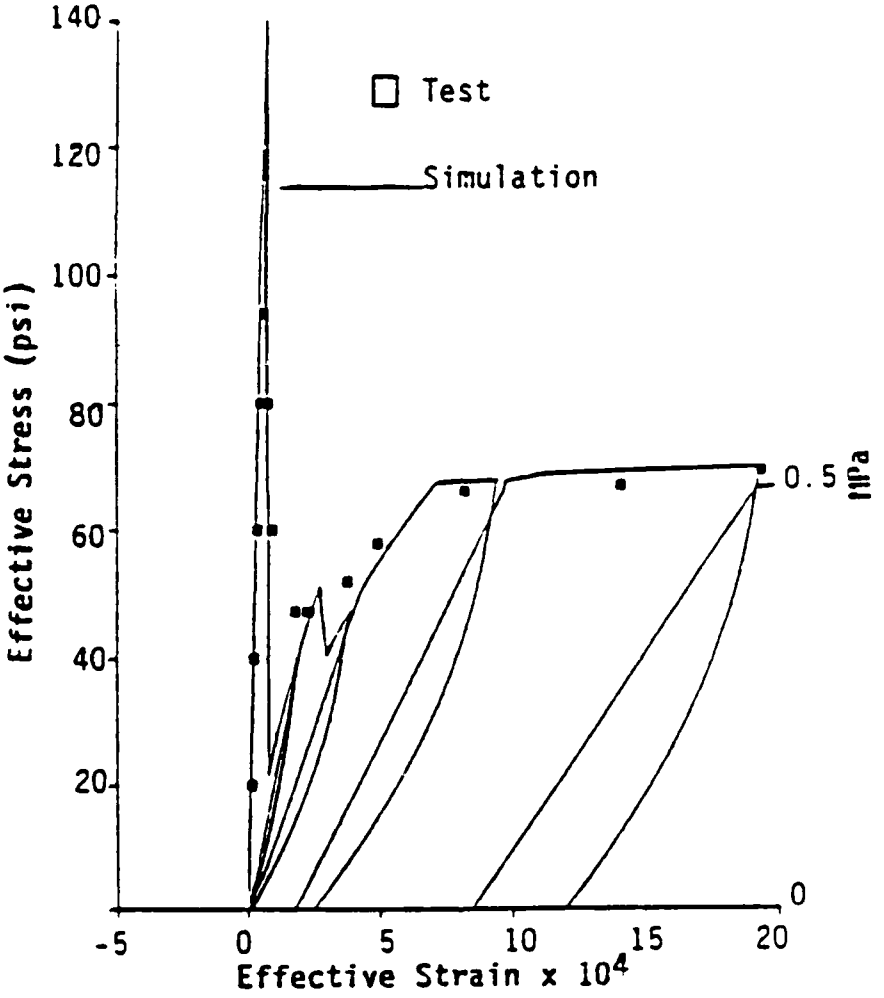

Figure 3.28. Comparison of test and simulation.

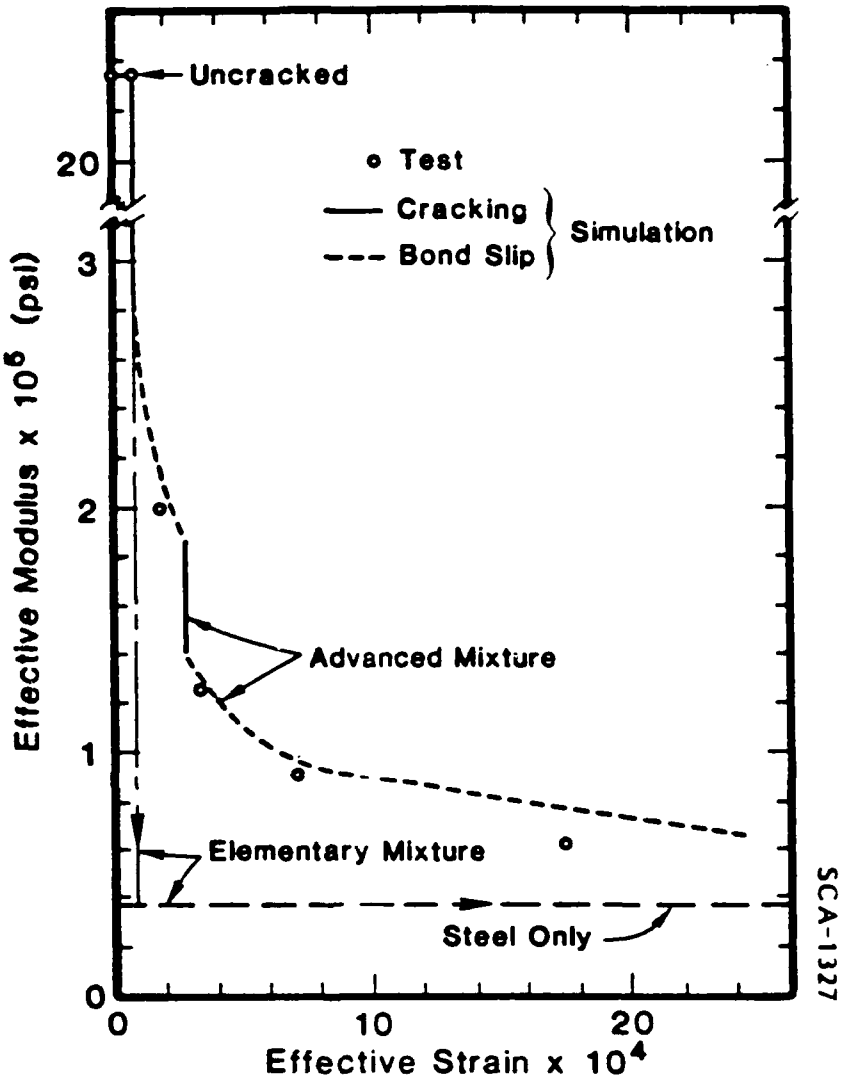

Figure 3.29. Comparison of test and simulation: Tangent stiffness degradation due to cracking and debonding.

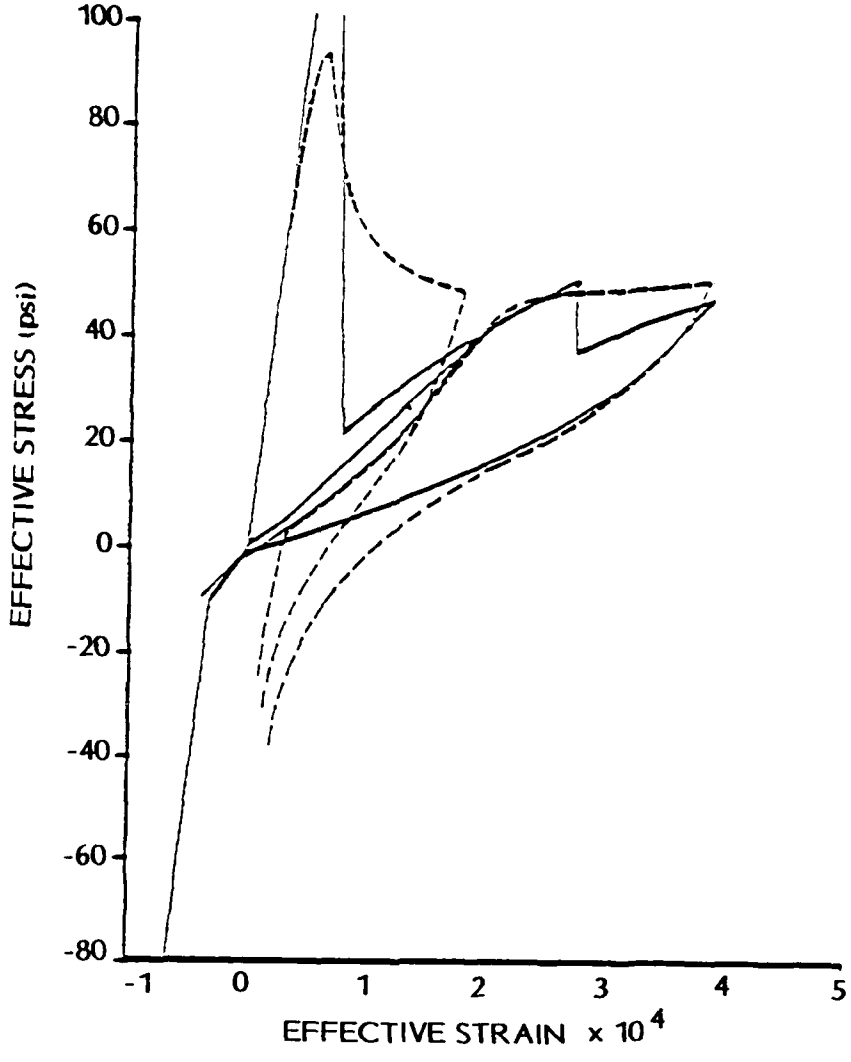

Figure 3.30. **Comparison of experiment (dashed lines) and theory (solid lines) effective stress versus effective strain curves for the first two deformation cycles.**

3.6.3 Simulation of R/C Under Shear (Dowel Problem).

The dowel problem is another classical problem associated with the response of R/C subsequent to cracking. This case, in its most elementary form, is depicted in Figure 3.31 for a dense array, and in Figure 3.32 for a "cell". Here a unidirectionally reinforced specimen with a preexisting crack perpendicular to the rebar is subjected to global shear. Of interest is the prediction of the global shear force or stress across the crack plane for a prescribed relative offset displacement of the concrete. In general, the response involves nonlinear geometric deformation (moderate rotations) of the steel, Figure 3.33., transverse deformation of the steel due to "dragging" through the concrete, steel-concrete bond slip, and aggregate interlock between opposing crack faces.

For the geometry depicted in Figure 3.32, the nonlinear mixture relations of Appendix C can be employed to deduce the appropriate governing equations. However, the description of Appendix C is Eulerian whereas a Lagrangian description is more convenient for this problem. Rather than presenting a general discussion of the nonlinear mixture relations in a Lagrangian description and then specializing to the present problem, a special derivation for the dowel case is furnished in Appendix I. The basic equations are:

(a) Equilibrium

$$N^{(1p)}_{11,1} + P_1 = 0 \quad , \tag{3-31}$$

$$N^{(1p)}_{12,1} + N^{(1p)}_{11} U^{(1)}_{2,11} + P_2 = 0 \quad , \tag{3-32}$$

$$M^{(1p)}_{11,1} - N^{(1p)}_{12} = 0 \tag{3-33}$$

(b) Stress Constitutive:

$$\begin{bmatrix} \dot{N}_{11} \\ \dot{N}_{12} \\ \dot{M}_{11} \end{bmatrix}^{(1p)} = \begin{bmatrix} C_{11} & C_{12} & 0 \\ C_{12} & C_{22} & 0 \\ 0 & 0 & C_{33} \end{bmatrix} \begin{bmatrix} \dot{U}_{1,1} + U_{2,1}\dot{U}_{2,1} \\ \dot{U}_{2,1} + \dot{S}_1 \\ \dot{S}_{1,1} \end{bmatrix} \tag{3-34}$$

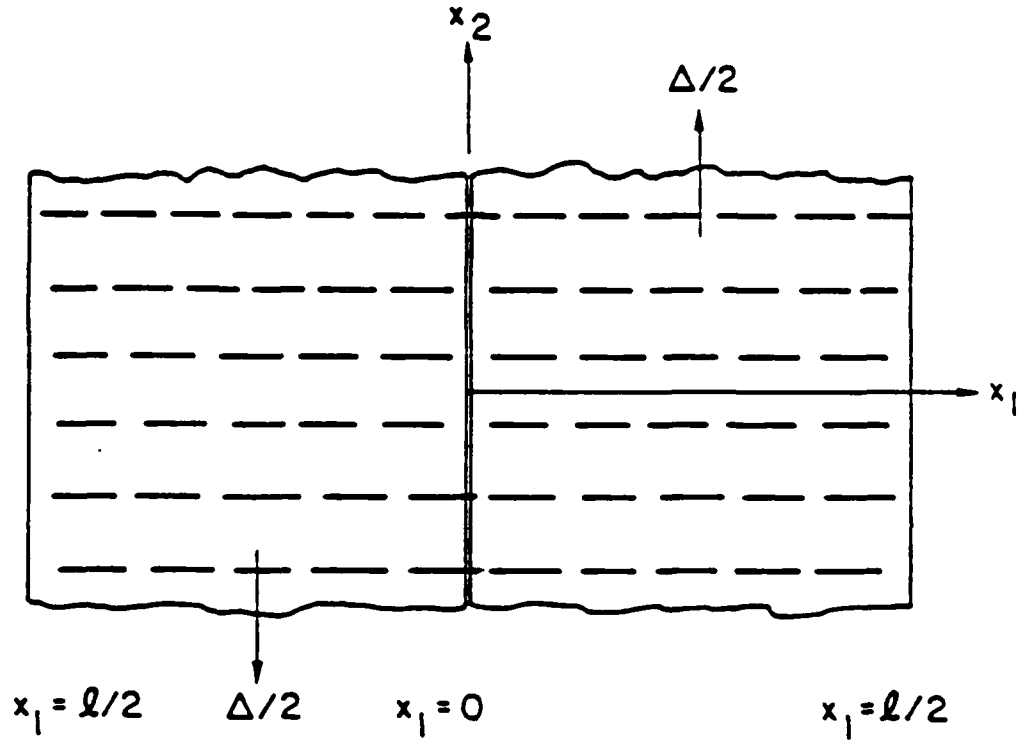

Figure 3.31. The dowel problem.

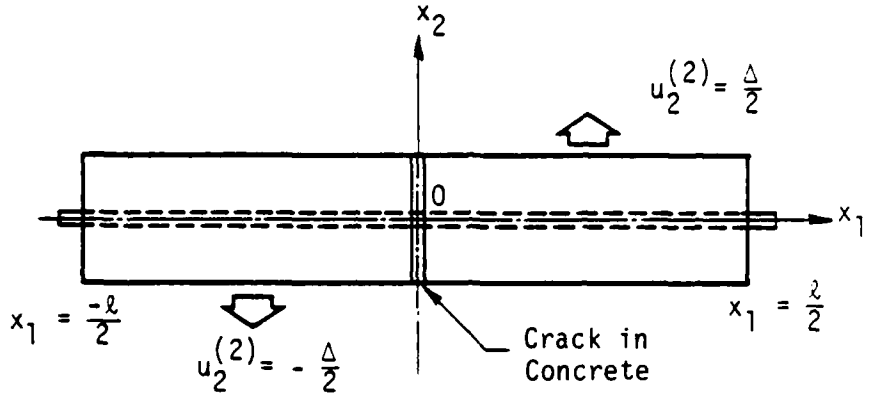

(a) Before deformation

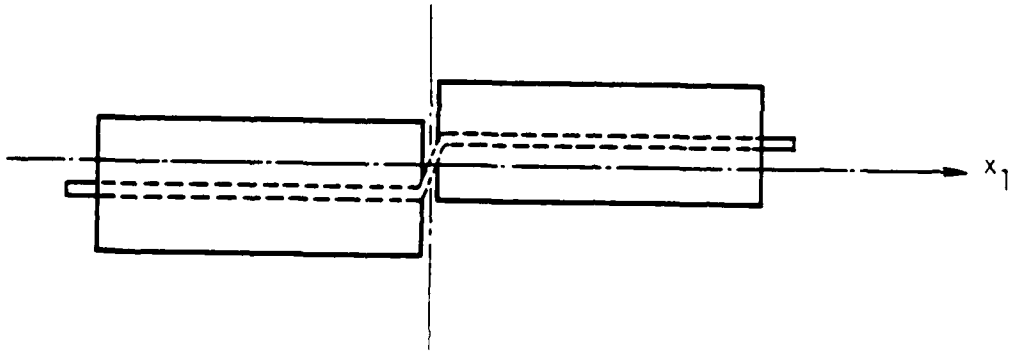

(b) After deformation.

Figure 3.32. A dowel action test simulation.

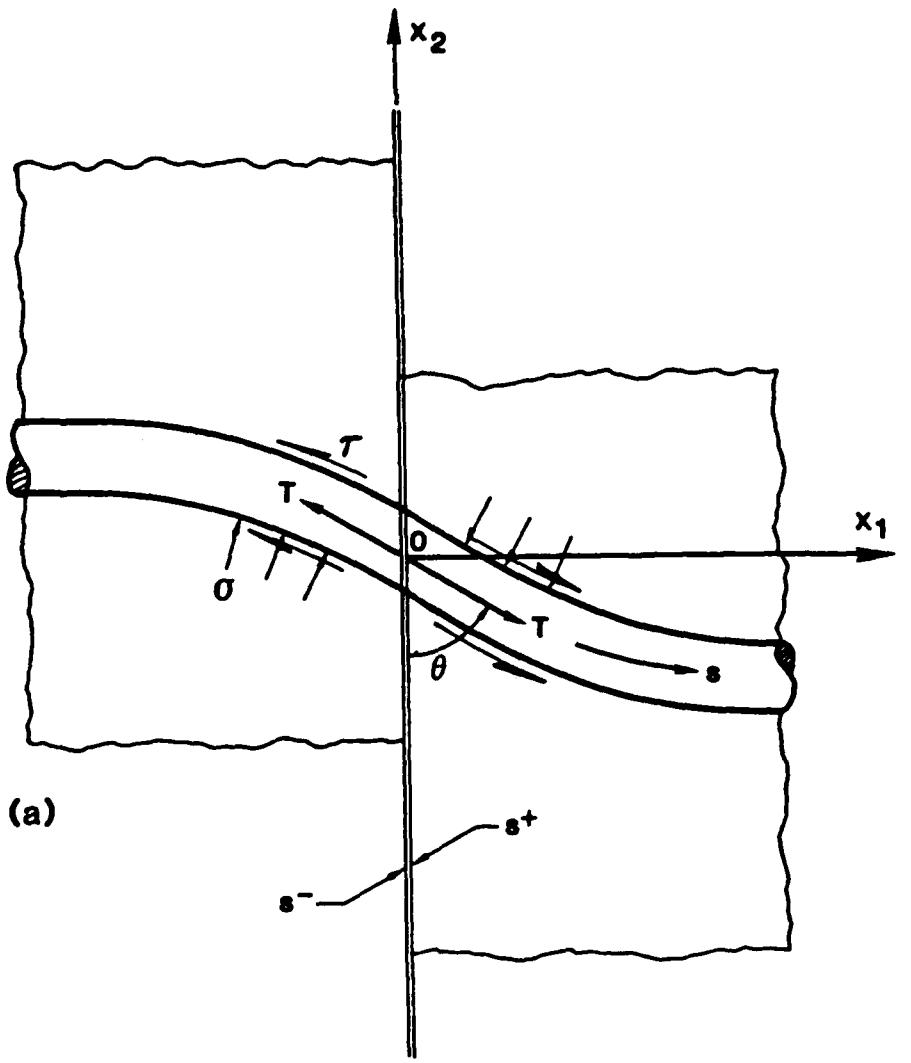

Figure 3.33. Local geometry.

where for $f < 0$ or $f = 0$ and $\dot{f} < 0$.

$$C_{11} = n^{(1)}E^{(1)}A,\ C_{12} = 0,\ C_{22} = n^{(1)}\mu^{(1)}A,\ C_{33} = E^{(1)}I^{(1)} \tag{3-35}$$

where E, μ denote Young's modulus and the shear modulus, respectively, and for $f = 0$ and $\dot{f} = 0$.

$$C_{11} = \left[\frac{E^{(1)}H}{E^{(1)} + H}\right]n^{(1)}A \quad , \quad C_{12} = -3\left[\frac{\mu^{(1)}}{E^{(1)} + H}\right]\frac{N_{12}^{(1p)}}{\sigma_y} \quad ,$$

$$C_{22} = n^{(1)}\mu^{(1)}A \quad , \quad C_{33} = \left[\frac{E^{(1)}H}{E^{(1)} + H}\right]I^{(1)} \quad . \tag{3-36}$$

Here

$$f = \left|N_{11}^{(1p)}\right| - \sigma_y \quad . \tag{3-37}$$

(c) Interaction Constitutive

$$\dot{P}_i = \beta_i[\dot{u}^i] \quad \text{for } |P_i| \leq (P_i)_y \tag{3-38a}$$

$$(i = 1,2;\ \text{no sum on } i)$$

$$P_i = \beta_i^{ep}[\dot{u}^i] \quad \text{for } |P_i| > (P_i)_y \ , \tag{3-38b}$$

where

$$\beta^{ep} = \beta_i\left[1 - \frac{\beta_i}{\beta_i + H_i}\right] \ , \tag{3-38c}$$

$$[u^1] \equiv \left[U_1^{(1)}\right], \quad [u^2] \equiv \left[U_2^{(1)}\right] + U_{2,1}^{(1)}\left[U_1^{(1)}\right] \tag{3-38d}$$

In the above, $N_{ij}^{(1p)}$ is the partial stress associated with the steel. A represents the "cell" area. P_i is the interaction body force in the *ith* direction. $M_{11}^{(1p)}$ is a weighted stress average. $E^{(1)}$ and $\mu^{(1)}$ denote Young's modulus and the shear modulus of the steel. H and H_i are hardening parameters, and S_1 is a displacement-type

variable. An assumption of moderate rotations of the steel is implicit in these relations.

(d) Boundary Conditions:

For the case of a smooth, lubricated crack interface, the appropriate boundary conditions are

$$N_{11}^{(1p)} = 0,\ N_{12}^{(1p)} = 0,\ M_{11}^{(1p)} = 0 \text{ at } x_1 = \pm \ell\ . \tag{3-39}$$

(e) Forcing Functions

The "forcing functions" of the problem are

$$[U_1] = -\ U_1^{(1)},\ [U_2] = (\text{sgn}(x_2))\frac{\Delta}{2} - U_2^{(1)} \tag{3-40}$$

where the offset Δ is prescribed.

The relations (3-39) above exclude interface shear transfer (IST). An elementary procedure for inclusion of IST is as follows: First, (3-31)-(3-40) are solved incrementally for $U_i^{(1)}$ and $T_i^{(1a)}$ at $x_1 = 0$ where $T_i^{(1a)} = N_{11}^{(1a)}$, $T_2^{(1a)} = N_{12}^{(1)} + U_{2,1}^{(1)} N_{11}^{(1)}$. Second, an effective normal stress $p = p_o + (T_1^{(1a)}/A)$ is defined on the crack face at $x_1 = 0$ where p_o is a confining pressure (see Figure 3.33) which is part of the test set-up for combined dowel action (DA) and IST experiments. Third, the effective normal stress p is applied to the concrete interface at $x_1 = 0$ and an IST law is postulated in the form $f(T_2^{(2a)}, p, \Delta) = 0$ and this relation is solved for $T_2^{(2a)}$ for a specified p and Δ. This latter quantity reflects IST. According to this procedure, IST influences the total effective shear stress, τ across $x_1 = 0$ but does not alter the DA contributions, $T_2^{(1a)}$. Here

$$\tau \equiv \left(T_2^{(1a)} + T_2^{(2a)}\right) \Big/ A \tag{3-41}$$

(1) <u>Monotonic Deformation</u>.

Let us now examine the simulation capability of the foregoing model for monotonic deformation. The first case to be considered is a simulation of the lubricated monotonic dowel tests by Paulay, Park and Phillips (1974). The test set-up and specimen are illustrated in Figures 3.34 and 3.35. Wax was used to lubricate

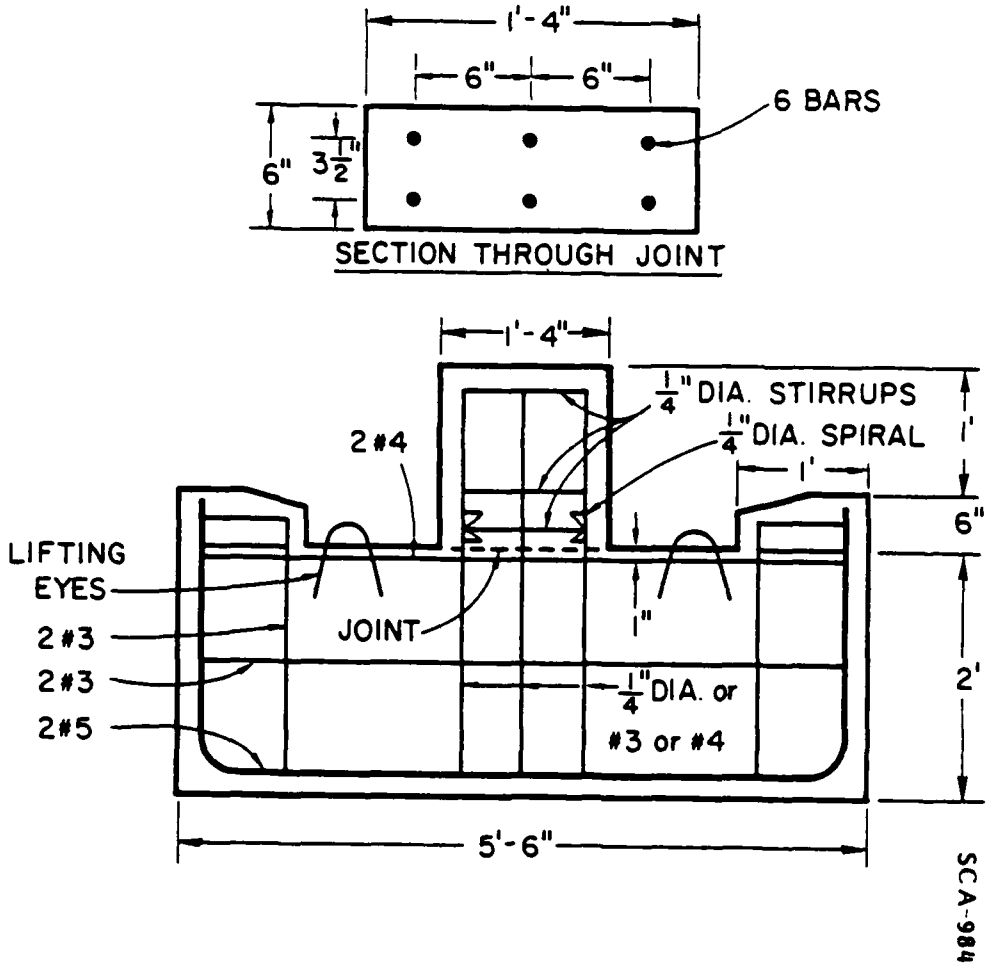

Figure 3.34. Test specimens by Paulay, *et al.* (1974).

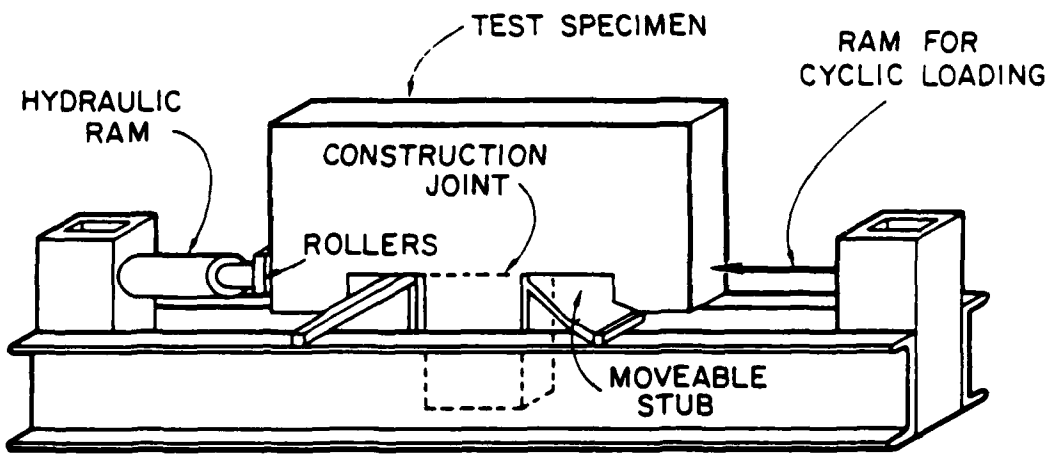

Figure 3.35. Test set up by Paulay, *et al.*, (1974).

the joint surface. Comparisons of theoretical and experimental results are shown in Figure 3.36 for three different steel volume fractions. Agreement is observed to be good. The "shear stress" in Figure 3.36 is based on (3-41) with $T_2^{(2a)} = 0$. Simulation of the test, which approximates pure DA, was performed using (3-31)-(3-40) and an appropriate incremental numerical procedure. The model parameters employed in the simulation are given in Table 3-1. The forms of the interaction terms used are depicted in Figures 3.37 and 3.38.

The second case to be considered includes IST; the tests were performed by Paulay, Park and Phillips (1974) using the test set-up and the test specimens (of different joint surface preparation) depicted in Figures 3.34 and 3.35. Figure 3.39 shows comparisons of experimental data and simulations for several different interface conditions. For simulation purposes, an IST relation of the form

$$\frac{1}{T_2^{(2a)}}(\Delta)/A = \left\{\tau_{max} - \tau_\infty\left(1 - e^{-\gamma}\right)\right\}\frac{\Delta}{\Delta_y}\exp\frac{1}{\beta}\left\{1 - \left(\frac{\Delta}{\Delta_y}\right)^{\beta}\right\} + \tau_\infty\left\{1 - \exp\left[-\gamma\frac{\Delta}{\Delta_y}\right]\right\} \quad . \tag{3-42}$$

was adopted. The model parameters used in the simulation are given in Table 3-2. Agreement between simulations and test data is observed to be excellent.

Another case of interest concerns the data produced by Karagozian and Case (1973). In these experiments the maximum slip Δ was much larger than that associated with the aforementioned tests. The test set-up and the specimens used are depicted in Figures 3.40 and 3.41. In order to include the effect of confining pressure p on the IST relation, τ_{max} and τ_∞ are expressed as:

$$\begin{aligned} \tau_{max} &= 979 + 1.53\ p\ (psi) \\ \tau_\infty &= 76 + 0.84\ p\ (psi). \end{aligned} \tag{3-43}$$

The remaining model parameters employed for simulation purposes are given in Table 3-3. comparisons between simulations and test results are illustrated in Figure 3.42 for a range of confining pressures. Agreement between predictions and experimental data is observed to be reasonable.

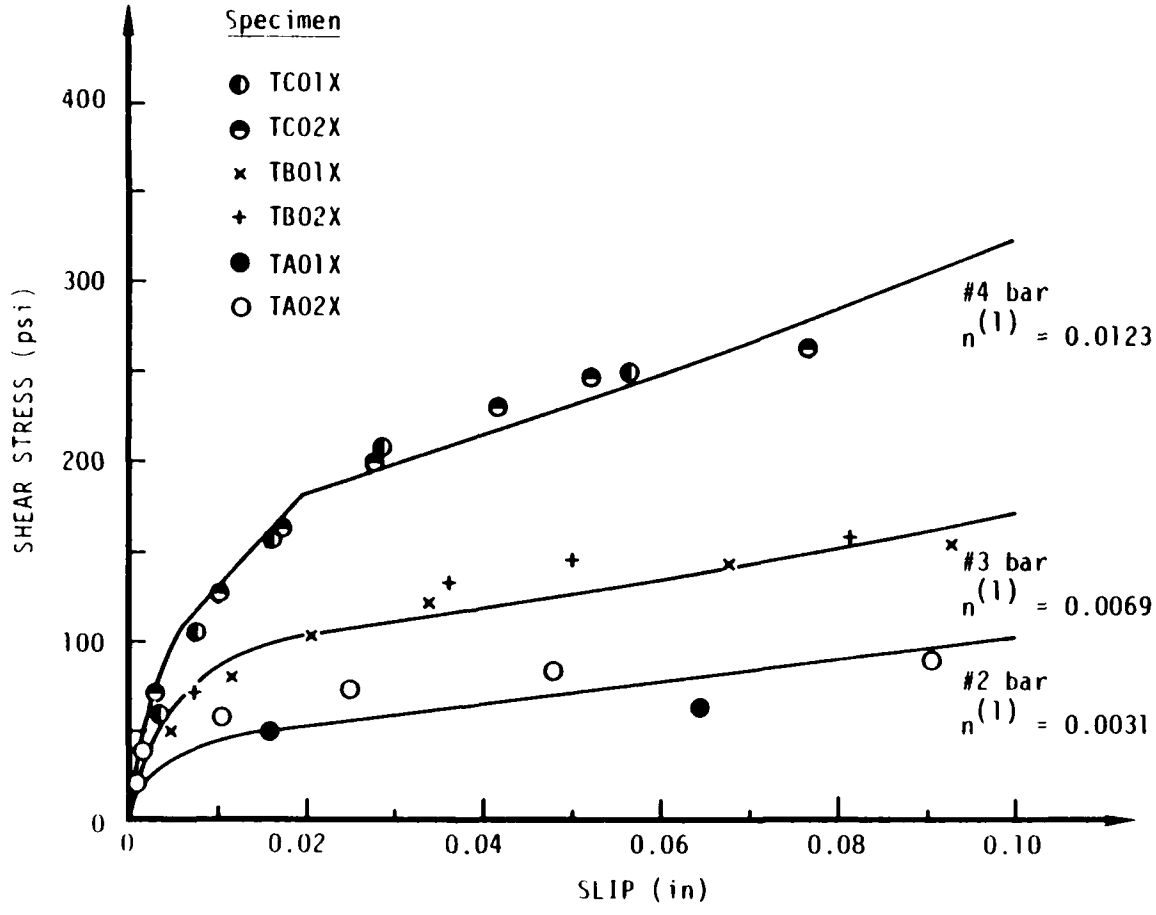

Figure 3.36.. Comparison of Paulay load-slip data with simulations.

TABLE 3-1
PARAMETERS USED IN SIMULATION OF DOWEL TESTS
Paulay, Park, and Phillips

Parameters / Specimens	n[1]	A in^2	β_1 psi	$(P_1)_y$ lb/in	H_1 psi	β_2 psi	$(P_2)\gamma$ lb/in	H_2 psi	ℓ in.
TA01,02	0.0031	16	2.11×10^6	1850	2×10^5	2.48×10^6	1700	1.2×10^5	2.4
TB01,02	0.0069	16	2.57×10^6	2770	2×10^5	2.91×10^6	2350	1.2×10^5	4
TC01,02	0.0123	16	3.03×10^6	3700	2×10^5	3.31×10^6	2800	2.5×10^5	6

TABLE 3-2
PARAMETERS USED IN SIMULATION OF IST TESTS
Paulay, Park, and Phillips

Parameters Specimens	β	γ	Δ_y in.	τ_{max} psi	τ_∞ psi
Scabbled, SB01	2.0	4.5	0.03	700	540
Keyed, KB01	2.0	4.5	0.03	700	540
Trowelled Plus Criss-Crossed ZB01	2.0	4.5	0.024	580	480
Retarder, No Bond RB01X	2.0	4.5	0.026	460	380
Trowelled, TB01	2.0	4.5	0.008	320	275

TABLE 3-3
PARAMETERS USED IN SIMULATION OF TESTS
Karagozian and Case

$n^{(1)}$	A_2 in^2	$E^{(1)}$ psi	$\mu^{(1)}$ psi	σ_y psi	H psi	β_1 psi	$(P_1)_y$ lb/in.
0.0035	56.25	30×10^6	11×10^6	50×10^3	15×10^3	2.17×10^6	2350

H_1 psi	β_2 psi	$(P_2)_y$ lb/in.	H_2 psi	ℓ in.	Δy in.	β	γ
0.338×10^6	2.51×10^6	2500	0.1×10^6	4.0	0.065	4.0	4.5

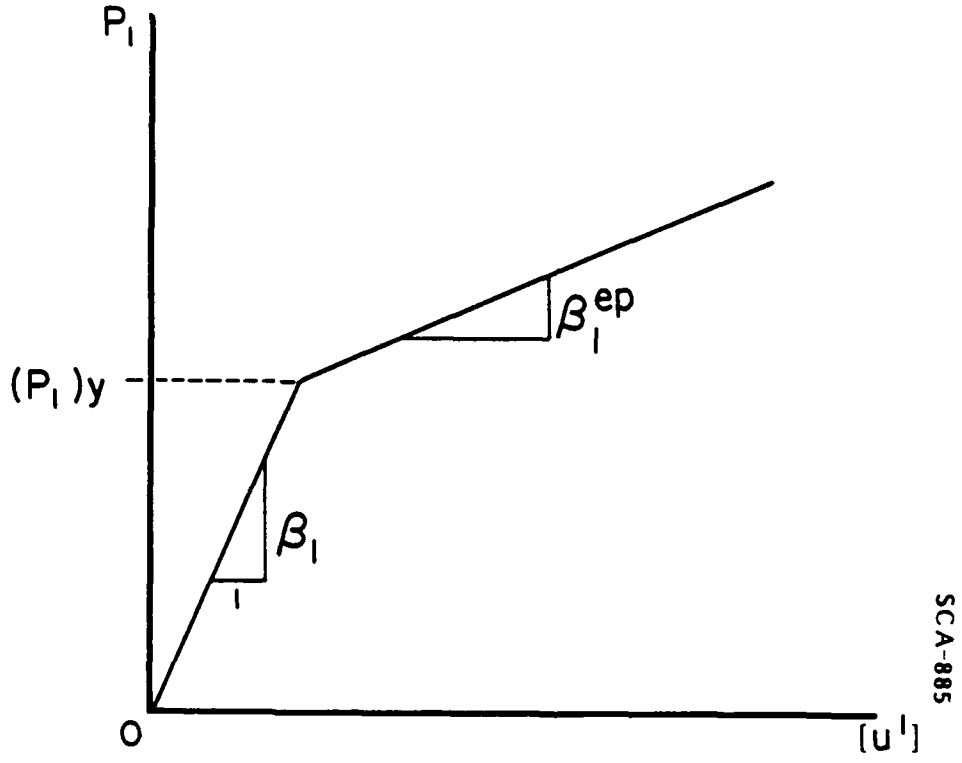

Figure 3.37. Interaction term P_1 for Paulay test.

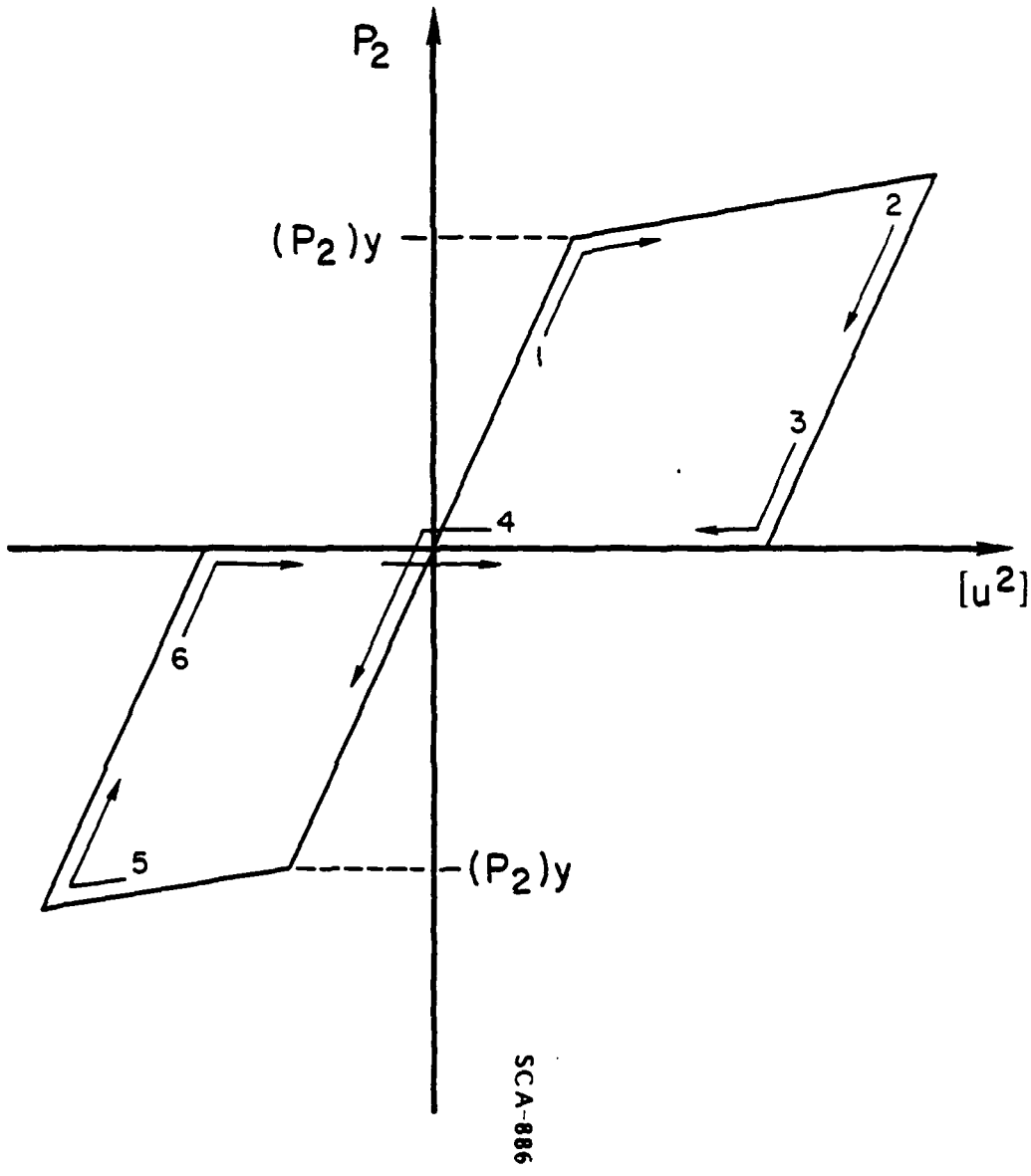

Figure 3.38. Interaction term P_2 for Paulay test.

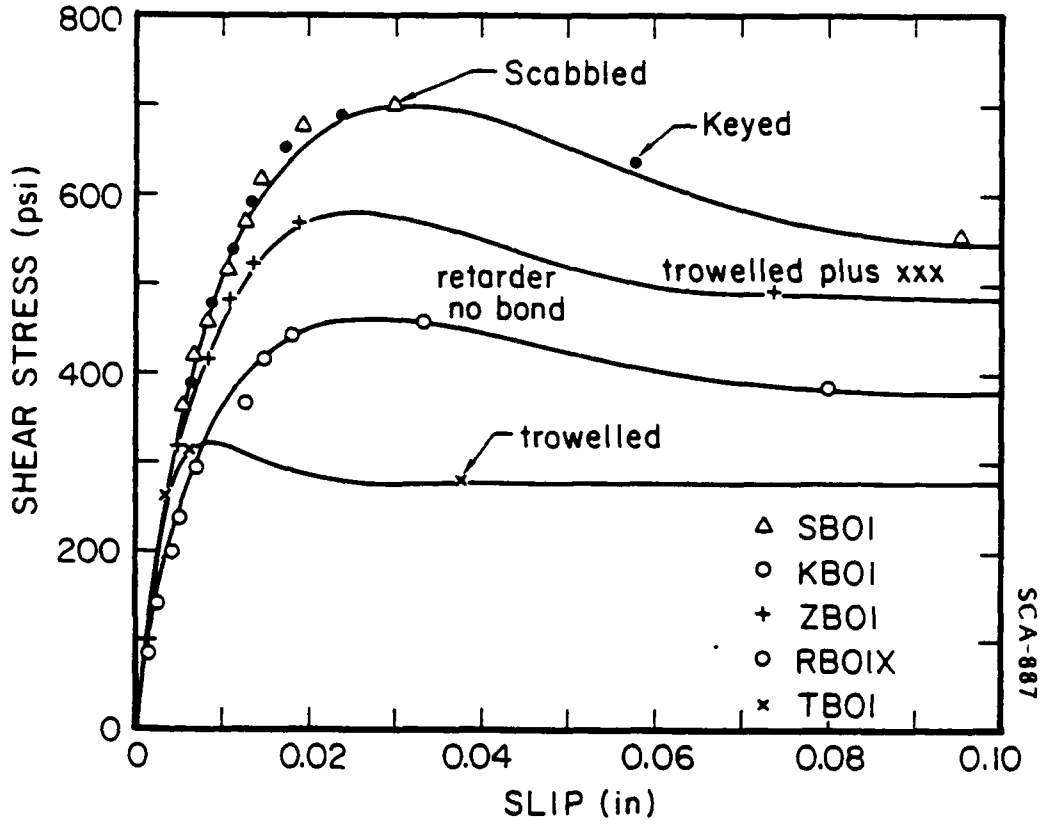

Figure 3.39. **Comparison of simulations and load-slip data for different surface conditions.**

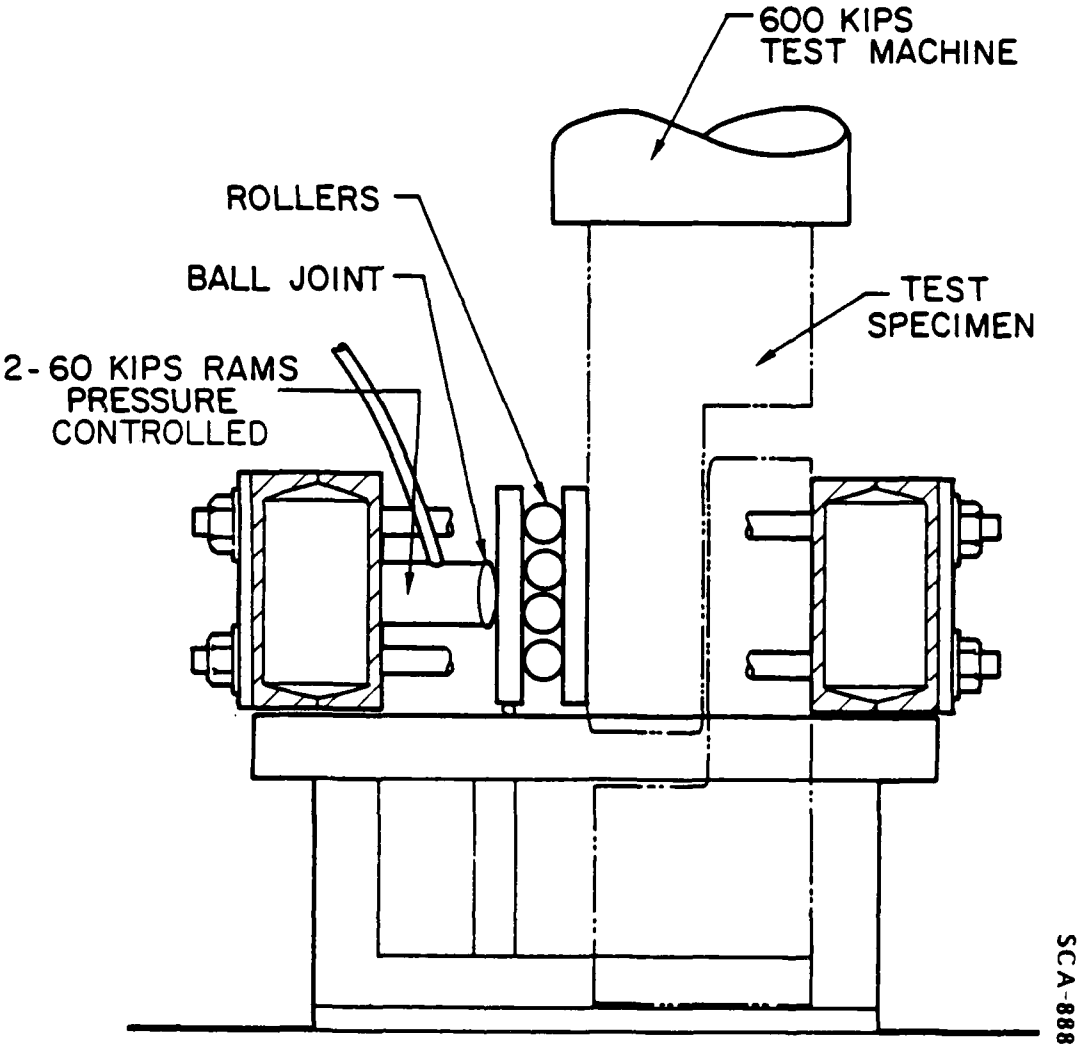

Figure 3.40. **Test set up used by Karagozian and Case (1973).**

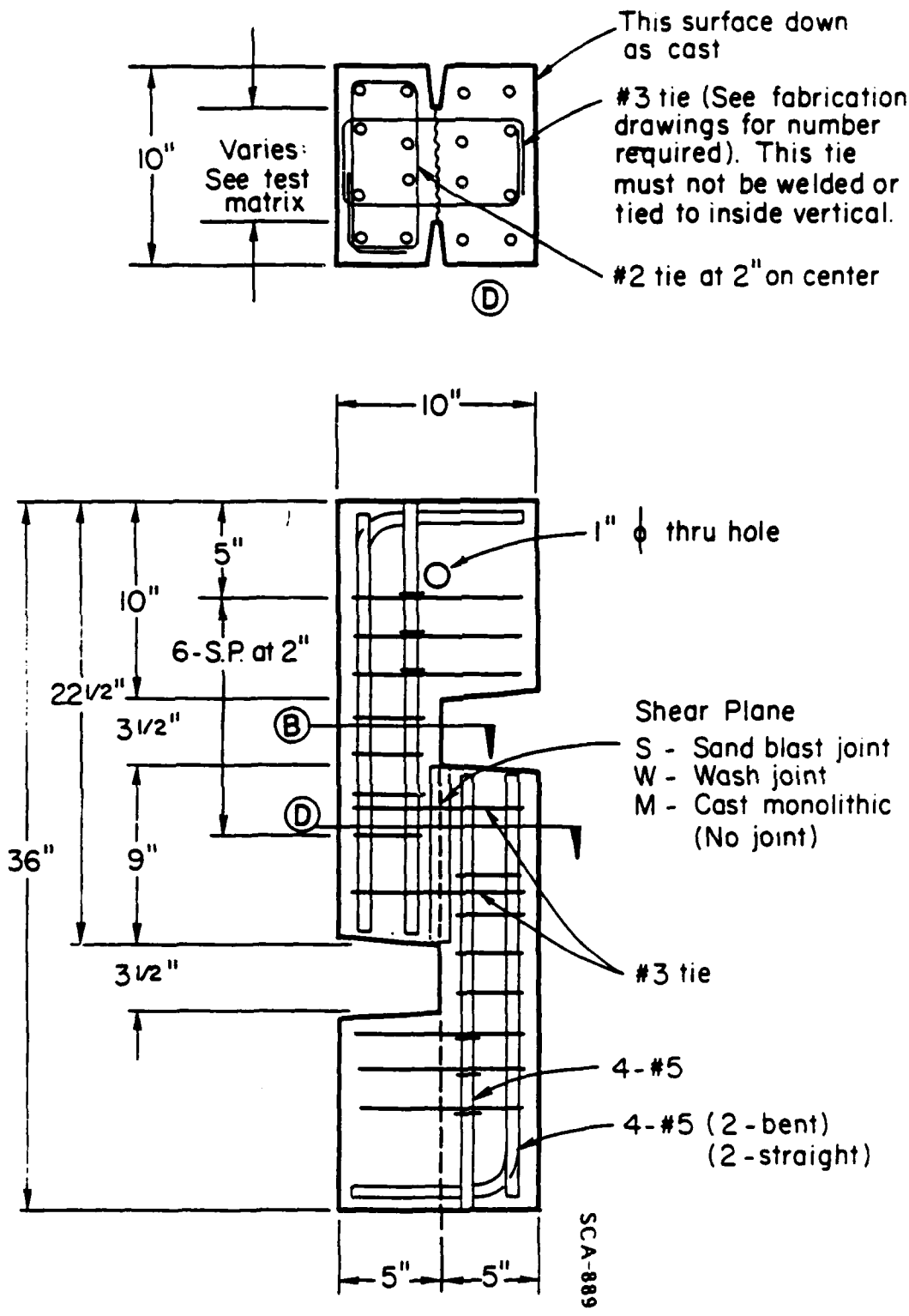

Figure 3.41. Test specimen used by Karagozian and Case (1973).

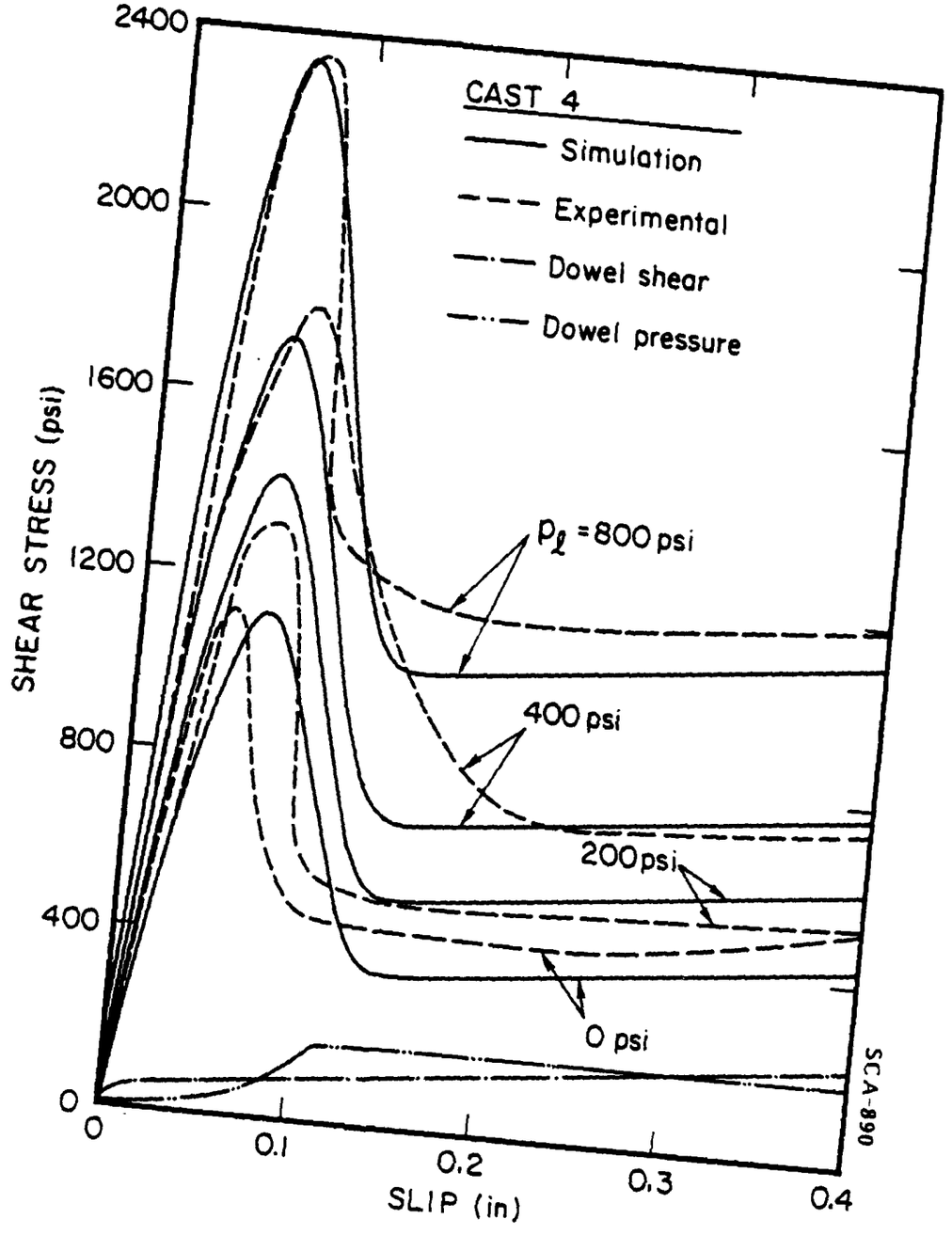

Figure 3.42. **Comparison between simulations and Karagozian test results.**

(3) **Hysteretic Deformation**.

A critical test of the model simulation capability is represented by hysteretic deformation. For validation purposes the experiments of Jimenez, Gergely and White (1978) were selected. The test set-up and specimen are illustrated in Figures 3.43 and 3.44. Thin brass sheets were used to lubricate the joint surface. A typical simulation versus experiment is shown in Figure 3.45. The agreement is observed to be good when one considers the complexity of the response. The model parameters employed in the simulation are provided in Table 3-4.

TABLE 3-4
PARAMETERS USED IN SIMULATION OF TESTS
Jimenez, Gergely, and White

Specimen	$n^{(1)}$	A_2 in^2	$E^{(1)}$ psi	$\mu^{(1)}$ psi	σ_y psi	H psi
DA-9A	0.0178	56.25	30×10^6	11×10^6	60×10^3	0.3×10^6

β_1 psi	β_2 psi	$(P_2)_y$ lb/in.	H_2 psi
3.41×10^6	3.57×10^6	4500	0.3×10^6

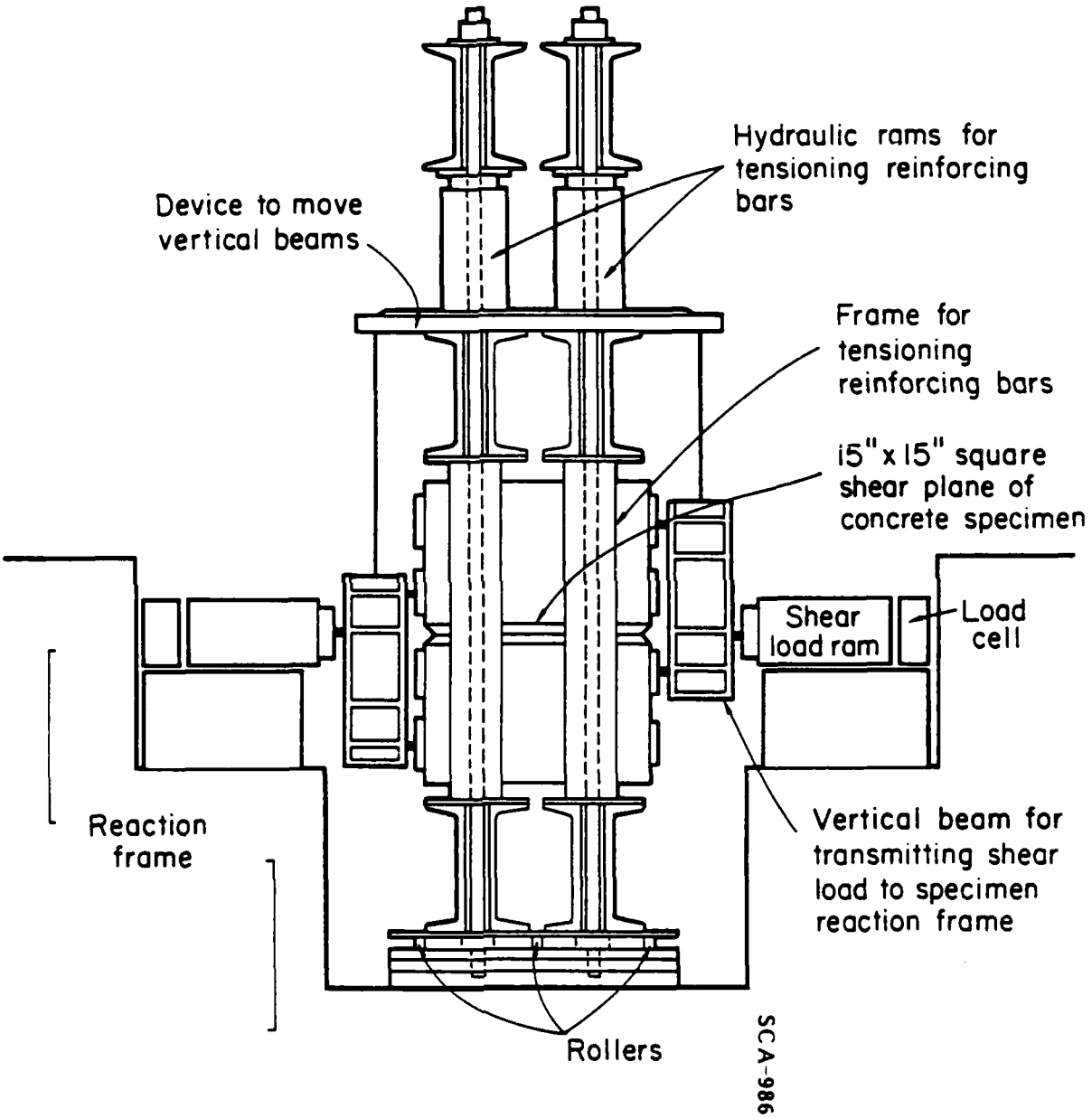

Figure 3.43. Test set up used by Jimenez, *et al.*, (1978).

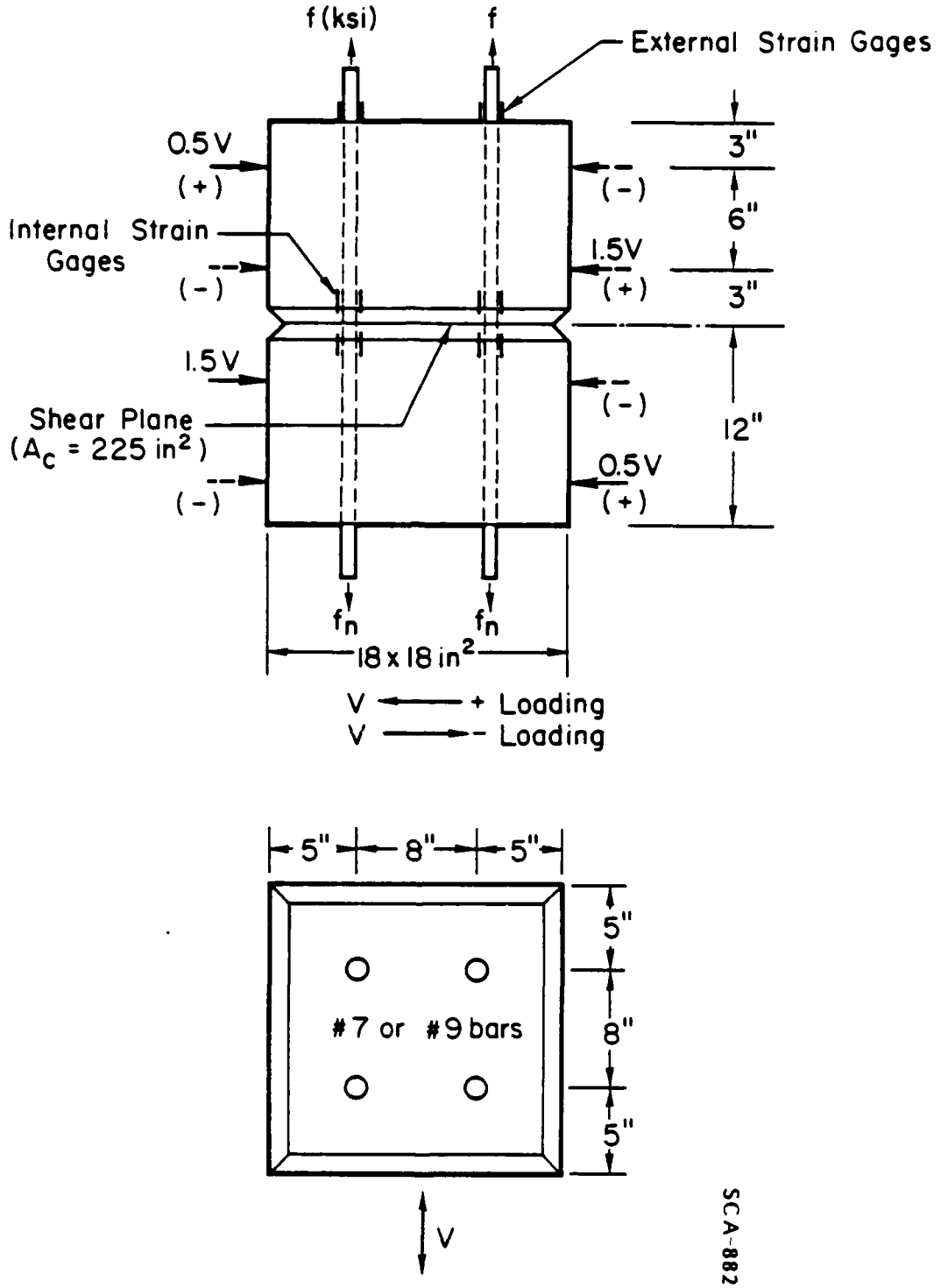

Figure 3.44. **Test specimen used by Jimenez, *et al.*, (1978).**

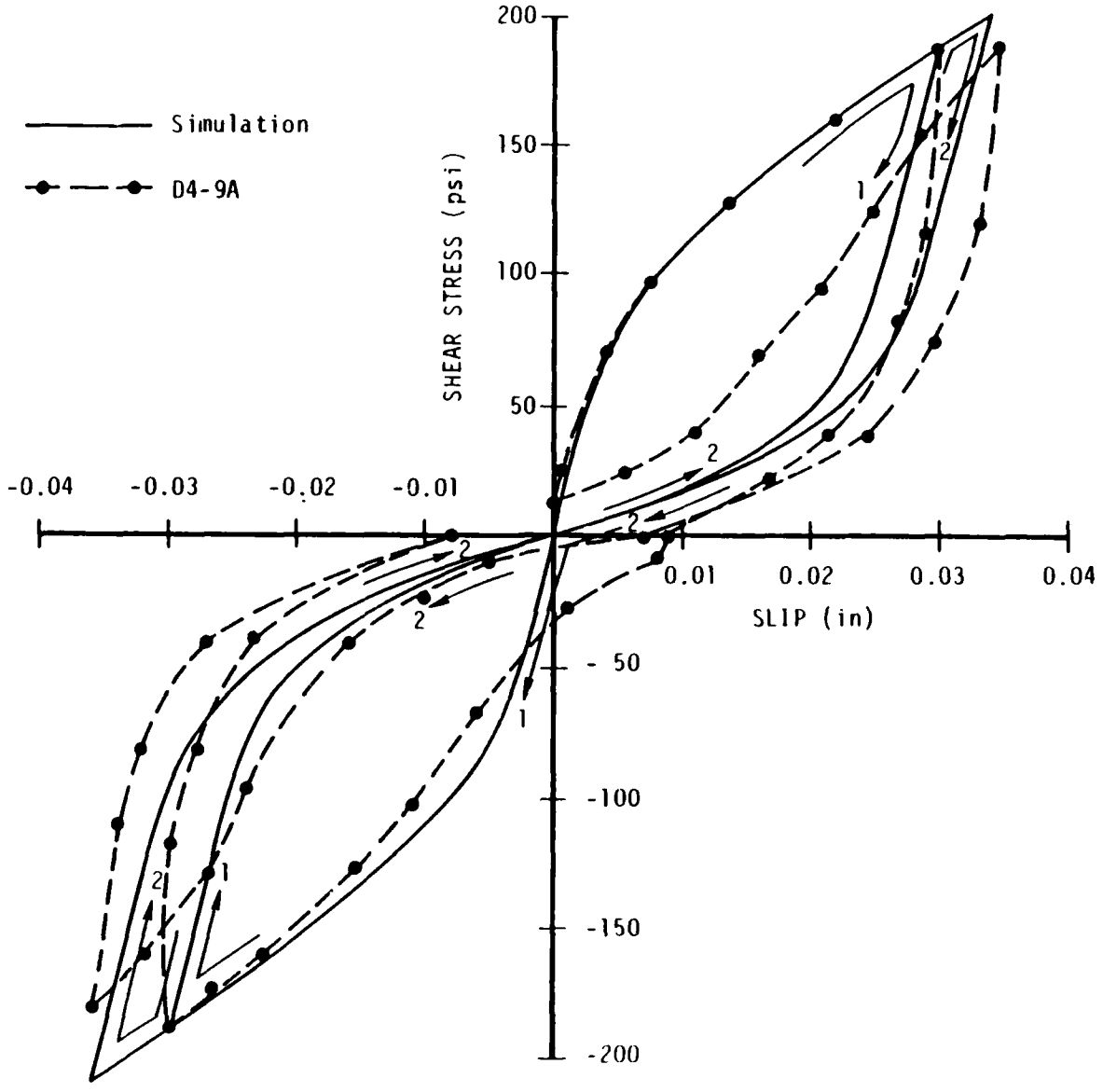

Figure 3.45. Hysteretic dowel action -- theoretical and experimental comparisons.

3.7 STUDIES IN PROGRESS.

A number of studies remained in progress as of the writing of this report. Two of the more important efforts are described below.

3.7.1 Biaxial Stress States.

The validation studies described previously were restricted with respect to the stress states (global) that were considered. For example, in the discussion of R/C under tension, the global stress state considered was uniaxial. Most practical problems, however, involve either global biaxial stress states (R/C plate) or global triaxial stress states (fully 3D R/C layout).

The models developed thus far are capable of simulating the response of R/C under either biaxial or triaxial conditions. In an effort to validate the theory for such cases, the problems depicted in Figures 3.46, 3.47 were considered. In all cases, the rebar layout is oblique to the global principal stress directions. In Figure 3.46(a) the objective was to understand how the rebar angle ϕ effects the global stiffness degradation as the crack field evolves. Figure 3.46(b) includes the effect of a second (compressive) principal global stress as well as ϕ. The problem depicted in Figure 3.47 is representative of a R/C shear wall with two extreme cases of boundary conditions.

In each of the foregoing cases, the intent was to compare simulations with laboratory data. For this reason, relevant test data on both model R/C and full-scale R/C tests have been collected. These data are currently under study.

3.7.2 Description of Concrete in Compression.

This subject matter concerns the behavior of reinforced concrete in compression. To model this behavior, it is necessary to adequately describe the plain concrete component in the mixture theory. This task was addressed in considerable detail. A complete presentation of the work is provided in Appendix J.

It is well known that the ductility of concrete increases as the mean compressive stress increases. The current approach followed by most investigators is to model this effect via a conventional elastic-plastic theory. However, substantial increases in global ductility of concrete are observed well below the brittle-ductile transition. Thus, it is unlikely that plastic flow is responsible for this effect. A more plausible explanation concerns "sliding" across distributed microcracks.

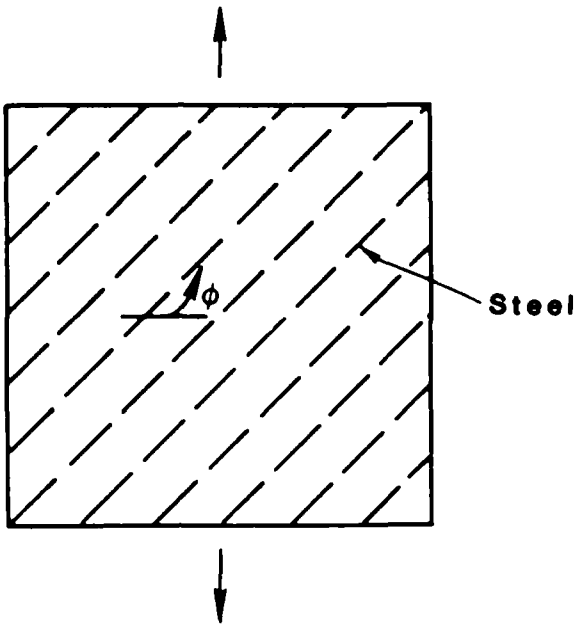

(a) Steel oblique to principal stress (uniaxial)

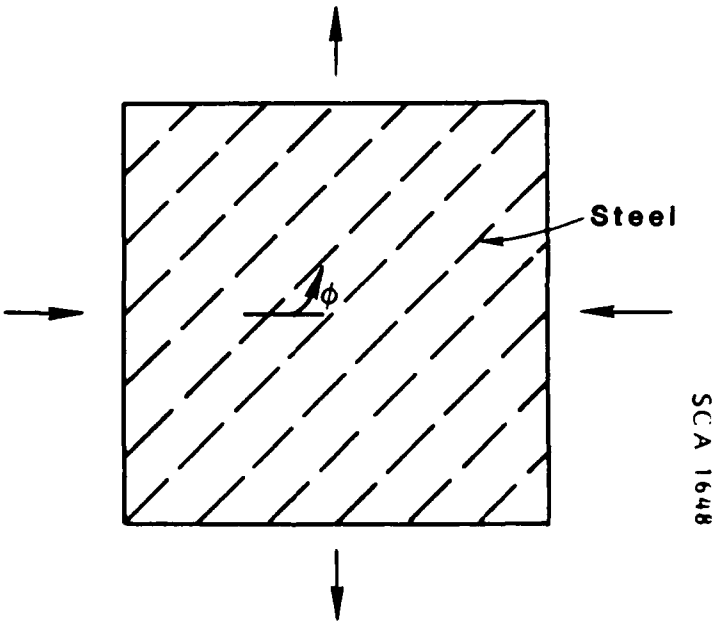

(b) Steel oblique to principal stress (biaxial)

Figure 3.46. Problems with steel oblique to principal stresses

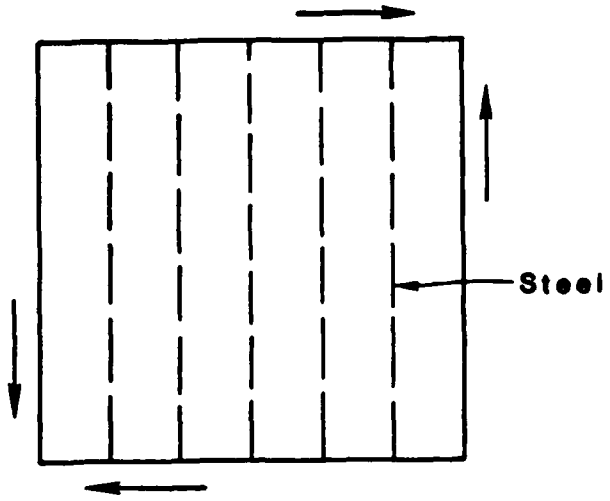

(a) R/C element (plate) subject to pure (macro) shear stress

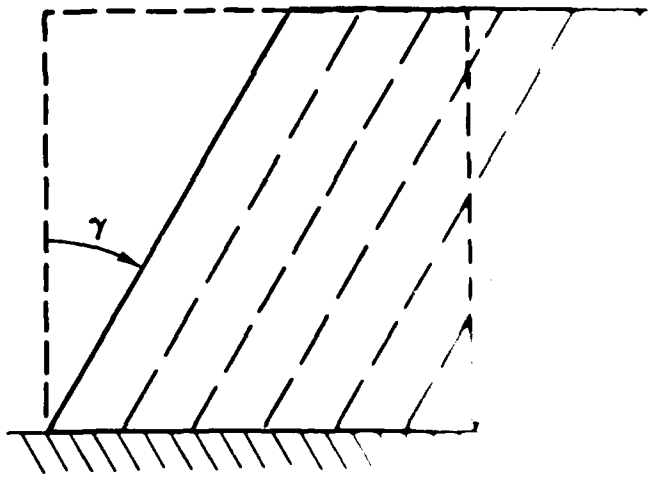

(b) R/C element (plate) subject to simple shear

Figure 3.47. Problems with steel orientation

AD-A187 337 DEVELOPMENT OF ADVANCEDCONSTITUTIVE MODELS FOR PLAIN AND REINFORCED CONCRETE(U) S-CUBED LA JOLLA CA G A HEGEMIER ET AL MAR 87 SSS-R-87-8454 2/3

UNCLASSIFIED AFOSR-TR-87-1391 F49620-84-C-0029 F/G 13/3 NL

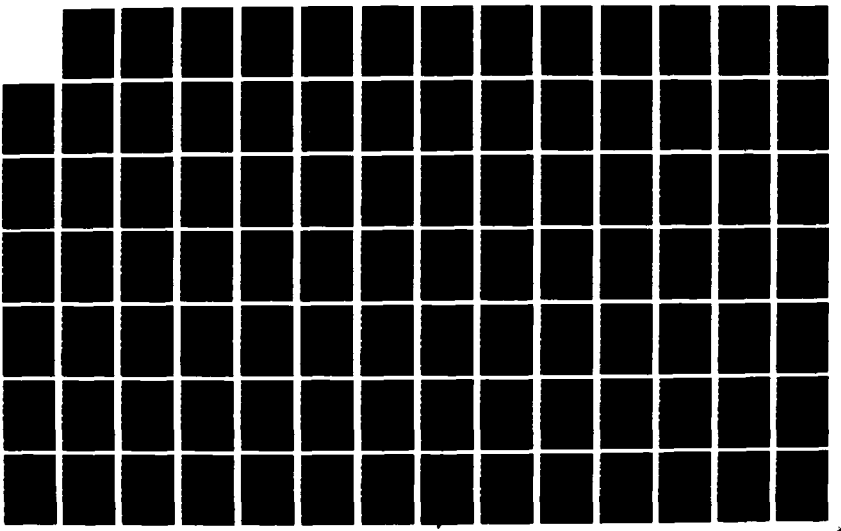

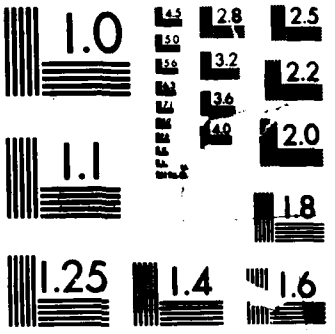

MICROCOPY RESOLUTION TEST CHART
NATIONAL BUREAU OF STANDARDS-1963-A

Recent analytical micromechanical studies appear to support the following view of the compression problem: under low confining stress microcracks tend to combine to form a single macrocrack or fault at failure; as the confinement is increased, the microcracks tend to form a distribution which resembles a slip system. Although final failure may again occur by faulting, relative sliding along such a system prior to faulting can lead to dramatic increases in ductility.

In an effort to incorporate the slip system premise, a new model of concrete was constructed. This model, the details of which are given in Appendix J, includes an arbitrary number of slip systems. It is planned to conduct validation studies to determine the simulation capability and accuracy of the theory during a future research period.

3.8 LIST OF REFERENCES FOR SECTION 3.

Murakami, H., and G. A. Hegemier (1986). "On Simulating Steel-Concrete Interaction in Reinforced Concrete. Part I: Theoretical Development," *Mechanics of Materials*, 5.

Hegemier, G. A., H. Murakami, and L. J. Hageman (1985). "On Tension Stiffening in Reinforced Concrete," *Mechanics of Materials*, 4, 161.

Hegemier, G. A., and H. Murakami (1985). "A Nonlinear Theory for Reinforced Concrete," *Proc. Second Symp. on Interaction of Non-Nuclear Munitions with Structures*, Panama City, Florida, April 15-18, p. 265.

Hegemier, G. A., H. Murakami and A. Maewal (1979). "On Construction of Mixture Theories for Composite Materials by the Method of Multivariable Asymptotic Expansions," *Proc. Third International Symp. on Continuum Models of Discrete Systems*, Freudenstadt, Germany.

Murakami, H., and G. A. Hegemier (1986b). "A Mixture Model for Unidirectionally Fiber-Reinforced Composites," *J. Appl. Mech.*, 53, p. 765.

Jimenez-Perez, R., P. Gergely and R. H. White (1978). "Shear Transfer Across Cracks in Reinforced Concrete," Report No. 78-4, Department of Structural Engineering, Cornell University, (NTIS PB-288 885/RC).

Karagozian and Case Structural Engineer (1973). "Construction Joint Test Program," Final Report for F04701-72-C-0358, submitted to Space and Missile Systems Organization, Air Force Systems Command, Norton Air Force Base, California.

Paulay, T., R. Park and M. H. Phillips (1974). "Horizontal Construction Joints in Cast-in-Place Reinforced Concrete," *ACI Special Publication, SP-42*, Vol. 2.

Hegemier, G. A., R. O. Nunn, and S. K. Arya (1978). "Behavior of Concrete Masonry Under Biaxial Stresses," *Proc. of North American Masonry Conference*, University of Colorado, Boulder, Colorado, August.

Mathey, R. G. and D. Watstein (1961), "Investigation of Bond in Beam and Pull-Out Specimens with High Yield Strength Deformed Bars," *ACI Journal*, 37, p. 1071.

Mirza, S. M. and J. Houde (1979), "Study of Bond Stress-Slip Relationship in Reinforced Concrete," *ACI Journal*, 76, p. 19.

Section 4

PLAIN CONCRETE

This section describes the research conducted on the theoretical description of the behavior of plain concrete. The discussion covers objectives, accomplishments, general mathematical forms and validation problems, which are intended to demonstrate the capability and accuracy of the models.

4.1 BASIC OBJECTIVES

The ultimate success of the mixture theory for reinforced concrete, discussed above, hinges very strongly on the ability of the constitutive model of plain concrete, used with the theory, to accurately describe the behavior of plain concrete over the wide range of response that can be expected in practice. Any deficiencies in the plain concrete model will surely be reflected -- and possibly enhanced -- when the model is used in conjunction with the mixture theory to describe reinforced concrete. Clearly, the accuracy of the mixture theory can never be greater than the accuracy of the plain concrete model used with it. Because of this, every effort should be made to develop an accurate model of plain concrete.

During the past ten years, considerable research has been devoted to understanding and modeling the constitutive behavior of plain concrete. From this has come a variety of different constitutive models for plain concrete which provide reasonably accurate descriptions of plain concrete behavior for stress paths which generally do not differ greatly from the standard paths followed in the usual laboratory testing. Largely, due to the lack of available appropriate data, little proof-testing of the models has been done to examine their predictive capabilities for complex stress or strain paths that are expected to occur in practice. Many of the models are limited to the stress range below failure, since they contain no provision for treating cracking. A few of the models do, however, attempt to treat cracking and post-cracking behavior as well. Generally speaking, however, the probems of developing a constitutive model of plain concrete capable of realistically describing the full spectrum of behavior from pre-cracking to cracking and finally post-cracking response still remains basically unresolved. The goal of the present research is to address this need.

4.2 ACCOMPLISHMENTS.

A new constitutive model of plain concrete was developed and validated with remarkable success against a variety of proof tests. The model is based on the endochronic theory of plasticity and exhibits the important features of nonlinear

concrete behavior for stress states below failure. Details of the model, together with example validations, are given in Section 4.3. An approach for extending the model to encompass cracking and post-cracking behavior has recently been made by Valanis (1987). This approach will be the basis of our future work to develop an *endochronic plastic fracturing model of plain concrete.*

In the course of exploring various approaches for mathematically representing cracking in plain concrete, a new continuous damage model was developed which has certain advantages, some of which are not found in other models. Details and features of the model are described in Section 4.4 and more fully in Appendix A. A number of examples are given to illustrate the various features of this new model.

In view of the Air Force's interest in the shock loading of concrete defense structures, and the need in design studies for a rate-dependent constitutive model of plain concrete, a comprehensive review of strain rate effects in plain concretes was conducted. The review focussed mainly on experimental issues related to strain rate testing and on the extent to which the data can be trusted. These issues are discussed in Section 4.

Finally, certain fundamental issues concerning the experimental basis for constitutive models for brittle materials have been explored and are discussed in Section 4.6. Problems related to standard quasi-static laboratory testing methods are treated. Included are the topics of strain softening, strain hardening, failure states and failure modes.

In those cases where the research accomplishments have been reported in detail in the published literature, only the main results are summarized here. The interested reader is referred to the appropriate papers for further details. The references for this section are listed at the end of the section.

4.3 A NEW CONSTITUTIVE MODEL FOR PLAIN CONCRETE

A new constitutive model of plain concrete was developed by Valanis and Read (1985,1986) which appears to have remarkable capabilities for predicting the nonlinear inelastic behavior of concrete for stress states below failure. The model is formulated on the basis of the endochronic theory of plasticity and, as such, does not require a yield surface nor the specification of loading or unloading criteria, as in classical

plasticity. It predicts that plastic flow will occur from the onset of loading, a feature which makes the model attractive and appropriate for describing the behavior of a material such as concrete which does not exhibit a well-defined yield point. Basically, the model is isotropic, rate-independent and satisfies the Clausius-Duhem dissipation inequality. It realistically portrays the major features of nonlinear inelastic behavior exhibited by plain concrete, including shear-volumetric coupling, effect of hydrostatic compression on shear response, hardening, hysteresis and stress-path dependence. For the case of isothermal deformation, the governing equations of the new model are as follows:

$$\underset{\sim}{s} = \int_0^{z_s} \rho(z_s - z') \frac{d\underset{\sim}{e}^p}{dz'} \, dz' \quad , \tag{4-1}$$

$$\sigma = \int_0^{z_H} \phi(z_H - z') \frac{d\epsilon^p}{dz'} \, dz' \quad , \tag{4-2}$$

$$d\underset{\sim}{e}^p = d\underset{\sim}{e} - d\underset{\sim}{s}/2\mu \quad , \tag{4-3}$$

$$d\epsilon^p = d\epsilon - d\sigma/K \quad , \tag{4-4}$$

$$dz^2 = \left|\left| d\underset{\sim}{e}^p \right|\right|^2 + k^2 |d\epsilon^p|^2 \quad , \tag{4-5}$$

$$dz_s = dz/F_s \quad , \quad dz_H = dz/kF_H \quad . \tag{4-6a,b}$$

Here $\underset{\sim}{s}$ denotes the deviatoric stress tensor, σ is the hydrostatic stress (pressure). $\underset{\sim}{e}^p$ represents the plastic component of the deviatoric strain tensor $\underset{\sim}{e}$, while ϵ^p is the plastic component of the volumetric strain ϵ. Moreover, μ and K are, respectively, the shear and bulk moduli, while k is a constant which determines the magnitude of shear-volumetric coupling. The double bars surrounding a symbol denote its norm, while single bars denote absolute value. Furthermore, F_s and F_H are, respectively, shear and hydrostatic hardening functions. In addition, z denotes the intrinsic time scale, while z_s and z_H are, respectively, the intrinsic times for shear and hydrostatic

behavior. Finally, $\rho(z)$ and $\phi(z)$ are weakly singular kernel functions satisfying the condition $\rho(0) = \phi(0) = \infty$, but integrable in the domain $0 \leq < \infty$.

The weakly singular nature of the kernel functions is a crucial feature of the model for two reasons:

(1) It provides for closure of hysteresis loops in the uniaxial or shear stress-strain space, however small they may be, and
(2) it ensures that, at points of unloading or reloading, the response is always elastic.

The specific forms of the kernel functions used in the present model are:

$$\rho(z_s) = \sum_r A_r e^{-\alpha_r z_s} , \tag{4-7}$$

$$\phi(z_H) = \sum_r B_r e^{-\beta_r z_H} ,$$

where the constants A_r, B_r, α_r, and β_r are all positive and finite. With such forms, it can be shown (Valanis and Read, 1984) that each of the hereditary integrals in (1) and (2) is reducible to a system of coupled linear ordinary differential equations; this greatly simplifies the computational strategy for dealing with the model.

The function F_H reflects the effect of compaction on hydrostatic behavior and therefore is taken to depend on the plastic volumetric strain, ϵ^p. The function F_s, on the other hand, accounts for the effect of hydrostatic pressure on shear response and failure, as well as the form of the trace of the failure surface in the π-plane. Generally speaking, F_s will depend on both σ and the third invariant of the deviatoric stress tensor, J_3'. In the present study, however, where the behavior of concrete for stress histories that do not produce significant macrocracking is considered, the model predictions are not likely to be sensitive to the fine details of the trace of the failure surface in the π-plane; this follows from the fact that the response regime of interest is not in the close proximity of the failure surface. Therefore, to simplify the model, F_s is taken to depend only on σ.*

---

* An extension of the model to include the effect of J_3 on failure is discussed in Appendix B.

It should be noted that the endochronic model described above is very different from previous endochronic models of concrete developed by Bazant and Bhat (1976) and Bazant and Shieh (1978) on the basis of earlier versions of endochronic theory. In the model discussed here, proper closure of hysteresis loops is guaranteed, and the instantaneous response at points where loading, unloading and reloading begin is elastic. The basic plastic flow properties of the model have been explored recently by Trangenstein and Read (1982) and Murakami and Read (1986;1987).

The foregoing endochronic model was applied to an extensive set of laboratory data recently generated by the University of Colorado, using a true triaxial device (Scavuzzo, *et al.*, 1983). The test program consisted of six different series of stress-controlled tests, each of which was designed to explore a different facet of concrete behavior. Altogether, the response of concrete to over 45 complex stress paths was investigated. In all cases, the stress paths were such that no significant cracking took place during the tests.

The model was fit to a very small subset of the data, after which it was proof-tested by exercising it around over 20 complex stress paths and predicting the corresponding deformation histories. None of the data from the complex stress path tests selected for proof-testing were used in fitting the model parameters and no optimization-techniques were employed.

The proof-tests were remarkably successful and revealed the powerful predictive capability of the model. Figures 4.1 to 4.4, for example, illustrate the results of the proof-tests for four of the many complex stress paths considered. The imposed stress paths are depicted at the top of each figure. It is seen that the comparisons between the model predictions and the measurements are excellent, considering the relatively large data scatter normally expected with concrete. The ability of the model to accurately describe the behavior of plain concrete around the complex stress paths not used in fitting the model reveal its remarkable predictive capabilities. Various other examples of the proof-tests can be found in the papers by Valanis and Read (1985,1986).

The above endochronic model has several limitations which restrict its application to stress states below failure. First, the model does not have the capability to describe macrocracking and its effect on material behavior. Secondly, since the model

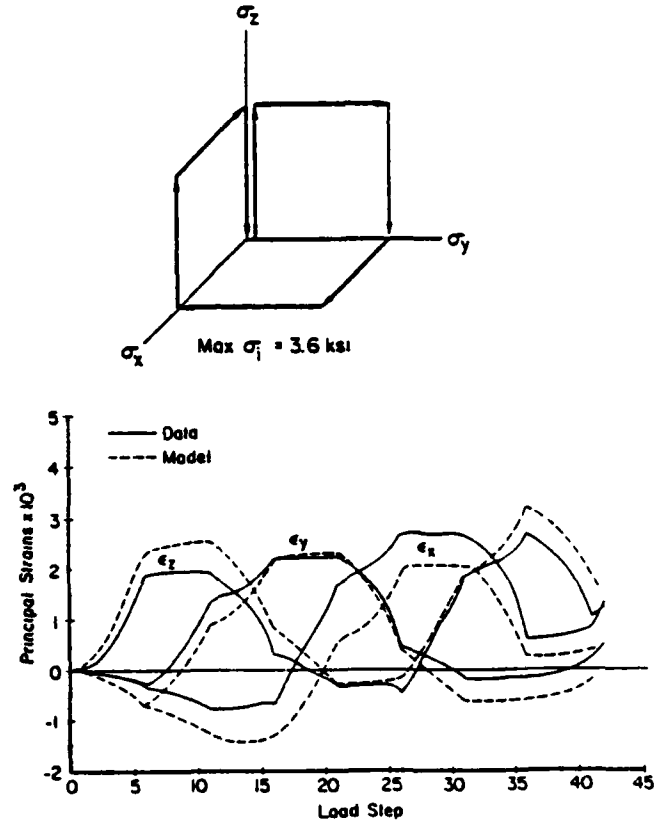

Figure 4.1 **Measured and predicted responses for complex stress path shown.**

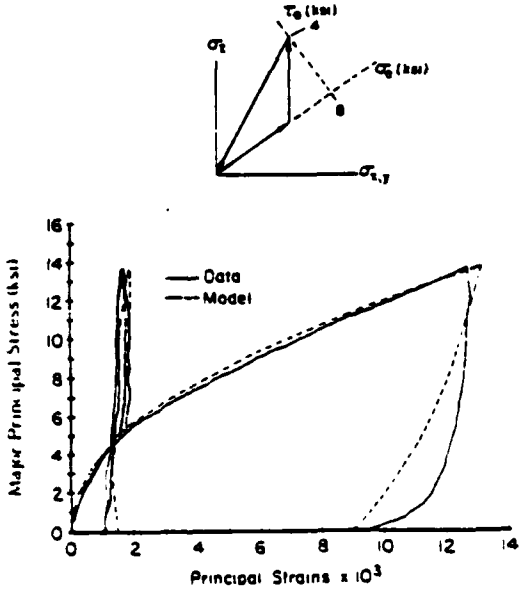

Figure 4.2. **Measured and predicted responses for complex stress path shown.**

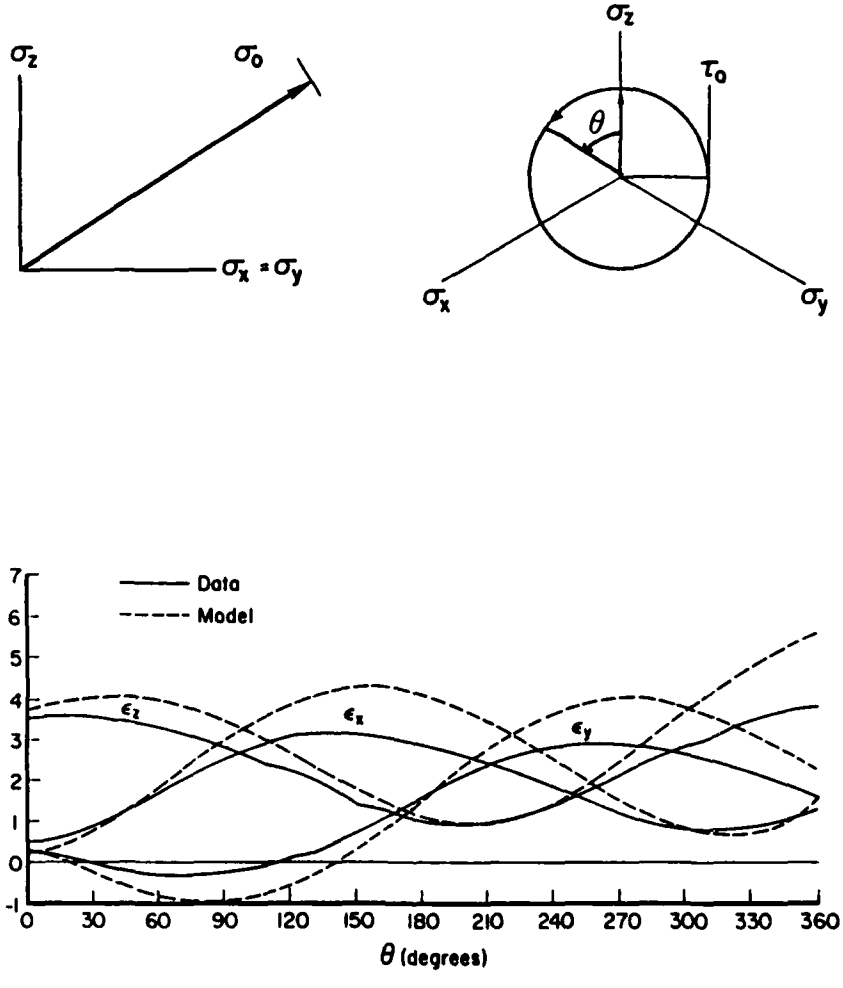

Figure 4.3 **Measured and predicted responses for circular stress path in the π-plane.**

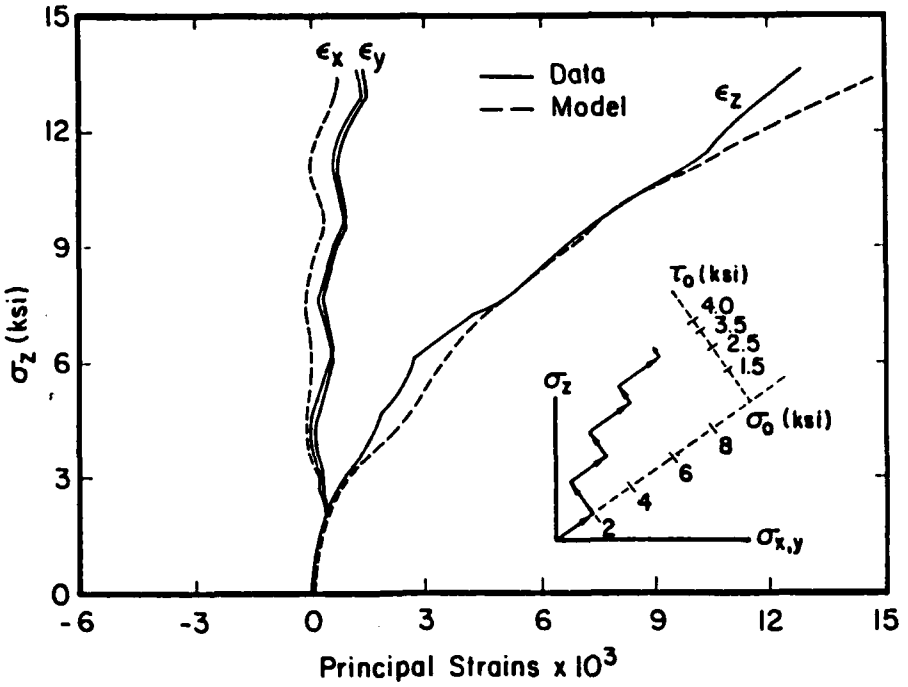

(a) Major principal stress σ_z versus principal strains. Insert depicts prescribed stress path.

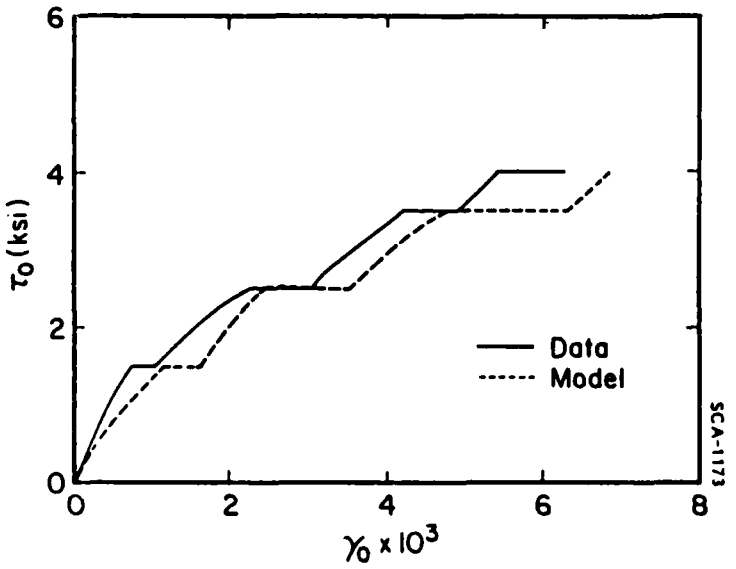

(b) Octahedral shear stress versus octahedral shear strain.

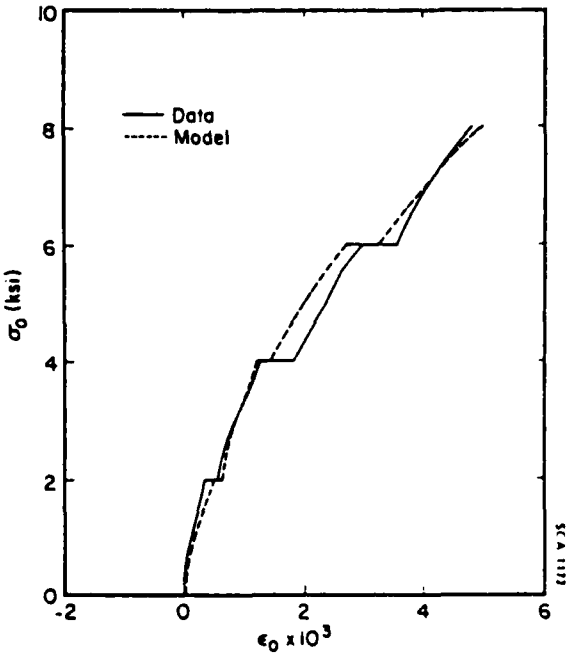

(c) Hydrostatic response.

Figure 4.4 Comparison between predicted and measured responses to prescribed complex stress path.

is isotropic, it cannot account for the anisotropy that can be expected to develop when significant macrocracking with preferred orientation occurs. Finally, when there is shearing in the presence of a fixed hydrostatic pressure, the model exhibits only compaction. Therefore, dilatant behavior usually observed when cracked material is sheared cannot be described by this model.

Recently, however, Valanis (1987) has developed an approach for generalizing the endochronic concrete model which overcomes all of the above limitations. By using a mapping between undamaged and damaged material, he found the form taken by the endochronic concrete model in the presence of cracking. This new model has been termed the endochronic plastic fracturing model (Valanis, 1987). The effect of cracking is reflected through a second order integrity tensor ϕ, which is governed by an evolution equation that relates the cracking to the tensile strain history. The plasticity of the non-cracked material is described by the endochronic concrete model. The resulting model appears to have the desired features for describing the full gamut of concrete behavior, including plastic flow and cracking. It exhibits anisotropy if cracking develops in preferred directions, as well as dilatancy during cracking. The anisotropy is accounted for in a clever way through the use of the second-order tensor ϕ, rather than by a fourth-order tensor, as is the usual approach. The use of a second-order tensor for this purpose greatly reduces the analytic complexity of the model and simplifies the experimental determination of the material parameters. Crack initiation and growth are governed by the evolution equation for ϕ. In its present form, the model is restricted to distributed damage, since it does not contain a characteristic length. The endochronic plastic fracturing model appears to offer considerable promise for describing the general behavior of plain concrete and, as such, will be the focus of our future efforts in this direction.

Many of the important questions faced by the Air Force today regarding the hardness of concrete defense structures requires a knowledge and understanding of the likelihood that a given structure will fail under a given loading environment. To address this issue in the most cost-effective manner, analytic methods must be available to allow system designers to systematically vary design parameters in an expedient and efficient manner so that an optimum structural design can be achieved. Finite element methods are now available for this purpose, but the results obtained with these methods can only be as good as the constitutive relations used in conjunction with them. To examine the hardness of concrete structures requires a

constitutive model of plain concrete which not only is capable of describing the inelastic behavior of intact unfractured material but is capable of describing developing damage and cracking and their effect on the overall constitutive behavior. For the endochronic concrete model to be useful in addressing these important issues, it must be able to treat elastic-plastic and cracking behavior. In the following section, our initial efforts to develop an advanced cracking model for this purpose are described.

4.4 A NEW CONTINUOUS DAMAGE MODEL.

The approach that we have taken to develop a cracking model appropriate for use in finite element framework utilizes the notion of an equivalent homogeneous continuum element to simulate the response of a finite volume of cracked or damaged material, as depicted in Figure 4.5. In effect, this means that instead of attempting to track and treat individual cracks in a finite volume of material and to account for their effect on the overall response of the element, we postulate an equivalent homogeneous continuum element whose constitutive properties are such that they provide the same response to applied loads as the actual cracked material element. The problem then is to find the appropriate constitutive relation for the equivalent continuum element.

With the above goal in mind, a new and very promising model for the equivalent homogeneous continuum was developed under this contract by Valanis (1985). Although the model described in this section applies to brittle elastic solids, the basic approach is extendable to elastic-plastic fracturing solids, as noted in the preceding section. The basic form of the model for elastic-fracturing solids is

$$\underset{\sim}{\sigma} = \underset{\sim}{\sigma}\left(\underset{\sim}{\varepsilon}, \underset{\sim}{\phi}\right) \tag{4-8}$$

where $\underset{\sim}{\sigma}$ and $\underset{\sim}{\varepsilon}$ denote, respectively, certain averages of the stress and strain taken over the volume of the material, while $\underset{\sim}{\phi}$, termed the integrity tensor, describes the orientation of damage, as well as its extent and character. It should be noted that the model is also capable of describing the evolution of damage in a material that has known pre-existing damage in the form of oriented cracks.

A unique feature of the model, which sets it apart from other cracking models, is that it can describe the development of anisotropy due to cracking without requiring the introduction of a fourth-order stiffness tensor into the formulation. Through a

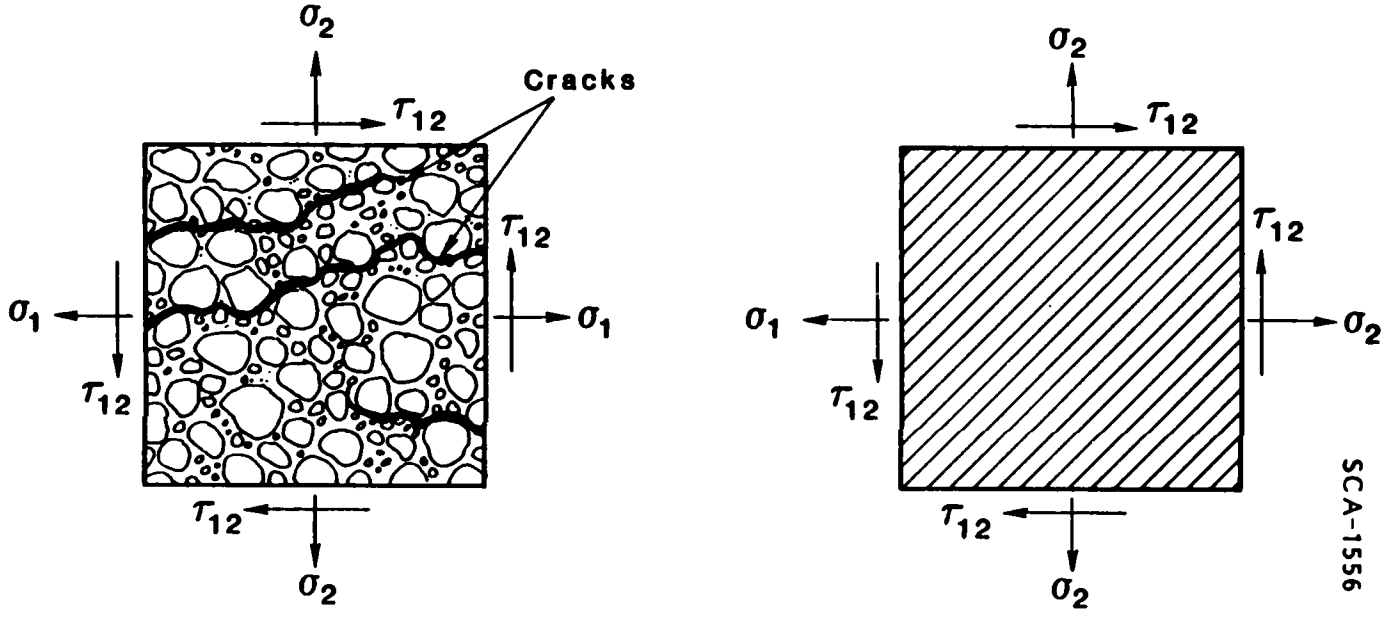

(a) Finite volume of damaged plain concrete

(b) Equivalent homogeneous continuum element

Figure 4.5 **Representation of a cracked multi-phase material element by an equivalent homogeneous continuum element.**

clever formulation described below, general anisotropy is represented by a constitutive equation that contains only second order tensors. The resulting model can describe the full spectrum of cracking, from the accumulation of microdamage up to complete fracture. In addition, it appears that the model can describe the standard modes of cracking, as well as the "splitting mode" under uniaxial compression (Horii and Nemat-Nasser, 1985), a mode which most of the existing fracture models cannot treat. Finally, the model predicts dilatancy during cracking, in accord with experimental observation, as we shall show in the sequel. In the following, a brief outline of the model will be given. A more extensive discussion of the model is given in Appendix A.

The fracturing theory is formulated below within the context of irreversible thermodynamics, although Valanis (1987) has recently shown that the same model can be developed by considering the mapping from undamaged to damaged material. We now introduce the free energy ψ per unit volume.* Since fracture produces a reduction in material integrity, an integrity tensor $\underset{\sim}{\phi}$ is introduced which has the following properties: It is a second-order symmetric tensor which is equal to the unit tensor $\underset{\sim}{\delta}$ in the undamaged virgin material and to the null tensor in the fully fractured material, i.e., material which cannot support tensile stress in any direction. We thus set

$$\psi = \psi(\underset{\sim}{\varepsilon}, \underset{\sim}{\phi}) \tag{4-9}$$

where isothermal conditions and small strains are assumed.

In a thermodynamic sense, $\underset{\sim}{\phi}$ plays the role of an internal variable, in which case we have the relations

$$\underset{\sim}{\sigma} = \frac{\partial \psi}{\partial \underset{\sim}{\varepsilon}} \quad , \quad \underset{\sim}{Q} = - \frac{\partial \psi}{\partial \underset{\sim}{\phi}} \tag{4-9a}$$

where $\underset{\sim}{\sigma}$ is the stress tensor and $\underset{\sim}{Q}$ the internal force, dual to $\underset{\sim}{\phi}$, which drives the fracturing process.

In view of the properties of $\underset{\sim}{\phi}$, the following relations must hold

$$\psi(\underset{\sim}{\varepsilon}, \underset{\sim}{Q}) = 0 \quad , \quad \psi(\underset{\sim}{Q}, \underset{\sim}{\phi}) = 0 \quad , \tag{4-9b}$$

---

* This nomenclature is preferred to free energy density, in view of the concept of "irreducible" material volume which must be introduced when dealing with heterogeneous, multi-phase materials, such as plain concrete.

the first meaning that a fully fractured material cannot contain free energy and the second that an unstrained material must have zero free energy (both relative to the reference state). The relations below must also hold:

$$\underset{\sim}{\mathcal{Q}}(\underset{\sim}{\varepsilon},\underset{\sim}{0}) = \underset{\sim}{0} \quad , \quad \underset{\sim}{\mathcal{Q}}(\underset{\sim}{0},\underset{\sim}{\phi}) = \underset{\sim}{0}$$

$$\underset{\sim}{\mathcal{Q}}(\underset{\sim}{\varepsilon},\underset{\sim}{0}) = \underset{\sim}{0} \qquad \text{(4-9c)}$$

The first two equations stipulate that the stress must vanish in the fully failed material and that, since the material remains elastic in the damaged state, the stress will vanish at zero strain. The last equation stipulates that the internal force $\underset{\sim}{Q}$ causing fracture must vanish in the fully failed material.

The free energy ψ is expanded in a Taylor series in $\underset{\sim}{\varepsilon}$ and terms no higher than quadratic are retained. In addition, it is assumed that ψ depends on $\underset{\sim}{\phi}$ in a quadratic manner.* On this basis, it follows that

$$\psi = C_{ijk\ell}\epsilon_{ij}\epsilon_{k\ell} \ , \qquad \text{(4-9d)}$$

where $\underset{\sim}{C}(\underset{\sim}{\phi})$ is purely quadratic in $\underset{\sim}{\phi}$. If the material is isotropic in the virgin state, it may be represented in terms of the outer products of the unit tensor and $\underset{\sim}{\phi}$. Since $\underset{\sim}{C}$ is purely quadratic in $\underset{\sim}{\phi}$, it must have the form

$$C_{ijk\ell} = \lambda\, \phi_{ij}\phi_{k\ell} + 2\mu\, \phi_{ik}\phi_{j\ell} \ , \qquad \text{(4-9e)}$$

in view of the symmetries imposed upon it by the symmetry of $\underset{\sim}{\varepsilon}$ via Eq. (4-9d). The constants in Eq. (4-9e) must indeed be the Lamé constants of the virgin material since

$$C_{ijk\ell} = \lambda\, \delta_{ij}\delta_{k\ell} + 2\mu\, \delta_{ik}\delta_{j\ell} \qquad \text{(4-10)}$$

when $\underset{\sim}{\phi} = \underset{\sim}{\delta}$. Therefore, from Eqs. (1-9d) and (4-9e) we can write

$$\psi = \tfrac{1}{2}\lambda(\phi_{ij}\epsilon_{ij})^2 + \mu\, \phi_{ik}\phi_{j\ell}\epsilon_{ik}\epsilon_{j\ell} \ , \qquad \text{(4-11)}$$

---

* This assumption has been validated through a completely independent (non-thermodynamic) approach based upon a mapping from undamaged to damaged material (Valanis, 1987).

which can be combined with the first of Eqs. (4-9a) to give

$$\sigma_{ij} = \lambda\, \phi_{ij}\phi_{k\ell}\epsilon_{k\ell} + 2\mu\, \phi_{ik}\phi_{j\ell}\epsilon_{k\ell} \tag{4-12}$$

To complete the specification of the model, it is necessary to establish an association between the mathematical structure of $\underline{\phi}$ and observed physical damage. This is discussed below.

In the initial version of the model, attention was focussed on the case in which developing damage is totally directed, that is, an advancing crack produces damage only in a direction normal to the crack. Attention to this case was originally motivated by the observation that in cementitious materials, such as plain concrete, when subjected to simple stress histories, the crack patterns, while locally quite tortuous, nevertheless are nominally normal to the direction of maximum tensile strain, as illustrated in Figure 4-6. With these notions in mind, an evolution equation for $\underline{\phi}$ was introduced on the basis of the following considerations.

When the material is not strain rate sensitive, an increment of tensile strain will produce an increment of damage. Specifically, given an increment in strain, $\Delta\underline{\epsilon}$, let $\Delta\epsilon^{\alpha}$ be its eigenvalue and n_i^{α} its eigenvectors ($\alpha = 1,2,3$). If $\Delta\underline{\epsilon}$ and $\underline{\epsilon}$ are coaxial, then $\Delta\epsilon^{\alpha}$ will constitute an increase in tensile strain if $\Delta\epsilon^{\alpha} > 0$ and $\epsilon^{\alpha} \geq 0$, where ϵ^{α} denote the eigenvalues of $\underline{\epsilon}$. In the more general case where $\Delta\underline{\epsilon}$ and $\underline{\epsilon}$ are not coaxial, $\Delta\epsilon^{\alpha}$ is said to be an increase in tensile strain if $\Delta\epsilon^{\alpha} > 0$ and $\epsilon_{ij} n_i^{\alpha} n_j^{\alpha} \equiv \epsilon_{\alpha}^{n} \geq 0$ (α not summed). Now let $\Delta\underline{\phi}$ be the change in the integrity tensor $\underline{\phi}$ due to the increment $d\underline{\epsilon}$, and let $\underline{n}_{\phi}^{\alpha}$ be the eigenvector of $\Delta\underline{\phi}$. With the above in mind, we now introduce the following two propositions:

(i) The tensors $\Delta\underline{\epsilon}$ and $\Delta\underline{\phi}$ are coaxial. The eigenvectors of $\Delta\underline{\phi}$ are then equal to the eigenvectors of $\Delta\underline{\epsilon}$, i.e.,

$$\underline{n}^{\alpha} = \underline{n}_{\phi}^{\alpha} \tag{4-13}$$

(ii) The eigenvalues of $\Delta\underline{\phi}$ are assumed to be related to the eigenvalues of $\Delta\underline{\epsilon}$ according to the following expression which has its roots in the physics of annihilation:

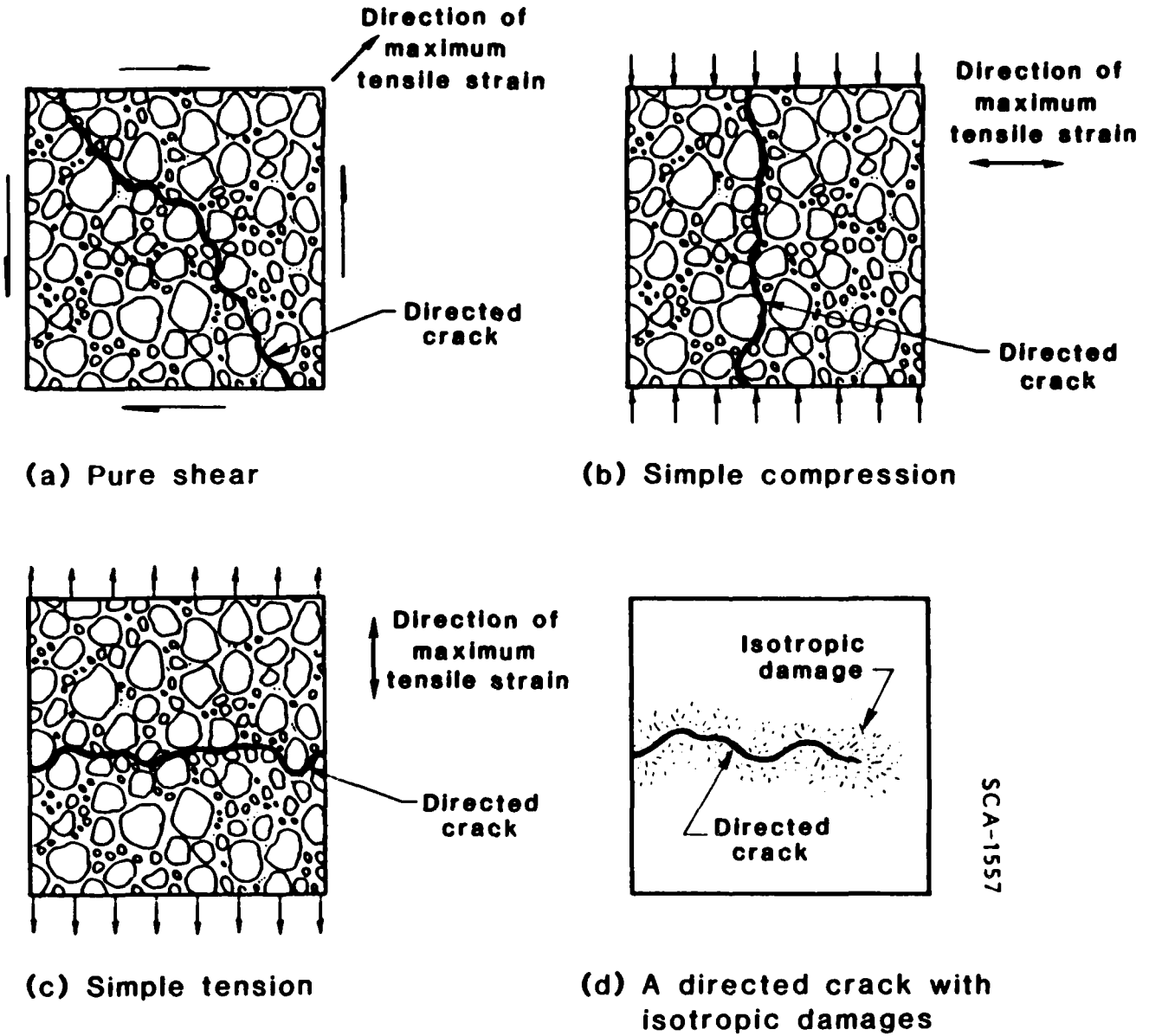

Figure 4.6 Observed fracture patterns in plain concrete.

$$\Delta\phi^{\alpha} = - \left(\phi_n^{\alpha}\right) \Delta\xi^{\alpha} \tag{4-14}$$

where

$$\Delta\xi^{\alpha} \quad \begin{cases} k\Delta\epsilon^{\alpha}, & \Delta\epsilon^{\alpha} > 0, \ \epsilon_n^{\alpha} \geq 0 \\ 0 \ , & \text{otherwise} \end{cases} \tag{4-15}$$

and

$$\begin{aligned} \phi_n^{\alpha} &= \phi_{ij} \, n_i^{\alpha} n_j^{\alpha} \\ \epsilon_n^{\alpha} &= \epsilon_{ij} \, n_i^{\alpha} n_j^{\alpha} \end{aligned} \tag{4-16}$$

In the above equations, k and m are positive material constants. In view of the above developments, we can write

$$\Delta\phi_{ij} = - \sum_{\alpha} \left(\phi_n^{\alpha}\right)^m d\xi^{\alpha} n_i^{\alpha} n_j^{\alpha} \tag{4-17}$$

By adjoining this evolution equation for ϕ to Eq. (4-12), the constitutive description for a brittle elastic solid which develops directed damage is complete, once the material parameters λ, μ, k and m have been specified. Applications of this theory to several cases involving homogeneous and non-homogeneous triaxial stress fields are described in Appendix A. As shown there, the theory leads to results which are in basic agreement with experimental observation and with theoretical solutions from linear elastic fracture mechanics.

Recently, in an effort to adapt the model specifically to plain concrete, a more general form of the evolution equation for ϕ was developed by Valanis (1986) which accounts for both directed and non-directed damage. This representation of ϕ was motivated by the results from the careful study done by Diamond and Bentur (1984) which clearly showed that directed cracking in cementitious materials is usually accompanied by the formation of small, randomly oriented cracks that develop near the crack tip (see Figure 4.6d). From a statistical standpoint, the damage produced by these small cracks can be considered isotropic, and we denote such damage by the scalar Ω. Thus Ω reduces the stress carrying capacity of a material by the same degree in all directions. As a result, the integrity tensor, which we now denote by ϕ_{Ω}, must be reduced by the presence of Ω and hence must be a state function of Ω. Accordingly, to account for both directed and isotropic damage, we write

$$\underline{\phi}_\Omega = \underline{\phi}_\Omega\left(\Omega, \xi^a\right) \quad , \tag{4-18}$$

subject to the following conditions which must always apply:

$$\underline{\phi}(0,0) = \underline{\delta} \ , \quad \underline{\phi}\left(1, \xi^a\right) = \underline{0} \tag{4-19}$$

Here, $\underline{\delta}$ denotes the unit tensor and ξ^a is defined by Eq. (4-15). To satisfy conditions (4-19), we take $\underline{\phi}$ to be of the form:

$$\underline{\phi}_\Omega = w(\Omega)\underline{\phi}\left(\xi^a\right) \quad , \tag{4-20}$$

where $\underline{\phi}$ is the integrity tensor for directed damage discussed above and $w(\Omega)$ is a monotonically decreasing function of Ω such that $w(0) = 1$ and $w(1) = 0$. A suitable function which satisfies the above constraints is

$$w(\Omega) = (1 - \Omega)^a \tag{4-21}$$

where $a \geq 0$. Thus, the integrity tensor $\underline{\phi}$ considered in the previous section is now modified by the presence of isotropic damage, as specified by Eqs. (4-20) and (4-21). The constitutive equation thus becomes

$$\sigma_{ij} = w^2\left\{\lambda\phi_{ij}\phi_{k\ell}\,\epsilon_{k\ell} + 2\mu\phi_{ik}\phi_{j\ell}\epsilon_{k\ell}\right\} \tag{4-22}$$

where λ and μ have the same meaning as before. Inasmuch as an expression for the evolution of $\underline{\phi}$ with damage was given earlier, an evolution equation for w is needed in order to complete the constitutive representation; this is considered below.

Physical considerations suggest that isotropic damage in cementitious materials is caused primarily by shearing which gives rise to local decohesion between the mortar and aggregate and/or the paste and the sand particles. Therefore, following similar reasoning that gave rise to Eq. (4-14), we take $d\Omega$ to be proportional to a positive monotonic function f of the isotropic integrity $1 - \Omega$, i.e.,

$$d\Omega = f(1 - \Omega)d\varsigma \tag{4-23}$$

where

$$d\varsigma = C||d\underline{\varepsilon}|| \tag{4-24}$$

Here, $C > 0$, $\underline{\underline{e}}$ is the deviatoric strain tensor, and the double bars around a symbol denote its Euclidean norm. Bearing in mind that the ultimate value of Ω is unity, a suitable form of f is

$$f = (1 - \Omega)^b \tag{4-25}$$

where $b > 0$. Upon substitution of Eq. (4-25) into Eq.(4-23), and solving the resulting differential equation, we obtain the result:

$$1 - \Omega = [1 - (1 - b)\zeta]^{\frac{1}{1-b}} , \tag{4-26}$$

which is similar in form to Eq. (A-26) given earlier in connection with directed damage. For the special case of $b = 1$, the above expression reduces to

$$1 - \Omega = e^{-b\zeta} \tag{4-27}$$

Note that C in Eq. (4-24) plays the role of an isotropic fracture toughness parameter which influences the rate of isotropic degradation. The specification of the constitutive model that accounts for both directed and isotropic damage is thus complete.

To illustrate the capability of the above model to describe the observed behavior of a real cementitious material, let us consider the case of axial compression of a plain concrete prism, which has been studied experimentally by Van Mier (1984). We denote by σ_1 and ϵ_1 the stress and strain in the axial direction and by ϵ_2 $(=\epsilon_3)$ the strain in the transverse direction. For this case, it can be shown (see Appendix A) that the model discussed above leads to the following set of coupled equations:

$$\sigma_1 = E\,\epsilon_1 \left\{a - (a - b)\, C^* \epsilon_2\right\}^{\frac{2a}{1-b}} \tag{4-28}$$

$$-\nu\epsilon_1 = \epsilon_2 \left\{1 - (1 - m)k\,\epsilon_2\right\}^{\frac{1}{1-m}} \tag{4-29}$$

Equations (4-28) and (4-29) were applied to the data reported by Van Mier (1984) for the case of axial compression of a prism having a height of 50 mm and lateral dimensions of 100 mm. From these data, the following values of the parameters in the above equations were determined:

$$\nu = 0.35 \quad k = 70 \quad m = 2.4$$

$$\frac{2a}{1-b} = 1.5 \qquad (1-b)C^* = 40 \tag{4-30}$$

Figures 4.7 to 4.9 illustrate the manner in which the model, with the values of the parameters listed above, describes the data from Van Mier (1984). Figure 4.7, for instance, shows the dependence of the axial strain ϵ_1 on the lateral strain ϵ_2, revealing the excellent agreement between the model and the data. Figure 4.8 depicts the relation between the axial strain ϵ_1 and the volumetric strain ϵ_{kk}, showing that the material initially experiences some small compaction before it becomes dilatant with increasing compressive strain. Finally, Figure 4.9 shows the dependence of the ratio $\sigma_1/(\sigma_1)_{max}$ on the axial strain ϵ_1. Here, $(\sigma_1)_{max}$ denotes the maximum value of σ_1 measured in the tests. This figure reveals that the model predicts softening beyond the peak stress which is in reasonable agreement with the data. Overall, the agreement between the model and the data is considered quite good.

Remarks

The fracture model presented in this section and further elaborated on in Appendix A is currently in the development stage. Based on the evidence presented in the preceding sections, the model clearly has a number of attractive and unique features which make it worthy of continued development.

- It can treat material that, in the initial state, is either uncracked and isotropic or has preexisting cracks.
- It model has the ability to develop anisotropy as damage occurs in preferred directions. Initially, the model is isotropic.
- The development of anisotropy is accounted for in the model in a very convenient manner involving only second order tensors. By comparison, the usual anisotropic model requires a fourth-order tensor, which greatly increases the complexity of the model, as well as the evaluation of the material parameters.

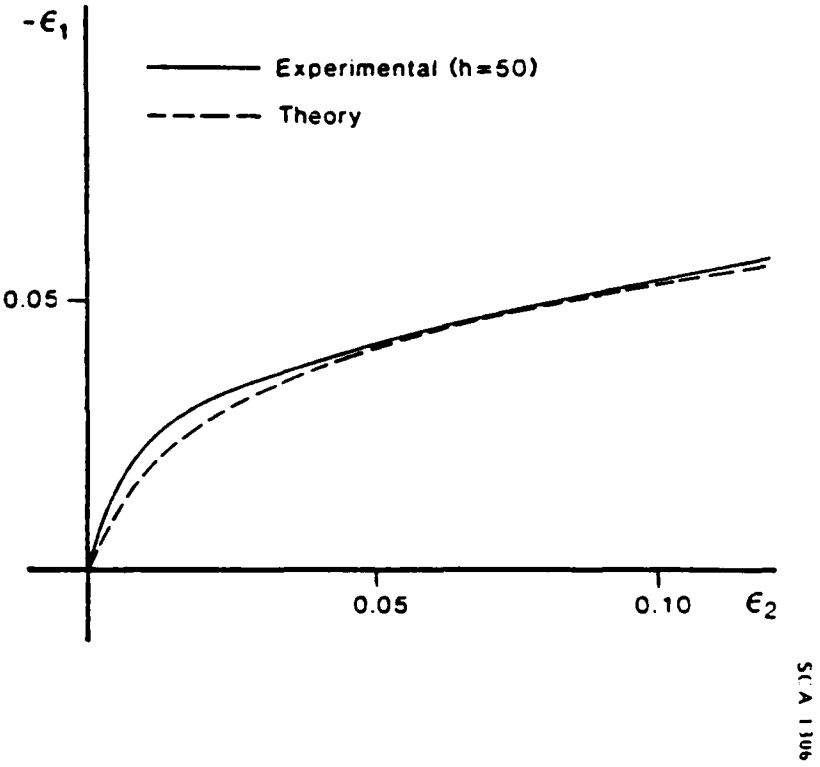

Figure 4.7 **Relation between axial and tranaverse strains under conditions of simple compression.**

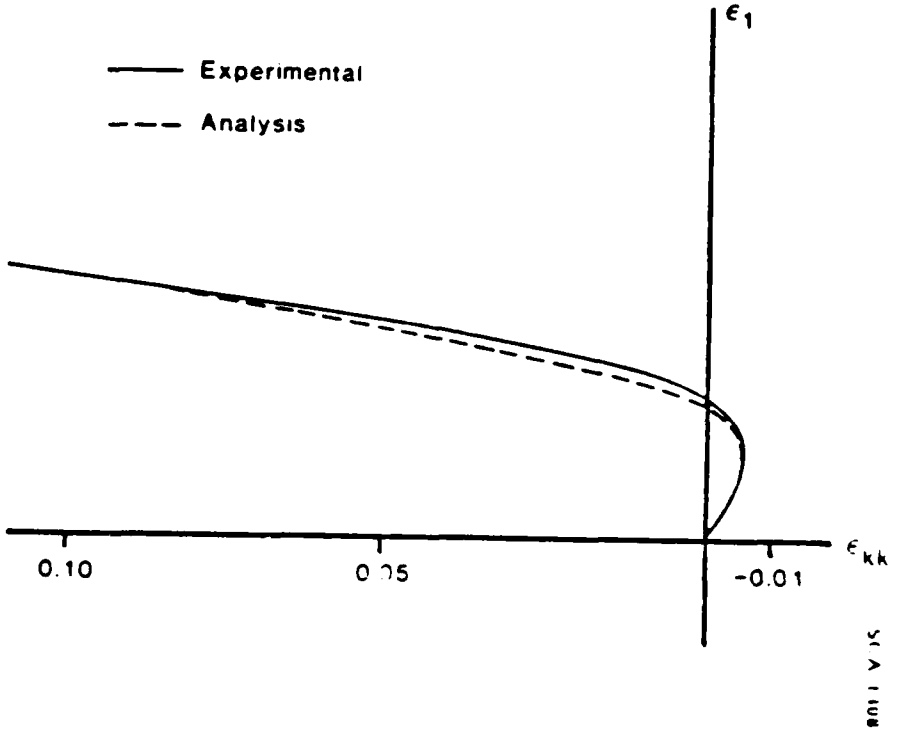

Figure 4.8 Dilatancy during simple compression.

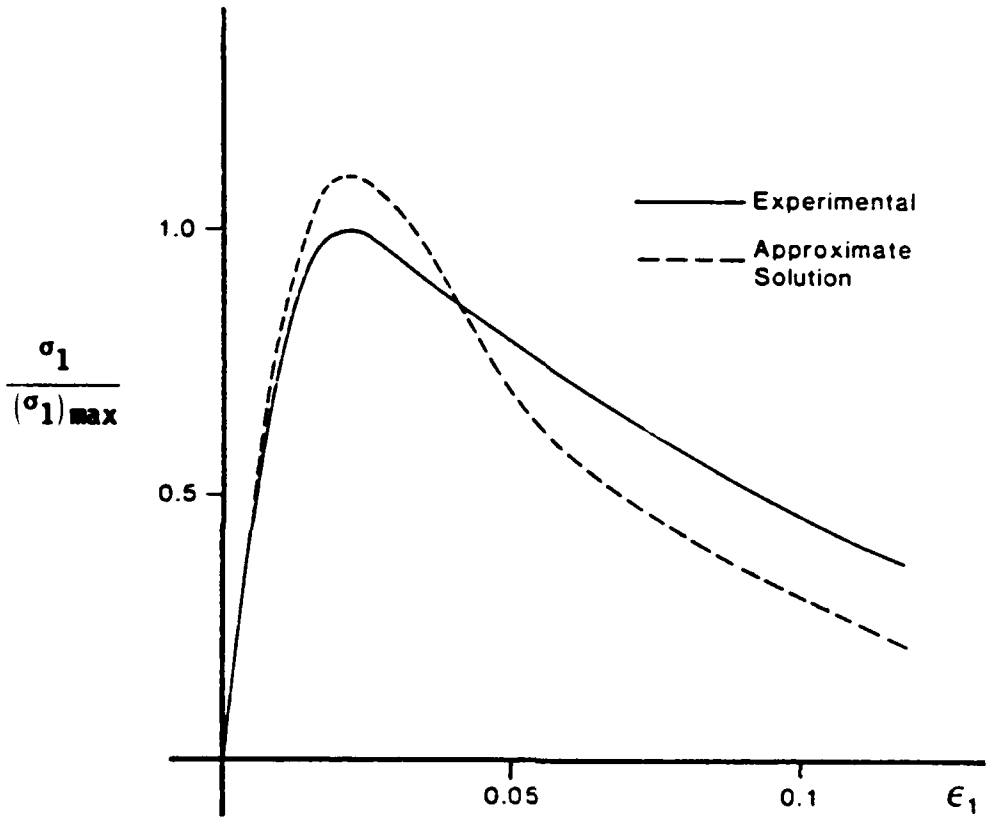

Figure 4.9 **Axial stress-strain relation showing softening in compression.**

- The model describes the full spectrum of developing damage, beginning with the gradual accumulation of distributed damage and continuing up to complete fracture.

- In addition to the standard modes of fracture, the model can describe the splitting modes under uniaxial compression, which most other fracture models are unable to treat.

- During the development of increasing damage, the model initially exhibits compaction and then dilatancy, in agreement with experimental observations on plain concrete.

- The model appears to be attractive for use in finite-element (FE) analysis. In the present study, we developed a computer program for the model and incorporated it into a FE code, which was then used to analyze several fracture problems described in Appendix A.

In its present form, the above fracture model applies specifically to elastic-fracturing solids. The approach has, however, been recently extended by Valanis (1987) to plastic fracturing solids, as noted earlier. In our future effort, we will pursue this new approach with the goal of developing an endochronic plastic fracturing model for plain concrete. The damage will be accounted for in the model by the ϕ tensor, while the endochronic concrete model will describe the concrete plasticity. The damage portion of the model will be calibrated from experimental data obtained for plain concret at low pressures, where the deformation is primarily due to cracking. Experiments conducted at high pressures, above the brittle-ductile transition where the deformation is mainly due to plastic flow, will be used to calibrate the plastic portion of the model. Once the model has been developed in this manner, it will then be proof-tested against data obtained at intermediate pressures.

It should also be noted that, as presently formulated, the model is not sensitive to specimen size. As a result, its application is essentially restricted to the case in which damage develops in a uniformly distributed manner over a specimen. In this case, the behavior does not depend on the size of the specimen. On the other hand, if the damage is not uniformly distributed but localizes, a size effect emerges and then must be reflected in the model. The notion of a size effect, and its

incorporation into fracture models for plain concrete, is currently a topic of considerable research and debate within the mechanics community. We plan to pursue this issue in our future efforts.

Finally, when the applications of interest involve rapid impulsive loading of concrete, as is the case here, the model should reflect the possible effect of strain-rate dependence on the behavior. Toward this end, a critical review of the existing state-of-the-art regarding strain rate effects, and their measurement, for plain concrete was prepared as part of this study. A discussion of the strain-rate issues and our findings are presented in the following section.

4.5 STRAIN-RATE EFFECTS IN PLAIN CONCRETE.

Understanding the manner in which concrete defense structures respond to rapidly applied, impulsive loadings -- such as produced, for example, by an explosive source -- continues to be a major concern for the Air Force. Generally speaking, typical threat scenarios can be expected to induce peak strain rates in concrete structures that range from 10^{-1} to 10^{2} sec^{-1}.

One of the complicating factors that arises when attempts are made to model such behavior is that concrete responds differently under high rates of loading than when loaded quasi-statically. Unfortunately, virtually all of the existing data used to develop and calibrate concrete constitutive models have been obtained from quasi-static laboratory tests. The existing evidence, which is inconsistent and confusing as we will show, nevertheless indicates that, as the rate of loading increases, concrete becomes more brittle (less ductile) and its strength increases. Because of this, constitutive models calibrated to quasi-static laboratory data are not likely to be adequate for describing the behavior of plain concrete at high rates of loading.

It appears that little is known about the mechanism that causes rate dependence in plain concrete. Some of the outstanding questions which need to be addressed experimentally include the following: Is the rate effect due mainly to cracking and the fact that cracks propagate at a finite velocity? Or is it due to plastic flow? Is the rate-effect observed both below and above the brittle-ductile transition? Answers to these questions would prove most valuable in future effort to introduce rate effects in the model in an appropriate manner.

With the goal of eventually introducing rate-dependence into the endochronic concrete model, we conducted, as part of this study, a critical review of the existing literature on strain rate effects in concrete, focussing primarily on the following question: Does the existing data base on strain rate effects in plain concrete have credibility and accurately portray the true strain rate dependence, or are the rate effects that have been inferred in the past from various experimental devices primarily due to system effects, inhomogeneous deformation of the test specimen or overly simplified methods of data analysis? In view of the importance to the Air Force of understanding the dynamic response of plain concrete in the range of strain rates from 10^{-1} to 10^{2} sec^{-1}, the review was primarily focussed on this range.

Inasmuch as detailed discussions of the results from this critical assessment of rate effects in concrete have been given in a paper (Hegemier and Read, 1985) and in a topical report (Read, 1984), we shall summarize the important findings below. Those interested in further details are referred to the references cited above, where more extensive discussions are given.

Drop-Hammer Tests.

With two exceptions (Birkimer, 1968; Malvern, *et al.*, 1985), all of the data in the literature on the strain rate dependence of plain concretes within the range from 10^{-1} to 10^{2} sec^{-1} have been obtained from drop-hammer tests. In such tests, which are schematically depicted in Figure 4-10, a concrete specimen is impacted on its upper flat surface by a flat heavy hammer which is released from a prescribed height and falls under the action of gravity. The test specimen rests as shown on an anvil, which is usually fabricated from a high strength steel and remains elastic during the impact process. By varying the height of drop, the impact velocity -- and hence the nominal strain induced in the specimen -- can be changed. Although not shown in Figure 4-10, there is a braking device which catches the hammer on rebound after impact and prevents it from making a second contact with the impacted specimen, or from crushing the remains of a failed specimen.

Figure 4-11 summarizes the results from all the known drop-hammer studies conducted on plain concrete which have been reported in the literature. Here, the effect of strain rate on the ratio of the dynamic strength, F_D, to the static strength, F_s, is shown. All of the data points which fall in the range from 10^{-6} to 10^{-2} sec^{-1}

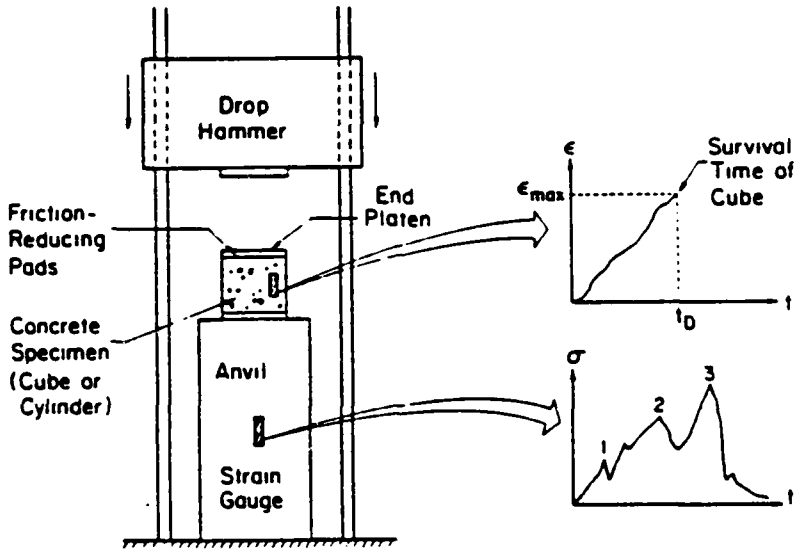

Figure 4.10 Typical features of drop-hammer devices.

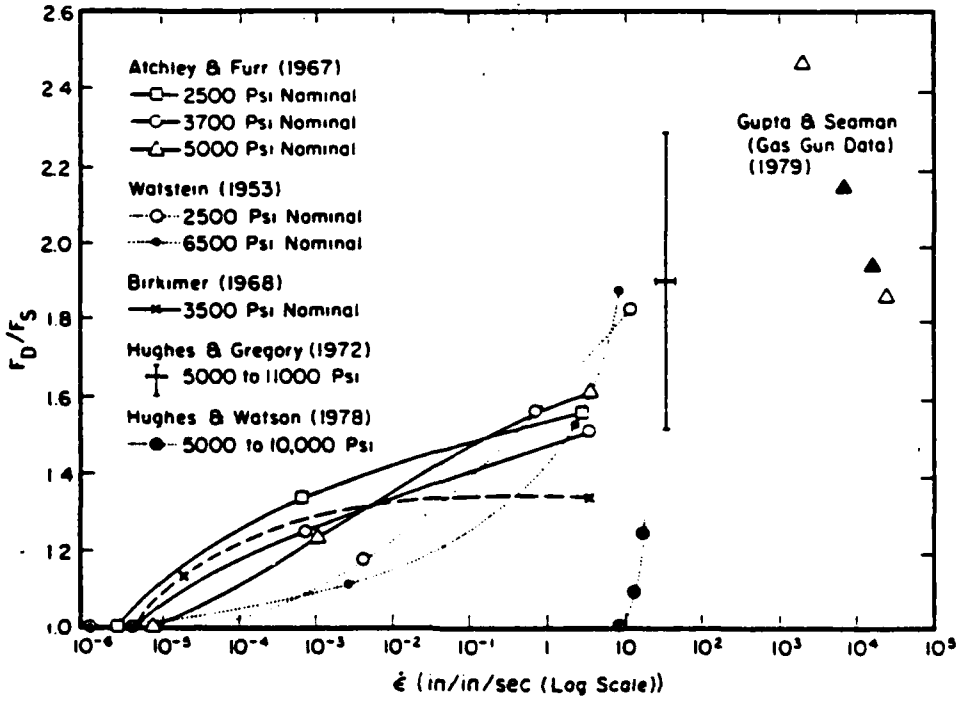

Figure 4.11 The effect of strain rate on the ratio of the dynamic to static strengths of plain concrete.

were obtained with conventional hydraulic testing devices, while the data between 10^{-1} and 10^{2} sec^{-1} are from drop-hammer tests, except for the single data point from Birkimer's investigation, which was obtained with a specially designed hydraulic testing machine.

An inspection of Figure 4-11 reveals that there are large inconsistencies between the results from the various investigations. Watstein's data, for example, show the dynamic strength of concrete increasing sharply with strain rate, while Atchley and Furr find a greater increase in strength at the low strain rates and less at the high rates. Birkimer's data reveal that the strength becomes independent of strain rate for strain rates above 10^{-1} sec^{-1}, which is in direct conflict with Watstein's data which show a very dramatic effect of strain rate. Hughes and Watson, on the other hand, find virtually no effect of strain rate up to 8 sec^{-1}, while Hughes and Gregory reported that, "No correlation was apparent (from their data) between the average rate of straining and either uniaxial compressive strength or mix proportions in the mixes used."

The results displayed in Figure 4-11 clearly illustrate the disturbing inconsistencies in the existing data, especially for the range of strain rates from 10^{-1} to 10^{2} sec^{-1}. Although we will not attempt to go into the details here, which can be found in the references cited near the beginning of this section, the data shown in Figures 4.11 appear to be strongly influenced by the differences in drop-hammer design between the various investigations, gauge placement, specimen shape, size and end capping, as well as methods of data interpretation. In addition, it is also possible, in view of the conclusions reached by Janach (1976) and Young and Powell (1979), that increased confinement of the specimen due to radial inertia effects present at the higher rates of loading can give rise to an "apparent" strain rate effect. Also, in all probability, the test specimens do not deform in a homogeneous manner during the gauge read time, which violates one of the crucial requirements for inferring constitutive properties.

In view of the above considerations, it appears that there are a number of serious complications with the drop-hammer test that make the extraction of credible constitutive property information from it very difficult. Because of this, the strain rate effect usually inferred from such tests is probably more apparent than real, due in large part to system effects. Further studies, both analytically and experimentally, need to be done to address the issues raised above and to determine the usefulness of drop-hammer tests for determining constitutive properties.

Split Hopkinson Bar Tests.

Another test device which has recently been used to investigate strain rate effects in plain concrete is the split Hopkinson bar (SHB). In a SHB test, a cylindrical specimen is positioned on axis between two long circular high strength steel bars of the same diameter, as shown in Figure 4-12. A compressive pulse is introduced into the input bar by various means and travels through the test specimen into the output bar. Strain gauges mounted on the input and output bars near the test specimen measure the strain histories. If it is assumed that the deformation of the specimen during the read time of the gauges is homogeneous and due to uniaxial stress, then the dynamic constitutive properties of the specimen can be inferred from the measured strain histories. The homogeneity assumption is therefore the key issue. Parenthetically, we note that the type of loading applied to a specimen by the SHB is the same as that produced by a drop hammer device, i.e., nominally uniaxial stress.

The SHB has been widely used in the past to study the strain rate dependence of various metals and other ductile solids and, for those materials, it is generally considered to be a credible approach. For brittle materials, however, the use of the SHB has raised serious questions which to date have not been resolved. The careful experimental studies by Janach (1976) and Young and Powell (1979) on rocks, for example, showed that the observed strain rate effects are most likely not the true rate dependence of the rocks but, instead, are due to strong lateral inertia effects arising from dilatancy (bulking) during failure.

To better appreciate the complexities associated with the use of a SHB in conjunction with brittle solids, consider the nature of the loading and its subsequent effect on the behavior of a brittle specimen. Because the impedance of test specimens is usually smaller than that of the high strength steel bars, the first wave to enter the specimen usually does not load it to the peak stress. Only after a number of reflections of the wave between the specimen-bar interfaces does the axial stress reach its peak. The loading time is proportional to the specimen length and to the number of reflections to reach the peak stress.

If the specimen is a brittle material, it will begin to fail near the lateral surface if the axial stress becomes sufficiently high, even though it has not reached its peak value. Thus, unlike ductile materials, failure in brittle materials can begin near the lateral surface while the axial loading process is still in progress. Such behavior is, of course, highly inhomogeneous.

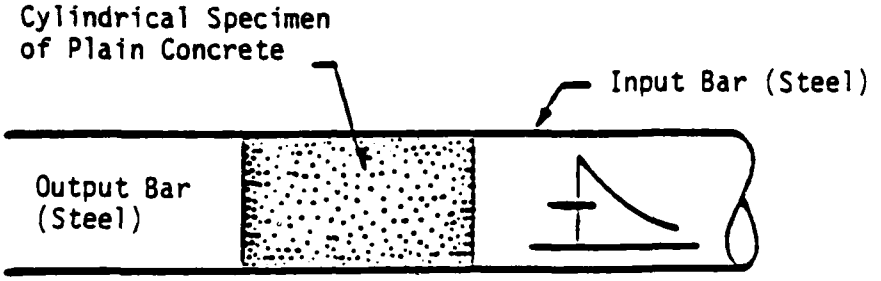

Figure 4.12 The standard split Hopkinson bar configuration.

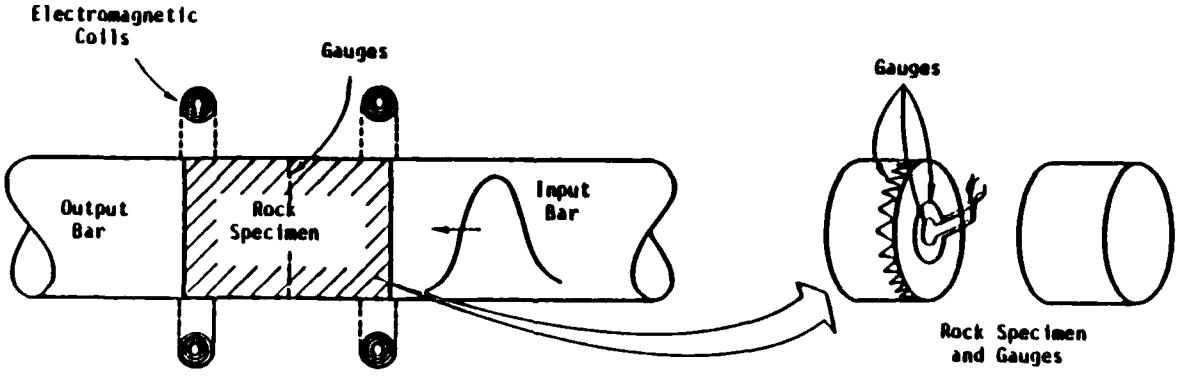

Figure 4.13 **Split Hopkinson bar configuration used by Young and Powell to study radial inertia effects in rocks.**

The behavior of brittle specimens in a SHB test is further complicated by dilatancy (bulking) during failure, which does not occur in ductile materials. During the process of brittle failure in compression, cracks develop and break the material into subregions, and these subregions, consisting of still intact material, must separate in order that the radial unloading process can be completed. The unloading process occurs through separations of these subregions of cracked material and is accompanied by frictional sliding and the formation of internal voids, which produce an inelastic bulking of the failing material. When this occurs, radial inertia can become very important because the reaction forces to radial acceleration of the fractured subregions produce a confining pressure on the not yet unloaded interior material. Inasmuch as the strength of most brittle materials increases with confining pressure, the effective confining pressure produced by the radial acceleration will increase the strength of the interior material. When this is the case, it becomes difficult, but not impossible as discussed below, to separate the true rate effect from the apparent rate effect due to radial inertia effects.

While the work of Janach (1976) was the first to point out the importance of considering radial inertia effects in SHB tests, Young and Powell (1979) were the first to actually measure them. Using embedded wire loops and an externally applied longitudinal magnetic field, as depicted in Figure 4.13, radial velocity histories were measured at interior points of rock specimens. From these histories, the radial accelerations were determined, as well as the confinement produced by the radial stress. Although the values of the peak axial strain rates achieved in the tests were not reported by Young and Powell, it is highly probable, in view of the high stresses generated in the specimens on impact, that the axial strain rates may have been as high as 10^4 to 10^5 sec^{-1}. Young and Powell concluded from this study that the effects of radial inertia were sufficiently large to account for the observed increases in compressive strength. They cautioned that it is not justifiable to attribute the increased strengths of the rock specimens considered to a strain rate effect.

A different conclusion was reached recently by Malvern *et al.* (1985), who performed a series of SHB tests on four different types of high strength plain concrete. The results are depicted in Figure 4.14, where the variation of the strength, σ_{max} with strain rate is shown for four different high strength concretes. To

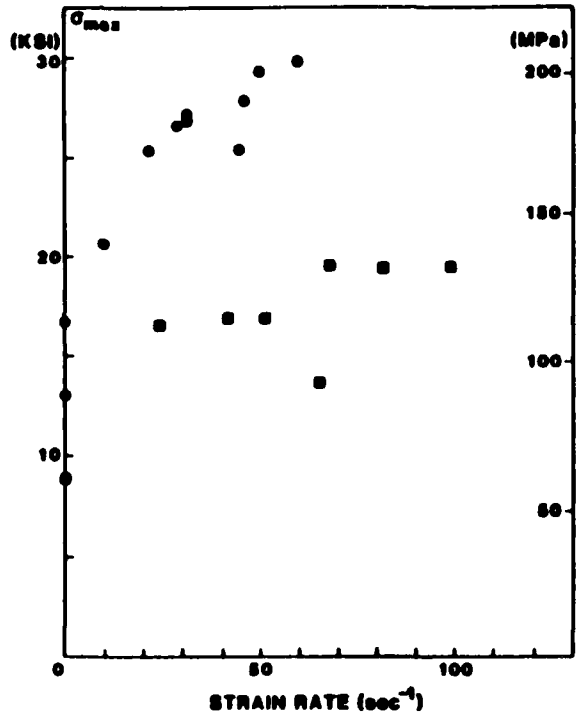

(a) Limestone aggregate (circles and Solite lightweight aggregate (squares).

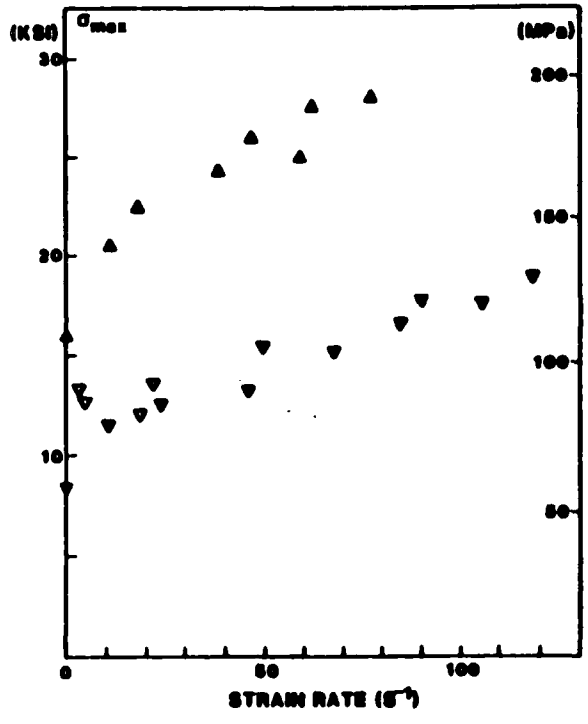

(b) Andesite (upper triangles) and Seattle gravel (lower inverted triangles).

Figure 4.14 Results from SHB tests on several high strength concretes. (From Malvern, *et al.*, 1985.)

accommodate the large tests specimens required for testing concrete, an unusually large SHB system was constructured for this purpose. In an effort to obtain insight into the possible effect of radial inertia, two additional strain gauges were mounted on the specimen surface midway between its ends. One gauge measured the axial strain while the other measured the hoop (ϵ_θ) strain. By numerically differentiating a smoothed history of ϵ_θ, the history of the strain rate $|\dot{\epsilon}_\theta|$ was constructed. Upon comparing this with the history of the axial stress, it was concluded that radial inertia could not be the cause of the increased strengths observed in the tests. However, there were some features of the data that could not be explained, which led Malvern *et al.*, to comment that, "There are some very important questions involved in these dynamic tests for which we do not yet have answers." It is also somewhat surprising that they find that tests conducted on longer specimens show higher strengths than those on shorter specimens at the same strain rates. A number of considerations would lead one to expect that the opposite might be true.

The conclusion reached by Janach (1976) and Young and Powell (1979) regarding the importance of radial inertia effects in SHB tests on rocks appears to be in disagreement with the conclusions reached by Malvern *et al.*, (1985) from SHB tests on plain concrete. These differing conclusions may, however, not be inconsistent if one takes into account the possible large differences in the strain rates between the studies. Malvern's tests were done at strain rates in the range from 10 to 10^2 sec^{-1}, while Young and Powell's tests appear to have been done at much higher rates, possibly as high as 10^4 to 10^5 sec^{-1}. It is to be expected that radial inertia effects will grow in importance as the strain rate increases. Consequently, it may be that Malvern's tests were done at sufficiently low strain rates that radial inertia was not important, while Young and Powell's tests, done at considerably higher rates, were in a range where radial inertia dominated the response. The studies by Malvern, *et al.* (1985) and by Young and Powell (1979) have provided valuable information, but there is still considerable uncertainty and unresolved issues in the way brittle specimens respond in a SHB test.

Gas Gun Tests.

Gas guns have been used in a very limited manner in the past to study the dynamic behavior of concrete. In fact, only two such studies have been reported, the first of which was conducted by Gregson (1971) and a more recent one by Gupta and Seaman (1979). Of these two, only the study by Gupta and Seaman provides direct

insight into the effect of strain rate on the behavior of plain concrete. The advantage that the gas gun has over the drop-hammer and SHB devices is that, because it subjects specimens to uniaxial strain deformation, it is free of radial inertia effects. Its disadvantage, at least as far as the present strain rate range of interest (10^{-1} to 10^{2} sec^{-1}) is concerned, is that it typically produces strain rates in concrete that are above this range. Nonetheless, gas gun data on concrete at the higher strain rates can serve as a guide in modeling the effects at the lower rates, since a suitable model should properly extrapolate to the higher rates.

In the gas gun study by Gupta and Seaman (1979), Lagrangian gauge analysis techniques were used to unfold the dynamic stress-strain relationship from the compressive loading data, and the results so obtained are depicted in Figure 4.15(a). Here, the measured dynamic stress-strain paths for two compressive loading shots are shown together with a corresponding quasi-static path (also obtained under uniaxial strain conditions). An inspection of this figure reveals that the dynamic stress-strain curve is well above the static stress-strain curve, indicating the presence of a substantial rate effect. The corresponding particle velocity histories measured at several depths in the high stress shot (93,000 psi) are shown in Figure 4.15(b). From this, one can observe the rapid attenuation of the pulse as it propagates through the specimen, as well as the increasing dispersion of the wave front.

Using the data from the high stress shot, the peak stress and the corresponding strain rate were determined for each of the four wave profiles shown in Figure 4.15-(b). The results are shown in Figure 4.11 presented earlier as the solid and open triangles. According to Seaman (1984), there is reasonable confidence in the data denoted by the solid triangles, but less confidence in that represented by the open triangles. Note that we have taken the liberty to plot in this figure the data from two different modes of deformation, i.e., drop-hammer data (uniaxial stress) and gas gun data (uniaxial strain). The validity of presenting such data on a single plot has not been explored.

4.6 EXPERIMENTAL METHODS AND FAILURE MODES.

In developing constitutive models for concrete and rock on the basis of data from laboratory tests, theoreticians often tacitly assume that certain fundamental premises, such as homogeneous fields and material continuity, are satisfied. In

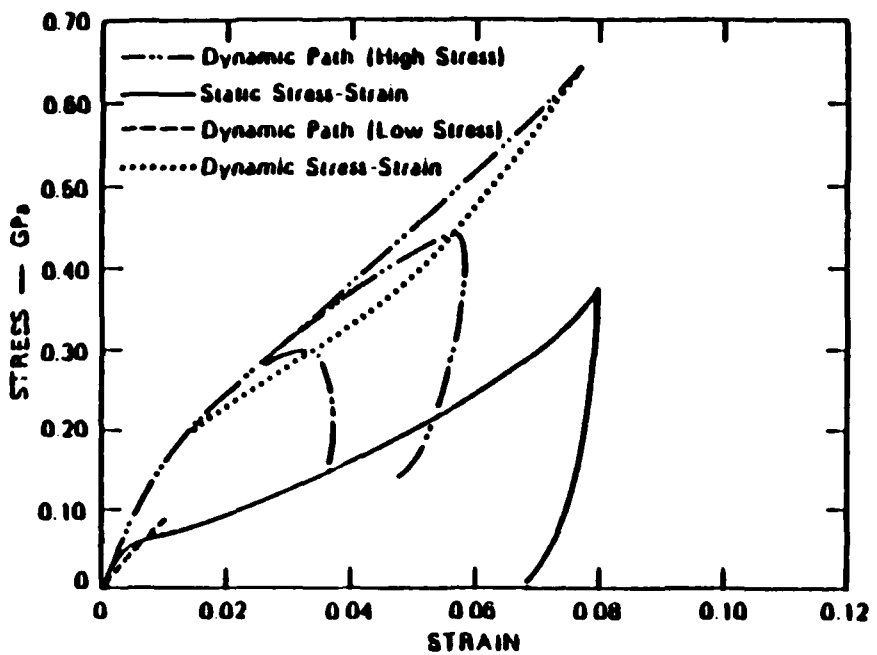

(a) Stress-strain relationship inferred from gas gun data by Lagrangian gauge analysis.

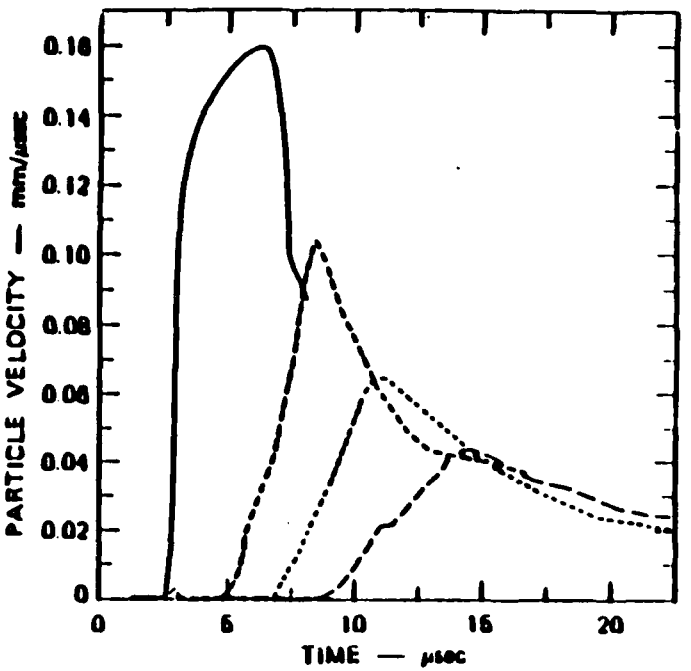

(b) Measured particle velocity histories at various depths in high stress shot (93,000 psi). The solid curve denotes the measured history at the impact surface, while the dashed curves represent the measured histories at various depths.

Figure 4.15. Results from gas gun tests on concrete (Gupta and Seaman [1979]).

many cases, appropriate information concerning these premises is not supplied by the experimenters. This is not necessarily the fault of the experimentalist, since he may not have been aware that certain features of a test were important to the theoretician and needed to be measured and reported. Also, it often happens that experiments are conducted before a model has been developed and the data needs are defined. In most all cases, the interaction between theoreticians and experimentalists appears to be insufficient, and has led to a propagation of misinformation for certain aspects of response. One such case involves the post-peak response of concrete and rock below the brittle/ductile transition (Read and Hegemier 1984; Hegemier and Read, 1984). Another concerns the dependence of concrete and rock properties on strain rate, as discussed in the preceding section.

To explore these issues in some depth, an extensive examination of experimental devices and test data normally used in the development of constitutive models for concrete and rock was conducted as part of the present study. Various issues pertaining to strain softening, strain hardening, failure states, failure modes and strain rate effects were considered. Since most of the results from this study have been described in detail elsewhere (Hegemier and Read, 1985), we shall focus here primarily on questions pertaining to failure, which have not been touched on before.

First of all, it should be noted that there is no unanimity among researchers on the definition of failure. In some cases, failure is defined in terms of the maximum attainable stress state. In others, failure is defined by the onset of dilatancy. In still other cases, failure is defined by a critical state of strain. Moreover, the term "failure" in the literature is often applied to brittle failure via cleavage or shear faulting, and the onset of ductile flow. The current presumption is that differences between definitions of failure do not lead to significant differences in failure data.

Comparison of data from tests in which the stress paths are prescribed reveals that test devices which employ "unconstrained" boundary conditions (of a type which do not lead to early failure via extrusion of lubricating materials) furnish failure data in stress space that is reasonably clustered. In contrast, measured strains at failure exhibit vast data scatter. It is suspected that part of this phemonenon may be due to inherent difficulties in measuring strains in unconstrained fluid-cushion type test systems. However, significant data scatter is also observed from specimen to specimen

within the same test system. In view of the above, it would appear preferable to describe failure in stress space rather than strain space. This does not, however, solve the problem, since deformation characterization is equally as important as stress characterization in most problems. In fact, in many cases, deformation plays the major role.

The mode of failure is also an important piece of information to the theoretician. Unfortunately, failure modes are poorly documented in the literature. While much effort has been devoted to exploring failure criteria in, for example, stress space, little correlation has been established between points on a failure surface and corresponding failure modes.

The paucity of data on failure modes is compounded by the fact that failure modes are, as one would expect, sensitive to the experimental test setup -- in particular, test boundary conditions. In the biaxial tests of mortar and concrete conducted by Andenaes, Gerstle and Ko (1977), the specimens in the fluid cushion boundary condition series failed by either splitting (tensile splitting) of the cube parallel to the free surface, by corner or edge failure, or by a combination of both. A different mode of failure was observed in their tests conducted with steel platens. Here, the failure surfaces formed characteristic shear cones at the free surfaces, with an angle varying between 12 degrees and 18 degrees with the major principal stress direction.

Information concerning failure modes in triaxial stress states is furnished by Mills and Zimmerman (1970), who conducted uniaxial, biaxial and triaxial experiments on cubical concrete specimens, using lubricated boundary conditions. Two types of basic triaxial tests were considered. Type I tests consisted of cases in which the largest principal stress is the major principal stress and the minor and intermediate principal stresses are smaller and equal. Type II tests were conducted in which the major and intermediate principal stresses are equal and larger than the minor principal stress. The failed cubes from the uniaxial and Type I triaxial tests were found to be cracked in planes parallel to the load. In the Type II tests, the cubes were found to be cracked in planes parallel to the plane of the two larger loads. The cracks in the tests with intermediate stress conditions indicated splitting in the direction of the smallest principal stress; however, the orientation of the crack planes with respect to the plane of the largest and intermediate principal stress did not exhibit predictable trends. The above mentioned failure modes are illustrated schematically in Figure 4.16.

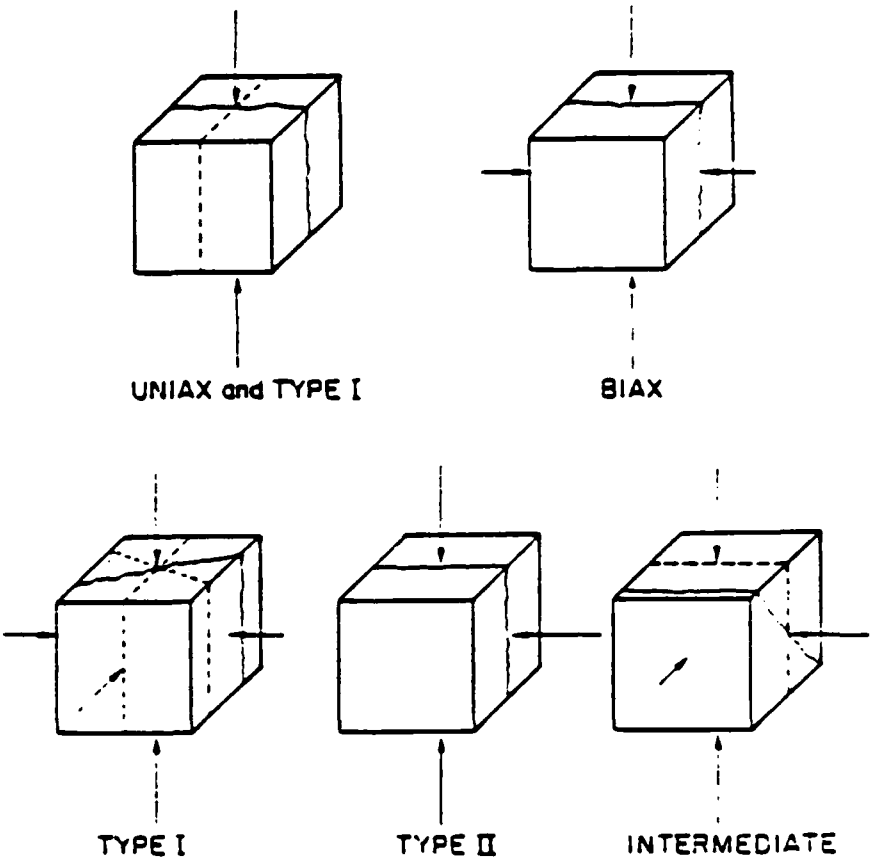

Figure 4.16. Summary of typical failure modes for concrete specimens.

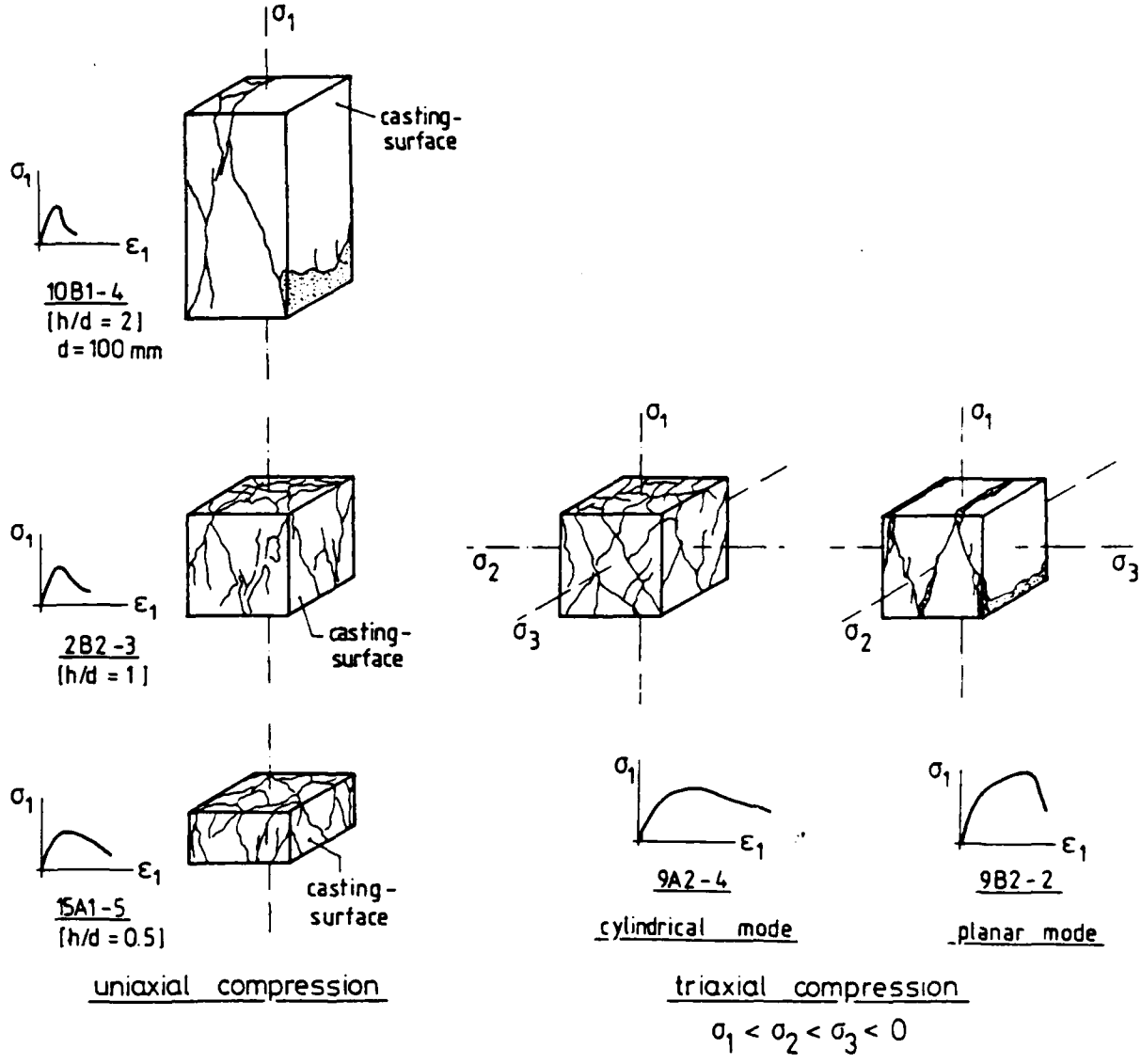

Figure 4.17. **Observed fracture modes in various tests of uni- and triaxial compression of concrete specimens (from van Mier, 1984).**

The recent experimental study by Van Mier (1984), however, reveals that the above picture of failure modes in concrete may be somewhat oversimplified. In this study, a new true triaxial device with servo-controls on all three axes was used to study the responses of cubes and prisms of a medium strength plain concrete to uniaxial and triaxial compression. The loads were applied to the test specimens through brush-bearing platens which deform them with reduced friction.

Uniaxial compression tests were performed on prisms of different slenderness-ratios ($h/d = 0.5$, 1.0 and 2.00). For the prisms with $h/d = 0.5$ and 1.0, failure occurred through fracture of the specimen into cone-shaped pieces in alternating positions, where the heights of the cones were restricted by the height of the specimen. In the case of the prisms with $h/d = 2.0$, eight tests were done and, of these, four failed by localized shear fracture, while the other four failed by formation of a multitude of axial cleavage cracks. Thus, even when specimens of the same concrete mix and slenderness ratio were tested in the same device, the fracture mode was not unique. The cracking patterns for several of the uniaxial compression tests are shown in Figure 4.17.

Triaxial tests were done only on cubical specimens. When the applied loading was such that extension occurred in only one direction (planar mode), the specimen failed through the development of localized shear bands. On the other hand, when loading caused extension in two directions (cylindrical mode), failure occurred by distributed fracture throughout the sample. Typical cracking patterns for the triaxial tests are also depicted in Figure 4.17.

The results from van Mier's study dramatically underscore the complex nature of failure in plain concrete. Inasmuch as van Mier took special care to reduce to the extent possible friction between the test specimens and the loading device by using brush-bearing platens, the observed modes of failure are believed to reflect true material behavior and not system effects. From these results, we see that the mode of failure depends on both a specimen's slenderness-ratio and the relative magnitudes of the applied principal stresses.

In conclusion, it is clear that failure modes are strongly influenced by a number of factors, including test boundary conditions. When unconstrained boundary conditions are used, similar general trends in failure modes are observed. Nonetheless,

quantitatively there is considerable data scatter with respect to failure modes, especially at low confining pressures. The above problems are further compounded by generally poor descriptions of the failure mode, failure sequence, and state of the specimen during and after failure. For further elaboration on the topics discussed in this section, see the paper by Hegemier and Read (1985).

4.5 REFERENCES FOR SECTION 4.

Andenaes, E., K. Gerstle and H. Y. Ko (1977), "Response of Mortar and Concrete to Biaxial Compression," *J. Engr. Mech. Div.*, ASCE, 103 (EM4), 515.

Atchley, B. L., and J. H. Furr (1967), "Strength and Energy Absorption Capabilities of Plain Concrete Under Dynamic and Static Loadings," *ACI Journal*, p. 745.

Bazant, Z. P., and P. D. Bhat (1976), "Endochronic Theory of Inelasticity and Failure of Concrete," *J. Engr. Mech. Div.*, ASCE, 102 (EM4), 701.

Bazant, Z. P., and C. L. Shieh (1978), "Endochronic Model for Nonlinear Triaxial Behavior of Concrete," *Nuclear Engng. Design*, 47, 305.

Birkimer, D. L. (1968), Discussion of paper by Atchley and Furr, *ACI Journal*, 414.

Diamond, S., and A. Bentur (1984), "On the Cracking in Concrete and Fiber-Reinforced Composites," *Procs. NATO Advanced Workshop on Application of Fracture Mechanics to Cementitious Composites*, Northwestern University, Evanston, Ill.

Gregson, V. L. (1971), "A Shock Wave Study of Fondu-Fyre WA-1 and A Concrete," General Motors Materials and Structures Laboratory, Warren, Michigan, Report MSL-70-30.

Gupta, Y. M., and L. Seaman (1979), "Local Response of Reinforced Concrete to Missile Impact," SRI Intl., Menlo Park, CA, Report NP-1217.

Hegemier, G. A., and H. E. Read (1985), "On Deformation and Failure of Brittle Solids: Some Outstanding Issues," *Mechanics of Materials*, 4, 215.

Hegemier, G. A., and H. E. Read (1984), "Strain Softening" Discussion, *Large-Scale Computations for Nonlinear Materials Behavior*, Edited by S. Nemat-Nasser, R. J. Asaro and G. A. Hegemier, Martinus Nijhoff, Pub.

Horii, H., and S. Nemat-Nasser (1985), "Compression-Induced Micro-Crack Growth in Brittle Solids: Axial Splitting and Shear Failure," *J. Geophys. Research*, 90, 3105.

Hughes, B. P., and R. Gregory (1972), "Concrete Subjected to High Rates of Loading in Compression," *Mag. Concrete Res.*, 24, 25.

Hughes, B. P., and A. J. Watson (1978), "Compressive Strength and Ultimate Strain of Concrete Under Impact Loading," *Mag. Concrete Res.*, 30, 189.

Janach, W. (1976), "The Role of Bulking in Brittle Failure of Rocks Under Rapid Compression," *Intl. J. Rock Mechs. Min. Sci.*, 13, 177.

Malvern, L. E., D. A. Jenkins, T. Tang and C. A. Ross (1985), "Dynamic Compressive Testing of Concrete," *Proc. 2nd Symp. on the Interaction of Non-Nuclear Munitions with Structures*, Panama City, Florida, April 15-17.

Mills, L. L., and R. M. Zimmerman (1970), "Compressive Strength of Plain Concrete Under Multiaxial Loading Conditions," *ACI Journal*, October, 802.

Murakami, H., and H. E. Read (1987), "Endochronic Plasticity: Some Basic Properties of Plastic Flow and Failure," *Intl. J. Solids Structs.*, 23(1), 133.

Murakami, H., and H. E. Read (1987), "Plastic Flow Properties of Endochronic Theory with Third Invariant Failure Surface," in preparation.

Read, H. E. (1984), "Strain Rate Effects in Concrete: A Review of Experimental Methods," S-CUBED Report SSS-R-85-6081, November.

Read, H. E., and G. A. Hegemier (1984), "Strain Softening of Rock, Soil and Concrete," *Mechanics of Materials*, 3, 271.

Scavuzzo, R., T. Stankowski, K. H. Gerstle and H. Y. Ko (1983), "Stress-Strain Curves for Concrete Under Multiaxial Load Histories," CEAE Department, University of Colorado, Boulder, Colorado.

Seaman, L., (1984), SRI Intl. Menlo Park, CA, Private Communication.

Trangenstein, J. A., and H. E. Read (1982), "The Inelastic Response Characteristics of the New Endochronic Theory with Singular kernel," *Intl. J. Solids Structs.*, 18, (11), 947.

Valanis, K. C., (1985), "A Fracture Theory for Brittle Materials," S-CUBED, La Jolla, California, Informal Report.

Valanis, K. C., and H. E. Read (1984), "An Endochronic Plasticity Theory for Concrete," S-CUBED, La Jolla, California Report No. SSS-R-85-7172.

Valanis, K. C., and H. E. Read (1985), "An Endochronic Plasticity Theory for Concrete," *Proc. 2nd Symp. on the Interaction of Non-Nuclear Munitions with Structures*, Panama City, Florida, April 15-17.

Valanis, K. C., and H. E. Read (1986), "An Endochronic Plasticity Theory for Concrete," *Mechanics of Materials*, 5, 277.

Valanis, K.C., (1986), S-CUBED, La Jolla, California, Unpublished report.

Valanis, K.C., (1987), ENDOCHRONICS, Vancouver, Washington, Unpublished report.

Van Mier, J. G. M. (1984), "Strain Softening of Concrete Under Multiaxial Loading Conditions," Ph.D. Dissertation, Eindhoven University of Technology, The Netherlands.

Watstein, D. (1953), "Effect of Straining Rate on the Compressive Strength and Elastic Properties of Concrete," *ACI Journal*, April, 729.

Young, C., and C. N. Powell (1979), "Lateral Inertia Effects on Rock Failure in Split-Hopkinson-Bar Experiments," *Proc. 20th U.S. Symp. on Rock Mechanics*.

APPENDIX A

NEW CONTINUOUS DAMAGE MODEL FOR CONCRETE

A.1 INTRODUCTION.

The purpose of this appendix is to describe, in detail, a damage-cracking model that has been developed under the present program. The model was formulated by Valanis (1985) and is presently under development. The discussion given below largely follows that given by Valanis (1985) but does not reflect various topics that are presently under study, which include (a) the addition of plasticity, (b) size effects and (c) strain rate dependence.

A.2 FORMULATION OF MODEL.

Consider a linearly elastic material which is isotropic in its virgin unstrained state and undergoes small deformation at isothermal conditions. As the deformation proceeds, damage gradually develops, which in turn reduces the material integrity. For sufficiently large deformation, the accumulated damage can lead to complete fracture, in which the material cannot support tensile stress in a direction normal to the damage. We shall formulate this damage-cracking process within the context of irreversible thermodynamics and, for this purpose, we introduce the free energy Ψ per unit volume.* Since fracture leads to a reduction in material integrity, we introduce an integrity tensor $\underset{\sim}{\phi}$ which will be discussed at length later and which is symmetrical such that $\underset{\sim}{\phi} = \underset{\sim}{\delta}$ (the unit tensor), when the material is in its virgin (undamaged) state, and $\underset{\sim}{\phi} = \underset{\sim}{0}$ when the material has fully failed, i.e., when the material cannot support stress in any direction. We thus set:

$$\Psi = \Psi(\underset{\sim}{\varepsilon}, \underset{\sim}{\phi}) \tag{A-1}$$

where $\underset{\sim}{\varepsilon}$ denotes the strain tensor. In a thermodynamic sense, $\underset{\sim}{\phi}$ now plays the role of an internal variable, in which case we can write the following relations:

$$\underset{\sim}{\sigma} = \frac{\partial \Psi}{\partial \underset{\sim}{\varepsilon}} \quad , \quad \underset{\sim}{Q} = - \frac{\partial \Psi}{\partial \underset{\sim}{\phi}} \tag{A-2}$$

---

* This nomenclature is preferred to free energy density, in view of the concept of "irreducible" material volume which must be introduced when dealing with heterogeneous multi-phase materials, such as plain concrete.

where $\underset{\sim}{\sigma}$ is the stress tensor and $\underset{\sim}{\mathcal{Q}}$ denotes the internal force, dual to $\underset{\sim}{\phi}$ which is driving the fracturing process.

In view of the definition of $\underset{\sim}{\phi}$, the following relations must hold:

$$\Psi(\underset{\sim}{\varepsilon},\underset{\sim}{Q}) = 0 \quad , \quad \Psi(\underset{\sim}{Q},\underset{\sim}{\phi}) = 0 \quad , \tag{A-3}$$

the first meaning that a fully failed material cannot contain free energy and the second that an unstrained material must have zero free energy; both conditions are relative to the reference state. Furthermore, the following conditions must also hold:

$$\underset{\sim}{\sigma}(\underset{\sim}{\varepsilon},\underset{\sim}{Q}) = \underset{\sim}{Q} \quad , \quad \underset{\sim}{\sigma}(\underset{\sim}{Q},\underset{\sim}{\phi}) = \underset{\sim}{Q} \tag{A-4}$$

$$\underset{\sim}{\mathcal{Q}}(\underset{\sim}{\varepsilon},\underset{\sim}{Q}) = \underset{\sim}{Q} \tag{A-5}$$

Equations (A-4) require that the stress vanish in the fully failed material and that, since the material remains elastic in the damaged state, the stress will vanish at zero strain. Equation (3.5) stipulates that the internal fracture causing force $\underset{\sim}{\mathcal{Q}}$ must vanish in the fully failed material.

If we now expand Ψ in a Taylor series in $\underset{\sim}{\varepsilon}$, retain terms no higher than the quadratic, and observe relations (3.3), we obtain the following form of Ψ:

$$\Psi = C_{ijk\ell}\epsilon_{ij}\epsilon_{k\ell} \tag{A-6}$$

where $\underset{\sim}{C} = \underset{\sim}{C}(\underset{\sim}{\phi})$. It is further assumed that $\underset{\sim}{C}$ depends upon $\underset{\sim}{\phi}$ in a purely quadratic manner. Since the material is assumed to be isotropic in its virgin state, $\underset{\sim}{C}$ may be represented in terms of outer products of the unit tensor $\underset{\sim}{\delta}$ and $\underset{\sim}{\phi}$. Furthermore, since $\underset{\sim}{C}$ is purely quadratic in $\underset{\sim}{\phi}$, it has no other representation than

$$C_{ijk\ell} = \lambda\, \phi_{ij}\phi_{k\ell} + 2\mu\, \phi_{ik}\phi_{j\ell}, \tag{A-7}$$

in view of the symmetries imposed upon it by the symmetry of $\underset{\sim}{\varepsilon}$ implied in Eq. (A-6). The constants λ and 2μ in Eq. (A-7) must indeed by the Lame constants of the virgin material, since

---

* This assumption has recently been verified by Valanis (1987), using a non-thermodynamic approach involving a mapping from undamaged to damaged material.

$$C_{ijk\ell} = \lambda\, \delta_{ij}\delta_{k\ell} + 2\mu\delta_{ik}\delta_{j\ell} \tag{A-8}$$

when $\underline{\phi} = \underline{\delta}$. Thus, we can write

$$\Psi = \frac{1}{2}\lambda\left(\phi_{ij}\epsilon_{ij}\right)^2 + \mu\,\phi_{ik}\phi_{j\ell}\epsilon_{ij}\epsilon_{k\ell} \quad , \tag{A-9}$$

so that, in view of Eq. (A-2a), $\underline{\sigma}$ us given by the expression:

$$\sigma_{ij} = \lambda\,\phi_{ij}\phi_{k\ell}\epsilon_{k\ell} + 2\mu\,\phi_{ik}\phi_{j\ell}\epsilon_{k\ell} \tag{A-10}$$

This equation defines the constitutive response of an elastic fracturing material, once we establish how the integrity tensor $\underline{\phi}$ is related to the fracturing process. In particular, an equation is needed which describes the manner in which $\underline{\phi}$ evolves with accumulated damage, and this is considered below.

A.3 EVOLUTION EQUATION FOR $\underline{\phi}$(DIRECTED DAMAGE)·

When the material is not strain rate sensitive, an increment of tensile strain will produce an increment of damage. Specifically, given an increment in strain, $d\underline{\epsilon}$, let $d\epsilon^{\alpha}$ be its eigenvalues and n_i^{α} its eigenvectors. If $d\underline{\epsilon}$ and $\underline{\epsilon}$ are coaxial, then $d\epsilon^{\alpha}$ will constitute an increase in tensile strain if $d\epsilon^{\alpha} > 0$ and $\epsilon^{\alpha} \geq 0$, where ϵ^{α} denote the eigenvalues of $\underline{\epsilon}$. In the more general case where $d\underline{\epsilon}$ and $\underline{\epsilon}$ are not co-axial, $d\epsilon^{\alpha}$ is said to be an increase in tensile strain if $d\epsilon^{\alpha} > 0$ and $\epsilon_{ij}n_i^{\alpha}n_j^{\alpha} \equiv \epsilon_{\alpha}^{n} \geq 0$ (α not summed). Now let $d\underline{\phi}$ be the change in the integrity tensor $\underline{\phi}$ due to the increment $d\underline{\epsilon}$, and let $\underline{\Omega}_{\phi}^{\alpha}$ be the eigenvectors of $d\underline{\phi}$. We now specify that $d\underline{\phi}$ and $d\underline{\epsilon}$ are co-axial, so that

$$\underline{\Omega}_{\phi}^{\alpha} = \underline{\Omega}^{\alpha} \tag{A-11}$$

The physical significance of Eq. (A-11) is examined in the discussion following Eq. (A-14).

To completely characterize the evolution of $\underline{\phi}$, the relation between $d\phi^{\alpha}$ and $d\epsilon^{\alpha}$ needs to be specified. In this section, we consider a type of damage that is completely "directed", that is, it develops in a specific direction without being accompanied by non-directed (or isotropic) damage. This type of damage is the variety dealt with in linear elastic fracture mechanics (LEFM) and appears to typify that which occurs in single phase brittle materials. Later on in Section A.7, we shall consider the more general case in which the advancing damage consists of both

directed and non-directed (isotropic) components. Such damage is characteristic of multi-phase materials, such as plain concrete, as discussed by Diamond and Bentur (1984).

Restricting attention now to completely "directed" damage, we adopt the following expression relating $d\phi^{\alpha}$ and $d\epsilon^{\alpha}$:

$$d\phi^{\alpha} = - \left(\phi_n^{\alpha}\right)^m d\xi^{\alpha} \tag{A-12}$$

where

$$d\xi^{\alpha} = \begin{cases} k d\epsilon^{\alpha} & , \text{ for } d\epsilon^{\alpha} > 0 \text{ and } \epsilon_n^{\alpha} \geq 0 \\ 0 & , \text{ otherwise} \end{cases} \tag{A-13}$$

Here, k and m are positive constants, and $\phi_n^{\alpha} = \phi_{ij} n_i^{\alpha} n_j^{\alpha}$ (α not summed). The form of Eq. (A-12) has its basis in the physics of annihilation, but may be changed to provide a more realistic description of damage accumulation for a particular material.

In view of Eq. (A-11), we can therefore write

$$d\phi_{ij} = - \sum_{\alpha} \left(\phi_n^{\alpha}\right)^m n_i^{\alpha} n_j^{\alpha} \, d\xi_{\alpha} \tag{A-14}$$

With this evolution equation for $\underset{\sim}{\phi}$, the constitutive description of the elastic fracturing solid is now complete, once the material parameters λ, μ, k and m have been specified.

Physical Interpretation of Equations

The physical meaning of the above equations, and their relation to the fracturing process, is best understood by reference to Eq. (A-10), which relates the stress tensor to the strain tensor. Let $\underset{\sim}{N}^{\alpha}$ be the eigenvectors of $\underset{\sim}{\phi}$ and let $\underset{\sim}{\sigma}$ and $\underset{\sim}{\epsilon}$ be referred to a system of coordinates $\bar{X}_{\alpha}$. Then, the components of $\underset{\sim}{\sigma}$ and $\underset{\sim}{\epsilon}$ on the $\bar{X}_{\alpha}$ coordinate system can be written as:

$$\bar{\sigma}_{rs} = \sigma_{ij} N_i^r N_j^s \tag{A-15}$$

$$\bar{\epsilon}_{rs} = \epsilon_{ij} N_i^r N_j^s \tag{A-16}$$

In this system of coordinates, $\bar{\phi}$ is diagonal, i.e., $\bar{\phi}_{rs} = 0$ for $r \neq s$, and Eq. (A-10) takes the form:

$$\bar{\sigma}_{rs} = \lambda\, \bar{\phi}_{rs}\bar{\phi}_{mn}\bar{\epsilon}_{mn} + 2\mu\, \bar{\phi}_{rm}\bar{\phi}_{sn}\bar{\epsilon}_{mn} \tag{A-17}$$

Since $\bar{\phi}$ is diagonal, we can write:

$$\bar{\sigma}_{11} = \lambda\, \bar{\phi}_{11} \sum_{r=1}^{3} \phi_{rr}\epsilon_{rr} + \bar{\phi}_{11}^2\bar{\epsilon}_{11}$$

$$\bar{\sigma}_{21} = \bar{\sigma}_{12} = 2\mu\, \bar{\phi}_{11}\bar{\phi}_{22}\bar{\epsilon}_{12} \tag{A-18}$$

$$\bar{\phi}_{31} = \bar{\phi}_{13} = 2\mu\, \bar{\phi}_{11}\bar{\phi}_{22}\bar{\epsilon}_{13}$$

Let us now single out the eigenvector N^1 and examine what happens to the stress when the eigenvalue $\phi^1 (= \bar{\phi}_{11})$ vanishes. Note from Eqs. (A-18) that, if $\bar{\phi}_{11} = 0$, it follows that $\sigma_{11} = \bar{\sigma}_{12} = \sigma_{13} = 0$, that is, the solid cannot support stresses on a plane normal to N^1, on which $\phi^1 \equiv \bar{\phi}_{11} = 0$. The physical meaning of this is that the decrease of ϕ^1 represents damage <u>normal</u> to the plane of N^1 and, as such, it is a measure of the plane microcracks that have developed normal to N^1 and/or the increase in the size of such cracks, so that when $\bar{\phi}_{11} = 0$, a plane crack in the accepted sense has formed across the material element on a plane with normal N^1, so that the element cannot support tensile or shear stresses on that plane.

On the basis of the above observations, the physical meaning of Eqs. (A-11), (A-12) and (A-13) now becomes clear. An increase in tensile strain $d\epsilon^\alpha$ on a plane with normal n^α causes planar damage $d\phi^\alpha$ on that plane, where $d\phi^\alpha$ is given by Eq. (A-12), in accordance with the observation that "planar microcracks form perpendicular to the direction of the principal tensile strain."

The constant k in Eq. (A-13) is a material parameter that reflects the fracture resistance or fracture toughness of the material. Eq. (A-12) is representative of processes involving annihilation of populations and catastrophic processes in systems where the increment of annihilation is proportional to the state of integrity, which is given here by the factor $(\phi_n^\alpha)^m$. This form is representative of such systems, even though any monotonically decreasing function $f(\phi_n^\alpha)$, such that $f(0) = 0$, will likely do as well. Finally, we note that the damage tensor $\underline{D}$ can be expressed in terms of $\bar{\phi}$ as follows:

$$D_{ij} = \sum_{\alpha} \left[1 - \left(\phi^{\alpha}\right)^2\right] N_i^{\alpha} N_j^{\alpha} \qquad \text{(A-19)}$$

The physical interpretation of the governing equations is now complete.

A.4 APPLICATION TO SOME SIMPLE CASES OF HOMOGENEOUS DEFORMATION.

In this section, analytic solutions, based upon the constitutive model described above, are presented for several simple cases of homogeneous deformation including simple tension, simple compression and simple shear. These solutions provide valuable insight into the characteristics of the model and reveal its remarkable predictive capabilities, despite the fact that it involves only four material parameters.

A.4.1 Homogeneous Triaxial Strain Fields.

As a preliminary development, consider the case in which the strain field is homogeneous and consists only of principal strains, i.e., $\epsilon_{ij} = 0$ for $i \neq j$. Thus, $d\underline{\xi}$ and $\underline{\xi}$ are always coaxial and $\underline{\phi}$ is coaxial with $\underline{\xi}$ by virtue of Eq. (A-11). As a result, $\underline{\phi}$ is diagonal. In view of Eq. (A-10), $\underline{q}$ is also diagonal. The principal stresses are given below in terms of the principal strains and the principal values of $\underline{\phi}$:

$$\sigma_1 = \lambda\, \phi_1 \sum_r \phi_r \epsilon_r + 2\mu \phi_1^2 \epsilon_1$$

$$\sigma_2 = \lambda\, \phi_2 \sum_r \phi_r \epsilon_r + 2\mu\, \phi_2^2 \epsilon_2 \qquad \text{(A-20)}$$

$$\sigma_3 = \lambda\, \phi_3 \sum_r \phi_r \epsilon_r + 2\mu\, \phi_3^2 \epsilon_3$$

The appropriate evolution equation for $\underline{\phi}$ is obtained from Eq. (A-14) and is given in terms of the principal components of $\underline{\phi}$ as follows:

$$d\phi_i = - \left(\phi_i\right)^m d\xi_i \qquad \text{(A-21)}$$

where

$$d\xi_i = \begin{cases} k\, d\epsilon_i \ , & \text{if } d\epsilon_i > 0 \ , \ \epsilon_i \geq 0 \\ 0 \ , & \text{otherwise} \end{cases}$$

We now consider two special cases of the above equations, namely, simple tension and simple compression.

A.4.2 Simple Tension.

Consider the case of monotonically increasing simple tension. In this case, $\sigma_2 = \sigma_3 = 0$, and integration of Eqs. (A-21) with $\epsilon_2 = \epsilon_3$ and the initial conditions $\phi_2 = \phi_3 = 1$, shows that $\phi_2 = \phi_3$ always. Hence, we find that

$$\phi_2\epsilon_2 = -\frac{\lambda}{2(\lambda+\mu)}\,\epsilon_1\phi_1 = -\nu\phi_1\epsilon_1 \qquad \text{(A-22)}$$

and

$$\sigma_1 = E\phi_1^2\epsilon_1 \qquad \text{(A-23)}$$

where

$$E = \frac{(2\mu+3\lambda)\mu}{\lambda+\mu} \qquad \text{(A-24)}$$

From Eq. (A-21a), the evolution equation for ϕ_1 is

$$d\xi_1\phi_1^m + d\phi_1 = 0 \ , \qquad \text{(A-25)}$$

subject to the initial condition $\phi_1(0) = 1$. Thus, the solution is

$$\phi_1 = \begin{cases} e^{-k\epsilon_1} & , \text{ if } m = 1 \\ \left\{1 - (1-m)k\epsilon_1\right\}^{\frac{1}{1-m}} & , \text{ if } m \neq 1 \end{cases} \qquad \text{(A-26)}$$

Combining Eqs. (A-23) and (A-26), we obtain the expression:

$$\sigma_1 = \begin{cases} e^{-2k\epsilon_1}, & \text{if } m = 1 \\ E\,\epsilon_1\left\{1-(1-m)k\epsilon_1\right\}^{\frac{2}{1-m}}, & \text{if } m \neq 1 \end{cases} \qquad \text{(A-27)}$$

Inspection of Eq. (A-27) reveals that, for $0 \leq m < 1$, σ_1 is not a monotonic function of ϵ_1, but reaches a maximum and then goes to zero for finite ϵ_1. For $1 \leq m < 3$, σ_1 again reaches a maximum and then decays monotonically to zero as $\epsilon_1 \to \infty$. For $m = 3$, σ_1 monotonically increases to an asymptotic constant value as $\epsilon_1 \to \infty$, while for $3 < m < \infty$, σ_1 increases monotonically with ϵ_1. The influence of m on the constitutive response is shown in Figure A.1a. Thus, in the range $0 \leq m < 3$, the model exhibits softening in tension in agreement with experimental data.

The model also unloads elasticity with an effective modulus of $E\phi_1^2$ which is diminished by the accumulated damage. Thus, the model has all of the characteristics of a fracturing elastic solid. It follows from Eq. (A-22) that $\epsilon_2 \leq 0$ and hence $\phi_2 = 1$, i.e., no damage is produced in the transverse direction due to the uniaxial tension loading.

A.4.3 Simple Compression.

Consider now the case of monotonically increasing uniaxial compression. Here, $\sigma_2 = \sigma_3 = 0$, while σ_1 and ϵ_1 are compressive. Again, Eqs. (A-21) together with $\epsilon_2 = \epsilon_3$, and the initial conditions $\phi_2 = \phi_3 = 1$, lead to the result that $\phi_2 = \phi_3$ always. Similar to the case of simple tension, we find that

$$\phi_2\epsilon_2 = -\nu\phi_1\epsilon_1 \qquad \text{(A-28)}$$

and

$$\sigma_1 = E\phi_1^2\epsilon_1 \qquad \text{(A-29)}$$

The damage evolution in this case is, however, entirely different from that for simple tension. Since both $d\epsilon_1$ and ϵ_1 are compressive at all times, we find from Eq. (A-21) that $d\phi_1 = 0$ and thus $\phi_1 = 1$ always. However, in view of Eq. (A-28), ϵ_2 is now tensile and hence ϕ_2 (and ϕ_3) will increase with the consequence that damage will develop on planes which are parallel to the axis of compression, in accordance with experimental observation; this is the so-called axial splitting mode (Horii and Nemat-Nasser, 1985).

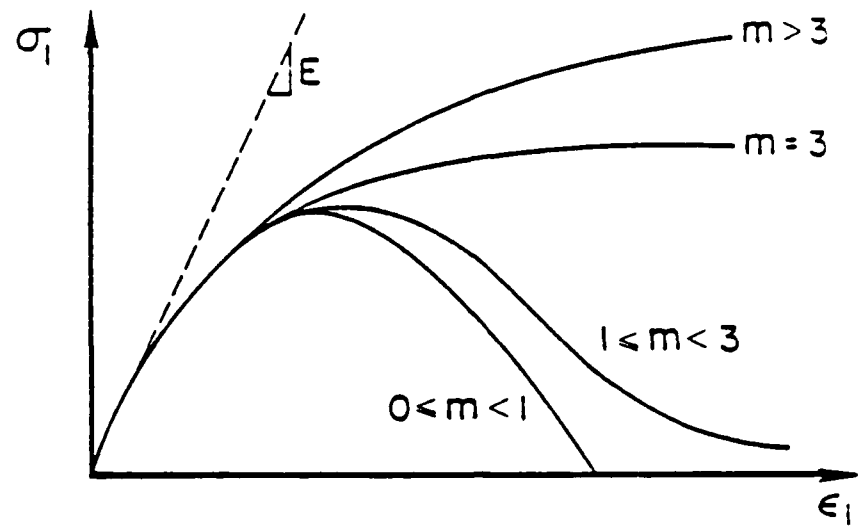

(a) Stress-strain relation in simple tension

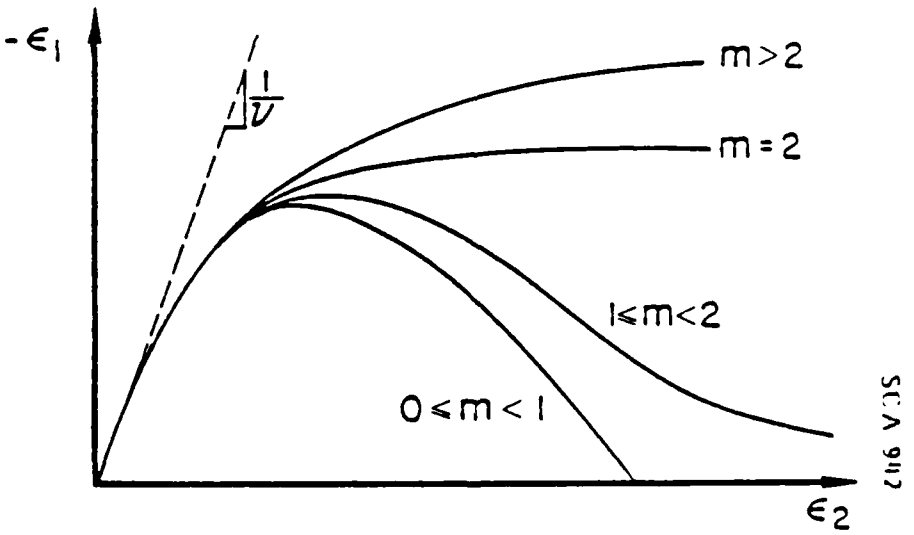

(b) Axial strain vs. lateral strain in simple compression

Figure A.1 Predicted responses for simple tension and simple compression, showing the effect of the parameters m on the resulting behavior.

From Eq. (A-21), we can write

$$d\phi_2 + \phi_2^m k \, d\epsilon_2 = 0 \quad , \tag{A-30}$$

the solution of which is

$$\phi_2 = \begin{cases} e^{-k\epsilon_2} & , \ m = 1 \\ \left\{1 - (1-m)k\epsilon_2\right\}^{\frac{1}{1-m}} & , \ m \neq 1 \end{cases} \tag{A-31}$$

Thus, in view of Eq. (A-29) and the condition $\phi_1 = 1$, the axial stress strain relation is

$$\sigma_1 = E \, \epsilon_1 \quad , \tag{A-32}$$

so that the response in the axial direction is purely elastic.

To find the relation between the strains, we use Eqs. (A-28) and (A-31) together with the fact that $\phi_1 = 1$. It then follows that

$$-\nu\epsilon_1 = \begin{cases} \epsilon_2 e^{-k\epsilon_2} & , \ m = 1 \\ \epsilon_2\left\{1 - (1-m)k\epsilon_2\right\}^{\frac{1}{1-m}} & , \ m \neq 1 \end{cases} \tag{A-33}$$

Here, we may distinguish three different cases:

(a) $0 \leq m < 1$

The strain ϵ_1 is not a monotonic function of ϵ_2. It reaches a maximum absolute value and then goes to zero for a finite value of ϵ_2. Specifically,

$$|\epsilon_1|_{max} = \frac{1}{k\nu}\left(\frac{n}{n+1}\right)^{n+1} \tag{A-34}$$

where $n = 1/(1-m)$.

(b) $1 \leq m < 2$

Again, the strain ϵ_1 is not a monotonic function of ϵ_2. It reaches a maximum absolute value again given by Eq. (A-34) for $1 < m$ and then goes to zero for infinite ϵ_2. For $m = 1$

$$|\epsilon_1|_{max} = \frac{1}{\nu e k} , \tag{A-35}$$

where e denotes the base of the natural logarithm.

(c) $2 \leq m < \infty$

In this case, ϵ_1 is a monotonic function of ϵ_2 and approaches the following limiting condition for increasing lateral strain:

$$\lim_{\epsilon_2 \to \infty} |\epsilon_1|_{max} = \begin{cases} \frac{1}{k} , & m = 2 \\ \infty , & m > 2 \end{cases} \tag{A-36}$$

The above cases are depicted graphically in Figure A.1(b).

A.4.4 Collapse of a Block Under Axial Compression.

It follows from the above discussion that a block consisting of elastic fracturing material will collapse under homogeneous axial compression if $0 \leq m \leq 2$, since ϵ_1 has an upper bound given by the expression:

$$|\epsilon_1|_{max} = \frac{1}{\nu k} \left(\frac{1}{2-m}\right)^{\frac{2-m}{1-m}} \tag{A-37}$$

The limiting cases are

$$|\epsilon_1|_{max} = \begin{cases} \frac{1}{\nu k e} , & m = 1 \\ \frac{1}{\nu k} , & m = 2 \end{cases} \tag{A-38}$$

The collapse stress may be calculated directly from Eq. (A-32), with the result:

$$|\sigma_1|_{max} = \frac{E}{\nu k} \left(\frac{1}{2-m}\right)^{\frac{2-m}{1-m}} \tag{A-39}$$

Thus, the theory predicts the collapse of a block under axial compression due to damage on planes parallel to the axis of compression. Again, this is the axial splitting mode.

A.4.5 Ratio of Collapse Stresses in Tension and Compression.

At this point, it is of interest to explore the rationality of the above results by comparing the ratio σ^c/σ^t, where σ^c and σ^t are collapse stresses in compression and tension, respectively, obtained analytically, with that observed experimentally for concrete, even though the end-grip conditions in the tests may not be ideal, as assumed in solutions obtained here. Restricting attention to the case m = 1, it follows from Eqs. (A-37) and (A-39) that

$$\frac{\sigma^c}{\sigma^t} = \frac{2}{\nu} \tag{A-40}$$

Since $\nu \simeq 0.2$ for concrete, we have

$$\frac{\sigma^c}{\sigma^t} \simeq 10 \quad , \tag{A-41}$$

which is close to experimental observation (Raphael, 1984).

A.4.6 Simple Shear.

Consider now the case of monotonically increasing shear strain under conditions of simple shear and small strain. The configuration of interest is depicted in Figure A.2. Inasmuch as the only non-zero strain component is ϵ_{12}, we can write

$$\phi_{k\ell}\epsilon_{k\ell} = 2\,\phi_{12}\epsilon_{12} \tag{A-42}$$

and

$$\phi_{ik}\phi_{j\ell}\epsilon_{k\ell} = (\phi_{i1}\phi_{j2} + \phi_{i2}\phi_{j1})\epsilon_{12} \tag{A-43}$$

Therefore, in this case, the general constitutive relation

$$\sigma_{ij} = \lambda\,\phi_{ij}\phi_{k\ell}\epsilon_{k\ell} + 2\mu\,\phi_{ik}\phi_{j\ell}\epsilon_{k\ell} \tag{A-44}$$

reduces to the form

$$\sigma_{ij} = 2\left[\lambda\,\phi_{ij}\phi_{12} + \mu\left(\phi_{i1}\phi_{j2} + \phi_{i2}\phi_{j1}\right)\right]\epsilon_{12} \tag{A-45}$$

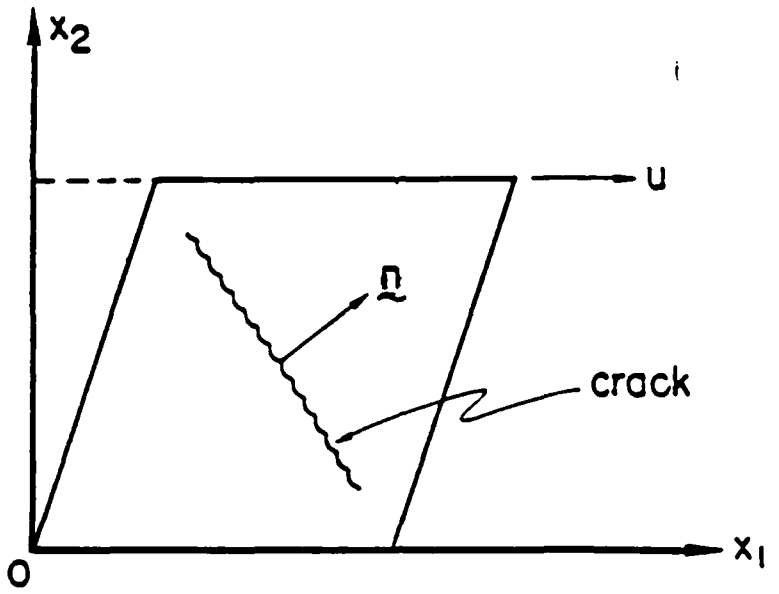

Figure A.2. Simple shear

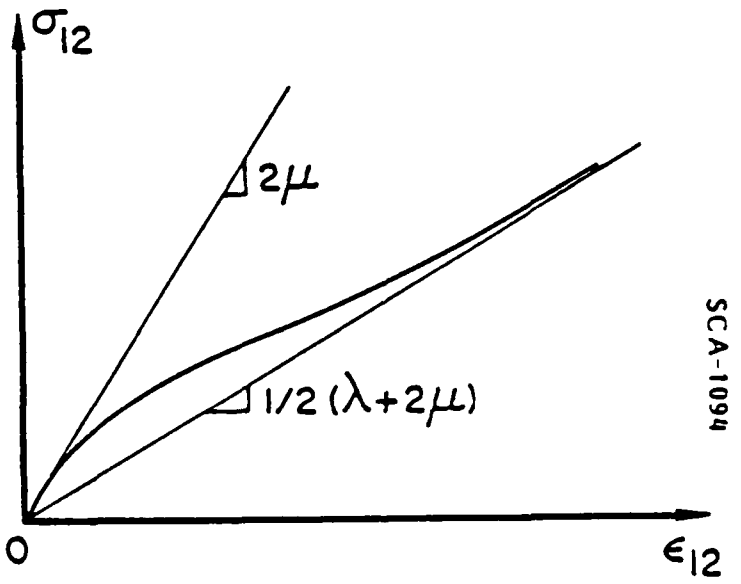

Figure A.3. General relationship between σ_{12} and ϵ_{12} for the case in which $\lambda > 2\mu$.

Therefore, we can write

$$\sigma_{12} = 2\left[\lambda\ \phi_{12}^2 + \mu\left(\phi_{11}\phi_{22} + \phi_{12}^2\right)\right]\epsilon_{12} \tag{A-46}$$

$$\sigma_{11} = 2(\lambda + 2\mu)\phi_{11}\phi_{12}\epsilon_{12} \tag{A-47}$$

$$\sigma_{22} = 2(\lambda + 2\mu)\phi_{22}\phi_{12}\epsilon_{12} \tag{A-48}$$

For a small shear strain, the maximum tensile strain will lie in a direction that makes a 45 degree angle with each of the coordinate axes. Consequently, cracks will develop in the material as shown in Figure A.2. The components of the unit normal $\underline{n}$ to the crack are $n_1 = n_2 = 1/\sqrt{2}$.

Since there is only one cracking direction, we set $\alpha = 1$ in the evolutionary equation for $d\phi_{ij}$ and write

$$d\phi_{ij} = -\ k(\phi_n)^m d\epsilon\ n_i n_j \tag{A-49}$$

where

$$\phi_n = \phi_{ij} n_i n_j$$
$$d\epsilon = d\epsilon_{12} \tag{A-50}$$

Since $n_1 = n_2 = 1/\sqrt{2}$, it follows from Eq. (A-49) that

$$d\phi_{11} = d\phi_{22} = d\phi_{12} \tag{A-51}$$

Hence

$$\int_1^{\phi_{11}} d\phi_{11} = \int_0^{\phi_{12}} d\phi_{12}\ , \tag{A-52}$$

since $\phi_{ij} = \delta_{ij}$ initially. From Eq. (A-53) we find

$$\phi_{11} = 1 + \phi_{12}\ , \tag{A-53}$$

and Eq. (A-50a) gives

$$\phi_n = \phi_{11} + \phi_{12}\ , \tag{A-54}$$

since $\phi_{11} = \phi_{22}$ according to Eq. (A-51).

Substitution of Eq. (A-53) into Eq. (A-54) yields

$$\phi_n = 1 + 2\,\phi_{12} \tag{A-55}$$

which, when combined with Eq. (A-49), leads to the result

$$d\phi_{ij} = -\,k\left(1 + 2\phi_{12}\right)^m d\epsilon_{12} n_i n_j \tag{A-56}$$

Therefore, since $n_1 = n_2 = 1/\sqrt{2}$, we can write

$$d\phi_{12} = -\,\frac{k}{2}\left(1 + 2\,\phi_{12}\right)^m d\epsilon_{12} \tag{A-57}$$

which can be integrated to give, for $m = 1$:

$$\phi_{12} = \frac{1}{2}\left[e^{-k\epsilon_{12}} - 1\right] \tag{A-58}$$

and for $m \neq 1$:

$$\phi_{12} = \frac{1}{2}\left\{\left[\frac{1}{k(m-1)\epsilon_{12}+1}\right]^{\frac{1}{m-1}} - 1\right\} \tag{A-59}$$

Recalling Eq. (A-53) and the fact that $\phi_{22} = \phi_{11}$, Eq. (A-46) can be placed in the following form:

$$\sigma_{12} = 2\left[(\lambda + 2\mu)\phi_{12}^2 + 2\mu\phi_{12} + \mu\right]\epsilon_{12} \tag{A-60}$$

Therefore, Eqs. (A-58) to (A-60) describe the relationship between σ_{12} and ϵ_{12}.

From Eqs. (A-58) and (A-59) note that

$$\lim_{\epsilon_{12}\to+\infty} \sigma_{12} = -\,\frac{1}{2}\,(\lambda + 2\mu)\epsilon \tag{A-61}$$

which in view of Eq. (A-60) leads to the result:

$$\lim_{\epsilon_{12}\to+\infty} \sigma_{12} = \frac{1}{2}\,(\lambda + 2\mu)\epsilon_{12} \tag{A-62}$$

Hence, when $\lambda < 2\mu$, the ultimate slope given by Eq. (A-62) will be less than the initial slope, 2μ, as shown in Figure A.3. The case $\lambda > 2\mu$ on the other hand, leads to the ultimate slope being greater than the initial slope, i.e., a hardening, which is difficult to visualize from a physical standpoint. These limiting cases, however, fall outside of the assumption of small strains made here and therefore may not be physically meaningful.

A.5 APPLICATION TO NON-HOMOGENEOUS STRAIN FIELDS.

In an effort to explore the capability of the continuous damage model to predict the proper trends for fracture problems involving non-homogeneous strain fields, we developed a computer program for the model and incorporated it into a finite element code. We then conducted a limited numerical study of a fracture problem, having a non-homogeneous strain field, for which a theoretical solution is available from linear elastic fracture mechanics (LEFM). The problem, depicted in Figure A.4(a), consists of a long flat plate of width w, which has a crack of length 2a and is acted upon by a uniform tensile stress σ. The problem is to find the magnitude of σ which causes the crack to grow catastrophically and thereby cause fracture of the plate.

The finite element grid used in the numerical study consisted of uniform, initially square zones of unit length. Because of symmetry, only the right half of the problem was considered. Vertically, there were 21 zones while 16 zones were used in the horizontal direction. Therefore, the width w had the value 32. The effect of an initial crack in the x-direction was introduced into the grid by simple setting $\phi_{yy} = 0$ in those zones through which the crack passed. In the study,. three different values of initial crack length were considered, namely, a = 1, 3 and 6.

The results from the numerical study are shown in Figure A.4(b), where the stress σ_f to fracture the plate is plotted against the dimensionless ratio a/w. Also shown on this figure is the corresponding theoretical prediction from LEFM (see Knott, 1973), which is given by the expression:

$$\sigma_f = \frac{K_{IC}}{\left[w \tan\left(\frac{\pi a}{w}\right)\right]^{1/2}} \quad , \tag{A.63}$$

where K_{IC}, the mode I fracture toughness, was set to the value 7.07 so that the theoretical curve would pass through the central numerical point shown in the figure. As an inspection of the figure reveals, the continuous damage model predicts a decay

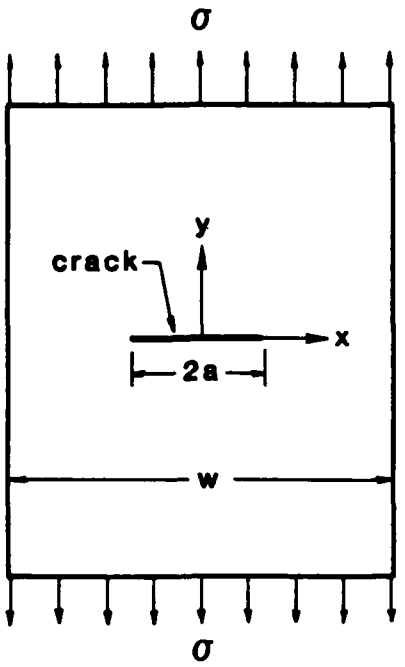

(a) Geometric configuration of flat plate.

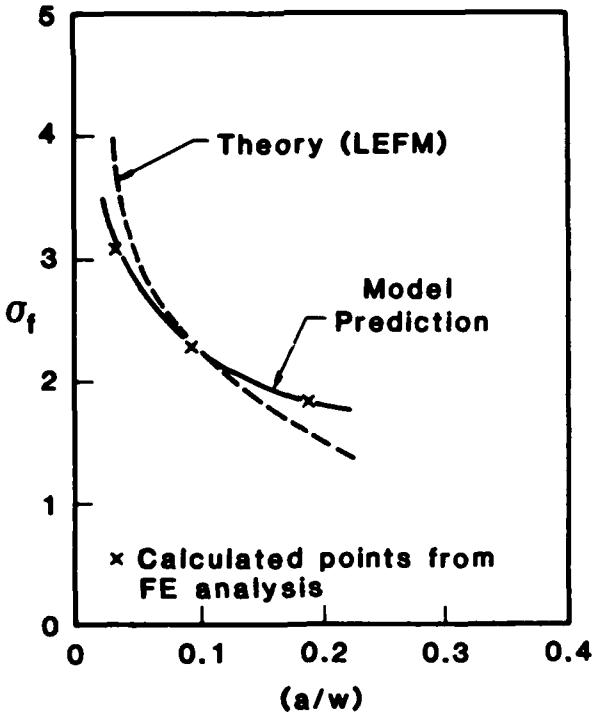

(b) Dependence of fracture stress σ_f on the ratio a/w.

Figure A.4. Response of a thin elastic plate with a crack to an applied uniform tensile stress.

of σ_f with increasing a/w, which is qualitatively in agreement with the theoretical result from LEFM.

Exact agreement between the model prediction and LEFM is not to be expected, however, for several reasons. First, the model produces some damage in every zone of the grid from the onset of the tensile loading, while in LEFM theory it is assumed that the damage remains confined to the original crack until there is catastrophic crack extension. Secondly, for the material region just ahead of the crack, the two approaches lead to significantly different stress fields. In LEFM, the material ahead of the crack remains linearly elastic and undamaged until overall failure occurs, while, in the numerical simulation with the model, the zones ahead of the crack experience increasingly greater damage as σ grows. Thus, the stress fields in the material just ahead of the crack are very much different in the two cases. In view of these considerations, the differences between the two predictions shown in Figure A.4 are not surprising. The general trends, however, are similar and indicate that the present model, when used in conjunction with a finite element code, leads to realistic results. Closer agreement between the two predictions could probably be obtained by revising the evolution equation for $\underline{\phi}$.

A.6 POST-FAILURE BEHAVIOR AND CRACK CLOSURE.

It was shown in Section A.3 that if an eigenvalue ϕ^A of $\underline{\phi}$ vanishes in a material element then the element cannot support stress on a plane normal to $\bar{N}^A$, the latter being the eigenvector of $\underline{\phi}$ associated with ϕ^A. In a structural sense the element has developed damage equivalent to a crack on the plane normal to $\bar{N}^A$. It follows that the element has developed kinematic freedom in directions normal and tangential fo $\bar{N}^A$ in the following sense. Let $\Delta\bar{\epsilon}_{\alpha\beta}$ be the components of the strain increments $\Delta\underline{\epsilon}$ defined relative to a system of coordinates x^α coincident with the eigenvectors $\bar{N}^\alpha$ of $\underline{\phi}$. Thus

$$\Delta\bar{\epsilon}_{\alpha\beta} = \begin{bmatrix} \Delta\bar{\epsilon}_{11} & \Delta\bar{\epsilon}_{12} & \Delta\bar{\epsilon}_{13} \\ \Delta\bar{\epsilon}_{21} & \Delta\bar{\epsilon}_{22} & \Delta\bar{\epsilon}_{23} \\ \Delta\bar{\epsilon}_{31} & \Delta\bar{\epsilon}_{32} & \Delta\bar{\epsilon}_{33} \end{bmatrix} \qquad \text{(A-64)}$$

Let $A = 1$. Perusal of Eqs. (A-18a.b.c) show that if $\phi^1 = \phi_{11} = 0$, then not only are $\bar{\sigma}_{11} = \bar{\sigma}_{12} = \bar{\sigma}_{13} = \bar{\sigma}_{31} = \bar{\sigma}_{21} = 0$ as discussed previously but the strains $\bar{\epsilon}_{11}$, $\bar{\epsilon}_{12} = \epsilon_{21}$, $\epsilon_{31} = \epsilon_{13}$ become indeterminate from the constitutive properties of the element.

A.7 DIRECTED AND ISOTROPIC DAMAGE.

It has recently been observed (Diamond and Bentur, 1984) that, in multi-phase materials, such as plain concrete, the formation of directional cracks is usually accompanied by the presence of small cracks randomly oriented, which from a statistical viewpoint amount to isotropic damage, denoted here by Ω. In this sense Ω reduces the stress carrying capacity of a material by the same degree in all directions. Thus the integrity tensor, now denoted by $\underset{\sim}{\phi}_\Omega$ must be reduced by the presence of Ω and hence it must be a state function of Ω. Thus, in symbolic form:

$$\underset{\sim}{\phi}_\Omega = \underset{\sim}{\phi}_\Omega(\Omega, \xi_\alpha) \tag{A-65}$$

subject to the following conditions which must always apply:

$$\underset{\sim}{\phi}_\Omega(0,0) = \underset{\sim}{\delta}$$

$$\underset{\sim}{\phi}_\Omega(1,\xi_\alpha) = \underset{\sim}{0} \tag{A-66}$$

where $\underset{\sim}{\delta}$ is the unit matrix.

To satisfy conditions (A-66) we adopt a relation of the multiplicative type, i.e., we set

$$\underset{\sim}{\phi}_\Omega = w(\Omega)\underset{\sim}{\phi}(\xi_\alpha) \tag{A-67}$$

such that $w(0) = 1$, $w(1) = 0$. Furthermore w must be a monotonically decreasing function of Ω. A suitable function that satisfies the above constraints is

$$w(\Omega) = (1 - \Omega)^a \tag{A-68}$$

where $a \geq 0$. Thus the integrity tensor $\underset{\sim}{\phi}$, considered in the previous sections, is now modified by the presence of isotropic damage as specified by Eqs. (A-67) and (A-68).

The constitutive equation thus becomes

$$\psi = \frac{1}{2}\omega^2\left\{\lambda\left(\phi_{ij}\epsilon_{ij}\right)^2 + \mu\,\phi_{ik}\phi_{j\ell}\epsilon_{ij}\epsilon_{k\ell}\right\} \tag{A-69}$$

and

$$\sigma_{ij} = \omega^2\left\{\lambda\phi_{ij}\phi_{k\ell}\epsilon_{k\ell} + 2\mu\,\phi_{ik}\phi_{j\ell}\epsilon_{k\ell}\right\} \tag{A-70}$$

A.7.1 The Rate Equation for Ω.

Physical considerations suggest that isotropic damage in cementitious materials is caused mainly by shearing which gives rise to local decohesion (between the mortar and the aggregate, and/or the paste and the sand particles). Thus following similar reasoning that gave rise to Eq. (A-12) and noting that the ultimate value of Ω is unity, we set $d\Omega$ to be proportional to a positive monotonic function of the isotropic integrity $(1-\Omega)$, i.e.,

$$d\Omega = f(1-\Omega)d\varsigma \quad , \tag{A-71}$$

where $d\varsigma$ is defined in terms of the increment in the deviatoric strain tensor de_{ij} as

$$d\varsigma^2 = c^2\left(de_{ij}de_{ij}\right) \tag{A-72}$$

and $c > 0$ is a material parameter A suitable form of the function f is as follows:

$$f(1-\Omega) = (1-\Omega)^b \tag{A-73}$$

where $b > 0$. Solution of Eq. (A-71) in the light of Eq. (A-73) gives rise to the expression

$$1-\Omega = \left(1-(1-b)\varsigma\right)^{\frac{1}{1-b}} \quad , \tag{A-74}$$

which is of the same form as Eq. (A-26). Specifically, if $b = 1$ then

$$(1-\Omega) = e^{-b\varsigma} \quad . \tag{A-75}$$

We note that c in Eq. (A-72) plays the role of an isotropic fracture toughness parameter which influences the rate of isotropic degradation.

A.7.2 Isotropic Damage in Homogeneous Triaxial Strain Fields.

In the presence of isotropic damage the counterparts of Eqs. (A-20) are:

$$\frac{\sigma_1}{\omega^2} = \lambda\phi_1 \sum \phi_k \epsilon_k + 2\mu\ \phi_1^2 \epsilon_1 \tag{A-76}$$

$$\frac{\sigma_2}{\omega^2} = \lambda\phi_2 \sum \phi_k \epsilon_k + 2\mu\ \phi_2^2 \epsilon_2 \tag{A-77}$$

$$\frac{\sigma_3}{\omega^2} = \lambda\phi_3 \sum \phi_k \epsilon_k + 2\mu\ \phi_3^2 \epsilon_3 \tag{A-78}$$

In that which follows, we illustrate the application of the above equations to two special cases of interest, namely, simple tension and simple compression.

(A) SIMPLE TENSION

Here $\sigma_2 = \sigma_3 = 0$ and the analysis follows very closely that of Section A.4.2. Specifically, in view of Eqs. (A-78):

$$\phi_2 \epsilon_2 = -\nu\ \phi_1 \epsilon_1 \tag{A-79}$$

$$\sigma_1 = \left(E\phi_1^2 \epsilon_1\right)\omega^2 \tag{A-80}$$

However, as opposed to the analysis in Section A.4.2 <u>two</u> functions ϕ_1 and ω are now necessary to determine the axial stress σ_1. In the absence of explicit coupling between directional and isotropic damage, ϕ_1 is still given by Eq. (A-26) in which case

$$\phi_1 = \left\{1 - (1 - m)k\epsilon_1\right\}^{\frac{1}{1-m}} \tag{A-81}$$

However, we expect that k in Eq. (A-81) will depend on Ω since clearly the material resistance to cracking will be greatly influenced by the presence of the isotropic damage. Specifically we expect that

$$k = k(\Omega) \tag{A-82}$$

where k is an increasing function of Ω. In this event Eq. (A-25) can no longer be integrated directly and Eq. (A-81) will not hold.

Evolution of Isotropic Damage.

In the presence of axial loading ($\sigma_2 = \sigma_3 = 0$)

$$d\zeta = c\sqrt{\frac{3}{2}} \left| d\epsilon_1 - d\epsilon_2 \right| \tag{A-83}$$

which in the light of Eq. (A-79) becomes

$$d\zeta = c\sqrt{\frac{3}{2}} \left| d\epsilon_1 + \nu\, d\left(\frac{\phi_1}{\phi_2}\,\epsilon_1\right) \right| \tag{A-84}$$

where use was made of Eq. (A-12). Thus, in general, we have the following coupled equations that govern simultaneously the evolution of directional and isotropic damage in simple tension:

$$d\phi_1 = -\,\phi_1^m\, k(\Omega)\, d\epsilon_1 \tag{A-85}$$

$$d\Omega = (1 - \Omega)^b\, c\sqrt{\frac{3}{2}} \left(1 + \nu\phi_1 - \nu k \phi_1^m \epsilon_1\right) d\epsilon_1 \tag{A-86}$$

Approximate Solution of Eqs. (A-85) and (A-86).

To obtain a qualitative understanding of the simultaneous effects of isotropic and directional damage we solve Eqs. (A-85) and (A-86) approximately. Specifically we uncouple the equations by setting $k(\Omega)$ equal to a constant k and setting equal to zero the terms on the righthand side of Eq. (A-86) that are multiplied by ν, since in the region of softening $\phi_1 < 1$ and the terms $\nu\phi_1$ and $k\phi_1^m$ are considerably less than unity. Then ϕ_1 is given by Eq. (A-81) while Ω is given by Eq. (A-87), i.e.,

$$1 - \Omega = \left\{1 - (1 - b)c\sqrt{\frac{3}{2}}\,\epsilon_1\right\}^{\frac{1}{1-b}} \tag{A-87}$$

in view of Eq. (A-74). Thus σ_1 may now be found upon use of Eqs. (A-80), (A-81) and (A-68) and is given below:

$$\sigma_1 = E\left(1 - (1 - m)k\epsilon_1\right)^{\frac{2}{1-m}} \epsilon_1 \left\{1 - (1 - b)c\sqrt{\frac{3}{2}}\,\epsilon_1\right\}^{\frac{2a}{1-b}} \tag{A-88}$$

In the very specific case where $m = b = 1$

$$\sigma_1 = E\epsilon_1 e^{-2\left(k + ac\sqrt{\frac{3}{2}}\right)\epsilon_1} \tag{A-89}$$

In other words, directional and isotropic degradation compound the effect of softening in simple tension. As we shall see this is not the case in compression. For comparison when isotropic damage is absent, see Eq. (A-27b).

(B) SIMPLE COMPRESSION

In this case Eqs. (A-79) and (A-80) apply but now $\phi_1 = 1$. Thus in this specific case

$$\phi_2\epsilon_2 = -\nu\,\epsilon_1 \tag{A-90}$$

$$\sigma_1 = E\epsilon_1\omega^2 \tag{A-91}$$

As opposed to tension, softening in compression is due entirely to volumetric damage. The appropriate rate equations in the presence of monotonic loading are:

$$d\phi_2 = -\phi_2^m\, k(\Omega)\, d\epsilon_2 \tag{A-92}$$

$$d\Omega = (1 - \Omega)^b c\sqrt{\frac{3}{2}}\left[1 + \frac{1}{\nu} - \frac{k(\Omega)}{\nu}\,\phi_2^m\epsilon_2\right]d\epsilon_2 \tag{A-93}$$

where Eqs. (A-71), (A-73), (A-90), and (A-92) were used. Eqs. (A-92) and (A-93) are coupled and cannot be integrated directly. We obtain, therefore, approximate solutions of these equations in order to study their qualitative trends. To that end we let $k(\Omega)$ be a constant k and define c^* by the relation

$$c\sqrt{\frac{3}{2}}\int_0^{\epsilon_2}\left[1 + \frac{1}{\nu} - \frac{k}{\nu}\,\phi_2^m\epsilon_2'\right]d\epsilon_2' = c^*\,\epsilon_2 \tag{A-94}$$

Equations (A-92) and (A-93) may now be integrated to give:

$$\phi_2 = \left\{1 - (1 - m)k\epsilon_2\right\}^{\frac{1}{1-m}} \tag{A-95}$$

$$1 - \Omega = \left\{1 - (1 - b)c^*\epsilon_2\right\}^{\frac{1}{1-b}} \tag{A-96}$$

$$-\nu\epsilon_1 = \epsilon_2\phi_2 = \epsilon_2\left\{1 - (1 - m)k\,\epsilon_2\right\}^{\frac{1}{1-m}} \tag{A-97}$$

$$\sigma_1 = E\epsilon_1\left\{1 - (1 - b)c^*\epsilon_2\right\}^{\frac{2a}{1-b}} \tag{A-98}$$

In Figure A.5 we show an experimental relation between the axial and transverse strains in the case of a concrete block under axial compression, according to Van Mier (1984), and the analytical relation according to Eq. (A-97) when $\nu = 0.35$, $k = 70$ and $m = 2.4$. Also shown is a compressive stress-strain relation for the same material and specimen. The approximate analytical axial stress-axial strain relation obtained on the basis of Eqs. (A-97) and (A-98) is shown in Figure A.6 when $2a/1\text{-}b = 1.5$ and $(1\text{-}b)c^* = 40$ (c^* assumed constant). For the same model, a comparison between the predicted and measured volume strain ϵ_{kk} as a function of the axial strain ϵ_1 is shown in Figure A.7. From this figure, it is evident that the model describes the observed dilatancy quite well.

A.7.3 Discussion.

The extensive and painstakingly precise investigations by Van Mier into the compressive deformation and fracture of concrete make it abundantly clear that the softening branch of the axial stress-strain curve represents the behavior of a geometric structure rather than that of a uniform material. The experiments in tension by Gopalaratnam and Shah (1985) lead to similar conclusions. There are therefore significant statistical variations in the behavior of concrete in the "softening regime."

The continuum damage theory which we have proposed in the previous sections captures, we believe, many of the essential features of the constitutive behavior of fracturing concrete. Further aspects of this approach shall be pursued in our future research.

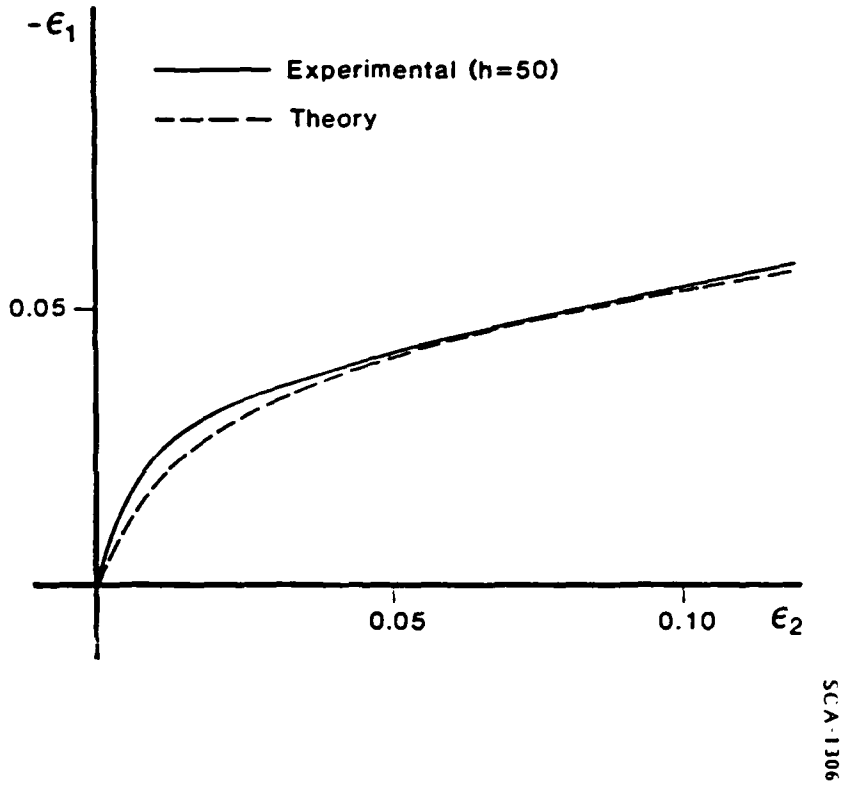

Figure A.5. **Relation between axial and transverse strains under conditions of simple compression.**

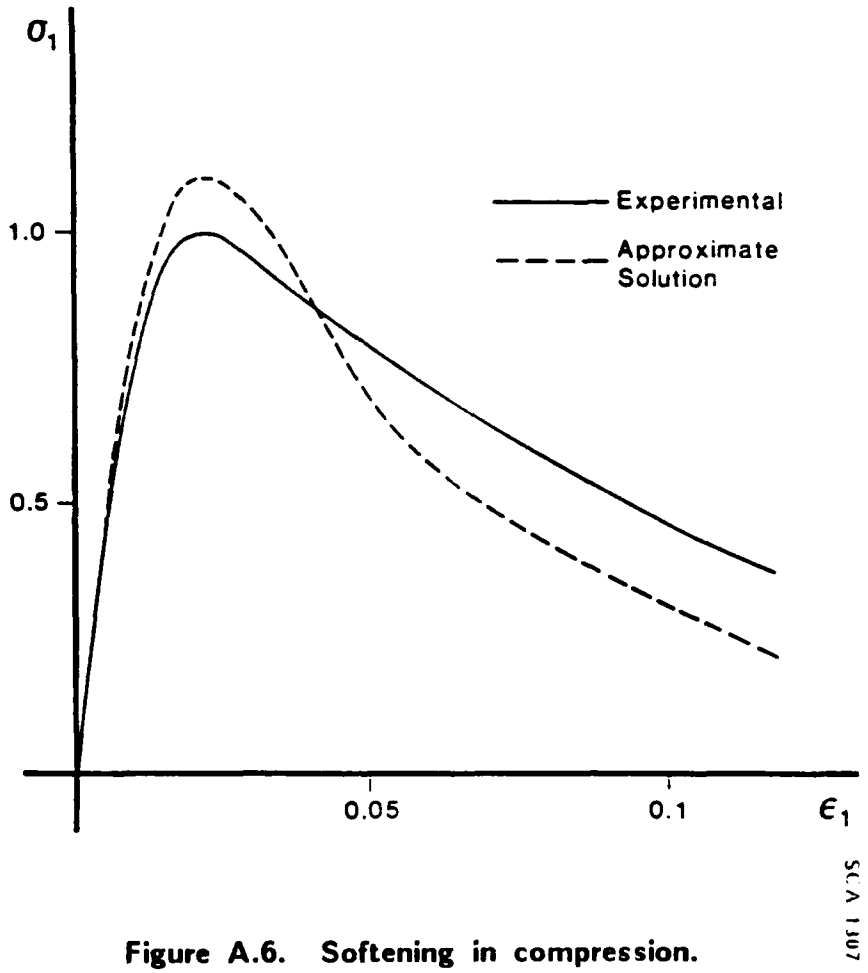

Figure A.6. Softening in compression.

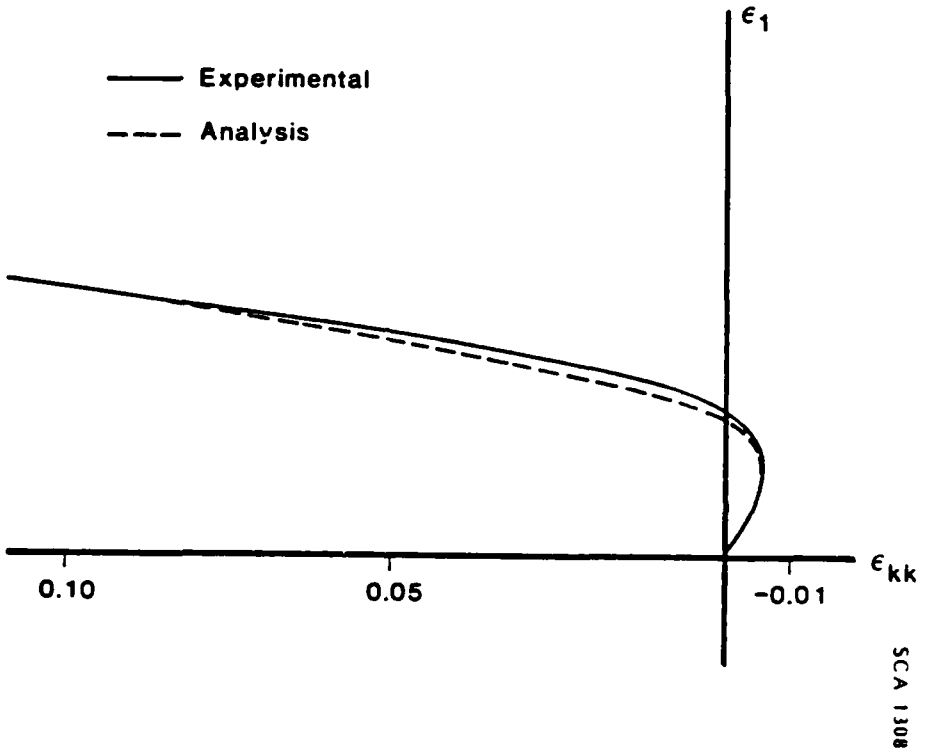

Figure A.7. Dilatancy during simple compression.

A.8 REFERENCES FOR APPENDIX A.

1. Gopalaratnam, V. S., and S. P. Shah (1985). "Softening Response of Plain Concrete in Direct Tension." ACI Journal, May-June, 310.

2. Horii, H., and S. Nemat-Nasser (1985). "Compression-Induced Microcrack Growth in Brittle Solids: Axial Splitting and Shear Failure." J. Geophys. Research, 90, 3105.

3. Knott, J. F., (1973). **Fundamentals of Fracture Mechanics**, Butterworth and Co. (Publishers) Ltd., London, England.

4. Raphael, J. M., (1984). "Tensile Strength of Concrete", ACI Journal, March-April, 158.

5. Diamond, S., and Bentur, A., (1984). "On the Cracking in Concrete and Fiber-Reinforced Cements," in Application of Fracture Mechanics to Cementitious Composites, NATO Advanced Research Workshop, Ed. S. P. Shah, Northwestern University, September.

6. Valanis, K. C., (1985). "A Fracture Theory for Brittle Materials," S-CUBED, La Jolla, California, Informal Report.

7. Van Mier, J. G. M., (1984). "Strain Softening of Concrete Under Multi-Axial Loading Conditions," Doctoral Dissertation, Technische Hohenschule, Eindhoven, The Netherlands, November.

APPENDIX B

RECENT ADVANCEMENTS IN THE ENDOCHRONIC CONCRETE MODEL

This Appendix describes several advancements that have recently been made in the endochronic model described earlier in Section 4.3 which extend its range of applicability to high pressures and provide a more realistic description of the failure surface. Details of these extensions of the model are given in the following sections of this appendix.

B.1 A THIRD INVARIANT FAILURE SURFACE FOR PLAIN CONCRETE.

Because the fine details of the failure surface were not expected to have a significant effect on the behavior of the endochronic model for peak stress states sufficiently far from failure, a simple failure surface was adopted in the model discussed in Section 4.3, with the function F_s taken to depend linearly on σ. When this is the case, it can be shown that the resulting failure is of the Drucker-Prager type, with the trace of this surface in the π-plane being a circle. Thus, such a surface does not account for the possible effect on failure of the intermediate principal stress. A more realistic failure surface for plain concrete allows F_s to depend not only on σ but also on the third invariant of the deviatoric stress tensor, J_3'. The incorporation of such a failure surface into the endochronic model is described in this section and illustrated through application to a suite of plain concrete failure data.

When the shear-kernel $\rho(z_s)$ is of such a form that a failure surface exists, the shear hardening function F_s defines the properties of the failure surface. For isotropic media, the most general form of the failure surface can be expressed in terms of the three independent invariants of the stress tensor, namely:

$$\sigma = \mathrm{tr}(\underset{\sim}{\sigma})$$

$$J_2 = \frac{1}{2}\ \underset{\sim}{s} : \underset{\sim}{s} \qquad \text{(B-1)}$$

$$J = \frac{3\sqrt{3}}{2}\ \frac{J_3}{(J_2)^{2/3}}\ ,$$

where

$$J_3 = \frac{1}{3} \det (\underset{\sim}{s}) \tag{B-2}$$

Here, the notation $\det(\underset{\sim}{s})$ denotes the determinant of the components of $\underset{\sim}{s}$. The most general form of the failure criterion for isotropic media can therefore be expressed in the form:

$$\sqrt{J_2} = \psi (\sigma, J) . \tag{B-3}$$

It was shown earlier by Hegemier, Read, Valanis and Murakami (1986) that the hardening function F_s can be expressed in terms of the function $\psi(\sigma,J)$ as follows:

$$F_s = \frac{\sqrt{2} \ \psi (\sigma, J)}{M_\infty} \tag{B-4}$$

where

$$M_\infty = \int_o^\infty \rho(x) \ dx \quad . \tag{B-5}$$

Therefore, to define F_s for a particular material, the function $\psi(\sigma,J)$ must be specified. This is done below for plain concrete.

There are a number of advanced failure criteria for plain concrete which have been proposed in the literature that have the general form of Eq. (B-3) (Mills and Zimmerman, 1970; Willam and Warnke, 1974; Ottosen, 1977; Lade, 1982; Peyton, 1983; Podgorski, 1985). Considering the large scatter in data between experimenters, as well as between different testing devices (see Hegemier and Read, 1986), most of the advanced failure criteria noted above provide satisfactory descriptions of existing plain concrete failure data. For critical assessments of most of the above failure models, the reader is referred to Ottosen (1977) and Podgorski (1985).

Inasmuch as all of the failure models noted above are reasonably accurate, and none appear to have significant advantages in predictive capability over the others, we select the model proposed by Peyton (1983) for specific consideration in this section because of our greater familiarity with it. A description of this failure model is given below, where the corresponding form of the function $\psi(\sigma,J)$ is defined. The model is then applied to failure data for plain concrete.

The failure criterion proposed by Peyton (1983) is given by the expression:

$$\frac{J_2}{\tau^2} - \alpha \frac{J_3}{\tau^3} = 1 \ , \tag{B-6}$$

where τ and α are, in general, smooth monotonic functions of the hydrostatic stress σ, i.e.,

$$\tau = \tau(\sigma) \ .$$
$$\alpha = \alpha(\sigma) \ . \tag{B-7}$$

The role of the function $\tau(\sigma)$ is to describe the effect of pressure on the meridians of the failure surface, while the function $\alpha(\sigma)$ determines the manner in which the trace of the failure surface in the π-plane changes with σ. In order for the trace to be convex, it is necessary that $0 \leq \alpha \leq 1$. If α is a continuous decreasing function of σ, the trace of the failure surface in the π-plane changes smoothly from a triangle ($\alpha=1$) to a circle ($\alpha=0$) with increasing σ.

To express Eq. (B-6) in the form of Eq. (B-3), we note that by defining an angle θ in the π-plane as shown in Figure B-1 it follows that:

$$J = -\sin 3\theta \tag{B-8}$$

Solving Eq. (B-1c) for J_3 and combining the result with Eq. (B-6) gives

$$\frac{J_2}{\tau^2} - \alpha \frac{2J}{3\sqrt{3}} \left[\frac{J_2}{\tau^2}\right]^{3/2} = 1 \ , \tag{B-9}$$

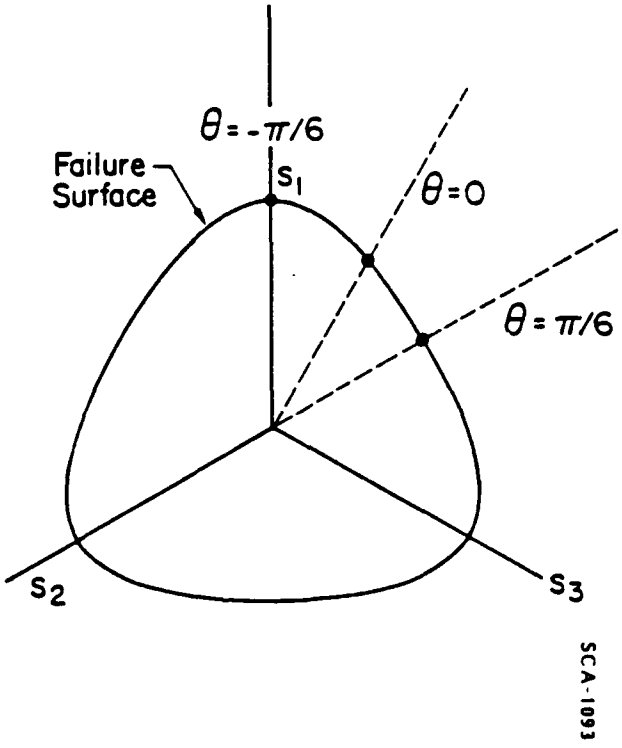

Figure B.1 Deviatoric stress plane, showing the manner in which the angle θ is defined.

which is of the form:

$$x^2 - q\,x^3 = 1. \tag{B-10}$$

if we set:

$$q \equiv \frac{2\alpha J}{3\sqrt{3}} \quad , \quad x \equiv \sqrt{\frac{J_2}{\tau^2}} \quad . \tag{B-11}$$

With the change of variable

$$x = \frac{1}{y} \tag{B-12}$$

Eq. (B-10) can be written in the form:

$$y^3 - y + 1 = 0 \; . \tag{B-13}$$

With a further change of variable,

$$y = \lambda \sin \phi \; . \tag{B-14}$$

Eq. (B-13) becomes

$$\sin^3 \phi - \frac{1}{\lambda^2} \sin \phi + \frac{q}{\lambda^3} = o \; . \tag{B-15}$$

We observe that this equation has the form of the following trigonometric identity:

$$\sin^3 \phi - \frac{3}{4} \sin \phi + \frac{1}{4} \sin 3\phi = o \; , \tag{B-16}$$

if we set

$$\lambda = \frac{2}{\sqrt{3}} \quad , \quad \sin 3\phi = \alpha J \; . \tag{B-17}$$

From Eq. (B-17b), it follows that

$$\phi = \frac{1}{3}\left[\sin^{-1}(\alpha J) + 2\pi\right] \quad . \tag{B-18}$$

Upon combining Eqs. (B-11b), (B-12), (B-14), (B-17) and (B-18), we can write

$$\sqrt{J_2} = \frac{\sqrt{3}\,\tau}{2\sin\left[\frac{1}{3}\sin^{-1}(\alpha J) + \frac{2\pi}{3}\right]} \quad , \tag{B-19}$$

which is of the form of Eq. (B-3). To apply this expression to a specific set of data, the functions $\alpha(\sigma)$ and $\tau(\sigma)$ must be specified. A procedure for doing this is described below.

Generally, failure data are obtained from triaxial compression and triaxial extension tests and, with this in mind, we define the ratio r as

$$r \equiv \frac{\left(\sqrt{J_2}\right)_c}{\left(\sqrt{J_2}\right)_e} \quad , \tag{B-20}$$

where the subscripts c and e refer, respectively, to compression and extension and both values of $\sqrt{J_2}$ are taken at the same hydrostatic pressure. Considering Eq. (B-19) with $J = +1$ for compression and $J = -1$ for extension, it can be shown that

$$r = \frac{\left(\sin\frac{2\pi}{3} - \frac{1}{3}\sin^{-1}\alpha\right)}{\left(\sin\frac{2\pi}{3} + \frac{1}{3}\sin^{-1}\alpha\right)} \quad . \tag{B-21}$$

Upon solving for α, we find

$$\alpha = \sin\left\{3\tan^{-1}\left[\sqrt{3}\,\frac{r-1}{r+1}\right]\right\} \quad . \tag{B-22}$$

Therefore, if we know the manner in which $(\sqrt{J_2})_c$ and $(\sqrt{J_2})_e$ depend on σ from data, then $r(\sigma)$ is known from Eq. (B-20) and $\alpha(\sigma)$ can be found from Eq. (B-22).

To determing $\tau(\sigma)$, we solve Eq. (B-19) for $\tau(\sigma)$ and set J = +1 to obtain

$$\tau(\sigma) = \frac{2}{\sqrt{3}} \sin\left[\frac{1}{3}\sin^{-1}\alpha + \frac{2\pi}{3}\right]\left(\sqrt{J_2}\right)_c \quad . \tag{B-23}$$

Therefore, since $\alpha(\sigma)$ and the variation of $(\sqrt{J_2})_c$ with σ are known, the function $\tau(\sigma)$ can be found.

The procedure described above was used to determine the forms of $\alpha(\sigma)$ and $\tau(\sigma)$ for plain concrete, using the failure data shown in Figure B-2. Here, data from both triaxial compression and triaxial extension tests on plain concretes conducted by several investigators on several different strengths of concrete are depicted. In this manner, it was found that the data could be well represented if we set

$$\alpha = \alpha_o$$

$$\tau = \tau_o + \beta_o\sqrt{\sigma - \gamma_o} \quad , \tag{B-24}$$

where

$$\alpha_o = 0.83$$

$$\tau_o = -1.91\ f_c'$$

$$\beta_o = 1.24\ \sqrt{f_c'} \tag{B-25}$$

$$\gamma_o = -2.69\ f_c'$$

The excellent ability of the failure model, with only four material parameters, to correlate the failure data is shown in Figure B-2.

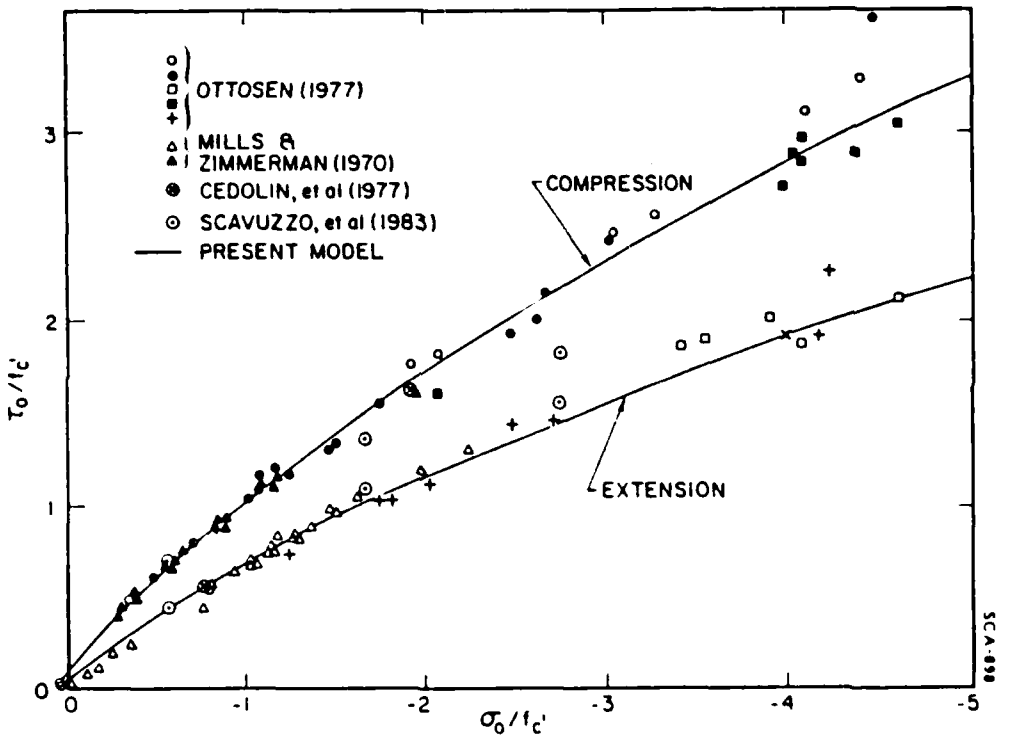

Figure B.2 **Correlation of concrete fracture data by present failure model.**

To determine the corresponding expression for the shear hardening function F_s, we first note that, since the shear kernel function $\rho(z_s)$ is assumed to be of the form of Eq. (6.7), it follows from Eq. (B-5) that

$$M_\infty = \sum \frac{A_r}{\alpha_r} \quad . \tag{B-26}$$

Upon substituting the values for A_r and α_r given by Valanis and Read (1986), we find

$$M_\infty = 17.5 \text{ ksi} \; . \tag{B-27}$$

Equations (B-3), (B-4) and (B-19) may be combined to give the following expression for F_s:

$$F_s = \frac{c_o \tau}{\sin\left[\frac{1}{3} \sin^{-1}(\alpha J) + \frac{2\pi}{3}\right]} \quad , \tag{B-28}$$

where $\alpha(\sigma)$ and $\tau(\sigma)$ are defined by Eqs. (B-24) and (B-25) and $c_o = 0.07 \text{ ksi}^{-1}$.

B.2 A HYDROSTATIC MODEL FOR HIGH PRESSURES.

Under monotonically increasing pressure, it is observed, as illustrated in Figure B-3, that the hydrostatic behavior of plain concrete is characterized by an initially convex stress-strain curve, which eventually becomes concave and finally (asymptotically) linear. The linear portion is reversible, indicating that the material has reached an elastic state. As the elastic state is approached, the stress and slope of the hydrostatic pressure - plastic volumetric strain curve tend to infinity as the plastic volumetric strain tends toward a critical value, ϵ_c^p, which corresponds to complete compaction. Further compression occurs elastically with $d\epsilon^p = o$.

The role of the hardening function F_H is to account for the effect of compaction on hydrostatic behavior and, since compaction is reflected through the plastic volumetric strain, ϵ^p, it is natural to take $F_H = F_H(\epsilon^p)$. It can be shown that, for

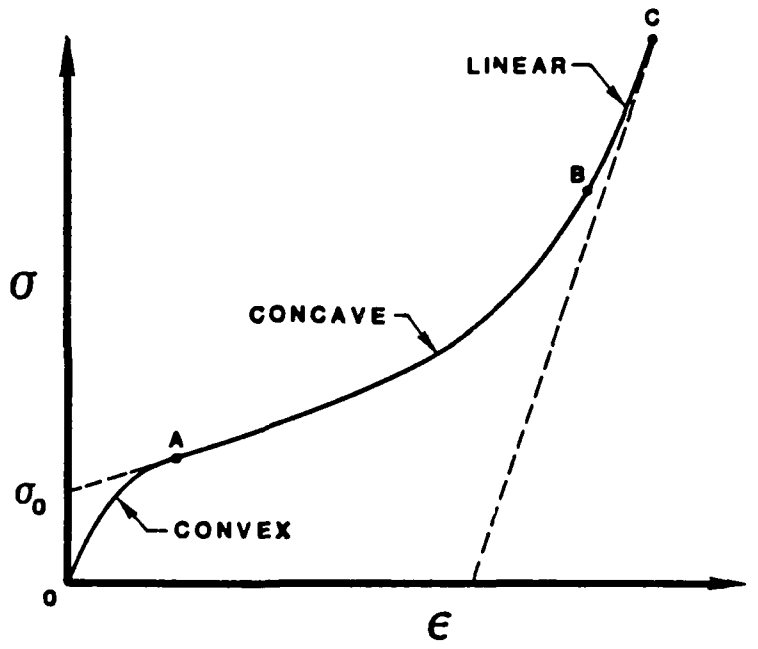

Figure B.3 Basic characteristics of virgin hydrostatic compression curve for plain concrete.

monotonic loading above the initial convex portion of the stress-strain curve, the hydrostatic stress σ and $F_H(\epsilon^p)$ are related by the expression

$$\sigma = K_o \, F_H(\epsilon^p) \, . \tag{B-29}$$

where K_o is a positive material constant. Therefore, except for the constant multiplier K_o, the function $F_H(\epsilon^p)$ describes the monotonic hydrostatic loading curve for all pressures above the initial convex part of this curve.

The general restrictions that the function F_H must satisfy, in addition to being a monotonically increasing function of ϵ^p, are:

$$\begin{aligned} &F_H(o) = 1 \\ &\lim_{\epsilon^p \to \epsilon_c^p} F_H = \infty \end{aligned} \tag{B-30}$$

The first restriction is imposed simply for convenience and allows us to set $K_o = \sigma_o$, where σ_o is the intercept on the σ-axis shown in Figure B.13. With K_o set to σ_o in Eq. (B-29), the virgin hydrostatic compression curve from A to C is then described by the equation

$$\sigma = \sigma_o \, F_H(\epsilon^p) \, . \tag{B-31}$$

which proves convenient in applying the model to specific materials.

The second restriction arises from the fact that it takes an infinite pressure to close all pores, that is:

$$\lim_{\epsilon^p \to \epsilon_c^p} \sigma = \infty \tag{B-32}$$

In view of Eq. (B-31), condition (B-32) is satisfied by taking F_H such that condition (B-30b) is fulfilled.

The hydrostatic data to which the endochronic model discussed in Section 4.1 was applied covered the range of pressures up to 15 ksi. Over this range, it was found that a simple linear expression for F_H, which satisfies condition (B-30a), led to an excellent description of the hydrostatic data. For higher pressures, however, this

linear form for F_H is inadequate and a more general expression which also satisfies condition (B-30b) is required.

To extend the range of the model to high pressures, including elastic behavior beyond full compaction, a suitable expression for F_H is as follows:

$$F_H = 1 + \beta_o \epsilon^p + \gamma_o \, (\epsilon_c^p - \epsilon^p)^{-m} \tag{B-33}$$

where β_o, γ_o and m are positive constants. This expression satisfies conditions (B-30) and is a monotonically increasing function of ϵ^p. There are, of course, other expressions that satisfy these general requirements, also, but that given by Eq. (B-33) appears to capture the behavior of plain concrete quite well, as shown in Figure B-4. Here, the response of the endochronic hydrostatic model, with F_H defined according to Eq. (B-33), to pure hydrostatic compression of plain concrete up to 65 ksi is compared with the corresponding data reported by Green and Swanson (1973), which unfortunately provided very limited unloading data. The agreement between the model and the data is considered quite good.

Finally, if pressures beyond point B in Figure B.3 are not of interest, the following simple expression for F_H has been found to be adequate in many cases:

$$F_H = e^{\beta \epsilon^p} \tag{B-34}$$

This expression satisfies only the first of the two conditions in Eq. (B-30) and, it reduces, for small ϵ^p, to the linear expression for F_H adopted in the model discussed in Section 4.3.

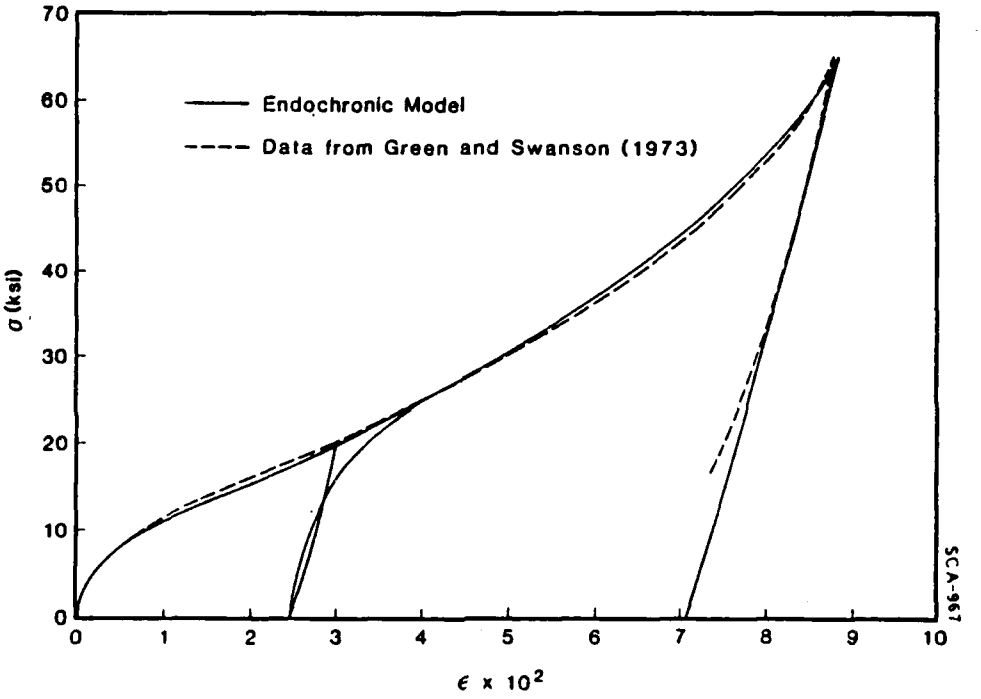

Figure B.4 Hydrostatic compression of plain concrete to high pressures.

B.3 REFERENCES FOR APPENDIX B.

1. Cedolin, L., R. J. Crutzen and S. Dei Poli (1977). "Triaxial Stress-Strain Relationship for Concrete," *J. Engr. Mechs. Div.*, 103 (EM3), 423.

2. Green, S. J., and S. R. Swanson (1973). "Static Constitutive Relations for Concrete," Terra Tek, Inc., Salt Lake City, Utah, Report AFWL-TR-782-244.

3. Hegemier, G. A., and H. E. Read (1986). "On Deformation and Failure of Brittle Solids: Some Outstanding Issues," *Mechanics of Materials*, 4, 215.

4. Hegemier, G. A., H. E. Read, K. C. Valanis and H. Murakami (1986). "Development of Advanced Constitutive Models for Plain and Reinforced Concrete," S-CUBED, La Jolla, California, 2nd Annual Report to AFOSR, SSS-R-86-7314.

5. Lade, P. V. (1982). "Three Parameter Failure Criterion for Concrete," *J. Engr. Mechs. Div.*, ASCE, 108, (EM5), October, 850.

6. Mills, L. L., and R. M. Zimmerman (1970). "Compressive Strength of Plain Concrete Under Multiaxial Loading Conditions," *ACI Journal*, October, 802.

7. Ottosen, N. S (1977). "A Failure Criterion for Concrete," *J. Engr. Mechs. Div.*, ASCE, 103 (EM5), October, 850.

8. Peyton, S. (1983). "A Failure Criterion for Rocks, Soils and Concretes," S-CUBED, La Jolla, California, unpublished report.

9. Podgorski, J (1985). "General Failure Criterion for Isotropic Media," *J. Engr. Mechs. Div.*, ASCE, 111 (EM2), 188.

10. Scavuzzo, R., T. Stankowski, K. H. Gerstle and H. Y. Ko (1983). "Stress-Strain Curves for Concrete Under Multiaxial Load Histories," CEAE Department, University of Colorado, Boulder.

11. Valanis, K. C., and H. E. Read (1986). "An Endochronic Plasticity Theory for Concrete," *Mechs. of Materials*, 5, 277.

12. Willam, K. J., and E. P. Warnke (1974), "Constitutive Model for the Triaxial Behavior of Concrete," *Proc. Intl. Assoc. Bridge and Structural Engrs. Seminar on Concrete Structs. Subjected to Triaxial Stresses*, Bergamo, Italy, May 17-19.

APPENDIX C

APPLICATION OF DIRECT VARIATIONAL METHOD TO DENSE STEEL LAYOUT - 3D PROBLEM

C.1 INTRODUCTION.

This Appendix furnishes a detailed derivation of an advanced mixture model for reinforced concrete (R/C). The development is based on the use of the Direct Variational Method.

The theoretical construction process to be discussed involves a number of key steps; these include: (1) a judicious scaling of the problem variables; (2) introduction of so-called microcoordinates and a two-space, asymptotic representation of all field variables; (3) a local periodicity condition; and (4) introduction of a variational principle. Each step is covered in some detail.

C.2 BASIC RELATIONS.

Consider a uniaxial steel layout with an initially local periodic array occupying a volume $\bar{V}_o$ with boundary $\partial\bar{V}_o$ in the initial configuration as illustrated in Figure C.1. In the current configuration the corresponding volume and surface will be denoted $\bar{V}$ and $\partial\bar{V}$, respectively.

If a spatial (Eulerian) description of motion is adopted, and if $\underset{\sim}{\bar{x}}$ denotes the global position vector of material particles, then the basic conservation equations of each constituent are:

$$D\bar{\rho}^{(\alpha)}/D\bar{t} + \bar{\rho}^{(\alpha)}\underset{\sim}{\bar{\nabla}}\cdot\underset{\sim}{\bar{v}}^{(\alpha)} = 0 \text{ in } \bar{V} \quad , \tag{C-1}$$

$$\underset{\sim}{\bar{\nabla}} \cdot \bar{\underset{\sim}{\sigma}}^{(\alpha)} + \underset{\sim}{\bar{f}}^{(\alpha)} = \bar{\rho}^{(\alpha)} D\underset{\sim}{\bar{v}}^{(\alpha)}/D\bar{t} \text{ in } \bar{V} \quad , \tag{C-2a}$$

$$\underset{\sim}{\bar{T}}^{(\alpha)} = \underset{\sim}{\nu}^{(\alpha)} \cdot \bar{\underset{\sim}{\sigma}}^{(\alpha)} \text{ on } \partial\bar{V}^{(\alpha)} \quad , \tag{C-2b}$$

$$\bar{\underset{\sim}{\sigma}}^{(\alpha)} = \bar{\underset{\sim}{\sigma}}^{(\alpha)T} \text{ in } \bar{V} \quad , \tag{C-3}$$

$$\bar{\rho}^{(\alpha)} D\bar{e}^{(\alpha)}/D\bar{t} = -\underset{\sim}{\bar{\nabla}} \cdot \underset{\sim}{\bar{E}}^{(\alpha)} + \bar{\rho}^{(\alpha)}\bar{q}^{(\alpha)} + \bar{\underset{\sim}{\sigma}}^{(\alpha)} : \underset{\sim}{\bar{d}}^{(\alpha)} \text{ in } \bar{V} \quad , \tag{C-4}$$

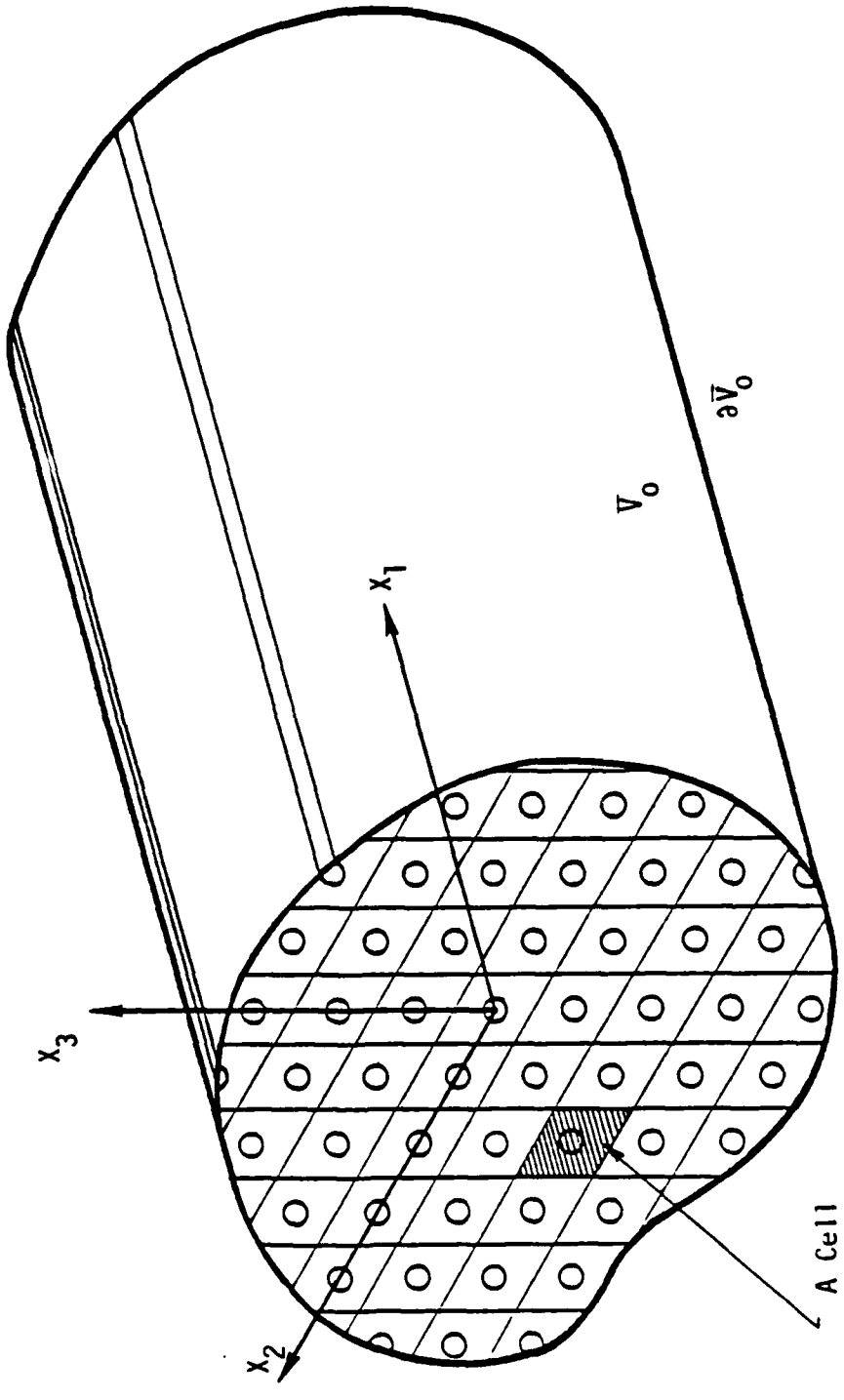

Figure C.1 Densely reinforced concrete; initial configuration.

where $\bar{\nabla}$ is the gradient operator with respect to $\bar{x}$, $\bar{v}$ is the velocity vector, $\bar{d}_{ij} \equiv (1/2)(\bar{v}_{i,j} + \bar{v}_{j,i})$ is the rate-of-deformation tensor, $\bar{\sigma}$ denotes the Cauchy stress tensor, $\bar{\rho}$ denotes material density, $\bar{f}$ is a body force per unit (current) volume, $\bar{T}$ is the traction vector acting on the surface $\partial\bar{V}$ with unit outer normal ν, $\bar{e}$ denotes internal energy per unit mass, $\bar{F}$ is the heat flux vector per unit time and current area, $\bar{q}$ is a heat source rate per unit time and mass, superscripts $\alpha = 1,2$ denote material α with $\alpha = 1$ representing steel and $\alpha = 2$ concrete, $(\ )^T$ denotes transposition of the tensor indices, $D(\ )/Dt$ is the material time derivative, and $\bar{V}^{(\alpha)}$ is the current volume occupied by material α with boundary $\partial\bar{V}^{(\alpha)}$. In what follows, both direct and index notations will be used. Lower case indices refer to a fixed rectangular Cartesian coordinate system and repeated subscripts are summed. Superscripts do not refer to tensor components. Repetition of unbracketed superscripts implies summation. Bracketed superscripts are not summed. Thus, α is not summed in the foregoing equations. Equations (C-1) - (C-4) represent the conservation of mass, linear momentum, angular momentum, and energy, respectively. In (C-2), the components of $\bar{\nabla}\cdot\bar{\sigma}$ and $\bar{\nu}\cdot\bar{\sigma}$ are $\bar{\sigma}_{ji,j}$ and $\bar{\nu}_j\bar{\sigma}_{ji}$, respectively. In (C-4) the components of $\bar{\sigma}:\bar{d}$ are $\bar{\sigma}_{ij}\bar{d}_{ij}$.

In what follows, attention will be focused upon physical processes that occur over time intervals that are small compared to typical thermal diffusion times. Consequently, an adiabatic premise will be adopted. Accordingly, in (C-4) one sets

$$\bar{q}^{(\alpha)} \simeq 0 \ , \quad \bar{F}^{(\alpha)} \simeq 0 \ . \tag{C-5}$$

The conservation equations must be supplemented by appropriate constitutive relations. A reasonably general class of constitutive behaviors may be characterized by assuming that an objective stress rate relates linearly to the rate-of-deformation tensor, i.e.,

$$\frac{\nabla}{\sigma}^{(\alpha)} = \bar{D}^{(\alpha)} : \bar{d}^{(\alpha)} \tag{C-6}$$

where $\bar{D}^{(\alpha)}$ is the instantaneous elastic-plastic modulus tensor for material α and the components of $\bar{D}:\bar{d}$ are $\bar{D}_{ijk\ell}d_{k\ell}$. The tensor $\bar{D}^{(\alpha)}$ is assumed to be independent of

the stress rate and the rate of deformation, but may depend upon the current stress state, internal energy, and certain deformation measures. Isotropy of $\bar{\underset{\sim}{D}}^{(\alpha)}$ may not be assumed in general due to plastic flow and/or prior cracking of the concrete. While $\bar{D}_{ijk\ell}^{(\alpha)}$ is symmetric with respect to the exchange of i and j, and k and ℓ, it is not, in general, symmetric with respect to the exchange of ij and kℓ.

The stress rate in (C-6) deserves comment. The Jaumann rate corotational with the material is most frequently adopted in constitutive relations of the type (C-6). In this case

$$\overset{\nabla}{\bar{\underset{\sim}{q}}}^{(\alpha)} \equiv D\bar{\underset{\sim}{q}}^{(\alpha)}/D\bar{t} - \bar{\underset{\sim}{w}}^{(\alpha)} \cdot \bar{\underset{\sim}{q}}^{(\alpha)} + \bar{\underset{\sim}{q}}^{(\alpha)} \cdot \bar{\underset{\sim}{w}}^{(\alpha)} \tag{C-7}$$

where components of, say, $\bar{\underset{\sim}{w}} \cdot \bar{\underset{\sim}{q}}$ are $\bar{w}_{ik}\bar{\sigma}_{kj}$. However, a number of other objective stress rates have been introduced by various authors. While each rate is admissible from the standpoint of being objective, each leads to a different constitutive relation. An appropriate choice depends upon the problem under consideration.

The constitutive form (C-6) covers a wide class of elastic-plastic and elastic-plastic-brittle fracture behavior. Yet, it is not intended to be comprehensive. Other constitutive relations can be incorporated into the theoretical development to follow. The incremental form (C-6) is the most convenient for demonstration purposes. Some important forms such as the endochronic theory, which is incrementally nonlinear, necessitate modification of (C-6).

A remark concerning the foregoing Eulerian description of motion is appropriate at this point. For computational purposes, it is often convenient to employ an "updated Lagrangian" description of motion. Accordingly, the Kirchhoff stress is adopted as the stress measure and the current configuration is used as the reference. In view of the latter,

$$\bar{\underset{\sim}{\tau}} = \bar{\underset{\sim}{q}} \tag{C-8}$$

where $\bar{\underset{\sim}{\tau}}$ denotes the Kirchhoff stress tensor. However, $D\bar{\underset{\sim}{\tau}}/D\bar{t} \neq D\bar{\underset{\sim}{q}}/D\bar{t}$ since

$$D\bar{\underset{\sim}{\tau}}/D\bar{t} = D\bar{\underset{\sim}{q}}/D\bar{t} + d\bar{\underset{\sim}{q}} \quad , \quad d \equiv \bar{\underset{\sim}{\nabla}} \cdot \bar{\underset{\sim}{v}} \quad . \tag{C-9}$$

Thus, for an updated Lagrangian description, one need only replace $\bar{\underset{\sim}{q}}$ by $\bar{\underset{\sim}{\tau}}$ in the conservation equations (C-1) - (C-4) and interpret $D(\ )/D\bar{t}$ as a material time derivative. However, the constitutive relations (C-6) must be altered. For this purpose (C-6) is replaced by

$$\overset{\nabla}{\underset{\sim}{\tau}}(\alpha) = \bar{\underset{\sim}{L}}(\alpha) : \bar{\underset{\sim}{d}}(\alpha) \quad . \tag{C-10}$$

From (C-6), (C-8), and (C-9), one finds

$$\bar{\underset{\sim}{D}}(\alpha) = \bar{\underset{\sim}{L}}(\alpha) - \bar{\underset{\sim}{q}}(\alpha)\underset{\sim}{\delta} \quad , \quad \text{or } \bar{\underset{\sim}{L}}(\alpha) = \bar{\underset{\sim}{D}}(\alpha) + \bar{\underset{\sim}{\tau}}(\alpha)\underset{\sim}{\delta} \tag{C-11}$$

where $\underset{\sim}{q}\underset{\sim}{\delta}$ denotes the tensor product, i.e., components of $\underset{\sim}{q}\underset{\sim}{\delta}$ are $\sigma_{ij}\delta_{k\ell}$ (this product is often written as $\underset{\sim}{q} \otimes \underset{\sim}{\delta}$).

In addition to the above conservation and constitutive equations, relations between tractions and velocities for each constituent across the steel-concrete interface must be specified. For modeling purposes this interface is idealized as smooth. Let $\bar{\mathcal{I}}^*$ denote that part of $\partial\bar{V}^{(1)}$ in contact with $\partial\bar{V}^{(2)}$, where both are smooth. Then, continuity of the traction vector requires that

$$\overset{\nu}{\underset{\sim}{\tau}}(1) = - \overset{\nu}{\underset{\sim}{\tau}}(2) \equiv \bar{\underset{\sim}{\tau}}^* \quad \text{on } \bar{\mathcal{I}}^* \quad . \tag{C-12}$$

With respect to displacements, relative slip across $\bar{\mathcal{I}}^*$ must be allowed to simulate steel-concrete bond slip and dowel action. Accordingly, a relative velocity $[\bar{\underset{\sim}{v}}]$ is defined by

$$\bar{\underset{\sim}{v}}(2) - \bar{\underset{\sim}{v}}(1) \equiv \left[\bar{\underset{\sim}{v}}\right] \text{ on } \bar{\mathcal{I}}^* \quad . \tag{C-13}$$

An interface "constitutive law" is next postulated in the form of a linear relation between an objective traction rate, $\overset{\circ}{\underset{\sim}{\tau}}{}^*$, and the relative velocity, i.e.,

$$\overset{\circ}{\underset{\sim}{\bar{T}}}{}^{*} = \underset{\sim}{\bar{\mathcal{B}}} \cdot \left[\underset{\sim}{\bar{v}}\right] \text{ on } \bar{\mathcal{I}}^{*} \quad , \tag{C-14a}$$

$$\overset{\circ}{\underset{\sim}{\bar{T}}}{}^{*} \equiv D\underset{\sim}{\bar{T}}^{*}/D\bar{t} - \underset{\sim}{\bar{w}} \cdot \underset{\sim}{\bar{T}}^{*} \quad , \tag{C-14b}$$

where $\underset{\sim}{\bar{\mathcal{B}}}$ is a second rank tangent modulus tensor which may depend on the current states of stress and relative slip on $\bar{\mathcal{I}}^{*}$.

It should be noted that the normal component of velocity (to the surface $\bar{\mathcal{I}}^{*}$) may be discontinuous as well as the tangential component in (C-14). This degree of freedom is necessary to allow proper simulation of actual steel-concrete interaction under certain conditions using the idealized smooth surface $\bar{\mathcal{I}}^{*}$.

If contact between $\partial\bar{V}^{(1)}$ and $\partial\bar{V}^{(2)}$ is lost, then one sets $\underset{\sim}{\bar{T}}^{(2)} = 0$, $\underset{\sim}{\bar{T}}^{(1)} = 0$ over those segments of $\partial\bar{V}^{(1)}$ and $\partial\bar{V}^{(2)}$ corresponding to no contact. This situation can also be incorporated into the form (C-14a) by a suitable choice of $\underset{\sim}{\bar{\mathcal{B}}}$.

The foregoing relations, (C-1) - (C-14), must be supplemented by initial conditions at $\bar{t} = 0$ and boundary conditions on $\partial\bar{V}$.

C.3 SCALING.

It will be convenient to nondimensionalize the basic equations. For this purpose let

$\bar{\Lambda}$ = typical macrosignal wavelength

$\bar{\Delta}$ = typical steel spacing

$\bar{c}_{(m)}, \bar{\rho}_{(m)}$ = reference wave velocity and macrodensity

$\bar{E}_{(m)} = \bar{\rho}_{(m)}\bar{c}^{2}_{(m)}$ = reference modulus

$\bar{t}_{(m)}$ = typical macrosignal travel time $(= \bar{\Lambda}/\bar{c}_{(m)})$

ϵ = $\bar{\Delta}/\bar{\Lambda}$ = ratio of micro-to-macrodimensions

With the aid of the above notation, nondimensional variables are now introduced according to

$$
\begin{aligned}
\underset{\sim}{x} &= \bar{\underset{\sim}{x}}/\bar{\Lambda}, \quad t = \bar{t}/\bar{t}_{(m)} \\
\underset{\sim}{v} &= \bar{\underset{\sim}{v}}/c_{(m)}, \quad \underset{\sim}{q} = \bar{\underset{\sim}{q}}/\bar{E}_{(m)} \\
\epsilon[\underset{\sim}{v}] &= [\bar{\underset{\sim}{v}}]/\bar{c}_{(m)}, \quad \underset{\sim}{T}^* = \bar{\underset{\sim}{T}}^*/\bar{E}_{(m)}, \\
\underset{\sim}{D} &= \bar{\underset{\sim}{D}}/\bar{E}_{(m)}, \quad (1/\epsilon)\mathcal{B} = \bar{\mathcal{B}}/(\bar{E}_{(m)}\bar{\Delta}). \\
\rho &= \bar{\rho}/\rho_{(m)}, \quad \underset{\sim}{f} = (\bar{\Lambda}/\bar{E}_{(m)})\bar{\underset{\sim}{f}}
\end{aligned}
\tag{C-15}
$$

C.4 MICROCOORDINATES.

It is expected that stress and deformation fields will vary significantly with respect to two basic length scales: (1) a "global" or "macro" length typical of the body size or loading condition; and (2) a "micro" length typical of a "cell" planar dimensions as depicted in Figure C.2. These macro and micro dimensions will be associated with the variables $\bar{\Lambda}$, $\bar{\Delta}$, respectively. Further, it is expected that these scales will differ by at least one order of magnitude in most cases. This suggests the use of multivariable asymptotic techniques, Hegemier, *et al.* (1979). This approach commences by introducing new independent variables according to

$$
\begin{aligned}
&\underset{\sim}{x}^* = \phi^{-1}(\epsilon)\underset{\sim}{x} \quad , \quad \phi(\epsilon) \to 0 \quad \text{as} \quad \epsilon \to 0 \\
&\tilde{\underset{\sim}{x}} = \psi(\epsilon)\underset{\sim}{x}, \quad \psi(\epsilon) \to 1 \quad \text{as} \quad \epsilon \to 0 \quad .
\end{aligned}
\tag{C-16}
$$

For the present analysis it will suffice to set

$$
\phi(\epsilon) = \epsilon \ , \quad \psi(\epsilon) = 1 \quad ; \tag{C-17}
$$

thus, all field variables $f(\underset{\sim}{x},t)$ are now functions of the "microcoordinates" $\underset{\sim}{x}^*$ as well as the "macrocoordinates" $\tilde{\underset{\sim}{x}} \equiv \underset{\sim}{x}$, i.e.,

AD-A187 337 DEVELOPMENT OF ADVANCEDCONSTITUTIVE MODELS FOR PLAIN AND REINFORCED CONCRETE(U) S-CUBED LA JOLLA CA G A HEGEMIER ET AL MAR 87 SSS-R-87-8454 3/3

UNCLASSIFIED AFOSR-TR-87-1391 F49620-84-C-0029 F/G 13/3 NL

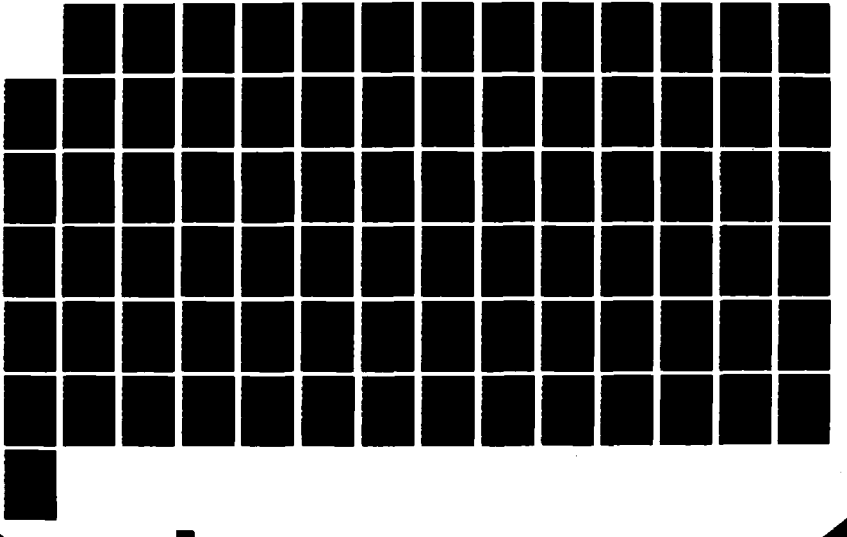

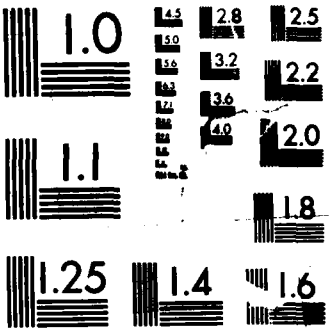

MICROCOPY RESOLUTION TEST CHART
NATIONAL BUREAU OF STANDARDS-1963-A

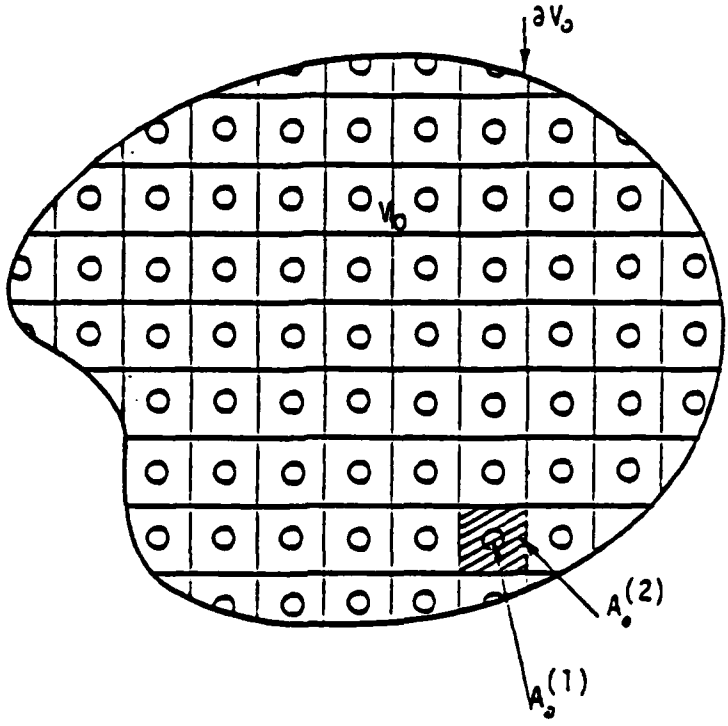

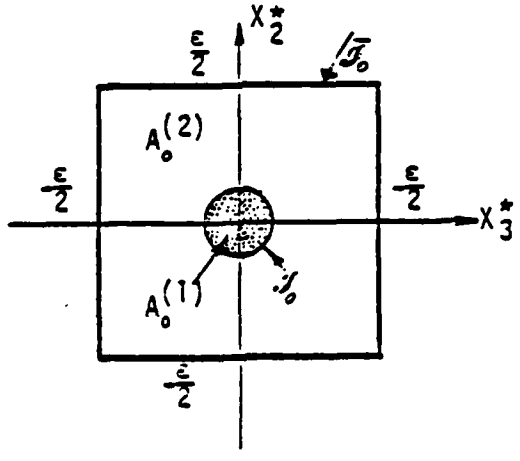

Figure C.2 Cell geometry for densely reinforced concrete (shown in initial configuration).

$$f(\underset{\sim}{x},t) = F(\underset{\sim}{x},t;\underset{\sim}{x}^*;\epsilon) \tag{C-18a}$$

Spatial derivatives of a function $f(\underset{\sim}{x},t)$ then take the form

$$\underset{\sim}{\nabla} f = \underset{\sim}{\nabla} F + \epsilon^{-1}\underset{\sim}{\nabla}^* F \ . \tag{C-18b}$$

For notational convenience in the following, the functions f and F will both be written as f.

For some problems it is necessary to introduce time-microvariables as well as the foregoing space-microvariables. These additional variables will not be advantageous for the present formulation, however.

It is noted that, for the present unidirectional steel layout, it is appropriate to constrain the vector $\underset{\sim}{x}^*$ according to

$$\underset{\sim}{x}^* \cdot \underset{\sim}{t} = 0 \tag{C-18c}$$

where $\underset{\sim}{t}$ denotes the tangent vector to the steel centerline.

C.5 SYNTHESIZED FIELD EQUATIONS.

The operations (C-18), when applied to all field variables, lead to the following synthesized governing field equations in nondimensional form:

(a) Conservation Relations

$$D\rho^{(\alpha)}/Dt + \rho^{(\alpha)}\underset{\sim}{\nabla} \cdot \underset{\sim}{v}^{(\alpha)} + \frac{1}{\epsilon}\underset{\sim}{\nabla}^* \cdot \left[\rho^{(\alpha)}\underset{\sim}{v}^{(\alpha)}\right] = 0 \quad \text{in } V^{(\alpha)}, \tag{C-19}$$

$$\underset{\sim}{\nabla} \cdot \underset{\sim}{q}^{(\alpha)} + \frac{1}{\epsilon}\underset{\sim}{\nabla}^* \cdot \underset{\sim}{q}^{(\alpha)} + \underset{\sim}{f}^{(\alpha)} = 0 \quad \text{in } V^{(\alpha)} \ , \tag{C-20a}$$

$$\underset{\sim}{t}^{(\alpha)} = \underset{\sim}{k}^{(\alpha)} \cdot \underset{\sim}{q}^{(\alpha)} \quad \text{on } \partial V^{(\alpha)} \ , \tag{C-20b}$$

$$\underset{\sim}{q}^{(\alpha)} = \underset{\sim}{q}^{(\alpha)^T} \text{ in } V^{(\alpha)} \ , \tag{C-21}$$

$$\rho^{(\alpha)} De^{(\alpha)}/Dt + \frac{1}{\epsilon}\underset{\sim}{v}^{(\alpha)} \cdot \underset{\sim}{\nabla}^* e^{(\alpha)} = \underset{\sim}{q}^{(\alpha)} : \left[\underset{\sim}{d}^{(\alpha)} + \underset{\sim}{d}^{*(\alpha)}\right] \text{ in } V^{(\alpha)}, \tag{C-22a}$$

$$\underset{\sim}{d}^{*(\alpha)} \equiv \frac{1}{2\epsilon}\left(\underset{\sim}{\nabla}^{*}\underset{\sim}{y} + \underset{\sim}{\nabla}^{*T}\underset{\sim}{y}\right) \quad . \tag{C-22b}$$

(b) Constitutive Relations

$$\underset{\sim}{\nabla}^{(\alpha)} = \underset{\sim}{D}^{(\alpha)} : \tilde{\underset{\sim}{d}}^{(\alpha)}, \quad \tilde{\underset{\sim}{d}}^{(\alpha)} \equiv \underset{\sim}{d}^{(\alpha)} + \underset{\sim}{d}^{*(\alpha)} \quad \text{in } V^{(\alpha)} \tag{C-23}$$

(c) Interface Relations

$$\overset{\nu}{\underset{\sim}{T}}{}^{(1)} = - \overset{\nu}{\underset{\sim}{T}}{}^{(2)} \equiv \underset{\sim}{T}^{*} \text{ on } \mathscr{I} \tag{C-24a}$$

$$\overset{\circ}{\underset{\sim}{T}}{}^{*} = \underset{\sim}{\mathscr{B}} \bullet [\underset{\sim}{y}] \quad , \quad [\underset{\sim}{y}] \equiv \underset{\sim}{y}^{(2)} - \underset{\sim}{y}^{(1)} \quad \text{on } \mathscr{I} \quad . \tag{C-24b}$$

(d) Initial Conditions at t = 0. Boundary Data on ∂V.

In the above, $\underset{\sim}{\nabla}^{*}$ is the gradient operator with respect to $\underset{\sim}{x}^{*}$, e.g., components of $\underset{\sim}{\nabla}^{*}\underset{\sim}{y}$ are $\partial v_i/\partial x_j^{*}$. The material derivative D()/Dt refers to the macrovariables x_i only.

C.6 CONSTRAINTS.

In the following, attention will be restricted to processes in which:

(1) The constitutive and interface relations do not depend on the internal energy.

(2) The microdeformation gradient is sufficiently small that micro-flux or micro-convection terms may be neglected in the material derivative.

(3) The micro-rotation is sufficiently small that its contribution to the stress rate may be neglected.

(4) The micro-deformation is sufficiently small that microvariations in the mass density may be neglected.

Under the above constraints, which are considered to be appropriate for R/C, the last term in (C-19) can be neglected, the energy equation (C-22a) need not be treated, and the material and stress-rate derivatives are to be interpreted in terms of the macrocoordinates only.

C.7 PERIODICITY CONDITION.

An important premise, called the local periodicity condition, is now introduced. This condition consists of the assumption that local periodicity in the microvariable $\underset{\sim}{x}^*$ may be invoked for all field variables. This premise allows one to analyze a single cell in an effort to determine the distribution of any field variable with respect to the microcoordinate $\underset{\sim}{x}^*$. A typical such cell is depicted in Figure C.2.

The local periodicity premise is motivated by extrapolation from linear analysis. It is expected to provide a good representation of the field variables for dense steel layouts.

C.8 DIRECT VARIATIONAL PRINCIPLE FOR SYNTHESIZED FIELDS.

A variational (weighted residual) principle is now constructed for the synthesized field variables. For this purpose consider the relation

$$\int_V \left\{ \sum_{\alpha=1}^{2} \int_{A^{(\alpha)}} \left(\underset{\sim}{\underset{\sim}{y}} \cdot \underset{\sim}{q}^{(\alpha)} + \epsilon^{-1} \underset{\sim}{\underset{\sim}{y}}^* \cdot \underset{\sim}{q}^{(\alpha)} + \underset{\sim}{f}^{(\alpha)} \right) \cdot \delta \underset{\sim}{v}^{(\alpha)} \, dA^* \right\} dV$$

$$+ \int_{\partial V} \left\{ \sum_{\alpha=1}^{2} \int_{A^{(\alpha)}} \left[\underset{\sim}{\underset{\sim}{I}}^{\nu} - \underset{\sim}{\underset{\sim}{\chi}} \cdot \underset{\sim}{q} \right]^{(\alpha)} \cdot \delta \underset{\sim}{v}^{(\alpha)} \, dA^* \right\} dS + \int_V \left\{ \sum_{\alpha=1}^{2} \oint_{\mathscr{I}} \epsilon^{-1} \left[\underset{\sim}{\underset{\sim}{I}}^{\nu} - \underset{\sim}{\underset{\sim}{\chi}} \cdot \underset{\sim}{q} \right]^{(\alpha)} \cdot \delta \underset{\sim}{v}^{(\alpha)} \, ds^* \right\} dV$$

$$+ \int_V \left\{ \int_{\partial A^{(2)}} \epsilon^{-1} \left[- \underset{\sim}{\chi}^{(2)} \cdot \underset{\sim}{q}^{(2)} \right] \cdot \delta \underset{\sim}{v}^{(2)} \, ds^* \right\} dV = 0 \, . \qquad \text{(C-25)}$$

In the above, $d\underset{\sim}{A}^* = dA^* \underset{\sim}{t}$, where $\underset{\sim}{t}$ is the unit tangent vector to the steel centerline

in a given cell. Thus, if a plane with normal $\underset{\sim}{t}$ intersects the steel centerline within a cell, then $A^{(\alpha)}$ is the projected area of material α on this plane. The integration is carried out over the microcoordinates, e.g., if x_k^*, k = 2,3 denote local Cartesian coordinates in the above plane, then $dA^* = dx_2^* dx_3^*$. The quantity $\mathscr{I} \equiv \partial A^{(1)}$, i.e., $\mathscr{I}$ is the projection of the steel-concrete boundary on this plane.

Let the boundary $\partial V = \partial V_T + \partial V_u$. Then, the following is assumed:

$$\begin{aligned} &\overset{\nu}{\underset{\sim}{I}}{}^{(\alpha)} = \text{prescribed on } \partial V_T \\ &\delta \underset{\sim}{y}^{(\alpha)} = 0 \quad \text{on } \partial V_u \quad . \end{aligned} \tag{C-26}$$

In addition, let

$$\begin{aligned} &\overset{\nu}{\underset{\sim}{I}}(1) = - \overset{\nu}{\underset{\sim}{I}}(2) \equiv \underset{\sim}{I}^* \quad \text{on } \partial A^{(1)}, \\ &\underset{\sim}{I}^* = \text{prescribed on } \partial A^{(1)} \quad . \end{aligned} \tag{C-27}$$

Finally, let

$$\begin{aligned} &\delta \underset{\sim}{y}^{(\alpha)} \ \epsilon C^1 \text{ on } A^{(\alpha)} \text{ with respect to } \underset{\sim}{x}, \underset{\sim}{x}^* , \\ &\delta \underset{\sim}{y}^{(\alpha)} \ \epsilon \underset{\sim}{x}^* \text{ - periodic.} \end{aligned} \tag{C-28}$$

If $\delta \underset{\sim}{y}^{(\alpha)}$ is the variation of the exact velocity field, then the first term of (C-25) vanishes due to (C-20a), the second vanishes due to (C-20b) and (C-26), the third vanishes due to (C-20b), and the last term vanishes due to (C-24). Thus, the validity of (C-25) is established if $\underset{\sim}{y}^{(\alpha)}$ is the exact velocity field.

If $\underset{\sim}{y}^{(\alpha)}$ is not the exact field, then (C-25) represents a weighted residual procedure for generating weak solutions of the governing equations. The weighting functions are $\delta \underset{\sim}{y}^{(\alpha)}$. In the latter case the solutions are of course approximate.

With the use of Gauss' Theorem, and (C-26) - (C-28), (C-25) can be placed in the following form:

$$\int_V \left\{ \sum_{\alpha=1}^{2} \int_{A(\alpha)} \underset{\sim}{q}^{(\alpha)} : \left[\underset{\sim}{\nabla} \delta \underset{\sim}{v}^{(\alpha)} + \epsilon^{-1} \underset{\sim}{\nabla}^* \delta \underset{\sim}{v}^{(\alpha)} \right] dA^* + \epsilon^{-1} \oint_{\mathcal{J}} \underset{\sim}{T}^* \cdot \delta [\underset{\sim}{v}] ds \right\} dV$$

(C-29)

$$= \int_V \left\{ \sum_{\alpha=1}^{2} \int_{A(\alpha)} \underset{\sim}{f}^{(\alpha)} \cdot \delta \underset{\sim}{v}^{(\alpha)} dA^* \right\} dV + \int_{\partial V_T} \left\{ \sum_{\alpha=1}^{2} \int_{A(\alpha)} \underset{\sim}{\mu}^{(\alpha)} \cdot \delta \underset{\sim}{v}^{(\alpha)} dA^* \right\} dS.$$

Equation (C-29) constitutes the principle of Virtual Work for the synthesized fields. This relation represents an important tool, in the form of a variational principle, for generating mixture field equations for the highly nonlinear class of problems of interest herein.

C.9 MODEL CONSTRUCTION: DIRECT METHOD.

Kantorovich's direct variational method is now applied to generate the desired mixture equations. The trial velocity field (test functions) is selected in the form

$$\underset{\sim}{v}^{(\alpha)} \left[\underset{\sim}{x}, t; \underset{\sim}{x}^*; \epsilon \right] = \overset{\circ}{\underset{\sim}{U}}{}^{(\alpha)} (x,t) + \epsilon \overset{\circ}{\underset{\sim}{\xi}}{}^{K(\alpha)} (\underset{\sim}{x}, t)\ g^{K(\alpha)} (\underset{\sim}{x}^*) + O\left[\epsilon^2\right] \qquad \text{(C-30)}$$

The "weight" functions $g^{K(\alpha)}(\underset{\sim}{x}^*)$ are to be prescribed for each material ($\alpha = 1,2$). The vector $\overset{\circ}{\underset{\sim}{U}}{}^{(\alpha)}$ reflects the macro contribution to the velocity field whereas the vectors $\overset{\circ}{\underset{\sim}{\xi}}{}^{K(\alpha)}$ reflect the micro contribution; these variables play the role of new dependent-type displacement variables. In the above, and in what follows, the summation convention is used with respect to the index K with range 1 to n.

C.9.1 Equations of Motion, Boundary Conditions.

Substitution of the test function (C-30) into the variational principle (C-25) furnishes, after some algebraic manipulations and integrations by parts, the following relation:

$$\int_{\partial V_T} \left[\sum_{\alpha=1}^{2} \delta \underset{\sim}{\dot{U}}^{(\alpha)} \cdot \left(\underset{\sim}{T}^{p(\alpha)} - \underset{\sim}{\kappa} \cdot \underset{\sim}{N}^{(\alpha)} \right) + \delta \underset{\sim}{S}^{K(\alpha)} \cdot \left(\underset{\sim}{T}^{K(\alpha)} - \underset{\sim}{\kappa} \cdot \underset{\sim}{M}^{K(\alpha)} \right) \right] dS$$

$$+ \int_{V} \left\{ \sum_{\alpha=1}^{2} \delta \underset{\sim}{\dot{U}}^{(\alpha)} \cdot \left(\underset{\sim}{\nabla} \cdot \underset{\sim}{N}^{(\alpha)} + \underset{\sim}{F}^{(\alpha)} + (-1)^{\alpha+1} \underset{\sim}{P} \right) \right. \tag{C-31}$$

$$\left. + \delta S^{K(\alpha)} \cdot \left(\underset{\sim}{\nabla} \cdot \underset{\sim}{M}^{K(\alpha)} - \overline{N}^{K(\alpha)} + \underset{\sim}{F}^{K(\alpha)} + (-1)^{\alpha+1} \underset{\sim}{Q}^{K} \right) \right\} dV = 0 \quad .$$

In (C-30), the following quantities have been defined:

$$\left(\underset{\sim}{F}^{(\alpha)}, \underset{\sim}{F}^{K(\alpha)} \right) \equiv \int_{A^{(\alpha)}} \left(1, \epsilon g^{K(\alpha)} \right) \underset{\sim}{f}^{(\alpha)} dA^{*} \quad ,$$

$$\left(\underset{\sim}{N}^{(\alpha)}, \underset{\sim}{M}^{K(\alpha)} \right) \equiv \int_{A^{(\alpha)}} \left(1, \epsilon g^{K(\alpha)} \right) \underset{\sim}{\ell}^{(\alpha)} dA^{*} \quad , \tag{C-31}$$

$$\overline{N}^{K(\alpha)} \equiv \int_{A^{(\alpha)}} \epsilon \underset{\sim}{\ell}^{(\alpha)} \cdot \underset{\sim}{\nabla}^{*} g^{K(\alpha)} dA^{*}, \quad \left(\underset{\sim}{T}^{\nu(\alpha)}, \underset{\sim}{T}^{\mu K(\alpha)} \right) \equiv \int_{A^{(\alpha)}} \left(1, \epsilon g^{K(\alpha)} \right) \underset{\sim}{T}^{\mu(\alpha)} dA^{*},$$

$$\underset{\sim}{P} \equiv \frac{1}{\epsilon} \oint_{\mathscr{I}} \underset{\sim}{T}^{*} ds^{*} \quad , \quad \underset{\sim}{Q}^{K} \equiv \oint_{\mathscr{I}} \underset{\sim}{T}^{*} \, g^{K(\alpha)} ds^{*} \quad (\alpha = 1 \text{ or } 2) \quad .$$

The Euler-Lagrange equations associated with the variational equation (C-30) are

$$\underset{\sim}{\nabla} \cdot \underset{\sim}{N}^{(\alpha)} + \underset{\sim}{F}^{(\alpha)} + (-1)^{\alpha+1} \underset{\sim}{P} = 0 \quad \text{in } V \tag{C-32}$$

$$\underset{\sim}{\nabla} \cdot \underset{\sim}{M}^{K(\alpha)} - \overline{N}^{K(\alpha)} + \underset{\sim}{F}^{K(\alpha)} + (-1)^{\alpha+1} \underset{\sim}{Q}^{K} = 0 \quad \text{in } V \tag{C-33}$$

The boundary conditions are

$$\overset{\nu}{\underset{\sim}{T}}(\alpha) = \underset{\sim}{\nu} \cdot \underset{\sim}{N}^{(\alpha)} \quad \text{or} \quad \delta\dot{\underset{\sim}{U}}^{(\alpha)} = 0 \quad \text{on } \partial V \ , \tag{C-34}$$

$$\overset{\nu}{\underset{\sim}{T}}^{K(\alpha)} = \underset{\sim}{\nu} \cdot \underset{\sim}{M}^{K(\alpha)} \quad \text{or} \quad \delta\dot{\underset{\sim}{S}}^{K(\alpha)} = 0 \quad \text{on } \partial V \ . \tag{C-35}$$

Equations (C-32) for $\alpha = 1,2$ are the "smoothed" equilibrium relations. They have the form of a binary mixture. The dependent variables $\underset{\sim}{N}^{(\alpha)}$ represent "partial stresses", i.e., stress averages over the cell area occupied by the appropriate constituent. The quantity $\underset{\sim}{P}$ represents a stress interaction vector which reflects stress transfer between the steel and the concrete across the interface.

In addition to direct averages of the stress field over the cell, weighted averages also enter the formulation via the variational principle. Equations (C-33) for $\alpha = 1,2$ govern these new dependent variables.

The variational principle provides appropriate boundary conditions for the displacement-type variables $\dot{\underset{\sim}{U}}^{(\alpha)}$, $\dot{\underset{\sim}{S}}^{K(\alpha)}$ and the stress-type variables $\underset{\sim}{N}^{(\alpha)}$, $\underset{\sim}{M}^{K(\alpha)}$. These conditions are expressed by (C-34) or (C-35).

C.9.2 Mixture Constitutive Relations.

The test functions (C-30) furnish the following rate-of-deformation tensor:

$$\underset{\sim}{d}^{(\alpha)} = \dot{\underset{\sim}{\mathscr{E}}}^{(\alpha)} + \epsilon \underset{\sim}{g}^{K(\alpha)} \dot{\mathscr{K}}^{(\alpha)} + \underset{\sim}{d}^{*(\alpha)} \tag{C-32}$$

where

$$\dot{\underset{\sim}{\mathscr{E}}}^{(\alpha)} \equiv \frac{1}{2}\left[\underset{\sim}{\nabla}\dot{\underset{\sim}{U}}^{(\alpha)} + \underset{\sim}{\nabla}^{T}\dot{\underset{\sim}{U}}^{(\alpha)}\right] , \dot{\mathscr{K}}^{K(\alpha)} \equiv \frac{1}{2}\left[\underset{\sim}{\nabla}\dot{\underset{\sim}{S}}^{K(\alpha)} + \underset{\sim}{\nabla}^{T}\dot{\underset{\sim}{S}}^{K(\alpha)}\right] ,$$

$$\underset{\sim}{d}^{*(\alpha)} \equiv \frac{1}{2}\left[\underset{\sim}{S}^{K(\alpha)}\underset{\sim}{\nabla}^{*}\underset{\sim}{g}^{K(\alpha)} + \underset{\sim}{S}^{K(\alpha)}\underset{\sim}{\nabla}^{*T}\underset{\sim}{g}^{K(\alpha)}\right] \ . \tag{C-33}$$

Substitution of (C-32) into the constitutive relation (C-23), and the latter into (C-31b,c) gives

$$\underset{\sim}{N}^{(\alpha)} = \underset{\sim}{E}^{(\alpha)} : \underset{\sim}{\mathscr{E}}^{(\alpha)} + \underset{\sim}{A}^{K(\alpha)} : \underset{\sim}{\mathscr{K}}^{K(\alpha)} + \underset{\sim}{B}^{K(\alpha)} \cdot \underset{\sim}{S}^{K(\alpha)} \quad , \tag{C-34}$$

$$\underset{\sim}{M}^{K(\alpha)} = \underset{\sim}{A}^{K(\alpha)} : \underset{\sim}{\mathscr{E}}^{(\alpha)} + \underset{\sim}{G}^{KL(\alpha)} : \underset{\sim}{\mathscr{K}}^{L(\alpha)} + \underset{\sim}{C}^{KL(\alpha)} \cdot \underset{\sim}{S}^{L(\alpha)} , \tag{C-35}$$

$$\underset{\sim}{N}^{(\alpha)} = \underset{\sim}{a}^{K(\alpha)} : \underset{\sim}{\mathscr{E}}^{(\alpha)} + \underset{\sim}{b}^{KL(\alpha)} : \underset{\sim}{\mathscr{K}}^{L(\alpha)} + c^{KL(\alpha)} \cdot \underset{\sim}{S}^{K(\alpha)} \quad . \tag{C-36}$$

where $\underset{\sim}{E}$. $\underset{\sim}{A}$. $\underset{\sim}{B}$. $\underset{\sim}{G}$. $\underset{\sim}{C}$. $\underset{\sim}{a}$. $\underset{\sim}{b}$. $\underset{\sim}{c}$ denote weighted averages of the material tensor $\underset{\sim}{D}$ over the cell. The latter quantities are given by

$$\left[\underset{\sim}{E}^{(\alpha)}, A^{K(\alpha)}, \underset{\sim}{B}^{K(\alpha)}, \underset{\sim}{G}^{KL(\alpha)}, \underset{\sim}{C}^{KL(\alpha)}\right] \equiv \int_{A(\alpha)} \Big[\underset{\sim}{D}^{(\alpha)}, \epsilon D^{(\alpha)} g^{K(\alpha)}, \tag{C-37a}$$

$$\underset{\sim}{D}^{(\alpha)} \cdot \underset{\sim}{\nabla}^* g^{K(\alpha)}, \ \epsilon^2 g^{K(\alpha)} g^{L(\alpha)} \underset{\sim}{D}^{(\alpha)}, \ \epsilon g^{K(\alpha)} \underset{\sim}{D}^{(\alpha)} \cdot \underset{\sim}{\nabla}^* g^{L(\alpha)}\Big] dA^* \ ;$$

$$\left[a^{K(\alpha)}, \underset{\sim}{b}^{KL(\alpha)}, \underset{\sim}{c}^{KL(\alpha)}\right] \equiv \int_{A(\alpha)} \Big[\epsilon \underset{\sim}{\nabla}^* g^{K(\alpha)} \cdot \underset{\sim}{D}^{(\alpha)}, \epsilon^2 g^{K(\alpha)} \underset{\sim}{\nabla}^* g^{K(\alpha)} \cdot \underset{\sim}{D}^{(\alpha)},$$

$$\epsilon \underset{\sim}{\nabla}^* g^{K(\alpha)} \cdot \underset{\sim}{D}^{(\alpha)} \cdot \underset{\sim}{\nabla}^* g^{L(\alpha)}\Big] dA^* \ ; \tag{C-37b}$$

C.9.3 Interaction Terms.

Using (C-31e), (C-30), and (C-24b), the interaction term $\underset{\sim}{P}$ can be expressed in the form

$$\overset{\nabla}{\underset{\sim}{P}} \simeq \underset{\sim}{\mathscr{L}} \cdot [\dot{\underset{\sim}{U}}] \quad , \quad \underset{\sim}{\mathscr{L}} \equiv \frac{1}{\epsilon} \int \underset{\sim}{\mathscr{B}} \, ds^* \quad . \tag{C-38a}$$

$$\overset{\nabla}{\underset{\sim}{Q}}{}^K \simeq \underset{\sim}{\mathscr{M}}{}^K \cdot [\dot{\underset{\sim}{U}}] \quad , \quad \underset{\sim}{\mathscr{M}}{}^K \equiv \int \underset{\sim}{\mathscr{B}} g^{K(1)} ds^* \quad . \tag{C-38b}$$

C.9.4 Summary of Mixture Equations.

The basic equations of the mixture model for dense, unidirectionally reinforced concrete can now be summarized as follows:

(a) Equations of Motion

$$\overset{\nabla}{\underset{\sim}{N}}{}^{(\alpha)} + \underset{\sim}{F}^{(\alpha)} + (-1)^{\alpha+1} \underset{\sim}{P} = 0 \, , \tag{C-39}$$

$$\overset{\nabla}{\underset{\sim}{M}}{}^{K(\alpha)} - \overset{\nabla}{\underset{\sim}{N}}{}^{K(\alpha)} + \underset{\sim}{F}^{K(\alpha)} + (-1)^{\alpha+1} \underset{\sim}{Q}^K = 0 \quad ; \tag{C-40}$$

(b) Constitutive Equations

$$\overset{\nabla}{\underset{\sim}{N}}{}^{(\alpha)} = \underset{\sim}{E}^{(\alpha)} : \dot{\underset{\sim}{\mathscr{E}}}^{(\alpha)} + \underset{\sim}{A}^{K(\alpha)} : \dot{\underset{\sim}{\mathscr{K}}}^{K(\alpha)} + \underset{\sim}{B}^{K(\alpha)} \cdot \dot{\underset{\sim}{S}}^{K(\alpha)} \, , \tag{C-41a}$$

$$\overset{\nabla}{\underset{\sim}{M}}{}^{K(\alpha)} = \underset{\sim}{A}^{K(\alpha)} : \dot{\underset{\sim}{\mathscr{E}}}^{(\alpha)} + \underset{\sim}{G}^{KL(\alpha)} : \dot{\underset{\sim}{\mathscr{K}}}^{L(\alpha)} + \underset{\sim}{C}^{KL(\alpha)} \cdot \dot{\underset{\sim}{S}}^{L(\alpha)} \, , \tag{C-41b}$$

$$\overset{\nabla}{\underset{\sim}{N}}{}^{K(\alpha)} = \underset{\sim}{a}^{K(\alpha)} : \dot{\underset{\sim}{\mathscr{E}}}^{(\alpha)} + \underset{\sim}{b}^{KL(\alpha)} : \dot{\underset{\sim}{\mathscr{K}}}^{L(\alpha)} + \underset{\sim}{c}^{KL(\alpha)} \cdot \dot{\underset{\sim}{S}}^{L(\alpha)} \, . \tag{C-41c}$$

(c) Interaction Terms

$$\overset{\nabla}{\underset{\sim}{P}} = \underset{\sim}{\mathscr{L}} \cdot [\dot{\underset{\sim}{U}}] \, , \quad \overset{\nabla}{\underset{\sim}{Q}}{}^K = \underset{\sim}{\mathscr{M}}{}^K \cdot [\dot{\underset{\sim}{U}}] \tag{C-42}$$

(d) Boundary Conditions on ∂V

$$\underset{\sim}{\overset{\nu}{T}}(\alpha) = \underset{\sim}{\kappa}\cdot\underset{\sim}{N}^{(\alpha)} \quad \text{or} \quad \delta\underset{\sim}{\dot{U}}^{(\alpha)} = 0 \quad \text{on} \quad \partial V_T \ , \tag{C-42b}$$

$$\underset{\sim}{\overset{\nu}{T}}{}^{K(\alpha)} = \underset{\sim}{\kappa}\cdot\underset{\sim}{M}^{K(\alpha)} \quad \text{or} \quad \delta\underset{\sim}{\dot{S}}^{K(\alpha)} = 0 \quad \text{on} \quad \partial V_T \tag{C-42b}$$

(e) Kinematic Relations

$$\underset{\sim}{\dot{\varepsilon}}^{(\alpha)} \equiv \frac{1}{2}\left[\underset{\sim}{\nabla}\underset{\sim}{\dot{U}}^{(\alpha)} + \underset{\sim}{\nabla}^{T}\underset{\sim}{\dot{U}}^{(\alpha)}\right] \ , \ \underset{\sim}{\dot{\kappa}}^{K(\alpha)} \equiv \frac{1}{2}\left[\underset{\sim}{\nabla}\underset{\sim}{\dot{S}}^{K(\alpha)} + \underset{\sim}{\nabla}^{T}\underset{\sim}{\dot{S}}^{K(\alpha)}\right] \tag{C-43a,b}$$

C.9.5 Weighting Functions.

In order to utilize the proceeding mixture equations, the weighting functions $g^{K(\alpha)}(\underset{\sim}{x}^*)$ must be specified. For a dense steel layout with a cell aspect ratio near unity, an adequate description of the microdeformation can be obtained in conjunction with a "concentric cylinders approximation". Accordingly, the outer cell boundary is approximated by a circle which is defined based upon equal area of the original and approximate cell. This procedure is depicted in Figure C.3 (for a hexagonal steel array).

Subsequent to the introduction of the approximate cell, the weighting functions are defined as follows:

$$g_2^{(1)}\left[x_2^*, x_3^*\right] = x_2^*/n^{(1)} \ ,$$

$$g^{(2)}\left[x_2^*, x_3^*\right] = -\left[x_2^* - \frac{x_2^*}{x_2^{*2} + x_3^{*2}}\right] \Big/ n^{(2)}$$

$$g_3^{(1)}\left[x_2^*, x_3^*\right] = x_3^*/n^{(1)} \ , \tag{C-44}$$

$$g_3^{(2)}\left[x_2^*, x_3^*\right] = -\left[x_3^* - \frac{x_3^*}{x_2^{*2} + x_3^{*2}}\right] \Big/ n^{(2)} \ .$$

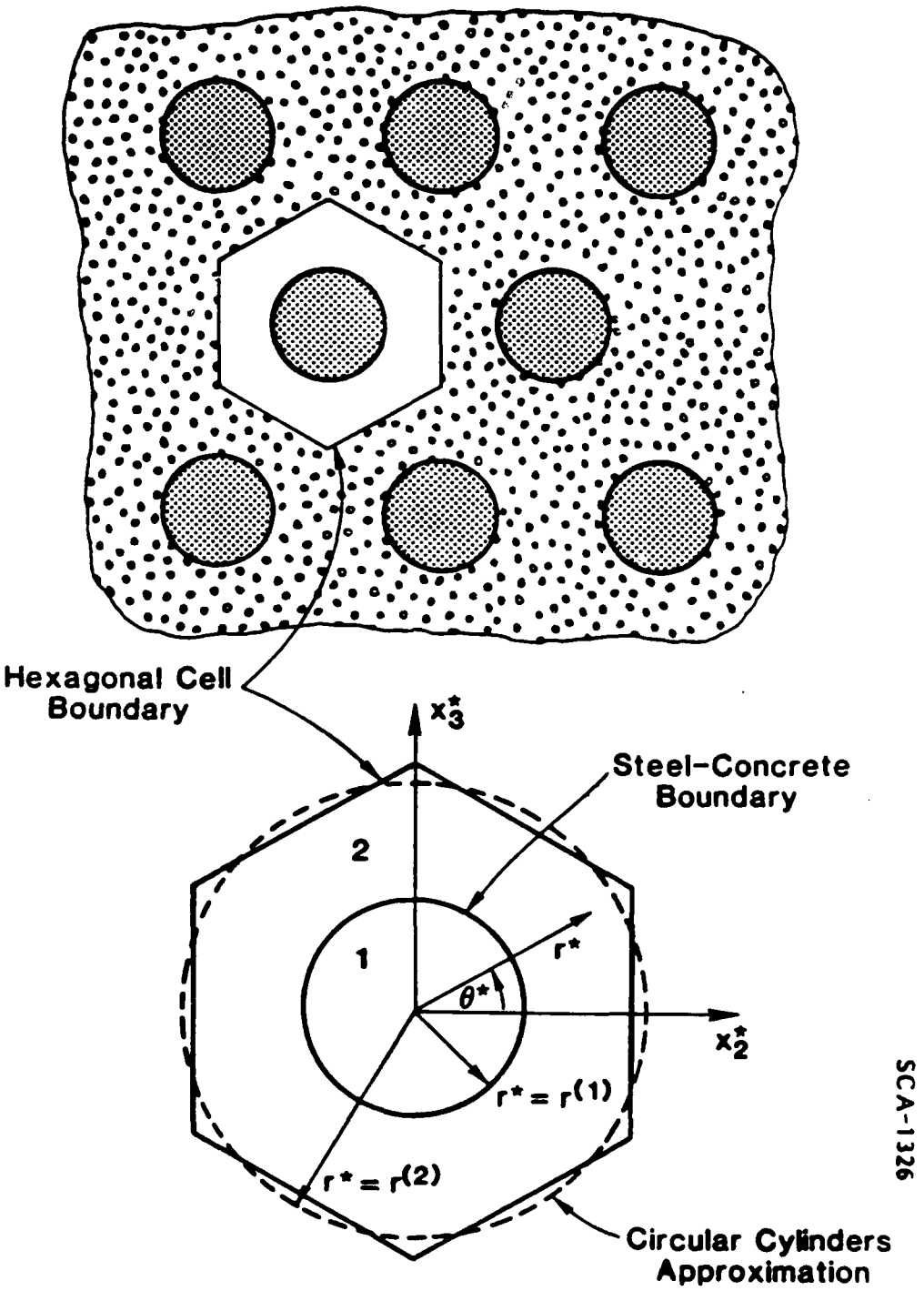

Figure C.3 Circular cylinders approximation (shown for periodic hexagonal steel array).

The relations (C-44) satisfy the $\underset{\sim}{x}^*$-periodicity condition on the (approximate) outer cell boundary. The form (C-44) represents the first relevant terms of a Taylor expansion in the singly connected region $A^{(1)}$ and a Laurent expansion in the annular region $A^{(2)}$. The quantities $n^{(1)}, n^{(2)}$ denote, respectively, the volume fraction of the steel and concrete. If $r^{(1)}, r^{(2)}$ represent the current steel and cell radii, respectively, then $n^{(1)} \equiv (r^{(1)}/r^{(2)})^2$, $n^{(2)} \equiv 1 - n^{(1)}$. The dimension $2r^{(2)}$ represents essentially the steel spacing.

If more accurate measures of the micro-deformation process are desired, they can be generated by a more sophisticated selection of weighting functions. A different set of weighting functions would also be necessary if the cell aspect ratio differed considerably from unity.

C.9.6 Constraints.

For some applications, it may be appropriate to introduce the constraint:

$$\underset{\sim}{S}^{K(1)} = \underset{\sim}{S}^{K(2)} \quad . \tag{C-45}$$

In accordance with the reduction of the number of dependent variables represented by (C-45), the relation (C-40) is replaced by

$$\underset{\sim}{\nabla} \cdot \underset{\sim}{M}^K - \bar{N}^K + \underset{\sim}{F}^K = 0 \tag{C-46}$$

where

$$\left(\underset{\sim}{M}^K, \bar{N}^K, \underset{\sim}{F}^K\right) \equiv \sum_{\alpha=1}^{2} \left(\underset{\sim}{M}^{K(\alpha)}, \bar{N}^{K(\alpha)}, \underset{\sim}{F}^{K(\alpha)}\right) \tag{C-47}$$

Constitutive equations for the new dependent variables $\underset{\sim}{M}^K$, $\underset{\sim}{N}^K$ are obtained by adding (C-35), for $\alpha = 1,2$; and by adding (C-36) for $\alpha = 1,2$. The result is

$$\overset{\nabla}{\underset{\sim}{M}}{}^K = \sum_{\alpha=1}^{2} \left[\underset{\sim}{A}^{K(\alpha)} : \overset{\bullet}{\underset{\sim}{\mathcal{E}}}(\alpha) + \underset{\sim}{G}^{KL(\alpha)} : \overset{\bullet}{\mathcal{K}}{}^L(\alpha) + \underset{\sim}{C}^{KL(\alpha)} \cdot \overset{\bullet}{\underset{\sim}{S}}{}^L\right] , \tag{C-48}$$

$$\overset{\nabla}{\underset{\sim}{N}}{}^{K} = \sum_{\alpha=1}^{2} \left[\underset{\approx}{a}^{K(\alpha)} : \overset{\bullet}{\underset{\approx}{\mathscr{E}}}(\alpha) + \underset{\approx}{b}^{KL(\alpha)} : \overset{\bullet}{\mathscr{K}}{}^{L}(\alpha) + \underset{\approx}{c}^{KL(\alpha)} \cdot \overset{\bullet}{\underset{\sim}{S}}{}^{L} \right] . \tag{C-49}$$

C.9.7 Coordinate Systems.

The mixture relations (C-47) - (C-52) are based on the premise that the current configuration is also the reference configuration. Otherwise, the equations are general. In particular, since direct notation has been used, the mixture relations are valid for arbitrary global (macro) coordinate systems. Care, however, must be exercised in performing coordinate transformations since the local or microcoordinates represent a preferred or "material"-type system. For example, the operator ∇^*, and the constitutive tensors $\mathscr{B}$, $\mathscr{L}$, and $\mathscr{M}$ are all referred to a local coordinate system with base vectors as illustrated in Figure C.4.

Let $(\,)^*$ denote tensor components referred to the preferred coordinate system. For simplicity, let this system be rectangular Cartesian. Then (see Figure C.4), with respect to any other (rectangular Cartesian) system, one finds

$$\overset{\nabla}{P}_i = \phi_{ik}\phi_{m\ell}\mathscr{L}^*_{k\ell}\left[\overset{\bullet}{U}_m\right] \ , \ \mathscr{L}^*_{k\ell} \equiv \frac{1}{\epsilon}\int \mathscr{B}^*_{k\ell}\, ds \ ; \tag{C-50a}$$

$$\overset{\nabla}{Q}{}^{K}_i = \phi_{ik}\phi_{m\ell}\mathscr{M}^{K*}_{k\ell}\left[\overset{\bullet}{U}_m\right] \ , \ \mathscr{M}^{K*}_{k\ell} \equiv \int_{\mathscr{I}} \mathscr{B}^*_{k\ell} g^{K(1)}\, ds \ ; \tag{C-50b}$$

$$B^{K(\alpha)}_{ijk} = \phi_{\ell m}\int_{A(\alpha)} D^{(\alpha)}_{ijk\ell}\, g^{K(\alpha)}_{,m^*}\, dA^* \ ; \tag{C-50c}$$

$$C^{KL(\alpha)}_{ijk} = \phi_{\ell m}\int_{A(\alpha)} \epsilon g^{K(\alpha)} D_{ijk\ell} g^{K(\alpha)}_{,m^*}\, dA^* \ ; \tag{C-50d}$$

$$a^{K(\alpha)}_{ijk} = \phi_{\ell m}\int_{A(\alpha)} \epsilon g^{K(\alpha)}_{,m^*} D_{\ell ijk}\, dA^* \ ; \tag{C-50e}$$

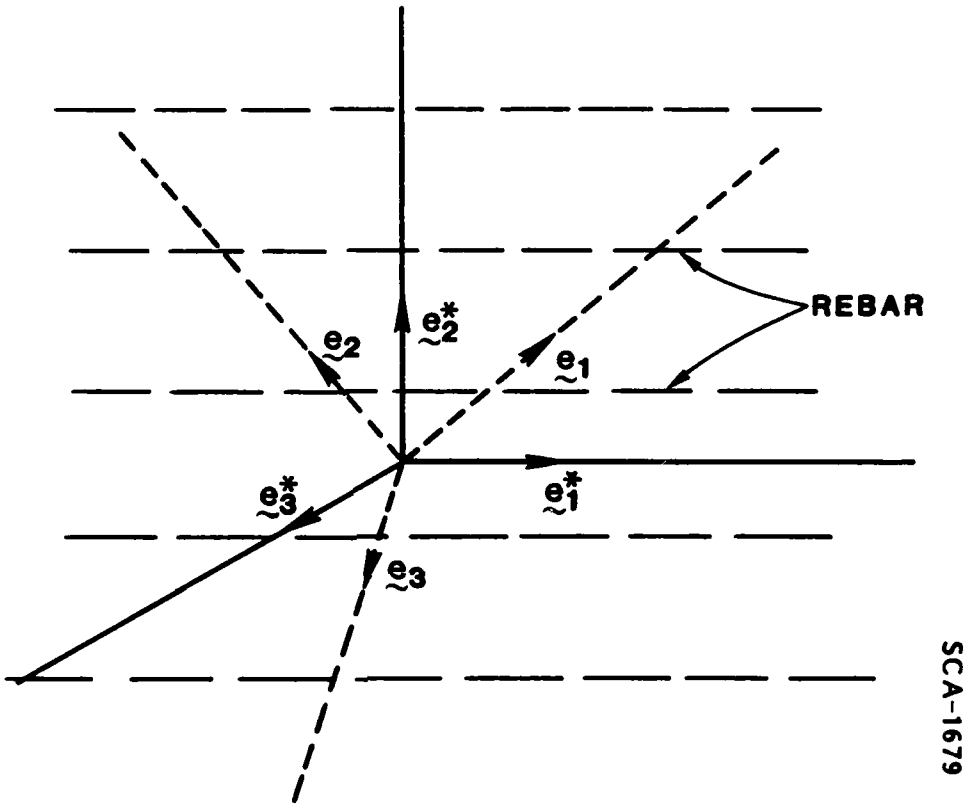

Figure C.4 Coordinate systems: ξ_i^*, ξ_i (i = 1,2,3) denote microcoordinates and macrocoordinates respectively.

$$b_{ijk}^{KL(\alpha)} = \phi_{\ell m} \int_{A(\alpha)} \epsilon^2 g^{K(\alpha)} g_{,m^*}^{K(\alpha)} D_{\ell ijk} dA^* \quad ; \tag{C-50f}$$

$$c_{ij}^{KL(\alpha)} = \phi_{\ell m} \phi_{kn} \int_{A(\alpha)} \epsilon g^{K(\alpha)} g_{,m^*}^{K(\alpha)} g_{,m^*}^{L(\alpha)} D_{\ell ijk} dA^* \tag{C-50g}$$

In the above, ϕ_{ij} denote angle cosines defined by

$$\phi_{ij} \equiv \underset{\sim}{e}_i \cdot \underset{\sim}{e}_j^* \tag{C-50h}$$

where $\underset{\sim}{e}_i$, $\underset{\sim}{e}_j^*$ are unit orthogonal base vectors associated with the general macrocoordinate system and the microcoordinate system, respectively. The components of all other tensors in (C-39) - (C-43) do not involve the microcoordinates and hence can be written directly without involvement of ϕ_{ij}.

APPENDIX D

MIXED VARIATIONAL PRINCIPLE FOR SYNTHESIZED FIELDS

The direct variational method, as outlined in Appendix C, is convenient from a theoretical construction standpoint. However, there are certain disadvantages associated with such an approach. For example, the constitutive relations for the interaction terms do not evolve naturally. Also, the microstresses resulting from the direct method will be rather crude unless complex weighting functions are utilized. Further, the system of equations generated by the direct method may be too "stiff".

In an effort to overcome problems such as those noted above, the use of other variational methods was explored. One such method -- a Reissner-type mixed variational formulation -- was found to be particularly useful. This technique is discussed next.

According to (C-25) of Appendix C, the conservation of linear momentum is satisfied in an average sense via a weighted residual procedure wherein the variations in velocity, $\delta \underset{\sim}{v}^{(\alpha)}$, constitute the weighting functions. In the mixed variational method, both the conservation of linear momentum and the constitutive relations are to be satisfied in an average sense via the following weighted residual procedure:

$$\int_V \left\{ \sum_{\alpha=1}^{2} \int_{A^{(\alpha)}} \left[\left(\underset{\sim}{\nabla} \cdot \overset{\nabla}{\underset{\sim}{q}}{}^{(\alpha)} + \epsilon^{-1} \underset{\sim}{\nabla}^* \cdot \overset{\nabla}{\underset{\sim}{q}}{}^{(\alpha)} + \underset{\sim}{f}^{(\alpha)} \right) \cdot \delta \underset{\sim}{v}^{(\alpha)} + \delta \overset{\nabla}{\underset{\sim}{q}}{}^{(\alpha)} : \left(\underset{\sim}{\tilde{d}}^{(\alpha)} - \underset{\sim}{\nabla} \underset{\sim}{v}^{(\alpha)} + \epsilon^{-1} \underset{\sim}{\nabla}^* \underset{\sim}{v}^{(\alpha)} \right) dA^* \right\} dV$$

$$+ \int_{V_{\mathscr{I}}} \epsilon^{-1} \delta \overset{\circ}{\underset{\sim}{I}}{}^* \cdot \left(\left[\underset{\sim}{\tilde{v}} \right] - \left[\underset{\sim}{v} \right] \right) ds \, dV + \int_{\partial V} \left\{ \sum_{\alpha=1}^{2} \int_{A^{(\alpha)}} \left(\overset{\circ}{\underset{\sim}{I}} - \underset{\sim}{\kappa} \cdot \overset{\nabla}{\underset{\sim}{q}} \right)^{(\alpha)} \cdot \delta \underset{\sim}{v}^{(\alpha)} dA^* \right\} dS \qquad \text{(D-1)}$$

$$+ \int_V \left\{ \sum_{\alpha=1}^{2} \int_{\mathscr{I}} \epsilon^{-1} \left(\overset{\circ}{\underset{\sim}{I}} - \underset{\sim}{\kappa} \cdot \overset{\nabla}{\underset{\sim}{q}} \right)^{(\alpha)} \cdot \delta \underset{\sim}{v}^{(\alpha)} ds^* dV \right\} + \int_V \left\{ \int_{\partial A^{(2)}} \epsilon^{-1} \left(-\underset{\sim}{\kappa}^{(2)} \cdot \overset{\nabla}{\underset{\sim}{q}}{}^{(2)} \right) \cdot \delta \underset{\sim}{v}^{(2)} ds^* \right\} dV = 0 \quad .$$

According to (D-1), both velocity and stress (increment) are to be varied in this principle. Equation (D-1) is (25) of Appendix C with stress in incremental form together with constraint conditions which are represented by the second and third terms of (D-1). In the second, $\underset{\sim}{d}$ is to be computed from the constitutive relation (C-30) given the stress increment, i.e., formally by

$$\underset{\sim}{\tilde{d}}^{(\alpha)} = \left[\underset{\sim}{\mathcal{D}}^{-1} : \overset{\nabla}{\underset{\sim}{\sigma}}\right]^{(\alpha)} \tag{D-2}$$

where $\underset{\sim}{\mathcal{D}}^{-1}$ denotes the inverse of $\underset{\sim}{\mathcal{D}}$. Similarly, in the third term, $[\underset{\sim}{v}]$ is to be computed from the interface constitutive relation (C-31), i.e., formally by

$$\left[\underset{\sim}{\tilde{v}}\right] = \underset{\sim}{\mathcal{B}}^{-1} \cdot \overset{\circ *}{\underset{\sim}{T}} \quad . \tag{D-3}$$

The variations of $\delta\underset{\sim}{v}^{(\alpha)}$ are to satisfy the same conditions as described for (C-25), Appendix C. The variations $\delta\overset{\nabla}{\underset{\sim}{\sigma}}$ are arbitrary over V, but are to satisfy the $\underset{\sim}{x}^*$ - periodicity condition. The variation $\delta\underset{\sim}{T}^*$ is arbitrary over the interface $\mathscr{I}$.

With application of Gauss' Theorem, use of (C-26) - (C-28) together with the $\underset{\sim}{x}^*$-periodicity of $\delta\underset{\sim}{q}^{(\alpha)}$, Equation (D-1) can be written

$$\int_V \left\{ \sum_{\alpha=1}^{2} \int_{A^{(\alpha)}} \left[\overset{\nabla}{\underset{\sim}{\sigma}}{}^{\alpha} : \left(\underset{\sim\sim}{\nabla}\delta\underset{\sim}{v}^{(\alpha)} + \epsilon^{-1}\underset{\sim}{\nabla}^*\delta\underset{\sim}{v}^{(\alpha)} \right) + \delta\overset{\nabla}{\underset{\sim}{\sigma}}{}^{(\alpha)} : \left(\underset{\sim\sim}{\nabla}\underset{\sim}{v}^{(\alpha)} + \epsilon^{-1}\underset{\sim}{\nabla}^*\delta\underset{\sim}{v}^{(\alpha)} - \underset{\sim}{\tilde{d}}^{(\alpha)} \right) \right] dA^* \right.$$

$$\left. + \epsilon^{-1} \oint_{\mathscr{I}} \left[\overset{\circ *}{\underset{\sim}{T}} \cdot \delta[\underset{\sim}{v}] + \delta\overset{\circ *}{\underset{\sim}{T}} \cdot \left([\underset{\sim}{v}] - [\underset{\sim}{\tilde{v}}] \right) \right] ds^* \right\} dV = \int_V \left\{ \sum_{\alpha=1}^{2} \int_{A^{(\alpha)}} \underset{\sim}{f}^{(\alpha)} \cdot \delta\underset{\sim}{v}^{(\alpha)} dA^* \right\} dV$$

$$+ \int_{\partial V_T} \left\{ \sum_{\alpha=1}^{2} \int_{A^{(\alpha)}} \overset{\nu}{\underset{\sim}{T}}{}^{(\alpha)} \cdot \delta\underset{\sim}{v}^{(\alpha)} dA^* \right\} dS \quad . \tag{D-4}$$

Equation (D-4) is an incremental form of the Principle of Virtual Work for the synthesized fields. The terms of (D-4) involving $\delta \underset{\sim}{q}^{(\alpha)}$ and $\delta \underset{\sim}{I}^{*}$ are constraint conditions that reflect satisfaction of the material and interface constitutive relations respectively; here $\delta \underset{\sim}{q}^{(\alpha)}$ and $\delta \underset{\sim}{I}^{*}$ play the roles of Lagrangian multipliers.

The mixed variational method has been used to generate mixture models for several important cases. This work is presented in Appendices E - H. In Appendix E, a model is derived for a dense 1D rebar layout, and for 3D deformation of the resulting composite. In Appendix F, a model is derived for a R/C plate; this is a 2D problem. In Appendix H, the basic equations for a R/C rod (1D problem) are obtained.

APPENDIX E

APPLICATION OF MIXED VARIATIONAL METHOD TO DENSE STEEL LAYOUT - 3-D PROBLEM

The purpose of this appendix is to demonstrate the application of the mixed variational method by a specific example calculation. For this purpose, a dense unidirectional steel layout, Figure E.1, will be considered. For simplicity, the development will be restricted to small deformations. Further, the concrete will be modeled as elastic-brittle fracture, and the steel as elastic. Only tangential steel-concrete slip will be allowed; otherwise, the interface constitutive relation will remain reasonably general.

If the rectangular Cartesian reference system illustrated in Figure E.1 is selected, a quasi-static process is considered without body forces, and small deformations are assumed, then the basic equations, (C-19) - (C-24) of Appendix C, of the synthesized fields reduce to:

(a) Equilibrium

$$\overset{\bullet}{\sigma}{}^{(\alpha)}_{ji,j} + \frac{1}{\epsilon}\,\overset{\bullet}{\sigma}{}^{(\alpha)}_{ji,j}{}^{*} = 0 \ , \ \sigma^{(\alpha)}_{ji} = \sigma^{(\alpha)}_{ij} \tag{E-1}$$

(b) Constitutive relations

$$\overset{\bullet}{\sigma}{}^{(\alpha)}_{ij} = \lambda^{(\alpha)} d_{ij}\, \overset{\bullet}{e}{}^{(\alpha)}_{kk} + 2\mu^{(\alpha)}\, \overset{\bullet}{e}{}^{(\alpha)}_{ij} \ , \tag{E-2a}$$

$$\overset{\bullet}{e}{}^{(\alpha)}_{ij} \equiv \frac{1}{2}\left[\overset{\bullet}{u}{}_{i,j}^{(\alpha)} + \overset{\bullet}{u}{}_{j,i}^{(\alpha)} + \frac{1}{\epsilon}\left[u_{i,j*}^{(\alpha)} + u_{j,i*}^{(\alpha)}\right]\right] \tag{E-2b}$$

(c) Interface relations

$$u_{\gamma}^{(1)} = u_{\gamma}^{(2)} \ (\gamma=2,3), \quad \sigma_{ji}^{(1)}\nu_j^{(1)} = \sigma_{ji}^{(2)}\nu_j^{(1)} \equiv T_i^{*} \quad \text{on } \mathcal{A} \tag{E-3}$$

$$\overset{\bullet}{T}{}_1^{*} = K_1 \left[\overset{\bullet}{u}_1\right] \ , \ \left[\overset{\bullet}{u}_1\right] \equiv \left[\overset{\bullet}{u}{}_1^{(2)} - \overset{\bullet}{u}{}_1^{(1)}\right] \tag{E-4}$$

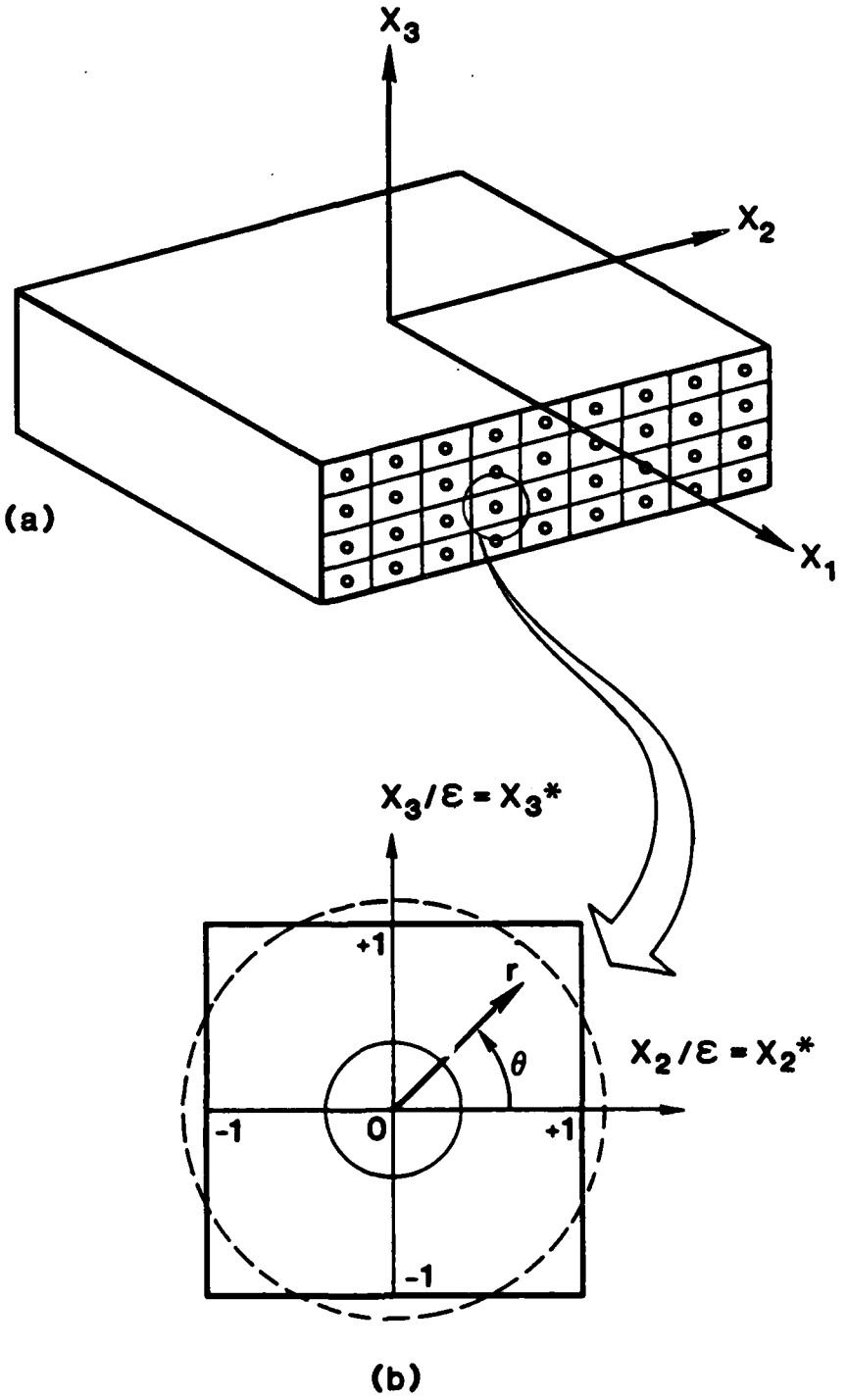

Figure E.1 Coordinate system.

In the above, $\lambda^{(\alpha)}$ and $\nu^{(\alpha)}$ are constants, whereas, K_1, is a (variable) tangent modulus.

Under the conditions noted above, the variational principle, (4) of Appendix C, can be written in component form as follows:

$$\int_V \left\{ \sum_{\alpha=1}^{2} \int_{A^{(\alpha)}} \left[\overset{\bullet}{\sigma}_{ij}^{(\alpha)} \left(\delta \overset{\bullet}{u}_{i,j}^{(\alpha)} + \bar{\epsilon}^{1} \delta \overset{\bullet}{u}_{i,j*}^{(\alpha)} \right) + \delta \overset{\bullet}{\sigma}_{ij}^{(\alpha)} \left(\overset{\bullet}{u}_{i,j}^{(\alpha)} + \bar{\epsilon}^{1} \overset{\bullet}{u}_{i,j*} - \overset{\bullet}{e}_{ij}^{(\alpha)} \; (\bullet\bullet\bullet) \right) \right] dA^{*} \right.$$

$$\left. + \bar{\epsilon}^{1} \oint_{\mathscr{S}} \left[\overset{\bullet}{T}_{i}^{*} \left(\delta \overset{\bullet}{u}_{i}^{(2)} - \delta \overset{\bullet}{u}_{i}^{(1)} \right) + \delta \overset{\bullet}{T}_{i}^{*} \left(\overset{\bullet}{u}_{i}^{(2)} - \overset{\bullet}{u}_{i}^{(1)} - \left[\overset{\bullet}{u}_{i} \right] (\bullet\bullet\bullet) \right) \right] ds^{*} \right\} dV$$

$$= \int_{\partial V_T} \left\{ \sum_{\alpha=1}^{2} \int_{A^{(\alpha)}} \overset{\bullet}{T}_{i}^{(\alpha)} \delta \overset{\bullet}{u}_{i}^{(\alpha)} \right\} dS \qquad \text{(E-5)}$$

In the above, u_i is the displacement vector, $(\overset{\bullet}{\;}) \equiv \partial(\;)/\partial t$ and $(\;)_j^{*} \equiv \partial(\;)/\partial x_j^{*}$ with $\partial(\;)/\partial x_1^{*} \equiv 0$. In what follows, all stress components will be varied with the exception of σ_{11}; thus $\delta\sigma_{11} \equiv 0$. The notation $\overset{\bullet}{e}_{ij}^{(\alpha)}(\bullet\bullet\bullet)$ implies inversion of the constitutive relations for (i,j) $\neq$ (1,1). Similarly, the notation $[\overset{\bullet}{u}_i](\bullet\bullet\bullet)$ implies inversion of the interface constitutive relation. Herein, only $\overset{\bullet}{T}_1$ will be varied; thus $\delta\overset{\bullet}{T}_2^{*} = \delta\overset{\bullet}{T}_3^{*} \equiv 0$.

Appropriate trial displacement and transverse stress fields for use in (E-5) can be obtained by an asymptotic procedure (Murakami, Maewal, and Hegemier [1981]). Accordingly, one invokes the premise that the macrodimension $\bar{\Lambda}$ is much smaller than the microdimension $\bar{\Delta}$, i.e., $\epsilon \equiv \bar{\Delta}/\bar{\Lambda} << 1$. This premise and the form of the scaled equations (E-1) and (E-2), suggest an expansion of the dependent variables in the asymptotic series:

$$\left\{u_i, \sigma_{ij}\right\}^{(\alpha)}\left(x_k, x_\ell^*, t; \epsilon\right) = \sum_{n=0}^{\infty} \epsilon^n \left\{u_{i(n)}, \sigma_{ij(n)}\right\}^{(\alpha)}\left(x_k, x_\ell^*, t\right) \qquad \text{(E-6)}$$

If (E-6) is substituted into (E-1) - (E-4), and the coefficients of different powers of ϵ are equated to zero, a sequence of problems defined on the cell is obtained. Consideration of this sequence to $O(\epsilon)$ provides the following form for the trial fields (see Murakami and Hegemier [1986]):

(a) Displacement trial functions

$$\overset{\bullet}{u}_i^{(\alpha)} = \overset{\bullet}{U}_i^{(\alpha)}(x_k, t) + \epsilon g^{(\alpha)}(r)\left\{{}^{2}\overset{\bullet}{S}_i(x_k, t)\cos\theta + {}^{3}\overset{\bullet}{S}_i(x_k, t)\sin\theta\right\} \qquad \text{(E-7a)}$$

where

$${}^{2}\overset{\bullet}{S}_3 = {}^{3}\overset{\bullet}{S}_2 \qquad \text{(E-7b)}$$

and

$$g^{(1)}(r) = \frac{r}{n^{(1)}} \quad , \quad g^{2}(r) = \frac{r}{n^{(2)}}\left[-r + \frac{1}{r}\right] \qquad \text{(E-7c)}$$

(b) Stress Trial Functions

$$\overset{\bullet}{\sigma}_{22}^{(1)} = \overset{\bullet}{\tau}_{22}^{(1)} + \epsilon \frac{g}{4}^{(1)}\left[3\overset{\bullet}{P}_2\cos\theta + \overset{\bullet}{P}_3\sin\theta\right] ,$$

$$\overset{\bullet}{\sigma}_{33}^{(1)} = \overset{\bullet}{\tau}_{33}^{(1)} + \epsilon \frac{g}{4}^{(1)}\left[\overset{\bullet}{P}_2\cos\theta + 3\overset{\bullet}{P}_3\sin\theta\right] ,$$

$$\overset{\bullet}{\sigma}_{23}^{(1)} = \overset{\bullet}{\tau}_{23}^{(1)} + \epsilon \frac{g}{4}^{(1)}\left[\overset{\bullet}{P}_2\cos\theta + \overset{\bullet}{P}_3\cos\theta\right] ,$$

$$\overset{\bullet}{\sigma}{}^{(1)}_{31} = \overset{\bullet}{\tau}{}^{(1)}_{31} + \epsilon \frac{g}{2}^{(1)} \overset{\bullet}{P}_1 \sin\theta \ ,$$

$$\overset{\bullet}{\sigma}{}^{(1)}_{12} = \overset{\bullet}{\tau}{}^{(1)}_{12} + \epsilon \frac{g}{2}^{(1)} \overset{\bullet}{P}_1 \cos\theta \ ,$$

$$\overset{\bullet}{\sigma}{}^{(2)}_{22} = \overset{\bullet}{\tau}{}^{(2)}_{22} + \overset{\bullet}{\tau}{}^{(2)}_{22} \frac{\cos 2\theta}{r^2} + \overset{\bullet}{\tau}{}^{(2)}_{33} \frac{\cos 2\theta}{r^2} + \overset{\bullet}{\tau}{}^{(2)}_{23} \frac{\sin 2\theta}{r^2} + \frac{\epsilon g}{4}^{(2)} \left[3\overset{\bullet}{P}_2 \cos\theta + \overset{\bullet}{P}_3 \sin\theta \right],$$

$$\overset{\bullet}{\sigma}{}^{(2)}_{33} = \overset{\bullet}{\tau}{}^{(2)}_{33} + \overset{\bullet}{t}{}^{(2)}_{22} \frac{\cos 2\theta}{r^2} - \overset{\bullet}{t}{}^{(2)}_{33} \frac{\cos 2\theta}{r^2} + \overset{\bullet}{t}{}^{(2)}_{23} \frac{\sin 2\theta}{r^2} + \frac{\epsilon g}{4}^{(2)} \left[(\overset{\bullet}{P}_2 \cos\theta + 3\overset{\bullet}{P}_3 \sin\theta \right],$$

$$\overset{\bullet}{\sigma}{}^{(2)}_{23} = \overset{\bullet}{\tau}{}^{(2)}_{23} + \overset{\bullet}{t}{}^{(2)}_{33} \frac{\sin 2\theta}{r^2} + \frac{\epsilon}{4} \left[\overset{\bullet}{P}_2 g^{(1)} \cos\theta + \overset{\bullet}{P}_3 \, g^{(2)} \cos\theta \right] \ ,$$

$$\overset{\bullet}{\sigma}{}^{(2)}_{31} = \overset{\bullet}{\tau}{}^{(2)}_{31} + \overset{\bullet}{t}{}^{(2)}_{12} \frac{\sin 2\theta}{r^2} + \overset{\bullet}{t}{}^{(2)}_{31} \frac{\cos 2\theta}{r^2} + \frac{\epsilon g}{2}^{(2)} \overset{\bullet}{P}_1 \sin\theta \ ,$$

$$\overset{\bullet}{\sigma}{}^{(2)}_{12} = \overset{\bullet}{\tau}{}^{(2)}_{12} + \overset{\bullet}{t}{}^{(2)}_{12} \frac{\cos 2\theta}{r^2} - \overset{\bullet}{t}{}^{(2)}_{31} \frac{\sin 2\theta}{r^2} + \frac{\epsilon}{2} \, g^{(2)} \cos\theta \ , \qquad \text{(E-8)}$$

where $\overset{\bullet}{\tau}{}^{(a)}_{ij}$, $\overset{\bullet}{t}{}^{(22)}_{22}$, $\overset{\bullet}{t}{}^{(2)}_{33}$ and $\overset{\bullet}{P}_i$ (i = 1-3) are functions of x_k and t.

Following substitution of the trial fields (E-7) and (E-8) into the variational principle (E-5), use of Cauchy's formula to evaluate T_i^* according to

$$T_i^* = \sigma_{ji}^{(1)} \nu_j^{(1)} \text{ on } \mathscr{S} \ , \qquad \text{(E-9)}$$

and appropriate integrations by parts, one obtains the Euler equations of the variational principle in the form

(a) Mixture Equilibrium - stress averages

$$n^{(\alpha)}\mathring{N}_{ji,j}^{(\alpha)} + (-1)^{\alpha+1}\,\mathring{P}_i = 0 \quad (i = 1\text{-}3) \quad , \tag{E-10}$$

(b) Mixture Equilibrium - stress moments

$$^{2}\mathring{M}_{ji,j} + \frac{1}{\epsilon^2}\left[\mathring{N}_{2i}^{(2)} - \mathring{N}_{2i}^{(1)} + \mathring{R}_{2i}^{(2)}\right] = 0 \quad (i = 1,2) \quad , \tag{E-11a}$$

$$^{3}\mathring{M}_{ji,j} + \frac{1}{\epsilon^2}\left[\mathring{N}_{3i}^{(2)} - \mathring{N}_{3i}^{(1)} + \mathring{R}_{3i}^{(2)}\right] = 0 \quad (i = 1,3) \quad , \tag{E-11b}$$

$$\frac{1}{2}\left[^{3}\mathring{M}_{j2,j} + {}^{2}\mathring{M}_{j3,j}\right] + \frac{1}{\epsilon^2}\left[\mathring{N}_{23}^{(2)} - \mathring{N}_{23}^{(1)} + \mathring{R}_{23}^{(2)}\right] = 0 \quad , \tag{E-11c}$$

where

$$\mathring{N}_{ij}^{(\alpha)} \equiv \frac{1}{n^{(\alpha)}A}\int_{A^{(\alpha)}} \mathring{\sigma}_{ij}^{(\alpha)}\, dA^* \quad , \tag{E-12a}$$

$$\epsilon\left[^{2}\mathring{M}_{ij} \;,\; {}^{3}\mathring{M}_{ij}\right] \equiv \frac{1}{A}\sum_{\alpha=1}^{2}\int_{A^{(\alpha)}} \mathring{\sigma}_{ij}^{(\alpha)}\, g^{(\alpha)}(\cos\theta,\ \sin\theta)\, dA^* \tag{E-12b}$$

(c) Constitutive Relations - transverse stress averages

$$\begin{Bmatrix}\mathring{N}_{22}\\ \mathring{N}_{33}\end{Bmatrix}^{(\alpha)} = \begin{Bmatrix}\mathring{\tau}_{22}\\ \mathring{\tau}_{33}\end{Bmatrix}^{(\alpha)} = \begin{bmatrix}\lambda+2\mu & \lambda\\ \lambda & \lambda+2\mu\end{bmatrix}\begin{bmatrix}\mathring{U}_{2,2}^{(\alpha)} + (-1)^{\alpha+1}\,{}^{2}\mathring{S}_{2}/n^{(\alpha)}\\ \mathring{U}_{3,3}^{(\alpha)} + (-1)^{\alpha+1}\,{}^{3}\mathring{S}_{3}/n^{(\alpha)}\end{bmatrix} + \lambda^{(\alpha)}\mathring{U}_{1,1}^{(\alpha)}\begin{Bmatrix}1\\ 1\end{Bmatrix}, \tag{E-13a}$$

$$\mathring{N}_{23}^{(\alpha)} = \mathring{\tau}_{23}^{(\alpha)} = \mu^{(\alpha)}\left[\mathring{U}_{2,3} + \mathring{U}_{3,2}\right]^{(\alpha)} + \frac{2(-1)^{\alpha+1}\,{}^{3}\mathring{S}_{2}}{n^{(\alpha)}} \quad , \tag{E-13b}$$

$$\overset{*}{N}{}_{31}^{(\alpha)} = \overset{*}{\tau}{}_{31}^{(\alpha)} = \left[\frac{1}{\mu(1)} + \delta_{\alpha 1}\frac{C_{11}}{\sqrt{n(1)}}\right]^{-1}\left[\overset{*}{U}{}_{3,1}^{(\alpha)} + \overset{*}{U}{}_{1,3}^{(\alpha)} + (-1)^{\alpha+1}\frac{3\overset{s}{S}_1}{n(\alpha)}\right] \qquad \text{(E-13c)}$$

$$\overset{*}{N}{}_{21}^{(\alpha)} = \overset{*}{\tau}{}_{21}^{(\alpha)} = \left[\frac{1}{\mu(1)} + \delta_{\alpha 1}\frac{C_{11}}{\sqrt{n(1)}}\right]^{-1}\left[\overset{*}{U}{}_{1,2}^{(\alpha)} + \overset{*}{U}{}_{2,1}^{(\alpha)} + (-1)^{\alpha+1}\frac{2\overset{s}{S}_1}{n(\alpha)}\right] \qquad \text{(E-13d)}$$

(d) Constitutive Relations - interaction terms

$$\overset{*}{P}_1 = \hat{\beta}_1\left\{\frac{\overset{*}{U}{}_1^{(2)} - \overset{*}{U}{}_1^{(1)}}{\epsilon^2} + \frac{\hat{\kappa}}{2}\left[{}^{2}\overset{s}{S}_{1,2} + {}^{2}\overset{s}{S}_{2,1}\right] + \frac{\hat{\kappa}}{2}\left[{}^{3}\overset{s}{S}_{3,1} + \overset{3*}{S}_{1,3}\right]\right\} \qquad \text{(E-14a)}$$

where

$$1/\hat{\beta}_1 = \tfrac{1}{2}\sum_{\alpha=1}^{2}\frac{\hat{\kappa}^{(\alpha)}}{\mu^{(\alpha)}} + \frac{C_{11}}{2\sqrt{n(1)}} \quad , \quad C_{11} \equiv K_1^{-1} \; ;$$

$$\hat{\kappa} = \sum_{\alpha=1}^{2}\hat{\kappa}^{(\alpha)} \quad , \qquad \text{(E-14b)}$$

$$\hat{\kappa}^{(\alpha)} = \frac{1}{\pi}\int_{A^{(\alpha)}}\left[g^{(\alpha)}\cos\theta\right]^2 dA^* \; ;$$

$$\overset{*}{P}_2 = \beta_2\left[\frac{\left(\overset{*}{U}{}_2^{(2)} - \overset{*}{U}{}_1^{(1)}\right)}{\epsilon^2} + \gamma\left[{}^{2}\overset{s}{S}_{1,1}\right] + \frac{h}{4}\left[3\left[{}^{2}\overset{s}{S}_{2,2}\right] + 2\left[{}^{3}\overset{s}{S}_{2,3}\right] + {}^{3}\overset{s}{S}_{3,2}\right]\right] \; , \qquad \text{(E-15)}$$

$$\overset{*}{P}_3 = \beta_3\left[\frac{\left(\overset{*}{U}{}_3^{(2)} - \overset{*}{U}{}_3^{(1)}\right)}{\epsilon^2} + \gamma\left[{}^{3}\overset{s}{S}_{1,1}\right] + \frac{h}{4}\left[{}^{2}\overset{s}{S}_{2,3} + 2\left[{}^{3}\overset{s}{S}_{2,2}\right] + 3\left[{}^{3}\overset{s}{S}_{3,3}\right]\right]\right] \; , \qquad \text{(E-16)}$$

where

$$\beta_2^{-1} = \beta_3^{-1} = \sum_{\alpha=1}^{2} \left[\frac{h^{(\alpha)} (\lambda+3\mu)^{(\alpha)}}{8\mu^{(\alpha)} (\lambda+\mu)^{(\alpha)}} \right] \quad , \tag{E-17a}$$

$$\gamma = \sum_{\alpha=1}^{2} h^{(\alpha)} \lambda^{(\alpha)} / 2(\lambda+\mu)^{(\alpha)} \quad , \quad h = \sum_{\alpha=1}^{2} h^{(\alpha)} \quad , \tag{E-17b}$$

$$h^{(1)} = \frac{1}{4} \; , \; h^{(2)} = \frac{-1}{4n^{(2)}} \left[2 + n^{(2)} + \frac{2}{n^{(2)}} \ell n \; n^{(1)} \right] \tag{E-17c}$$

(e) Constitutive Relations - stress moments

$$^{2}\mathring{M}_{22} = \frac{3}{4} h \mathring{p}_2 \quad , \quad ^{2}\mathring{M}_{33} = \frac{h}{4} \quad , \quad ^{2}\mathring{M}_{12} = \frac{h}{2} \mathring{p}_1 \quad , \tag{E-18a}$$

$$^{3}\mathring{M}_{22} = \frac{h}{4} \mathring{p}_3 \quad , \quad ^{3}\mathring{M}_{33} = \frac{3}{4} h \mathring{p}_3 \quad , \quad ^{3}\mathring{M}_{31} = \frac{h}{2} \mathring{p}_1 \quad , \tag{E-18b}$$

$$^{2}\mathring{M}_{23} = ^{2}\mathring{M}_{31} = ^{3}\mathring{M}_{23} = ^{3}\mathring{M}_{12} = 0 \tag{E-18c}$$

where it is understood that $^{2}M_{ij} = ^{2}M_{ji}$, $^{3}M_{ji} = ^{3}M_{ij}$.

Additional definitions used in the foregoing equations include

$$R_{21}^{(2)} \equiv t_{12}^{(2)} / n^{(1)}, \quad R_{22}^{(2)} \equiv \left[t_{22}^{(2)} / 2 + t_{33}^{(2)} \right] / n^{(1)} \; ,$$

$$R_{31}^{(2)} \equiv - t_{31}^{(2)} / n^{(1)} \; , \; R_{23}^{(2)} \equiv t_{23}^{(2)} / 2n^{(1)}, \; R_{33}^{(2)} \equiv \left[-t_{22}^{(2)} / 2 + t_{33}^{(2)} \right] / n^{(1)}$$

$$t_{12}^{(2)} = -\mu^{(2)} {}^{2}S_1 \; / \; n^{(2)} \; , \; t_{31}^{(2)} = \mu^{(2)} {}^{3}S_1 \; / \; n^{(2)} \quad ,$$

$$t_{22}^{(2)} = -(\lambda+\mu)^{(2)} \left[{}^2S_2 - {}^3S_3\right]/n^{(2)} \ , \ t_{33}^{(2)} = -\mu^{(2)} \left[{}^2S_2 + {}^3S_3\right]/n^{(2)} \ , \qquad \text{(E-19)}$$

$$t_{23}^{(2)} \equiv -(\lambda+\mu)^{(2)} \left[2\ {}^3S_2\right]/n^{(2)} \ .$$

(f) Constitutive Relations - axial stresses

The remaining constitutive relations associated with $\sigma_{11}^{(\alpha)}$ are obtained from (E-2a) with i=j≡1: the result is

$$\dot{N}_{11}^{(\alpha)} = (\lambda+2\mu)^{(\alpha)} \dot{U}_{1,1}^{(\alpha)} + \lambda^{(\alpha)} \left\{ \dot{U}_{2,2}^{(\alpha)} + \dot{U}_{3,3}^{(\alpha)} + (-1)^{\alpha+1} \left[{}^2\dot{S}_2 + {}^3\dot{S}_3\right]/n^{(\alpha)} \right\} \ , \qquad \text{(E-20)}$$

$$\begin{Bmatrix} {}^2\dot{M}_{11} \\ {}^3\dot{M}_{11} \end{Bmatrix} = \sum_{\alpha=1}^{2} h^{(\alpha)} \left[(\lambda+2\mu)^{(\alpha)} - \frac{\lambda^{(\alpha)2}}{(\lambda+\mu)^{(\alpha)}} \right] \begin{Bmatrix} {}^2\dot{S}_{1,1} \\ {}^3\dot{S}_{1,1} \end{Bmatrix} + \gamma \begin{Bmatrix} \dot{P}_2 \\ \dot{P}_3 \end{Bmatrix} \ . \qquad \text{(E-21)}$$

(g) Boundary Conditions

The boundary conditions on ∂V associated with Euler equations are

$$n^{(\alpha)}\ \dot{N}_{ji}^{(\alpha)} \nu_j = \dot{T}_i^{\nu\ (\alpha p)} \text{ or } \delta \dot{U}_i^{(\alpha)} = 0 \ , \ i=1\text{-}3 \ ; \qquad \text{(E-22a)}$$

$$\dot{M}_{ji}^{2} \nu_j = {}^{2\nu}\dot{T}_i \text{ or } \delta\ {}^2\dot{S}_i = 0 \ , \ i=1,2 \ ; \qquad \text{(E-22b)}$$

$${}^3\dot{M}_{ji} \nu_j = {}^{3\nu}\dot{T}_i \text{ or } \delta\ {}^3\dot{S}_i = 0 \ , \ i=1,3 \ ; \qquad \text{(E-22c)}$$

$$\left[{}^3\dot{M}_{j2} + {}^2\dot{M}_{j3}\right] \nu_j = {}^{3\nu}\dot{T}_2 + {}^{2\nu}\dot{T}_3 \text{ or } \delta\ {}^3\dot{S}_2 = 0 \ ; \qquad \text{(E-22d)}$$

where

$$\overset{\nu}{T}_i{}^{(\alpha p)} \equiv \frac{1}{A} \int_{A^{(\alpha)}} \overset{\nu}{T}_i{}^{(\alpha)}\ dA^* \ , \qquad \text{(E-23a)}$$

$$\epsilon\left[{}^{2}_{\nu}T_i \ , \ {}^{3}_{\nu}T_i\right] = \frac{1}{A}\sum_{\alpha=1}^{2}\int_{A^{(\alpha)}} {}^{\nu}_{\alpha}T_i^{(\alpha)}\ g^{(\alpha)}\ (\cos\theta,\sin\theta)\ dA^{*} \qquad \text{(E-23b)}$$

Equations (E-10) - (E-23) define a well-posed boundary value problem with respect to the macrocoordinates x_k.

APPENDIX F

APPLICATION OF MIXED VARIATIONAL METHOD TO R/C PLATE - 2D PROBLEM

The purpose of this appendix is to furnish a second example application of the mixed variational method. In this example, mixture equations are derived for the planar deformations of a R/C plate, Figure F.1. The rebar layout is unidirectional, small deformations will be considered. The concrete is modeled as elastic-brittle fracture, and the steel remains elastic. The development includes tangential steel-concrete slip.

As in the first example, the basic equations of the synthesized field (C-19)-(C-24) of Appendix C are:

(a) Equilibrium

$$\sigma^{(\alpha)}_{ji,j} + \frac{1}{\epsilon}\sigma^{(\sigma)}_{ji,j*} = 0 \quad , \quad \sigma^{(\sigma)}_{ji} = \sigma^{(\alpha)}_{ij} \quad ; \tag{F-1}$$

(b) Constitutive Relations

$$\dot{\sigma}^{(\alpha)}_{ij} = \lambda^{(\alpha)}\delta_{ij}\dot{e}^{(\alpha)}_{kk} + 2\mu^{(\alpha)}\dot{e}^{(\alpha)}_{ij} \quad , \tag{F-2a}$$

$$\dot{e}^{(\alpha)}_{ij} \equiv \frac{1}{2}\left[\dot{u}^{(\alpha)}_{i,j} + \dot{u}^{(\alpha)}_{j,i} + \frac{1}{\epsilon}\left(\dot{u}^{(\alpha)}_{i,j*} + \dot{u}^{(\alpha)}_{j,i*}\right)\right] \quad ; \tag{F-2b}$$

(c) Interface Relations

$$u^{(1)}_{\gamma} = u^{(2)}_{\gamma} \quad (\gamma=2,3) \quad , \quad \sigma_{ji}{}^{(1)}\nu_j{}^{(1)} = \sigma_{ji}{}^{(1)}\nu_j{}^{(1)} \equiv T^*_i \text{ on } \mathcal{A} \quad , \tag{F-3}$$

$$\dot{T}^*_1 = \beta_1\left[\dot{u}_1\right] \quad , \quad \left[\dot{u}_1\right] \equiv \left[\dot{u}^{(2)}_1 - \dot{u}^{(1)}_1\right] \tag{F-4}$$

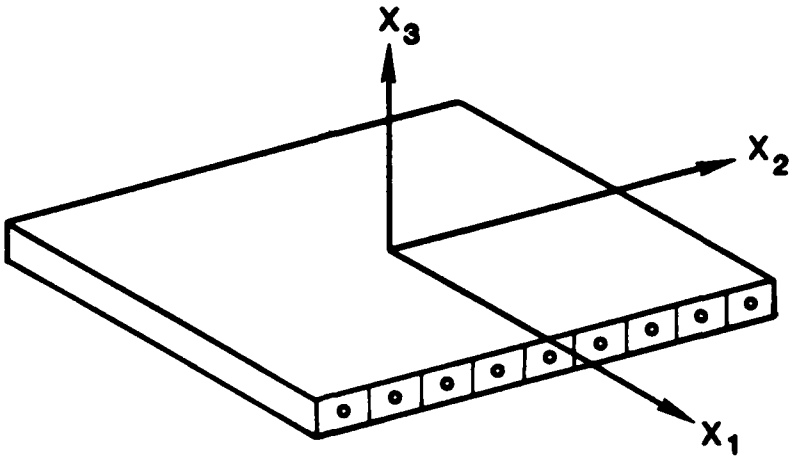

Figure F.1 Coordinate system.

In addition, the variational principle (4) of Appendix D can be written

$$\int_V \left\{ \sum_{\alpha=1}^{2} \int_{A^{(\alpha)}} \left[\overset{\bullet}{\sigma}{}_{ij}^{(\alpha)} \left(\delta \overset{\bullet}{u}{}_{i,j}^{(\alpha)} + \bar{\epsilon}^{1} \delta \, \overset{\bullet}{u}{}_{i,j*}^{(\alpha)} \right) + \delta \overset{\bullet}{\sigma}{}_{ij}^{(\alpha)} \left(\overset{\bullet}{u}{}_{ij}^{(\alpha)} + \bar{\epsilon}^{1} \overset{\bullet}{u}{}_{i,j*} - \overset{\bullet}{e}{}_{ij}^{(\alpha)} (\ldots) \right) \right] dA^{*} \right.$$

$$\left. + \bar{\epsilon}^{1} \oint \left[\overset{\bullet}{T}{}_{i}^{*} \left(\delta \overset{\bullet}{u}{}_{i}^{(2)} - \delta \overset{\bullet}{u}{}_{i}^{(1)} \right) + \delta \overset{\bullet}{T}{}_{i}^{*} \left(\overset{\bullet}{u}{}_{i}^{(2)} - \overset{\bullet}{u}{}_{i}^{(1)} - [u_i](\ldots) \right) \right] ds \right\} dV$$

$$= \int_{\partial V_T} \left\{ \sum_{\alpha=1}^{2} \int_{A^{(\alpha)}} \overset{\nu}{\overset{\bullet}{T}}{}_{i}^{(\alpha)} \, \delta \overset{\bullet}{u}{}_{i}^{(\alpha)} \right\} dS \quad . \tag{F-5}$$

Consider now a preferred rectangular Cartesian Coordinate system as depicted in Figure F.1. The x_i-axis in this system is aligned with the rebar axis, and x_3 is normal to the plate.

The analysis commences by invoking the following premise concerning the global stress fields:

$$N_{31}^{(\alpha)} = N_{32}^{(\alpha)} = N_{33}^{(\alpha)} = 0 \quad , \quad \alpha = 1,2 \tag{F-6}$$

where, as in Appendix C

$$N_{ij}^{(\alpha)} \equiv \frac{1}{n^{(\alpha)} A} \int_{A^{(\alpha)}} \sigma_{ij}^{(\alpha)} \, dA^{*} \tag{F-7}$$

Equation (F-6) represents a type of global "plane stress".

Next, the following trial displacement field is selected:

$$\begin{aligned} \overset{\bullet}{u}_i^{(\alpha)} &= \overset{\bullet}{U}_i^{(\alpha)} + \epsilon \left[{}^{2}\overset{\bullet}{S}_i \right] g^{(\alpha)}(r) \cos\theta \quad , \quad i=1,2 \quad ; \\ u_3^{(\alpha)} &= 0 \quad . \end{aligned} \tag{F-8}$$

Here again,

$$g^{(1)}(r) = \frac{r}{n^{(1)}} \quad , \quad g^{(2)}(r) = \frac{r}{n^{(2)}} \left[-r + \frac{1}{r} \right] \quad . \tag{F-9}$$

It is evident that (F-8) is a special case of (E-7), Appendix E, for which $U_3=0$, ${}^{3}S_i=0$, ${}^{2}S_3=0$.

The stress trial field is selected in the following form:

$$\left.\begin{aligned} \overset{\bullet}{\sigma}_{22}^{(1)} &= \overset{\bullet}{\tau}_{22}^{(1)} + \epsilon \frac{3\overset{\bullet}{\beta}_2}{4} g^{(1)}(r) \cos\theta \quad , \\ \overset{\bullet}{\sigma}_{33}^{(1)} &= \frac{\epsilon}{4} \overset{\bullet}{\beta}_2 g^{(1)}(r) \cos\theta \quad , \\ \overset{\bullet}{\sigma}_{23}^{(1)} &= \frac{\epsilon}{4} \overset{\bullet}{\beta}_2 g^{(1)}(r) \sin\theta \quad , \\ \overset{\bullet}{\sigma}_{31}^{(1)} &= \frac{\epsilon}{2} \overset{\bullet}{\beta}_1 g^{(1)}(r) \sin\theta \quad , \\ \overset{\bullet}{\sigma}_{12}^{(1)} &= \overset{\bullet}{\tau}_{12} + \frac{\epsilon}{2} \overset{\bullet}{\beta}_1 g^{(1)}(r) \cos\theta \quad , \end{aligned}\right\} \tag{F-10a}$$

$$\left.\begin{aligned}
\overset{\bullet}{\sigma}{}^{(2)}_{22} &= \overset{\bullet}{\tau}{}^{(2)}_{22} + 2\overset{\bullet}{t}{}^{(2)}_{22}\,\frac{\cos 2\theta}{r^2} + \frac{3\epsilon}{4}\,\overset{\bullet}{\beta}_2\, g^{(2)}(r)\,\cos\theta \quad , \\
\overset{\bullet}{\sigma}{}^{(2)}_{23} &= \overset{\bullet}{t}{}^{(2)}_{22}\,\frac{\sin 2\theta}{r^2} + \frac{\epsilon}{4}\,\overset{\bullet}{\beta}_2\, g^{(2)}(r)\,\sin\theta \quad , \\
\overset{\bullet}{\sigma}{}^{(2)}_{31} &= \overset{\bullet}{t}{}^{(2)}_{12}\,\frac{\sin 2\theta}{r^2} + \frac{\epsilon}{2}\,\overset{\bullet}{\beta}_1\, g^{(2)}(r)\,\sin\theta \quad , \\
\overset{\bullet}{\sigma}{}^{(2)}_{12} &= \overset{\bullet}{\tau}{}^{(2)}_{12} + \overset{\bullet}{t}{}^{(2)}_{12}\,\frac{\cos 2\theta}{r^2} + \frac{\epsilon}{2}\,\overset{\bullet}{\beta}_1\, g^{(2)}(r)\,\cos\theta \quad .
\end{aligned}\right\} \qquad \text{(F-10b)}$$

where $\overset{\bullet}{\tau}{}^{(\alpha)}_{ij}$, $\overset{\bullet}{t}{}^{(\alpha)}_{ij}$, and P_i are functions of x_2, x_3 and t.

Equations (F-10) are a special case of (E-8), Appendix E, for which

$$\tau_{33}{}^{(\alpha)} = \tau_{23}{}^{(\alpha)} = \tau_{13}{}^{(\alpha)} = 0 \quad , \qquad \text{(F-11a)}$$

$$P_3 = 0 \quad , \qquad \text{(F-11b)}$$

$$t^{(2)}_{22} = t^{(2)}_{33} \quad , \quad t^{(2)}_{31} = 0 \quad , \quad t^{(2)}_{23} = 0 \qquad \text{(F-11c)}$$

Equations (F-11a,b) result from the premise (F-6) whereas (F-11c) arises from the constraint

$$\sigma^{(2)}_{33} = \sigma^{(2)}_{32} = \sigma^{(2)}_{31} = 0 \quad \text{at} \quad \theta = \pm\frac{\pi}{2} \quad , \qquad \text{(F-12)}$$

i.e., the top and bottom concrete surfaces are assumed to be traction free.

Substitution of the trial displacement and stress fields into the variational principle (F-5), noting that $\delta\sigma_{11}^{(\alpha)} \equiv 0$, evaluating T_i^* by

$$T_i^* = \sigma_{ji}^{(1)} \nu_j^{(1)} \quad \text{on} \quad \mathscr{S} \quad , \tag{F-13}$$

and performing necessary integration by parts furnishes the Euler equations of the variational problem is the form

(a) Mixture Equilibrium - Stress Averages

$$n^{(\alpha)} \left[\mathring{N}_{11,1}^{(\alpha)} + \mathring{N}_{21,2}^{(\alpha)} \right] + (-1)^{\alpha+1} \mathring{P}_1 = 0 \quad , \tag{F-14a}$$

$$n^{(\alpha)} \left[\mathring{N}_{12,1}^{(\alpha)} + \mathring{N}_{22,2}^{(\alpha)} \right] + (-1)^{\alpha+1} \mathring{P}_2 = 0 \quad , \tag{F-14b}$$

(b) Mixture Equilibrium - Stress Moments

$$2\mathring{M}_{11,1} + 2\mathring{M}_{21,2} + \frac{1}{\epsilon^2} \left[\mathring{N}_{12}^{(2)} - \mathring{N}_{12}^{(1)} + \frac{\mathring{t}_{12}^{(2)}}{2n^{(1)}} \right] = 0 \quad , \tag{F-15a}$$

$$2\mathring{M}_{12,1} + 2\mathring{M}_{22,2} + \frac{1}{\epsilon^2} \left[\mathring{N}_{22}^{(2)} - \mathring{N}_{22}^{(1)} + \frac{\mathring{t}_{22}^{(2)}}{n^{(1)}} \right] = 0 \tag{F-15b}$$

where

$$\epsilon\, M^2_{ij} \equiv \frac{1}{A} \sum_{\alpha=1}^{2} \int_{A^{(\alpha)}} \sigma^{(\alpha)}_{ij}\, g^{(\alpha)}(r) \cos\theta \; dA^* \quad ; \tag{F-15c}$$

(c) Constitutive Relations - Stress Averages

$$\dot{N}^{(\alpha)}_{11} = \left[\frac{E}{1-\nu^2}\right]^{(\alpha)} \left[\dot{U}^{(\alpha)}_{1,1} + \nu^{(\alpha)}\, \dot{U}^{(\alpha)}_{2,2} + (-1)^{\alpha+1}\, \frac{\nu^{(\alpha)}}{n^{(\alpha)}}\, 2\dot{S}_2\right] , \tag{F-16a}$$

$$\dot{N}^{(\alpha)}_{22} = \left[\frac{E}{1-\nu^2}\right]^{(\alpha)} \left[\nu^{(\alpha)}\, \dot{U}^{(\alpha)}_{1,1} + \dot{U}^{(\alpha)}_{2,2} + \frac{(-1)^{\alpha+1}}{n^{(\alpha)}}\, 2\dot{S}_2\right] , \tag{F-16b}$$

$$\dot{N}^{(\alpha)}_{12} = \left[\frac{1}{\mu^{(\alpha)}} + \delta\alpha 1\, \frac{C_{11}}{\sqrt{n^{(1)}}}\right]^{-1} \left[\dot{U}^{(\alpha)}_{1,2} + \dot{U}^{(\alpha)}_{2,1} + \frac{(-1)^{\alpha+1}}{n^{(\alpha)}}\, 2\dot{S}_1\right] \quad ; \tag{F-16c}$$

(d) Constitutive Relations - Interaction Terms

$$\dot{P}_1 = \hat{\beta}_1 \left\{\frac{\dot{V}^{(2)}_1 - \dot{V}^{(1)}_1}{\epsilon^2} + \frac{1}{2} \sum_{\alpha=1}^{2} \kappa^{(\alpha)} \left[2\dot{S}_{1,2} + 2\dot{S}_{2,1}\right]\right\}, \tag{F-17a}$$

$$\dot{P}_2 = \beta_2 \left\{\frac{\dot{V}^{(2)}_2 - \dot{V}^{(1)}_1}{\epsilon^2} + \sum_{\alpha=1}^{2} \kappa^{(\alpha)} \nu^{(\alpha)}\, 2\dot{S}_{1,1} + \frac{3}{4} \sum_{\alpha=1}^{2} \kappa^{(\alpha)} 2\dot{S}_{2,2}\right\} \tag{F-17b}$$

$$\frac{1}{\hat{\beta}_1} = \sum_{\alpha=1}^{2} \frac{\kappa^{(\alpha)}}{2\mu^{(\alpha)}} + \frac{C_{11}}{2\sqrt{n^{(1)}}} \quad , \quad C_{11} \equiv K_1^{-1} \quad ; \tag{F-17c}$$

$$\frac{1}{\beta_2} = \sum_{\alpha=1}^{2} \left\{\frac{5}{8}\, \kappa^{(\alpha)} \left(1-\nu^2\right)^{(\alpha)} - \frac{3}{8}\, \kappa^{(\alpha)} \nu^{(\alpha)} \left[\frac{1+\nu}{E}\right]^{(\alpha)} + \frac{\kappa^{(\alpha)}}{16\mu^{(\alpha)}}\right\} \quad ; \tag{F-17d}$$

$$\kappa^{(1)} = \frac{1}{4} \quad , \quad \kappa^{(2)} = -\frac{1}{4n^{(2)}} \left[2+n^{(2)} + \frac{2}{n^{(2)}} \ell n \, n^{(1)} \right] \quad ; \qquad \text{(F-17e)}$$

(e) Constitutive Relations - Stress Moments

$$2\overset{\bullet}{M}_{11} = \sum_{\alpha=1}^{2} \kappa^{(\alpha)} \nu^{(\alpha)} \overset{\bullet}{\beta}_2 + \sum_{\alpha=1}^{2} \kappa^{(\alpha)} E^{(\alpha)} \, 2\overset{s}{S}_{1,1} \quad , \qquad \text{(F-18a)}$$

$$2\overset{\bullet}{M}_{21} = 2\overset{\bullet}{M}_{12} = \frac{1}{2} \sum_{\alpha=1}^{2} \kappa^{(\alpha)} \overset{\bullet}{\beta}_1 \quad , \qquad \text{(F-18b)}$$

$$2\overset{\bullet}{M}_{22} = \frac{3}{4} \sum_{\alpha=1}^{2} \kappa^{(\alpha)} \overset{\bullet}{\beta}_2 \quad , \qquad \text{(F-18c)}$$

(f) Additional Definitions

$$\overset{\bullet}{t}{}^{(2)}_{12} = -\gamma_1 \left[2\overset{s}{S}_1 \right] \quad , \quad \overset{\bullet}{t}{}^{(2)}_{22} = -\gamma_2 \left[2\overset{s}{S}_2 \right] \quad ; \qquad \text{(F-19a)}$$

$$\gamma_1 = \frac{\mu^{(2)}}{n^{(2)}} \quad , \quad \gamma_2 = \frac{3}{n^{(2)}} \frac{E^{(2)} \mu^{(2)}}{4\left(1-\nu^2\right)^{(2)} \mu^{(2)} + E^{(2)}} \quad . \qquad \text{(F-19b)}$$

In the above, ν and E denote Poisson's ratio and Young's modulus, respectively.

APPENDIX G

MIXTURE EQUATIONS FOR ROTATED COORDINATE SYSTEM

The coordinate system selected in Appendix F is a preferred system. For many problems, another reference system may be desirable.

Consider Figure G.1, where the arbitrary coordinate system is related to the preferred system by

$$\left.\begin{aligned} x_1 &= \hat{x}_1 \cos\theta - \hat{x}_2 \sin\theta \quad , \\ x_2 &= \hat{x}_1 \sin\theta + \hat{x}_2 \cos\theta \quad , \\ x_3 &= \hat{x}_3 \quad . \end{aligned}\right\} \tag{G-1}$$

Under the transformation (G-1), the basic mixture relations for the two-dimensional R/C plate take the form

$$n^{(\alpha)} \left[\overset{\circ}{N}{}^{(\alpha)}_{11,1} + \overset{\circ}{N}{}^{(\alpha)}_{21,2} \right] + (-1)^{\alpha+1} \overset{\circ}{P}_1 = 0 \quad ; \tag{G-2a}$$

$$n^{(\alpha)} \left[\overset{\circ}{N}{}^{(\alpha)}_{12,1} + \overset{\circ}{N}{}^{(\alpha)}_{22,2} \right] + (-1)^{\alpha+1} \overset{\circ}{P}_2 = 0 \quad ; \tag{G-2b}$$

(b) Mixture Equilibrium - stress moments

$$\epsilon^2 \left[\overset{2\circ}{M}_{11,1} + \overset{2\circ}{M}_{21,2} \right] + \cos\phi \left[\overset{\circ}{N}{}^{(2)}_{12} - \overset{\circ}{N}{}^{(1)}_{12} \right] + \sin\phi \left[\overset{\circ}{N}{}^{(2)}_{11} - \overset{\circ}{N}{}^{(1)}_{11} \right]$$

$$+ \frac{\sin\phi}{n^{(2)}\pi} \int_{A^{(2)}} \frac{1}{r^2} \cos 2\theta \, \overset{\circ}{\sigma}{}^{(2)}_{11} dA^* + \frac{\cos\phi}{n^{(2)}\pi} \int_{A^{(2)}} \frac{1}{r^2} \cos 2\theta \, \overset{\circ}{\sigma}{}^{(2)}_{12} dA^* \quad , \tag{G-3a}$$

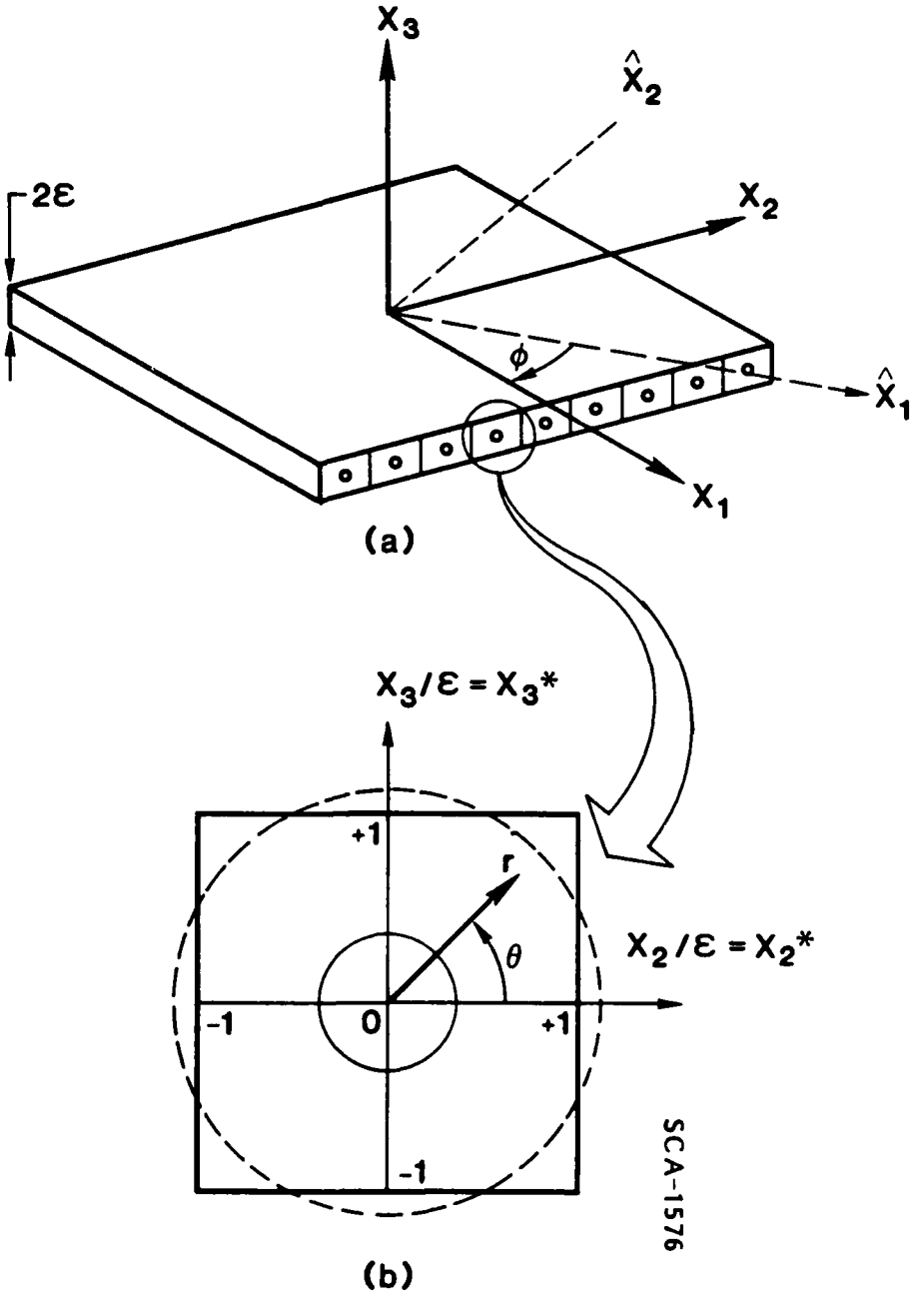

Figure G.1 Coordinate system.

$$\epsilon^2\left[\overset{2}{M}_{12,1} + \overset{2}{M}_{22,2}\right] + \sin\phi\left[\overset{1}{N}_{12}^{(2)} - \overset{1}{N}_{12}^{(1)}\right]\cos\phi\left[\overset{1}{N}_{22}^{(2)} - \overset{1}{N}_{22}^{(1)}\right]$$

$$+ \frac{\sin\phi}{n^{(2)}\pi}\int_{A^{(2)}}\frac{1}{r^2}\cos 2\theta\ \overset{1}{\sigma}_{12}\ dA^* + \frac{\cos\phi}{n^{(2)}\pi}\int_{A^{(2)}}\frac{1}{r^2}\cos 2\theta\ \overset{1}{\sigma}_{22}^{(2)}\ dA^* = 0 \qquad \text{(G-3b)}$$

(c) Constitutive Relations - stress average

$$\overset{1}{N}_{11}^{(\alpha)} = \left[\frac{E}{1-\nu^2}\right]^{(\alpha)}\left[\overset{1}{U}_{1,1}^{(\alpha)} + (-1)^{\alpha+1}\frac{\sin\phi}{n^{(\alpha)}}\left[\overset{2}{S}_1\right]\right] + \left[\frac{\nu E}{1-\nu^2}\right]^{(\alpha)}\left[\overset{1}{U}_{2,2}^{(\alpha)} + (-1)^{\alpha+1}\frac{\cos\phi}{n^{(\alpha)}}\left[\overset{2}{S}_2\right]\right], \qquad \text{(G-4a)}$$

$$\overset{1}{N}_{22}^{(\alpha)} = \left[\frac{\nu E}{1-\nu^2}\right]^{(\alpha)}\left[\overset{1}{U}_{1,2}^{(\alpha)} + (-1)^{\alpha+1}\frac{\sin\phi}{n^{(\alpha)}}\left[\overset{2}{S}_1\right]\right] + \left[\frac{E}{1-\nu^2}\right]^{(\alpha)}\left[\overset{1}{U}_{2,2}^{(\alpha)} + (-1)^{\alpha+1}\frac{\cos\phi}{n^{(\alpha)}}\left[\overset{2}{S}_2\right]\right], \qquad \text{(G-4b)}$$

$$\overset{1}{N}_{12}^{(\alpha)} = \left[\frac{1}{\mu^{(\alpha)}} + \frac{\delta_{\alpha 1}C_{11}}{n^{(1)}}\right]\left\{\overset{1}{U}_{1,2}^{(\alpha)} + \overset{1}{U}_{2,1}^{(\alpha)} + (-1)^{\alpha+1}\left[\frac{\cos\phi}{n^{(\alpha)}}\left[\overset{2}{S}_1\right] + \frac{\sin\phi}{n^{(\alpha)}}\left[\overset{2}{S}_2\right]\right]\right\} \qquad \text{(G-4c)}$$

(d) Constitutive Relations - stress moments

$$\overset{2}{M}_{11} = \left\{\sum_\alpha \kappa^{(\alpha)}\left(1-\tfrac{1}{4}\sin^2\phi\right) + \sum_\alpha \kappa^{(\alpha)}\nu^{(\alpha)}\cos^2\phi\right\}\sin\phi\ \overset{1}{P}_1$$

$$+\left\{-\frac{1}{4}\sum_\alpha \kappa^{(\alpha)}\sin^2\phi + \sum_\alpha \kappa^{(\alpha)}\nu^{(\alpha)}\cos^2\phi\right\}\cos\phi\ \overset{1}{P}_2$$

$$+\sum_\alpha \kappa^{(\alpha)}E^{(\alpha)}\cos^2\phi\left\{\cos^2\phi\left[\overset{2}{S}_{1,1}\right] + \sin^2\phi\left[\overset{2}{S}_{2,2}\right] - \sin\phi\cos\phi\left[\overset{2}{S}_{1,2} + \overset{2}{S}_{2,1}\right]\right\}, \qquad \text{(G-5a)}$$

$$\overset{2}{M}_{22}=\left\{-\frac{1}{4}\sum_{\alpha}\kappa^{(\alpha)}\cos^2\phi+\sum_{\alpha}\kappa^{(\alpha)}\nu^{(\alpha)}\sin^2\phi\right\}\sin\phi\ \overset{1}{P}_1$$

$$+\left\{\sum_{\alpha}\kappa^{(\alpha)}\left(1-\frac{1}{4}\cos^2\phi\right)+\sum_{\alpha}\kappa^{(\alpha)}\nu^{(\alpha)}\sin^2\phi\right\}\cos\phi\ \overset{2}{P}_2$$

$$+\sum_{\alpha}\kappa^{(\alpha)}E^{(\alpha)}\sin^2\phi\left\{\cos^2\phi\ \overset{2}{S}_{1,1}+\sin^2\phi\ \overset{2}{S}_{2,2}-\sin\phi\cos\phi\left[\overset{2}{S}_{1,2}+\overset{2}{S}_{2,1}\right]\right\},$$

(G-5b)

$$\overset{2}{M}_{12}=\overset{2}{M}_{21}=\left\{\left(\frac{1}{2}-\frac{1}{4}\sin^2\phi\right)\sum_{\alpha}\kappa^{(\alpha)}-\sum_{\alpha}\kappa^{(\alpha)}\nu^{(\alpha)}\sin^2\phi\right\}\cos\phi\ \overset{1}{P}_1$$

$$+\left\{\left(\frac{1}{2}-\frac{1}{4}\cos^2\phi\right)\sum_{\alpha}\kappa^{(\alpha)}-\sum_{\alpha}\kappa^{(\alpha)}\nu^{(\alpha)}\cos^2\phi\right\}\sin\phi\ \overset{2}{P}_2$$

$$-\sum_{\alpha}\kappa^{(\alpha)}E^{(\alpha)}\sin\phi\cos\phi\left\{\cos^2\phi\left[\overset{2}{S}_{1,1}\right]+\sin^2\phi\left[\overset{2}{S}_{2,2}\right]-\sin\phi\cos\phi\left[\overset{2}{S}_{12}+\overset{2}{S}_{2,1}\right]\right\}\quad\text{(G-5c)}$$

(d) Constitutive Relations - interaction terms

$$\overset{1}{P}_1=\left(\hat{\beta}_1\cos^2\phi+\beta_2\sin^2\phi\right)\left[\frac{\overset{1}{U}_1^{(2)}-\overset{1}{U}_1^{(1)}}{\epsilon^2}\right]+\left(\beta_2-\hat{\beta}_1\right)\sin\phi\cos\phi\left[\frac{\overset{2}{U}_2^{(2)}-\overset{2}{U}_2^{(1)}}{\epsilon^2}\right]$$

$$+\left\{\sum_{\alpha}\kappa^{(\alpha)}\ \hat{\beta}_1\cos^2\phi+\sum_{\alpha}\kappa^{(\alpha)}\nu^{(\alpha)}\beta_2\cos^2\phi+\frac{3}{4}\sum_{\alpha}\beta_2\sin^2\phi\right\}\sin\phi\left[\overset{2}{S}_{1,1}\right]$$

$$+\left\{-\sum_{\alpha}\kappa^{(\alpha)}\ \hat{\beta}_1\cos^2\phi+\sum_{\alpha}\kappa^{(\alpha)}\nu^{(\alpha)}\beta_2\sin^2\phi+\frac{3}{4}\sum_{\alpha}\kappa^{(\alpha)}\beta_2\cos^2\phi\right\}\sin\phi\left[\overset{2}{S}_{2,2}\right]$$

$$+\left\{\frac{1}{2}\sum_{\alpha}\kappa^{(\alpha)}\ \hat{\beta}_1\left(\cos^2\phi-\sin^{-2}\phi\right)-\sum_{\alpha}\kappa^{(\alpha)}\nu^{(\alpha)}\beta_2\sin^2\phi+\frac{3}{4}\sum_{\alpha}\kappa^{(\alpha)}\beta_2\sin^2\phi\right\}\cdot$$

$$\cdot\cos\phi\left[\overset{2}{S}_{1,2}+\overset{2}{S}_{2,1}\right], \qquad \text{(G-6a)}$$

$$\overset{2}{P}_2=\left(\beta_2-\hat{\beta}_1\right)\sin\phi\cos\phi\left[\frac{\overset{2}{U}_1^{(2)}-\overset{2}{U}_1^{(1)}}{\epsilon^2}\right]+\left(\beta_2\cos^2\phi+\beta_1\sin^2\phi\right)\left[\frac{\overset{2}{U}_2^{(2)}-\overset{2}{U}_2^{(1)}}{\epsilon^2}\right]$$

$$+\left\{-\sum_{\alpha}\kappa^{(\alpha)}\ \hat{\beta}_1\sin^{-2}\phi+\sum_{\alpha}\kappa^{(\alpha)}\nu^{(\alpha)}\beta_2\cos^2\phi+\frac{3}{4}\sum_{\alpha}\kappa^{(\alpha)}\beta_2\sin^{-2}\phi\right\}\cos\phi\left[\overset{2}{S}_{1,1}\right]$$

$$+\left\{\sum_{\alpha}\kappa^{(\alpha)}\ \hat{\beta}_1\sin^2\phi+\sum_{\alpha}\kappa^{(\alpha)}\nu^{(\alpha)}\beta_2\sin^2\phi+\frac{3}{4}\sum_{\alpha}\kappa^{(\alpha)}\beta_2\cos^2\phi\right\}\cos\phi\left[\overset{2}{S}_{2,2}\right]$$

$$+\left\{-\frac{1}{2}\sum_{\alpha}\kappa^{(\alpha)}\ \hat{\beta}_1\left(\cos^2\phi-\sin^2\phi\right)-\sum_{\alpha}\kappa^{(\alpha)}\nu^{(\alpha)}\beta_2\cos^2\phi+\frac{3}{4}\sum_{\alpha}\kappa^{(\alpha)}\beta_2\cos^2\phi\right\}\cdot$$

$$\cdot\ \sin\phi\left[\overset{2}{S}_{1,2}+\overset{2}{S}_{2,1}\right]$$

APPENDIX H

APPLICATION OF MIXED VARIATIONAL METHOD TO R/C ROD - ID PROBLEM

In this appendix, the governing mixture relations for a R/C Rod, Figure 1, are presented. This geometry is relevant since it represents specimens that are most often used to investigate steel-concrete bond properties in the laboratory. Tension tests are also frequently performed using this geometry.

The mixture equations for the R/C rod can be obtained from the analysis of Appendix E by imposing a number of constraints. With reference to Equation (8), Appendix E, the appropriate displacement constraints are

$$U_2^{(a)} = \overset{2}{S}_1 = \overset{2}{S}_2 = 0 \tag{H-1}$$

while the necessary stress constraints (see Equation 10 of Appendix E) are

$$\tau_{22}^{(a)} = \tau_{12}^{(a)} = t_{22}^{(2)} = t_{12}^{(2)} = P_2 = 0 \tag{H-2}$$

Therefore, the trial displacement field becomes

$$u_1^{(a)} = u_1^{(a)}(x_1) \quad , \quad u_2^{(a)} = u_3^{(a)} = 0 \quad , \tag{H-3}$$

whereas the trial stress field becomes

$$\sigma_{22}^{(a)} = \sigma_{33}^{(a)} = \sigma_{23}^{(a)} = 0 \ , \tag{H-4a}$$

$$\sigma_{31}^{(a)} = \frac{\epsilon}{2} P_1 g^{(a)}(r) \sin\theta \quad , \quad \sigma_{12}^{(a)} = \frac{\epsilon}{2} P_1 g^{(a)}(r)\cos\theta \ . \tag{H-4b}$$

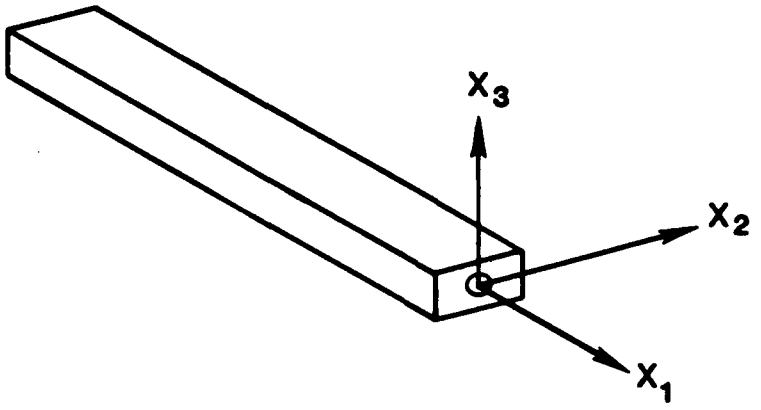

Figure H.1 Coordinate system.

In view of (H-4a), the appropriate constitutive relations are

$$\sigma_{11}^{(\alpha)} = E^{(\alpha)} e_{11}^{(\alpha)} \quad , \quad e_{11}^{(\alpha)} = U_{1,1}^{(\alpha)} \quad ; \tag{H-5a}$$

$$\left[2e_{31}, 2e_{12}\right]^{(\alpha)} = \frac{1}{\mu^{(\alpha)}} \left[\sigma_{31}, \sigma_{12}\right]^{(\alpha)} \tag{H-5b}$$

where $E^{(\alpha)}$, $\mu^{(\alpha)}$ denote Young's modulus and the shear modulus, respectively.

The desired mixture relations can be obtained by substituting (H-3)-(H-5) into the mixed variational principle of Appendix D. This same result can be obtained by invoking (H-1) and (H-2) in the R/C plate equations of Appendix F, and by noting that $(\ )_2 = 0$. The result is

(a) Mixture Equilibrium

$$N_{11,1}^{(\alpha p)} + (-1)^{\alpha+1} P_1 = 0 \quad (\alpha = 1,2) \quad ; \tag{H-6}$$

(b) Mixture Constitutive

$$n^{(\alpha)} \dot{N}_{11}^{(\alpha p)} = E^{(\alpha)} \dot{U}_{1,1}^{(\alpha)} \quad ; \tag{H-7}$$

(c) Interaction Term

$$\dot{\beta}_1 = \beta_1 \left[\frac{\dot{U}_1^{(2)} - \dot{U}_1^{(1)}}{\epsilon^2}\right] \tag{H-8}$$

where

$$\left.\begin{aligned} \beta_1^{-1} &= \sum_{\alpha} \kappa^{(\alpha)}/2\mu^{(\alpha)} \quad , \quad \kappa^{(1)} = 1/4 \ , \\ \kappa^{(2)} &= \frac{-1}{4n^{(2)}} \left[2+n^{(2)}+ \frac{2}{n^{(2)}} \ell n \ n^{(1)}\right] \quad . \end{aligned}\right\} \tag{H-9}$$

In the above, $N_{11}^{(\alpha p)} \equiv n^{(\alpha)} N_{11}^{(\alpha p)}$ denotes a "partial" stress.

The foregoing relations apply prior to local bond slip and prior to plastic deformation of the rebar. Where the latter nonlinearities occur, the quantities β_1 and $E^{(\alpha)}$ must be interpreted as tangent moduli as in Appendix C.

APPENDIX I

ON DOWEL ACTION IN REINFORCED CONCRETE

I.1 INTRODUCTION.

The nonlinear response of reinforced concrete subsequent to initial cracking is often dominated by complex mechanisms associated with steel-concrete interactions. These mechanisms include aggregate interlock or interface shear transfer (IST), dowel action (DA), nonlinear dowel effects (NDE), and steel-concrete bond action (BA). They are, in general, interdependent. This interdependence places a severe limitation on experimental attempts to quantify the contribution of each mechanism.

The foregoing experimental difficulties are amplified by a dependence of test data on the test set-up. For example, Fenwick and Paulay [1] have shown that the measured global force versus displacement relations from DA and DA plus IST tests depend strongly on the geometry of the test specimen and the test set-up, i.e., on structural constraints. The inability to separate structural effects and basic material properties within a framework of continuum mechanics renders the development of empirical relations for the response of reinforced concrete members of arbitrary geometry and boundary conditions intractable.

Problems such as those noted above demonstrate the need for analytical descriptions of the basic interaction mechanisms. Even one-dimensional analytical models (Friberg [2]; Rehm [3]; Hegemier, *et al.* [4]) have proved to be very useful in studies of certain coupled interaction mechanisms in reinforced concrete members.

To achieve optimum utility and simulation capability, the analytical descriptions noted above should be nonphenomenological. In particular, the global behavior of a reinforced concrete member should be synthesized from the properties and geometries of the composite (steel, concrete, interfaces). Further, the description should provide measures of local fields (e.g., average stress states in the steel and concrete, stress states at interfaces, interface slip, etc.) as well as global fields.

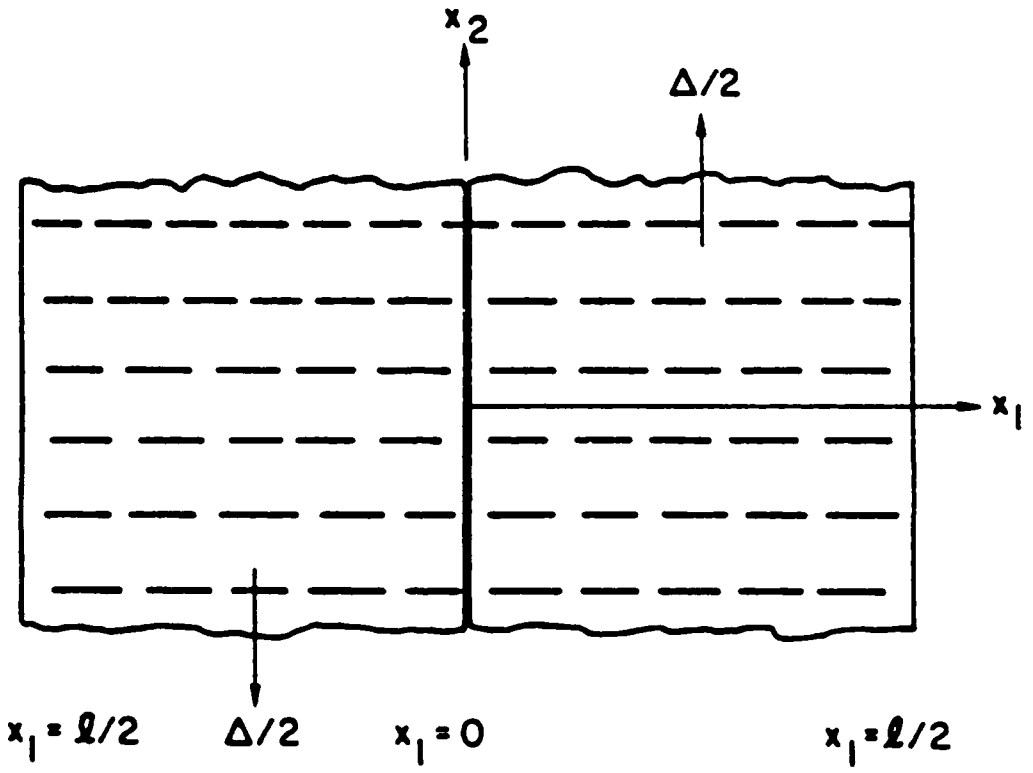

Figure I.1 The dowel problem.

The construction of an analytical model of reinforced concrete that can synthesize global behavior from component responses is a difficult task which requires some level of micromechanical analysis. This is especially true when a DA-type interaction mechanism is active. In this paper one procedure for accomplishing this task is discussed. For this purpose a specific problem is selected. The latter, and the developed model, involve combined DA, NDE, IST and BA. This work represents a generalization of a linear dowel action model (Murakami and Hegemier [5]) to include large deflections, moderately large rotations, and small-strain plastic deformation of the rebars. As a result, and in contrast to the previous work, the developed analytical description is capable of simulating large slip dowel tests (Karagozian and Case [6]; Paulay, Park and Phillips [7]).

Following model development, the simulation capability of the theory is demonstrated for both monotonic and hysteretic dowel-deformation time histories. The monotonic cases are conducted with and without IST. The hysteretic example excludes IST. BA and NDE effects are included in all examples.

The discussion herein focuses on a special case of a more general problem. In particular, the crack plane is assumed to be normal to the principal rebar direction. The general case in which concrete crack planes occur at arbitrary angles with respect to the principal steel directions will be treated in a subsequent work.

I.2 FORMULATION.

Consider a reinforced concrete element of length 2ℓ with a pre-existing crack (in the concrete) normal to the rebar at the center of the undeformed specimen. (This element may represent an actual structure or a "cell" in a periodic undirectional steel layout, see Murakami and Hegemier [5]). Let rectangular Cartesian coordinates X_1, X_2, X_3 be selected with X_1 in the axial (rebar) direction as shown in Figure I.1. The crack surface in the undeformed configuration is thus located at $X_1 = 0$. For notational convenience, $(\ )^{(\alpha)}$, $\alpha = 1,2$, will denote quantities associated with material α with $\alpha = 1$ representing the rebar and $\alpha = 2$ the concrete. In the cross-sectional X_2, X_3-plane the rebar center is located at the origin of the coordinates, and material

α occupies the domain $A^{(\alpha)}$; the exterior boundary of $A^{(1)} \cup A^{(2)}$ and the interface between the steel and concrete are denoted by ∂A and I, respectively.

In what follows, a dowel-type problem will be considered for which the displacements on ∂A are prescribed as depicted in Figure I.1. For a given history, the corresponding global forces in the coordinate directions are sought, as well as details concerning the stress states in material α which relate to failure.

Model Construction for DA

A model for deformation in the $X_1.X_2$-plane is developed by application of the direct variational method in conjunction with an appropriate trial displacement field, and by invoking an approximation of plane stress in the $X_1.X_2$-plane at a certain point of the analysis. Both the trial functions and the plane stress assumption have been previously adopted in the derivations of classical beam-type theories.

Analysis of the dowel problem commences by application of the principal of virtual work to each material in the undeformed configuration. Addition of the results furnishes

$$\int_0^{\ell} \int_{\partial A_T} \overset{\nu}{T}{}_i^{(2)} \, \delta u_i^{(2)} ds_0 \, d X_1 + \left[\sum_{\alpha=1}^{2} \iint_{A^{(\alpha)}} \overset{1}{T}{}_i^{(\alpha)} \, \delta u_i^{(\alpha)} \, d X_2 d X_3 \right]_{X_1 = 0}^{X_1 = \ell}$$

$$= \int_0^{\ell} \left\{ \sum_{\alpha=1}^{2} \iint_{A^{(\alpha)}} S_{ij}^{(\alpha)} \, \delta E_{ij}^{(\alpha)} \, d X_2 d X_3 + \oint \overset{\nu}{T}{}_i^{*} \, \delta [u_i] ds_0 \right\} d X_1 \qquad \text{(I-1)}$$

where $S_{ij}^{(\alpha)}$ is the second Piola-Kirchhoff stress, $E_{ij}^{(\alpha)}$ is the Green-Lagrange strain, u_i is the displacement, $[u_i] \equiv u_i^{(2)} - u_i^{(1)}$ is the displacement discontinuity (slip) at the surface I, T_i is the stress vector defined on the surface with exterior normal ν_i, and T_i^* denotes the stress vector on I; both T_i and ν_i are defined in the undeformed configuration. In (I-1) the virtual displacement and strain are expressed by δu_i and

δE_{ij}, respectively, and ds_0 denotes an infinitesimal line element on ∂A_T and I; the quantity ∂A_T denotes the subdomain of ∂A on which the traction is specified.

In the development, it is assumed that the rebar experiences large deflections and moderate rotations with small strain plastic deformation. At the interface I, the rebar is allowed to suffer axial slip $[u_1]$; the concrete in the neighborhood of I may experience cracking or crushing due to the relative transverse displacement $[u_2]$ between the rebar and concrete. The interface I is an "effective" surface associated with a bar that is actually deformed.

The assumed trial displacement field for use in (I-1) has the form

$$u_i^{(\alpha)}(X_1, X_2, X_3) = U_i^{(\alpha)}(X_1) + \delta_{i1}\, \psi_1^{(\alpha)}(X_1) X_2 \quad , \tag{I-2}$$

where δ_{i1} is the Kronecker delta.

Under (I-2), the Green-Lagrange strains become

$$E_{11}^{(\alpha)} = U_{1,1}^{(\alpha)} + \psi_{1,1}^{(\alpha)} X_2 + \frac{1}{2}\left(U_{2,1}^{(\alpha)}\right)^2, \quad E_{22}^{(\alpha)} = 0 \quad ,$$

$$E_{12}^{(\alpha)} = \frac{1}{2}\left(U_{2,1}^{(\alpha)} + \psi_1^{(\alpha)}\right) \quad . \tag{I-3}$$

For simplicity, and consistent with the premise of moderate rotations, the von Karmon approximation [8] has been adopted in which only the nonlinear terms associated with $U_{2,1}$ have been retained in (I-3).

Substitution of (I-2) and (I-3) into (I-1) and integration by parts furnishes

$$\int_0^{\ell} \Big\{ \Big[N^{(\alpha)}_{11,1} + (-1)^{\alpha+1} P_1 + \delta_{\alpha 2} Q_1 \Big] \delta U^{(\alpha)}_1 + \Big[\Big(N^{(\alpha)}_{12} + U^{(\alpha)}_{2,1} N^{(\alpha)}_{11} \Big)_{,1}$$

$$+ (-1)^{\alpha+1} \Big(P_2 + U^{(\alpha)}_{2,1} P_1 \Big) + \delta_{\alpha 2} \Big(Q_2 + U^{(\alpha)}_{2,1} Q_1 \Big) \Big] \delta U^{(\alpha)}_2$$

$$+ \Big[M^{(\alpha)}_{11,1} - N^{(\alpha)}_{12} + (-1)^{\alpha+1} P^{II}_1 + \delta_{\alpha 2} Q^{II}_1 \Big] \delta \psi^{(\alpha)}_1 \Big\} \, dX_1$$

$$- \Big[\Big(N^{(\alpha)}_{11} - \overset{1}{T}{}^{(\alpha a)}_1 \Big) \delta U^{(\alpha)}_1 + \Big(N^{(\alpha)}_{12} + U^{(\alpha)}_{2,1} N^{(\alpha)}_{11} - \overset{1}{T}{}^{(\alpha a)}_2 \Big) \delta U^{(\alpha)}_2$$

$$+ \Big(M^{(\alpha)}_{11} - \overset{1}{T}{}^{II(\alpha a)}_1 \Big) \delta \psi^{(\alpha)}_1 \Big]_{X_1=0}^{X_1=\ell} = 0 \quad , \tag{I-4}$$

where

$$[N_{11}, N_{12}, M_{11}]^{(\alpha)} \equiv \iint_{A^{(\alpha)}} [S_{11}, S_{12}, X_2 S_{11}]^{(\alpha)} dX_2 dX_3, \tag{I-5a}$$

$$\Big[P_1, P_2, P^{II}_1 \Big] \equiv \int_{\ell} \Big[\overset{\nu}{T}{}^{(K)}_1, \overset{\nu}{T}{}^{(K)}_2, X_2 \overset{\nu}{T}{}^{(K)}_1 \Big]^* ds_0 \quad , \tag{I-5b}$$

$$\Big[\overset{1}{T}{}^{(\alpha a)}_1, \overset{1}{T}{}^{(\alpha a)}_2, \overset{1}{T}{}_1 II(\alpha) \Big] \equiv \iint_{A^{(\alpha)}} \Big[\overset{1}{T}{}^{(\alpha)}_1, \overset{1}{T}{}^{(\alpha)}_2, X_2 \overset{1}{T}{}^{(\alpha)}_1 \Big] dX_2 dX_3 \quad , \tag{I-5c}$$

$$\Big[Q_1, Q_2, Q^{II}_1 \Big] \equiv \oint_{\partial A_T} \Big[\overset{\nu}{T}{}^{(K)}_1, \overset{\nu}{T}{}^{(K)}_2, X_2 \overset{\nu}{T}{}^{(K)}_1 \Big] ds_0 \tag{I-5d}$$

and where $(\,)^*$ implies that $(\,)$ is evaluated on the interface I of the undeformed configuration.

In the derivation of (I-4), the following expressions were employed:

$$\overset{\nu}{T}{}^{*}_{i} = T_{ji}\nu_j = \frac{\partial x_i}{\partial X_k} S_{jk}\nu_j = \frac{\partial x_i}{\partial X_k} \overset{\nu}{T}{}^{(K)}_{k} , \tag{I-6a}$$

$$\overset{1}{T}{}^{(\alpha)}_{i} = T^{(\alpha)}_{ji}\nu_j = T^{(\alpha)}_{1i} = \frac{\partial x_i}{\partial X_k} S_{1k} \tag{I-6b}$$

where T_{ij} is the <u>first</u> Piola-Kirchhoff stress and $\overset{\nu}{T}{}^{(K)}_{k} = S_{jk}\nu_j$ is the stress vector related to the <u>second</u> Piola-Kirchhoff stress. In the spirit of the von Karmon approximation for moderate rotations, the undeformed coordinates X_k were related to the deformed coordinates x_i by

$$\partial x_1/\partial X_1 = 1 . \qquad \partial x_1/\partial X_2 = 0$$

$$\partial x_2/\partial X_1 = U_{2,1} . \quad \partial x_2/\partial X_2 = 1 \tag{I-6c}$$

Equation (I-4) indicates that the Euler-Lagrange relations of the variational problem on $0 < X_1 < \ell$ are:

$$\text{either } \delta U^{(\alpha)}_1 \equiv 0 \text{ or } N^{(\alpha)}_{11,1} + (-1)^{\alpha+1} P_1 + \delta_{\alpha 2} Q_1 = 0, \tag{I-7a}$$

$$\text{either } \delta U^{(\alpha)}_2 \equiv 0 \text{ or } N^{(\alpha)}_{12,1} + N^{(\alpha)}_{11} U^{(\alpha)}_{2,11} + (-1)^{\alpha+1} P_2 + \delta_{\alpha 2} Q_2 = 0, \tag{I-7b}$$

$$\text{either } \delta \psi^{(\alpha)}_1 \equiv 0 \text{ or } M^{(\alpha)}_{11,1} - N^{(\alpha)}_{12} + (-1)^{\alpha+1} P^{II}_1 + \delta_{\alpha 2} Q^{II}_1 = 0, \tag{I-7c}$$

where (I-7a) was used to simplify (I-7b). In addition, the appropriate boundary conditions to (I-7) at $X_1 = 0$ and $X_1 = \pm \ell$ are

$$\text{either } \delta U_1^{(\alpha)} = 0 \text{ or } N_{11}^{(\alpha)} = \overset{1}{T}{}_1^{(\alpha a)} \quad , \tag{I-8a}$$

$$\text{either } \delta U_2^{(\alpha)} = 0 \text{ or } \left[N_{12}^{(\alpha)} + U_{2,1}^{(\alpha)}\, N_{11}^{(\alpha)}\right] = \overset{1}{T}{}_2^{(\alpha a)} \tag{I-8b}$$

$$\text{either } \delta \psi_1^{(\alpha)} = 0 \text{ or } M_{11}^{(\alpha)} = \overset{1}{T}{}_1^{II(\alpha a)} \quad . \tag{I-8c}$$

Equations (I-7) are of the <u>mixture</u> form. The quantities P_1, P_2, P_1^{II} are <u>interaction</u> terms, which reflect stress transfer between the rebar and concrete across the interface *I*. The quantities Q_1, Q_2, Q^{II} denote forces or moments resulting from tractions on the <u>exterior</u> cell boundary ∂A_T.

In the remainder of the analysis, attention is focused on a special dowel problem for which

$$U_1^{(2)} = 0,\ U_2^{(2)} = \text{sgn}\ (X_1)\ \Delta/2,\ \psi_1^{(2)} = 0 \quad . \tag{I-9}$$

where $\text{sgn}(X_1) = 1$ for $X_1 > 0$ and $= -1$ for $X_1 < 0$.

This case corresponds to a <u>uniform</u> displacement of the exterior boundary ∂A of the concrete cover (see Figure I.1). Under (I-9) $\delta U_i^{(2)} = 0$ on $0 < X_1 < \ell$, and the relevant mixture relations reduce to

$$N_{11,1}^{(1)} + P_1 = 0 \quad , \tag{I-10a}$$

$$N_{12,1}^{(1)} + N_{11}^{(1)}\, U_{2,11}^{(1)} + P_2 = 0 \quad , \tag{I-10b}$$

$$M_{11,1}^{(1)} - N_{12}^{(1)} + P_1^{II} = 0 \tag{I-10c}$$

on $0 < X_1 < \ell$ and

$$\text{either } \delta U_1^{(1)} = 0 \text{ or } N_{11}^{(1)} = {}^{1}T_1^{(1a)} \quad , \tag{I-11a}$$

$$\text{either } \delta U_2^{(1)} = 0 \text{ or } \left[N_{12}^{(1)} + U_{2,1}^{(1)}\, N_{11}^{(1)}\right] = {}^{1}T_2^{(1a)} \quad , \tag{I-11b}$$

$$\text{either } \delta \psi_1^{(1)} = 0 \text{ or } M_{11}^{(1)} = {}^{1}T_1^{II(1a)} \quad , \tag{I-11c}$$

$$\text{on } X_1 = 0 \, , \, \ell \, .$$

For the case of DA only, a lubricated interface is assumed at $X_1 = 0$. Further, a test set-up is considered for which the concrete is traction free at the termini $X_1 = \pm \ell$. This condition corresponds to

$${}^{1}T_2^{(2a)} = 0 \text{ at } X_1 = 0 \, , \pm \ell \tag{I-12a}$$

$${}^{1}T_1^{(2a)} = 0 \text{ at } X_1 = \pm \ell \, . \tag{I-12b}$$

In addition to (I-10), constitutive relations are required for $N_{11}^{(1)}$, $N_{12}^{(1)}$, $M_{11}^{(1)}$, P_1, P_2, P_1^{II} to close the model. For this purpose it is necessary to relate the time rate of change of the second Piola-Kirchhoff stress $\overset{\circ}{\underset{\sim}{S}}$ and the time rate of change of the Green-Lagrange strain $\overset{\circ}{\underset{\sim}{E}} \equiv \partial \underset{\sim}{E}/\partial t$ at time t to the corresponding quantities in the deformed configuration. For <u>small strain</u> problems it is possible to interpret the components of $\underset{\sim}{S}$ as those of the Cauchy stress $\underset{\sim}{\sigma}$ with respect to the covariant bases, and the components of $\overset{\circ}{\underset{\sim}{E}}$ as those of the rate of deformation tensor $\underset{\sim}{D}$, with respect to the convected contravariant bases in the deformed configuration. The premise of small strain implies that the convected covariant bases (g_1, g_2) can be approximated by the rotated rectangular Cartesian bases (g^*_1, g^*_2) at $X_2 = 0$, one of which is g_1 and the other orthogonal to g_1 to form a right-handed system. Figure I.2.

As a result of these approximations, one may interpret $N_{ij}^{(1)}$, $M_{11}^{(1)}$, P_i and P_1^{II} as the corresponding quantities defined in terms of the Cauchy stress with respect to rotated rectangular Cartesian bases.

For elastic response, the appropriate <u>stress</u> constitutive relations are, under the approximation of plane stress in the X_1, X_2 plane,

$$\overset{\circ}{S}_{11}^{(1)} = E^{(1)} \overset{\circ}{E}_{11}^{(1)} , \tag{I-13a}$$

$$\overset{\circ}{S}_{12}^{(1)} = 2\mu^{(1)} \overset{\circ}{E}_{12}^{(1)} . \tag{I-13b}$$

Substitution of (I-13) into (I-5a) with use of (I-3) for $\alpha = 1$ furnishes the elastic segment of the constitutive relations in the form:

$$\overset{\circ}{N}_{11}^{(1)} = n^{(1)} AE^{(1)} \left[\overset{\circ}{U}_{1,1}^{(1)} + U_{2,1}^{(1)} \overset{\circ}{U}_{2,1}^{(1)}\right] , \tag{I-14a}$$

$$\overset{\circ}{N}_{12}^{(1)} = n^{(1)}\mu^{(1)}A\left[\overset{\circ}{U}_{2,1}^{(1)} + \overset{\circ}{\psi}_1^{(1)}\right] . \tag{I-14b}$$

$$\overset{\circ}{M}_{11}^{(1)} = E^{(1)} I^{(1)} \overset{\circ}{\psi}_{1,1}^{(1)} \tag{I-14c}$$

where $n^{(1)}A$ is the area of the subdomain $A^{(1)}$ and $n^{(1)}$ denotes the area fraction of the rebar in the X_2, X_3-plane. A is the total area of the slip plane, and

$$I^{(1)} \equiv \iint_{A^{(1)}} (X_2)^2 \, dX_2 \, dX_3 . \tag{I-15}$$

For plastic response of the rebar, the von Mises yield criterion with the associated flow rule is employed with respect to the rotated coordinate bases as follows:

$$f(\underset{\sim}{\sigma}) = \sqrt{3J_2} - \sigma_y(\kappa) = 0 \tag{I-16}$$

where, for plane stress,

$$3J_2 = \sigma_{11}^2 + \frac{3}{2}\left(\sigma_{12}^2 + \sigma_{21}^2\right) \tag{I-17}$$

and σ_y is the yield stress in simple tension; the latter is a function of the plastic work κ where

$$\dot{\kappa} = \sigma_{ij}\, D_{ij}^P \quad . \tag{I-18}$$

The quantity D_{ij}^P is the plastic part of the rate of deformation tensor. Application of the associative flow law gives

$$D_{11}^P = \frac{\lambda}{\sigma_y}\sigma_{11}, \quad D_{12}^P = \frac{3\lambda}{2\sigma_y}\sigma_{12} \tag{I-19}$$

where λ is the plastic multiplier. By invoking the consistency condition, λ can be evaluated. By further invoking the premise of small strains, $\underset{\sim}{\sigma}$ and $\underset{\sim}{D}$ can be interchanged with $\dot{\underset{\sim}{S}}$ and $\dot{\underset{\sim}{E}}$, respectively, as was noted previously. Following use of (I-13) for the elastic part of $\underset{\sim}{D}$, i.e., $\underset{\sim}{D}^e = \underset{\sim}{D} - \underset{\sim}{D}^p$, one obtains the following local constitutive relations:

$$\begin{bmatrix} \dot{S}_{11} \\ \dot{S}_{12} \end{bmatrix}^{(1)} = \frac{1}{\left[1 + \dfrac{ES_{11}^2 + 9\mu S_{12}^2}{\sigma_y^2 H}\right]} \begin{bmatrix} E\left[1 + \dfrac{9\mu S_{12}^2}{\sigma_y^2 H}\right] & \dfrac{-3E\mu S_{11}S_{12}}{\sigma_y^2 H} \\ \dfrac{-3E\mu S_{11}S_{12}}{\sigma_y^2 H} & \mu\left[1 + \dfrac{ES_{11}^2}{\sigma_y^2 H}\right] \end{bmatrix}^{(1)} \begin{bmatrix} \dot{E}_{11} \\ 2\dot{E}_{12} \end{bmatrix}^{(1)} \tag{I-20}$$

where

$$H \equiv \sigma_y \frac{d\sigma_y}{d\kappa} \quad . \tag{I-21}$$

Equation (I-20) can now be employed to furnish constitutive relations for the global quantities $N^{(1)}_{11}$, $N^{(1)}_{12}$ and $M^{(1)}_{11}$ by substitution into (I-5a). To facilitate the resulting integrations, and in order to arrive at a result of practical utility, three approximations are made prior to integration. The first consists of dropping terms of $0(S^2_{12})$ compared to unity in the diagonal elements and denominator of (I-20); the second consists of approximating σ^2_y by S^2_{11} in (I-20), i.e., assuming $S^2_{12} << S^2_{11}$; the third involves the assumption that the cross-section is <u>fully</u> plastic. The result of these approximations, which are judged to be reasonable for the problem class under consideration, is

$$\begin{bmatrix} \dot{N}_{11} \\ \dot{N}_{12} \\ \dot{M}_{11} \end{bmatrix}^{(1)} = \begin{bmatrix} C_{11} & C_{12} & 0 \\ C_{12} & C_{22} & 0 \\ 0 & 0 & C_{33} \end{bmatrix} \begin{bmatrix} \dot{U}_{1,1} + U_{2,1}\,\dot{U}_{2,1} \\ \dot{U}_{2,1} + \dot{\psi}_1 \\ \dot{\psi}_{1,1} \end{bmatrix}^{(1)} \tag{I-22}$$

where

$$C_{11} = \frac{E^{(1)}H}{E^{(1)}+H} n^{(1)} A \quad , \quad C_{12} = \frac{-3\mu^{(1)} N^{(1)}_{12}}{\sigma_y \left[E^{(1)}+H\right]}$$

$$C_{22} = \mu^{(1)} n^{(1)} A \quad , \quad C_{33} = \frac{E^{(1)} H I^{(1)}}{E^{(1)}+H} \tag{I-23}$$

The quantity $E^{(1)}H/E^{(1)}+H$ in (I-23) is the elasto-plastic tangent modulus. The relation (I-22) was obtained with the aid of a quadratic interpolation of S_{12} over the cross-section $A^{(1)}$, i.e.

$$S_{12}^{(1)} = \gamma N_{12}^{(1)} \left[a^2 - X_2^2\right] \quad , \quad \frac{1}{\gamma} \equiv \iint_{A^{(1)}} \left[a^2 - X_2^2\right] dX_2 dX_3 \quad . \tag{I-24}$$

where a is the radius of the domain $A^{(1)}$.

In addition to the foregoing global stress constitutive relations, expressions must be considered that define the constitutive behavior of the interaction terms $P_i (i = 1.2)$. Here P_i, e.g., in (I-10a) and (I-10b), represent the forces exerted on the rebar by the concrete. In general, one may write

$$P_i = F_i\left([u^i]\right) \tag{I-25}$$

where F_i denote functionals and

$$\left[u^1\right] = \left[U_1\right] \quad , \quad \left[u^2\right] = U_{2,1}\left[U_1\right] + \left[U_2\right] \quad . \tag{I-26a}$$

For the present problem

$$\left[U_i\right] \equiv \delta_{i2}\, \mathrm{sgn}\left(X_2\right) \Delta/2 - U_i^{(1)} \tag{I-26b}$$

where δ_{ij} is the Kroncher delta. In (I-26), $[U_i]$ is the interface displacement discontinuity defined in the undeformed configuration; the transformation (I-26a) has been introduced such that $[u^i]$ are components with respect to the rotated coordinate

bases in the deformed configuration.

The interaction term P_1 in (I-10a) reflects "bond" action between the steel and concrete, and represents a tangential force on the steel due to the concrete. In previous studies by Hegemier *et al.* [4] and Hageman *et al.* [9] it was found that this interaction term can be adequately expressed in the form

$$\mathring{P}_1 = K_1[\overset{\bullet}{u}^1] \tag{I-27}$$

where K_1 denotes a (non-constant) tangent modulus. For monotonic deformation, the following bilinear form of (I-27) has been found to be adequate:

$$\begin{aligned} \mathring{P}_1 &= \beta_1[\overset{\bullet}{u}^1] \text{ for } |P_1| \leq (P_1)_y \text{ ,} \\ \mathring{P}_1 &= \beta_1^{ep}[\overset{\bullet}{u}^1] \text{ for } |P_1| > (P_1)_y \end{aligned} \tag{I-28a}$$

where $(P_1)_y$ denotes a critical value at which the modulus changes from β_1 to β_1^{ep}. If one introduces the hardening parameter H_1, then β_1^{ep} can be written as

$$\beta_1^{ep} = \beta_1\left[1 - \frac{\beta_1}{\beta_1 + H_1}\right] \text{ .} \tag{I-28b}$$

The constant β_1 in (I-28), which corresponds to no bond slip (perfect bond), has been evaluated analytically in a previous work by Murakami and Hegemier [5]. For dowel problems involving hysteretic bond slip, a more complex representation of K_1 is necessary. The form used for computational purposes herein is depicted in Figure I.3.

The interaction term P_2 reflects a normal force on the steel due to the concrete. Again, for monotonic deformation the bilinear expression below has been adopted

$$\overset{\circ}{P}_2 = \beta_2[\overset{\bullet}{u}^2] \quad \text{for} \quad |P_2| \leq (P_2)_y$$
$$\overset{\circ}{P}_2 = \beta_2^{ep}[\overset{\bullet}{u}^2] \quad \text{for} \quad |P_2| > (P_2)_y \qquad \text{(I-28c)}$$

where

$$\beta_2^{ep} = \beta_2\left[1 - \frac{\beta_2}{\beta_2 + H_2}\right] \qquad \text{(I-28d)}$$

and where β_2 has been evaluated analytically in Murakami and Hegemier [5]. For hysteretic deformation, the form of K_2 depicted in Figure I.4 has been found to be adequate; in general, the incremental form

$$\overset{\circ}{P}_2 = K_2[\overset{\bullet}{u}^2] \quad , \qquad \text{(I-28e)}$$

where K_2 is a tangent modulus, should suffice for most applications.

It is noted, that in contrast to P_1 where the nonlinear part of the bond behavior must be postulated, the nonlinear part of P_2 should be derivable from the component constitutive behavior and geometry. This, however, requires the introduction of a nonlinear model of the concrete and the conduct of a detailed 3-D microanalysis.

This is a formidable task which is outside the scope of the present paper. For purposes of examining the general features of the current modeling process, the constitutive relation for P_2 has been postulated beyond the linear range.

Finally, the interaction term P_1^{II} must be considered. From (I-5b) it is evident that this quantity represents a moment generated by the steel-concrete interface shear stress S_{21}. In general, this moment can be shown to be negligible for problems of practical interest which necessitate bond breakage prior to independent bending action of the rebar. As a consequence of this point, it is assumed that

$$P_1^{II} \simeq 0 \quad . \tag{I-29}$$

The formulation of the model is now complete for DA and NDE without IST. The basic equations are (I-10), (I-14), or (I-22), (I-28) and (I-29), and the boundary conditions (I-8) with $\alpha = 1$. For convenience, these relations are summarized below; the interaction terms listed refer to the case of monotonic deformation:

Summary of Basic Equations for DA

(1) Equilibrium:

$$\begin{aligned} &N_{11,1}^{(1)} + P_1 = 0 \quad , \\ &N_{12,1}^{(1)} + N_{11}^{(1)} U_{2,11}^{(1)} + P_2 = 0 \quad , \\ &M_{11,1}^{(1)} - N_{12}^{(1)} = 0 \quad . \end{aligned} \tag{I-30}$$

(2) Stress Constitutive Relations:

$$\begin{bmatrix} \dot{N}_{11} \\ \dot{N}_{12} \\ \dot{M}_{11} \end{bmatrix}^{(1)} = \begin{bmatrix} C_{11} & C_{12} & 0 \\ C_{12} & C_{22} & 0 \\ 0 & 0 & C_{33} \end{bmatrix} \begin{bmatrix} \dot{U}_{1,1} + U_{2,1}\dot{U}_{2,1} \\ \dot{U}_{2,1} + \dot{\Psi}_1 \\ \dot{\Psi}_{1,1} \end{bmatrix}^{(1)} \tag{I-31a}$$

where

$$C_{11} = E^{(1)} n^{(1)} A \ , \quad C_{12} = 0 \ , \quad C_{22} = \mu^{(1)} n^{(1)} A \ , \quad C_{33} = E^{(1)} I^{(1)}$$

$$\text{for } f < 0 \text{ or } f = 0 \text{ and } \dot{f} < 0 \tag{I-31b}$$

where

$$f = \sqrt{3J_2} - \sigma_y \ , \quad 3J_2 = N_{11}^{(1)^2}$$

and

$$C_{11} = \left[\frac{E^{(1)} H}{E^{(1)} + H}\right] n^{(1)} A \ , \quad C_{12} = -3 \left[\frac{\mu^{(1)}}{E^{(1)} + H}\right] \frac{N_{12}^{(1)}}{\sigma_y}$$

$$C_{22} = \mu^{(1)} n^{(1)} A \ , \quad C_{33} = \left[\frac{E^{(1)} H}{E^{(1)} + H}\right] I^{(1)} \tag{I-31c}$$

$$\text{for } f = 0 \text{ and } \dot{f} = 0 \ .$$

(3) Interaction Constitutive Relations:

$$\dot{P}_i = \beta_i \left[\dot{u}^i\right] \quad \text{for} \quad |P_i| \leq (P_i)_y$$

$$\dot{P}_i = \beta_i^{ep} \left[\dot{u}^i\right] \quad \text{for} \quad |P_i| > (P_i)_y \ , \quad (i = 1,2, \text{ no sum on } i) \tag{I-32a}$$

where

$$\beta_i^{ep} = \beta_i \left[1 - \frac{\beta_i}{\beta_i + H_i}\right] \quad , \tag{I-32b}$$

$$\left[u^1\right] \equiv \left[U_1\right], \quad \left[u^2\right] \equiv \left[U_2\right] + U_{2,1}\left[U_1\right] \quad . \tag{I-32c}$$

(4) Boundary Conditions:

$$N_{11}^{(1)} = 0 \quad , \quad N_{12}^{(1)} = 0 \quad , \quad M_{11}^{(1)} = 0 \quad \text{at} \quad X_1 = \pm \ell \quad . \tag{I-33}$$

(5) "Driving" terms:

$$\left[U_i\right] = \delta_{i2} \, \text{sgn} \, (X_2) \, \Delta/2 - U_i^{(1)} \quad . \tag{I-34}$$

Addition of IST

An elementary procedure for inclusion of IST in the foregoing dowel problem is now considered as follows: First, (I-30) - (I-34) are solved incrementally for $U_i^{(1)}$ and $T_i^{(1a)}$ at $X_1 = 0$ where $\overset{1}{T}{}_i^{(1a)} = N_{11}^{(1)}$, $\overset{1}{T}{}_2^{(1a)} = N_{12}^{(1)} + U_{2.1}^{(1)} N_{11}^{(1)}$. Second, an effective normal stress $p = p_o + (\overset{1}{T}{}_1^{(1a)}/A)$ is defined on the crack face at $X_1 = 0$, where p_o is a confining pressure (see Figure I.1) which is part of the test set-up for combined DA + IST experiments. Third, the effective normal stress p is applied to the concrete interface at $X_1 = 0$ and an IST law is postulated in the form $f(\overset{1}{T}{}_2^{(2a)}, p, \Delta) = 0$ and this relation is solved for $\overset{1}{T}{}_2^{(2a)}$ for a specified p and Δ. This latter quantity reflects IST. According to this procedure, IST influences the total effective shear stress, τ, across $X_1 = 0$ but does not alter the DA contribution, $\overset{1}{T}{}_2^{(1a)}$. Here

$$\tau \equiv \left[\frac{1}{T_2(1a)} + \frac{1}{T_2(2a)} \right] \Big/ A \quad . \tag{I-35}$$

I.3 REFERENCES FOR APPENDIX I.

1. Fenwick, R. C., and T. Paulay, "Mechanisms of Shear Resistance of Concrete Beams," *ASCE Journal of the Structural Division*, Vol. 94, No. ST10, 2325-2350 (1968).

2. Friberg, B. F., "Design of Dowels in Transverse Joints of Concrete Pavements," *Transaction of ASCE*, Vol. 105, 1076-1116 (1940).

3. Rehm, G., "Über die Grundlager des Verbundes Zwischen Stahl und Beton," Deutscher Ausschluss für Stahlbeton, H. 138 (1961); "The Basic Principles of the Bond Between Steel and Concrete," *Cement and Concrete Association*, Translation No. 134, London (1963).

4. Hegemier, G. A., H. Murakami, and J. L. Hageman, "On Tension Stiffening in Reinforced Concrete," *Mechanics of Materials*, Vol. 4, 161-179 (1985).

5. Murakami, H., and G. A. Hegemier, "On Simulating Steel-Concrete Interaction in Reinforced Concrete, Part I: Theoretical Development," *Mechanics of Materials*, Vol. 5, (1986).

6. Karagozian and Case Structural Engineers, "Construction Joint Test Program," Final Report for F04701-72-C-0358 , submitted to Space and Missile Systems Organization, Air Force Systems Command, Norton AFB, CA (1973).

7. Paulay, T., R. Park, and M. H. Phillips, "Horizontal Construction Joints in Cast-in-Place Reinforced Concrete," ACI Special Publications, SP-42, *Shear in Reinforced Concrete*, Vol. 2, 599-616 (1974).

8. von Karman, T. "Festigkeits Probleme im Maschinenbau," *Encyklopädie der Mathematischen Wissenschaften*, Vol. IV, 4, Chap. 27 (1970).

APPENDIX J

DESCRIPTION OF CONCRETE UNDER COMPRESSIVE STRESS STATES

J.1 INTRODUCTION.

It is well known that the strength of concrete increases with increasing mean confinement stress. This effect can be observed in the triaxial failure surface of concrete in stress space, Figure J.1.

In addition to strength, the ductility of concrete is observed to increase with increasing mean compressive stress. Typical increases in ductility during standard triaxial tests are shown in Figure J.2. The effect of confinement on ductility is seen to be much greater than that on strength. This can also be deduced from the behavior of reinforced concrete in the presence of confinement steel, Figure J.3.

Analytical and experimental studies (see Nemat-Nasser, *et al.*, [1]) on brittle materials such as concrete suggest that, at low confining stress levels failure occurs by the growth and connection of a narrow zone of microcracks to form one or at most several macrocracks or macrofaults, Figure J.4a,b. The onset of this event (formation of a macrocrack) corresponds to the onset of "strain softening" [2]. In contrast, at higher levels of confining stress microcracks grow in a more uniform manner and a distribution of microcracks evidently develops, Figure J.4c. Although failure may again occur via localization, the formation of this distribution appears to be responsible for the observed increase in ductility.

Below the brittle-ductile transition, slip along the planes that constitute the above distribution is a more plausible explanation of increased ductility than is true plastic flow. Consequently, conventional phenomenological elastoplastic descriptions of concrete under moderate compressive stress states appear to be inappropriate.

In view of the above discussion, an effort was made to construct a theory of concrete based on a "slip system" concept. A description of progress made to-date on this subject follows.

J.2 THE SLIP SYSTEM.

Slip system models have been used previously to describe both metals and frictional materials. A representative cross-section of such models includes the works of Mandel [3], Spencer [4], Asaro [5], and Nemat-Nasser, *et al.*, [6]. An excellent discussion and in-depth treatment of the subject is given by Nemat-Nasser [7].

Figure J.5 describes the slip concept in the case of a single slip system. Locally $\underset{\sim}{n}$ represents a unit normal to the slip surface and $\underset{\sim}{s}$ is a unit tangent vector which describes the direction of slip. The quantity Δ denotes an effective slip surface spacing. The slip system and its geometry is presumed to form at a certain critical stress state. The collection of these states forms a surface in stress space.

In the sequel, a theory is described for an arbitrary number of slip systems. Associated with the αth system is a normal vector $\underset{\sim}{n}^{(\alpha)}$, tangent vector $\underset{\sim}{s}^{(\alpha)}$, and spacing $\Delta^{(\alpha)}$, Figure J.5, where $\alpha = 1,2 \ldots, N$.

According to the slip concept, all irreversible deformation (i.e., "plastic slip") is assumed to take place along the slip surfaces. The material between these surfaces will be modeled as elastic.

J.3 DEFORMATION.

Let the relative rate of slip across a slip surface, Figure J.5, be denoted as $[v_{(s)}]$. Further, let $\underset{\sim}{e}_i$ (i = 1 to 3) denote the unit orthogonal base vectors of a rectangular Cartesian reference system. Then, if the rate of deformation tensor

$$d_{ij} = \frac{1}{2}\left(v_{i,j} + v_{j,i}\right) \qquad \text{(J-1)}$$

where $\underset{\sim}{v}$ is the velocity vector, is decomposed into elastic and inelastic parts according to

$$d_{ij} = d^e_{ij} + d^p_{ij} \tag{J-2}$$

one obtains

$$d^p_{ij} = \frac{1}{2}\left(s_i n_j + s_j n_i\right)\frac{[v_{(s)}]}{\Delta} \tag{J-3}$$

where

$$s_i \equiv \underset{\sim}{s} \cdot \underset{\sim}{e}_i \quad , \quad n_i \equiv \underset{\sim}{n} \cdot \underset{\sim}{e}_i \quad . \tag{J-4}$$

In the case of multiple slip systems, the effects are superposed to give

$$d^p_{ij} = \sum_{\alpha=1}^{N} \frac{1}{2}\left(s^\alpha_i n^\alpha_j + s^\alpha_j n^\alpha_i\right)\frac{[v_{(s)}]^\alpha}{\Delta^\alpha} \quad . \tag{J-5}$$

Since $\underset{\sim}{s}\cdot\underset{\sim}{n} = s_i n_i = 0$, it is evident that the inelastic deformation characterized by (J-5) does not involve volume change. There are three plausible ways that inelastic volume change may accompany plastic flow within the context of a slip system (Nemat-Nasser[7]): (a) plastic volumetric expansion may occur normal to the slip plane as slip takes place; (b) uniform isotropic expansion or contraction may accompany slip; and (c) uniform inelastic volumetric deformation may take place independently of slip.

The physical cause of (a) is asperities in the form of aggregate interlock. Let $[v_{(n)}]$ denote the rate of separation of the $\pm$ slip surfaces in the normal direction. Then

$$\sum_{\alpha=1}^{N} n_i n_j \frac{[v_{(n)}]^\alpha}{\Delta^\alpha}$$

represents the dilatancy due to $[v_{(n)}]$. If the latter is related to the slip $[v_{(s)}]$ according to

$$[v_{(n)}] = \theta_1 [v_{(s)}] \tag{J-6}$$

where θ_1 is a scalar function, then (J-5) can be generalized to give

$$d^p_{ij} = \sum_{\alpha=1}^{N} \left[\frac{1}{2}\left(s^\alpha_i n^\alpha_j + s^\alpha_j n^\alpha_i\right) + n^\alpha_i n^\alpha_j \theta^\alpha_1\right] \frac{\left[v_{(s)}\right]^\alpha}{\Delta^\alpha} \qquad \text{(J-7)}$$

The physical basis for (b) is the formation of microvoids and microcracks due to slip, while that for (c) is the collapse of voids under hydrostatic compression. These effects can be modeled by adding to (J-7) terms of the form

$$\sum_{\alpha=1}^{N} \left[s^\alpha_i s^\alpha_j \theta^\alpha_2 + \delta_{ij}\theta^\alpha_3\right] \frac{v^\alpha_{(s)}}{\Delta^\alpha} + \delta_{ij}\theta^\alpha_3 \quad .$$

Consequently, the inelastic deformation rate tensor becomes

$$d^p_{ij} = \sum_{\alpha=1}^{N} p^\alpha_{ij} \frac{\left[v_{(s)}\right]^\alpha}{\Delta^\alpha} + \dot{\theta}\delta_{ij} \qquad \text{(J-8a)}$$

where

$$p^\alpha_{ij} \equiv \frac{1}{2}\left(s^\alpha_i n^\alpha_j + s^\alpha_j n^\alpha_i\right) + n^\alpha_i n^\alpha_j \theta^\alpha_1 + s^\alpha_i s^\alpha_j \theta^\alpha_2 + \delta_{ij}\theta^\alpha_3 \quad . \qquad \text{(J-8b)}$$

In addition to the rate of deformation tensor d^p_{ij}, a spin tensor w^p_{ij} is now defined according to (Asaro [5])

$$w^p_{ij} = \sum_{\alpha=1}^{N} w^\alpha_{ij} \frac{\left[v_{(s)}\right]^\alpha}{\Delta^\alpha} \qquad \text{(J-9a)}$$

where

$$w^\alpha_{ij} \equiv \frac{1}{2}\left(s^\alpha_i n^\alpha_j - s^\alpha_j n^\alpha_i\right) \quad . \qquad \text{(J-9b)}$$

J.4 INTERFACE BEHAVIOR.

The αth slip system is assumed to be activated if the resultant shear stress τ^α has attained a critical value defined by

$$f^{\alpha}(\tau^{\alpha},\sigma^{\alpha},p,\epsilon^{\alpha\beta}) = 0 \;; \quad \alpha,\beta = 1 \text{ to } N \tag{J-10}$$

where σ^{α} denotes the normal stress on the slip surface, p is the mean pressure, and $\epsilon^{\alpha\beta}$ are measures of the history of slip. Slip occurs if, in addition to (J-10),

$$\overset{*}{f}{}^{\alpha}(\tau^{\alpha},\sigma^{\alpha},p,\epsilon^{\alpha\beta}) = 0 \quad . \tag{J-11}$$

Equation (J-11) can be expressed in the form

$$\overset{\bullet}{\tau}{}^{\alpha} + \overset{\bullet}{\sigma}{}^{\alpha} \tan\eta_1 + \overset{\bullet}{p} \tan\eta_2 - \sum_{\beta=1}^{N} h^{\alpha\beta}\frac{[v_{(s)}]^{\beta}}{\Delta^{\beta}} = 0 \tag{J-12}$$

where $\tan\eta_1$ and $\tan\eta_2$ are material parameters that characterize, respectively, the effects of normal stress and hydrostatic stress on slip. Here η_1 corresponds to the usual friction. The quantity η_2 reflects the influence of pressure on plastic flow: e.g., in crystal plasticity this term would represent the influence of pressure on the motion of dislocations [1]. (In two-dimensional problems (J-12) can be re-written in terms of σ^{α} only.) The parameters $h^{\alpha\beta}$ characterize the manner by which the slip system's resistance changes due to slip. In what follows $h^{\alpha\beta}$ is assumed to be symmetric (but not necessarily positive definite). Finally, the effect of cohesion has been excluded in the above formulation.

Consider now the problem of calculating the time rate of change of τ^{α} and σ^{α} in (J-10) - (J-12). Since

$$\tau^{\alpha} = \underset{\sim}{T}{}^{\alpha} \cdot \underset{\sim}{s}{}^{\alpha} = \sigma_{ij} n_i^{\alpha} s_j^{\alpha} \quad , \quad \sigma^{\alpha} = \underset{\sim}{T}{}^{\alpha} \cdot \underset{\sim}{n}{}^{\alpha} = \sigma_{ij} n_i^{\alpha} n_j^{\alpha} \tag{J-13}$$

it is clear that one must determine $\overset{\bullet}{\underset{\sim}{n}}{}^{\alpha}$ and $\overset{\bullet}{\underset{\sim}{s}}{}^{\alpha}$ in order to calculate $\overset{\bullet}{\tau}{}^{\alpha}$ and $\overset{\bullet}{\sigma}{}^{\alpha}$. The former rates must be objective. Based on the physical processes under consideration, the following rates of change of the unit vectors $\underset{\sim}{n}{}^{\alpha}$ and $\underset{\sim}{s}{}^{\alpha}$ are defined

$$\overset{\bullet}{n}{}_i^\alpha = w_{ij}^e n_j^\alpha \quad , \quad \overset{\bullet}{s}{}_i^\alpha = w_{ij}^e s_j^\alpha \quad . \tag{J-14}$$

According to (J-14). the unit vectors are corotational with the elastic deformation of the slip system. With use of (J-14). equations (J-13) furnish

$$\overset{\bullet}{\tau}{}^\alpha = \overset{\nabla}{\sigma}_{ij} n_i^\alpha s_j^\alpha \quad , \quad \overset{\bullet}{\sigma}{}^\alpha = \overset{\nabla}{\sigma}_{ij} n_i^\alpha n_j^\alpha \tag{J-15}$$

where

$$\overset{\nabla}{\sigma}_{ij} \equiv \overset{\bullet}{\sigma}_{ij} - w_{ik}^e \sigma_{kj} \sigma_{ki} - w_{jk}^e \sigma_{ki} \quad . \tag{J-16}$$

If one defines the quantity q_{ij}^α according to

$$q_{ij}^\alpha \equiv \frac{1}{2} \left(s_i^\alpha n_j^\alpha + s_j^\alpha n_i^\alpha \right) + n_i^\alpha n_j^\alpha \tan \eta_1 + \delta_{ij} \tan \eta_2 \tag{J-17}$$

then (J-12) furnishes the following relation which can be used to calculate $\overset{\nabla}{\sigma}_{ij}$:

$$\overset{\nabla}{\sigma}_{ij} q_{ij}^\alpha = \sum_{\beta=1}^{N} h^{\alpha\beta} \frac{\left[v_{(s)} \right]^\beta}{\Delta^\beta} \quad . \tag{J-18}$$

J.5 GLOBAL CONSTITUTIVE RELATIONS.

In this section the global constitutive relation for σ_{ij} is assembled. For this purpose the elastic part of the slip system deformation is postulated in the form

$$\overset{\nabla}{\sigma}_{ij} = L_{ijk\ell} d_{k\ell}^e \tag{J-19}$$

where $L_{ijk\ell}$ is the instantaneous elastic tensor modulus. If the material between slip planes is isotropic. then

$$L_{ijk\ell} = G\left(\delta_{ik}\delta_{j\ell} + \delta_{i\ell}\delta_{jk} \right) + \lambda \delta_{ij}\delta_{k\ell} \quad . \tag{J-20}$$

It will be assumed that L_{ijkl} is independent of the rate of elastic deformation.

With use of (J-2), (J-8a), and (J-18), the relation (J-19) can be cast in the following form:

$$\overset{\nabla}{\sigma}_{ij} = C^*_{ijkl}\,(d_{kl} - \delta_{kl}\,\theta) \tag{J-21}$$

where C^*_{ijkl} is an "elastic-plastic" modulus defined by

$$C^*_{ijkl} \equiv L_{ijkl} - \sum_{\alpha,\beta=1}^{N} \left[L_{ijmn}p^{\alpha}_{mn} + \omega^{\alpha}_{im}\sigma_{mj} + \omega^{\alpha}_{jm}\sigma_{mi}\right] M^{\alpha\beta} q^{\beta}_{mn} L_{mnkl} \tag{J-22}$$

where

$$M^{\alpha\beta} \equiv \left(h^{\alpha\beta} + q^{\alpha}_{ij} L_{ijkl} p^{\beta}_{kl}\right)^{-1} \quad . \tag{J-23}$$

J.6 REMARKS.

The constitutive relations (J-21) are fully nonlinear and incorporate an arbitrary number of slip systems. Their form is identical, for all practical purposes, to the relations obtained by Nemat-Nasser [7]. The only relevant difference concerns the interpretation of the tensor L_{ijkl}. The definition of this quantity, which may depend on the current stress and the history of deformation, is somewhat vague for brittle materials such as concrete.

The constitutive relations (J-21) include classical plasticity as a special case. However, there is an important difference. It can be easily shown that the current model is such that the stress tensor σ_{ij} is noncoaxial with the inelastic deformation rate tensor d^p_{ij}. This feature furnishes an ability to model localization phenomena.

A number of special case studies using the foregoing results are under current study. These investigations are intended to determine the modeling capabilities and limitations of the slip-system description of concrete behavior.

J.7 REFERENCES FOR APPENDIX J.

1. Horii, H. and S. Nemat-Nasser, "Compression-induced Micro-crack Growth in Brittle Solids: Axial Splitting and Shear Failure," *J. Geophys. Research*, 90 (1985), 3105.

2. Read, H. E., and G. A. Hegemier, "Strain Softening of Rock, Soil and Concrete," *Mechanics of Materials*, 3 (1985), 271.

3. Mandel, J., "Sur les lignes de glissement et le calcul des déplacements dans la déformation plastique," *Comptes rendus de l'Academie des Sciences*, 225 (1947), 1272.

4. Spencer, A. J. M., "A Theory of Kinematics of Ideal Soil Under Plane Strain Conditions," *J. Mech. Phys. Sol., 12 (1964), 337.*

5. *Asaro, R., "Geometrical Effects in the Inhomogeneous Deformation of Ductile Single Crystals," Acta. Met.*, 27 (1979), 445.

6. Nemat-Nasser, S., M. Mehrabadi and T. Iwakuma, "On Certain Macroscopic and Microscopic Aspects of Plastic Flow of Ductile Materials," *Three-dimensional Constitutive Relations and Ductile Fracture*, (ed. by Nemat-Nasser, S.), North-Holland, Amsterdam, Proc. IUTAM Symp., Dourdan, France (1980), 157.

7. Nemat-Nasser, S., "Generalization of the Mandel-Spencer Double-Slip Model," to be published.

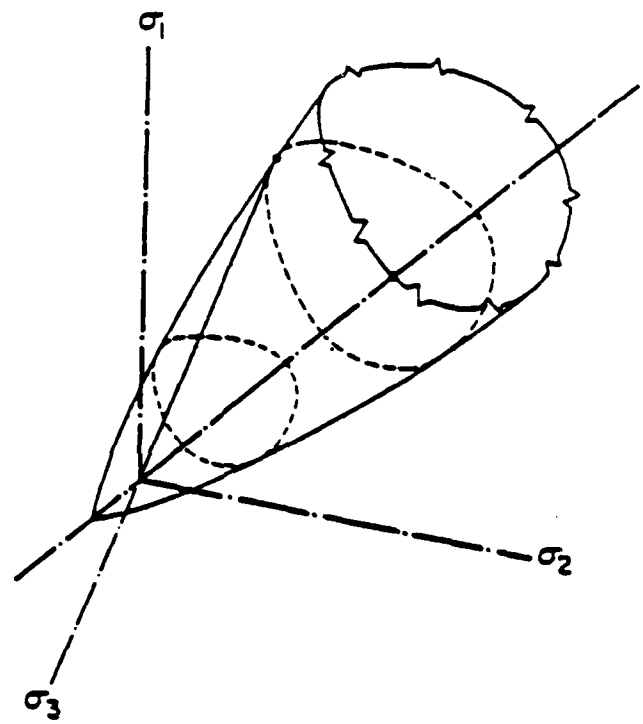

Figure J.1. Triaxial failure surface of concrete.

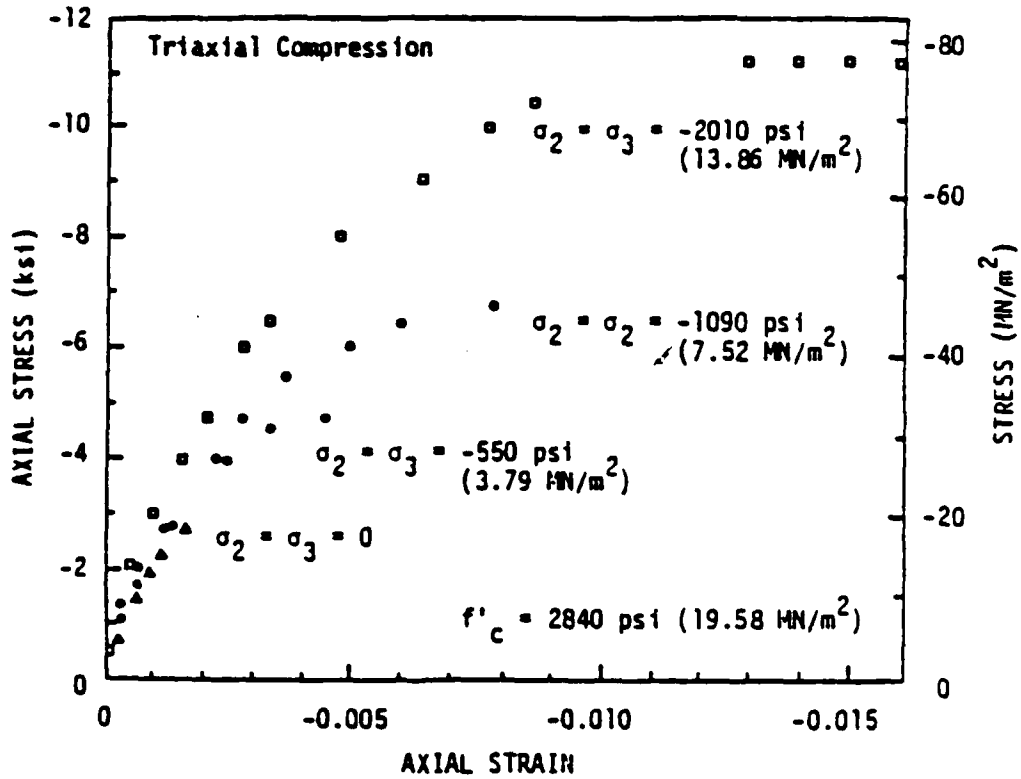

Figure J.2. Influence of confinement on strength and ductility.

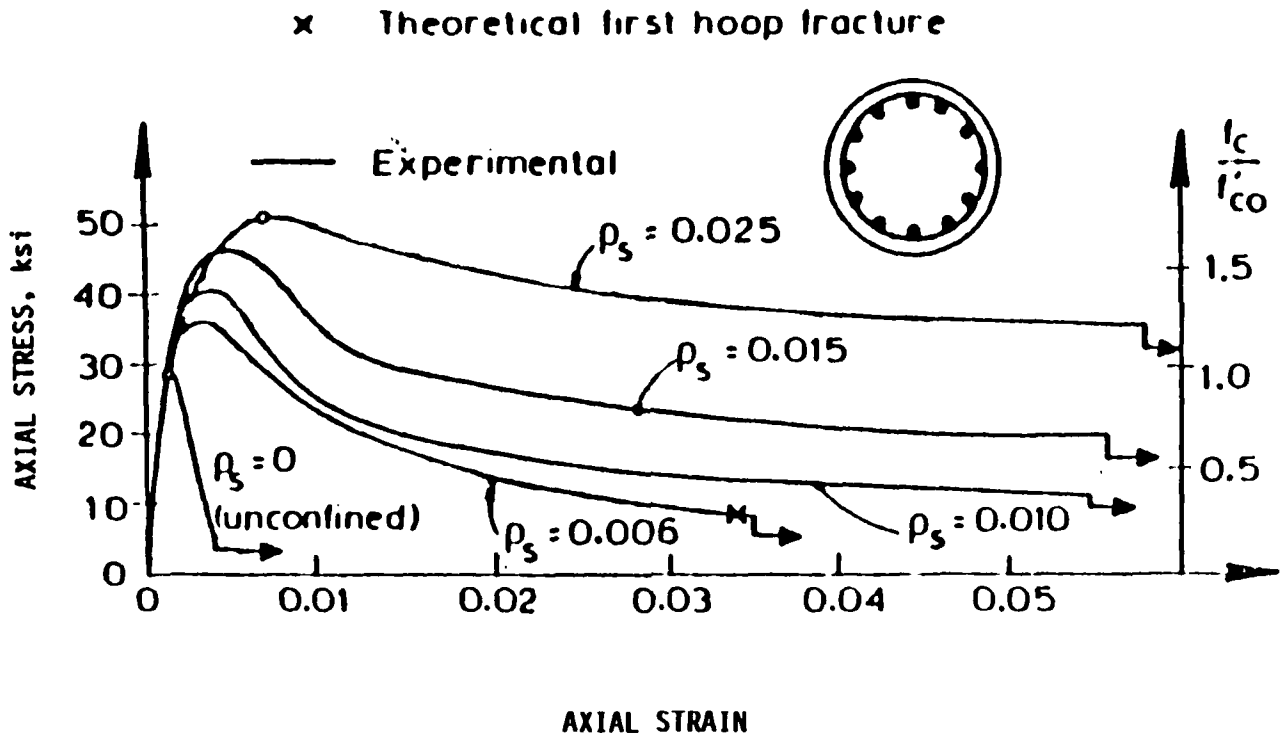

Figure J.3. Behavior of reinforced concrete in compression.

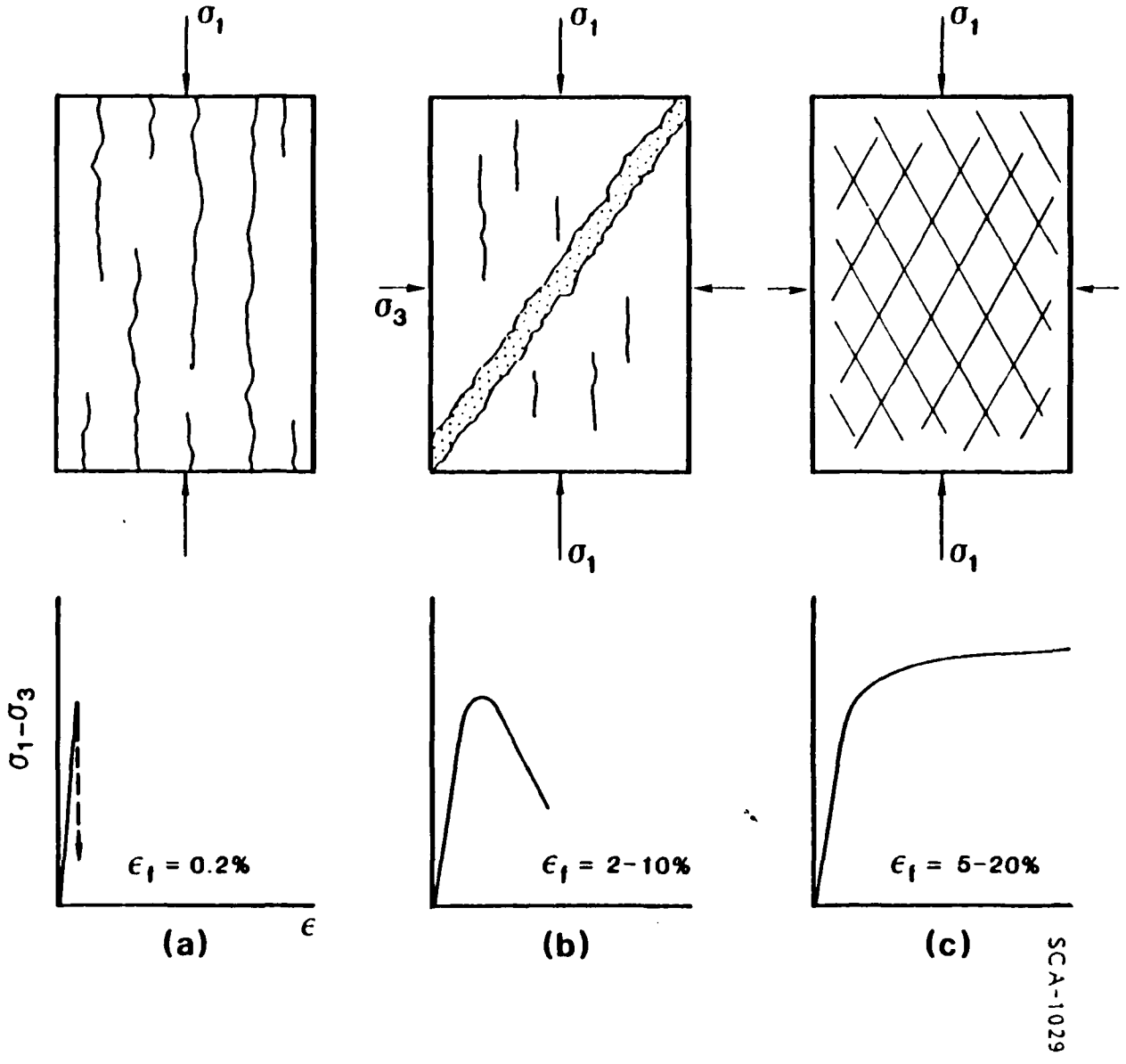

Figure J.4. Behavior of plain concrete in compression.

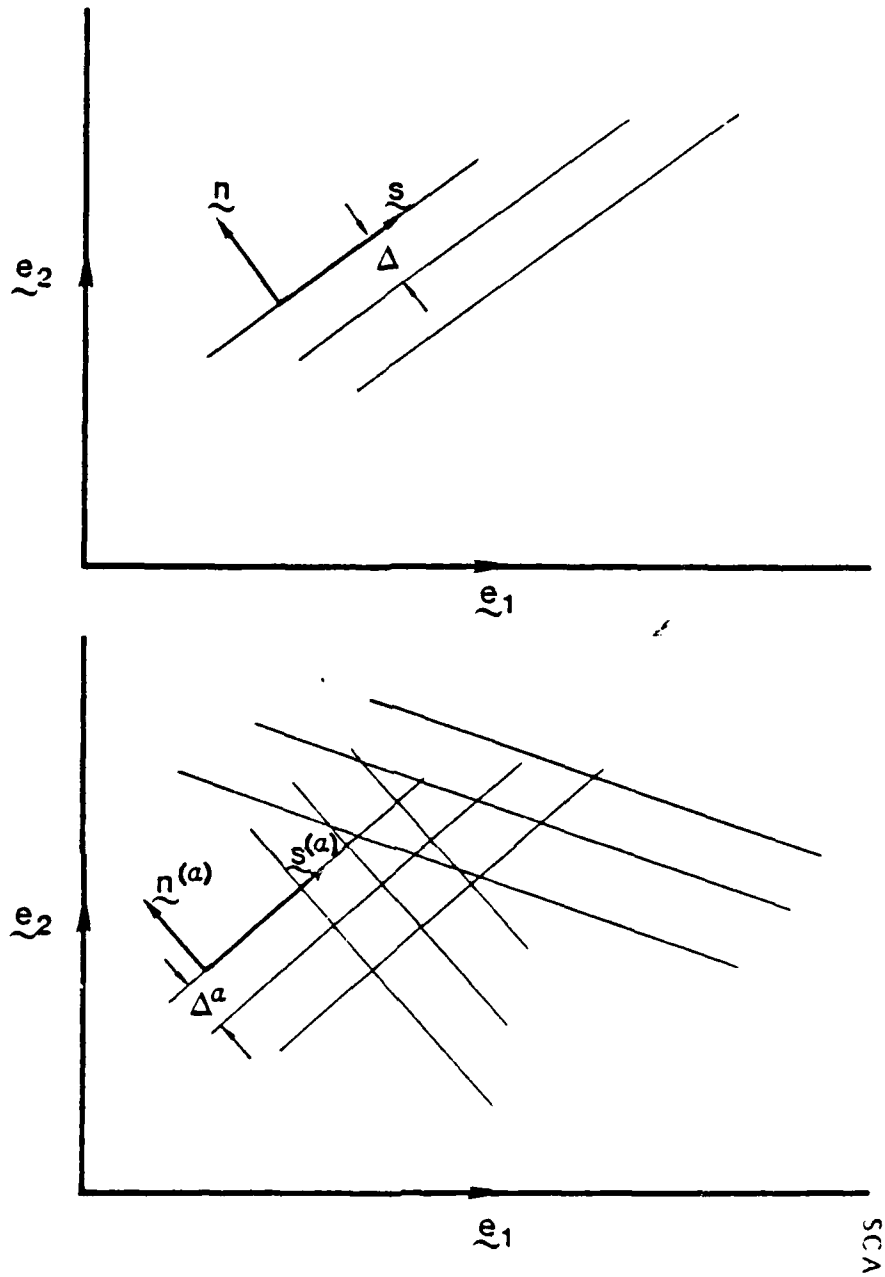

Figure J.5. Slip system concept.

END

Feb.

1988

DTIC